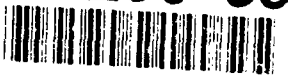

PULSED LASER DEPOSITION OF HIGH T_c SUPERCONDUCTING THIN FILMS

J. B. Boyce and G. A. N. Connell

Xerox Palo Alto Research Center
Palo Alto, California 94304

Final Technical Report
15 April 1992

REPORT DOCUMENTATION PAGE

Form Approved
OMB No. 0704-0188

1. AGENCY USE ONLY (Leave blank)	2. REPORT DATE	3. REPORT TYPE AND DATES COVERED
	15 April 1992	Final Technical Report: 7/1/90-11/1/91

4. TITLE AND SUBTITLE

Pulsed Laser Deposition of High T_c Superconducting Thin Films

5. FUNDING NUMBERS

F49620-90-C-0069

6. AUTHOR(S)

J. B. Boyce and G. A. N. Connell

7. PERFORMING ORGANIZATION NAME(S) AND ADDRESS(ES)

Xerox Corporation
Palo Alto Research Center
3333 Coyote Hill Road
Palo Alto, CA 94304

8. PERFORMING ORGANIZATION REPORT NUMBER

9. SPONSORING/MONITORING AGENCY NAME(S) AND ADDRESS(ES)

USAF, AFSC
Air Force Office of Scientific Research
Building 410
Bolling AFB, DC 20332-6448

NE

10. SPONSORING/MONITORING AGENCY REPORT NUMBER

2306/C1

11. SUPPLEMENTARY NOTES

12a. DISTRIBUTION/AVAILABILITY STATEMENT

unlimited

12b. DISTRIBUTION CODE

13. ABSTRACT (Maximum 200 words)

Superconducting thin films have been deposited *in-situ* on several substrate materials using pulsed excimer laser deposition. The major accomplishments were in four separate areas:

(1) we were the first to grow excellent quality $YBa_2Cu_3O_7$ on Si and on silicon-on-sapphire. The quality of these films has enabled several applications and other studies to be realized. These include infrared detectors and superconducting metal-insulator-semiconductor structures, as well as flux motion studies.

(2) we were the first to grow excellent quality YBCO on GaAs.This success allows superconductors to be combined with high-speed GaAs for future device applications.

(3) we were the first to grow a-axis oriented YBCO films using monolayer buffers of PrO_2. This structural orientation favors technical applications, such as, Josephson devices or tunnel junctions.

(4) we were the first to observe an extreme sensitivity of T_c to cool-down rate for epitaxial Fe-doped YBCO films. These results not only may yield information on the role of the Cu-O chains and planes in the superconductivity of this material but also may lead to procedures to increase the flux pinning.

14. SUBJECT TERMS	15. NUMBER OF PAGES
	8
	16. PRICE CODE

17. SECURITY CLASSIFICATION OF REPORT	18. SECURITY CLASSIFICATION OF THIS PAGE	19. SECURITY CLASSIFICATION OF ABSTRACT	20. LIMITATION OF ABSTRACT
Unclassified	Unclassified	Unclassified	UL

Final Technical Report on AFOSR Contract F49620-90-C-0069

Title: Pulsed Laser Deposition of High T_c Superconducting Thin Films

Investigators: James B. Boyce
G. A. Neville Connell
Xerox Palo Alto Research Center
3333 Coyote Hill Road
Palo Alto, CA 94304

1) **Statement of Work:** We will use laser deposition to grow thin film superconductors that cover a wide range of compositions, substrates, and deposition conditions. These films will be characterized and provided for in-depth study and device processing both by ourselves and collaborators at Xerox and Stanford University and their associates.

2) **Status of the Research Effort**

During the period of support on this contract (7/90-11/91), we have used our versatile PolyGun excimer laser deposition system to grow excellent quality thin films of $YBa_2Cu_3O_7$ on different substrates and with Fe dopants. We have achieved success in the following four areas:

(1) We were the first to grow excellent quality YBCO on Si and on silicon-on-sapphire, and, in collaboration with others, some YBCO/Si devices and applications have been studied.
(2) We were the first to grow excellent quality YBCO on GaAs.
(3) We were the first to grow a-axis oriented YBCO films using monolayer buffers of PrO_2.
(4) We were the first to observe an extreme sensitivity of T_c to cool-down rate for epitaxial Fe-doped YBCO films.

In the first area of YBCO/Si, we have extended our earlier work using bulk Si substrates to using silicon-on-sapphire (SOS). In both cases, an intermediate buffer layer of YSZ is used to achieve epitaxy and prevent reactions between the YBCO and the Si. The use of SOS allows the growth of thick (about 4000 Å) films without the thermally induced cracking characteristic of epitaxial films on bulk Si. Consequently, higher critical currents are obtained due to the reduction of strain in YBCO (4.6×10^6

A/cm^2 versus 2.2$\times$10^6 A/cm^2 at 77K). In addition, a low surface resistance of 72 $\mu\Omega$ is obtained at 4.2K and 11.8 GHz.

This capability of growing good quality YBCO films on Si, either bulk Si or SOS, has enabled several applications and other studies to be realized. These include infrared detectors and superconducting metal–insulator–semiconductor (MIS) structures, as well as flux motion studies. The infrared detectors, made at the University of California at Berkeley, are superconducting transition edge bolometers with outstanding figures of merit at long wavelengths. Voltage noise in YBCO films on YSZ /Si imply that for wavelengths of 20 microns and more, such detectors offer the highest sensitivity of any conceived IR detector. In addition, flux motion studies have been made by this group using our films of YBCO grown on 0.003" thick silicon wafers. The thin substrates enabled these measurements, and the results indicate that, in 20 nm thick films, the quantized flux tubes are moving as rigid rods. Also, MIS structures have been fabricated in collaboration with Santa Clara University in order to assess the utility of YBCO as a gate and/or interconnect material. The ionic conductivity of the insulating YSZ layer is manifested as hysteresis in C–V measurements and is frozen out at 77K. This could be exploited to "program" the threshold shift with a gate bias during cooling. To control hysteresis, other materials are being considered such as cerium oxide.

The second accomplishment is the growth of good quality YBCO on GaAs. The high speed and optical applications of GaAs make it a prime candidate for hybrid devices utilizing selected epitaxial oxides. Since YBCO is chemically incompatible with GaAs, buffer layers have been explored to provide a chemical barrier and structural template for epitaxy. To this end, MgO and yttria–stabilized zirconia were tested and successfully grown epitaxially on GaAs by pulsed laser deposition. Work has focused on MgO because it is more chemically inert. We have shown that improved epitaxy is achieved if the first several unit cells are grown slowly, allowing sufficient time for nucleation and ordering. Additional improvement occurs if growth is carried out on GaAs polished 10 degrees off toward [110]. Subsequent to the growth of the MgO buffer layer on GaAs, epitaxial, superconducting YBCO was grown *in situ*. The T_c and transition width were 87 K and 1.5 K, respectively. Critical currents measured by transport from 77 K to 4.2 K exceeded all prior literature values by at least a factor of ten, reaching 9 x10^6 A/cm^2 at 4.2 K. Scanning electron micrographs reveal smooth, almost featureless surfaces. This success allows

superconductors to be combined with high-speed GaAs for future device applications.

The third result is the growth of a-axis oriented YBCO thin films. For many applications, it is desirable to have YBCO films with the crystallographic a-axis out of the film plane. The structure of YBCO causes the superconducting coherence length to be about an order of magnitude larger along the a- and b-directions than along the c-direction. This favors technical applications, such as, Josephson devices or tunnel junctions, based on YBCO films grown with the a-axis normal to the substrate surface plane (a-axis oriented films). Epitaxial c-axis oriented YBCO is readily fabricated whereas a-axis films are more difficult to prepare. c-axis films with a critical temperature T_c of 86K and a transition width ΔT_c of 1K have been grown on $LaAlO_3(001)$ in a two temperature process by pulsed laser deposition. Under identical experimental conditions, an additional intermediate buffer of praseodymium oxide (PrO_2) of only about 2 Å thickness results in the growth of almost exclusive a-axis oriented YBCO, as indicated by x-ray diffraction studies and resistivity measurements. Critical temperatures of these a-axis oriented films are typically 10 K lower than those for the c-axis oriented films. Our findings suggest that a single layer of $PrBa_2Cu_3O_{7-\delta}$ is formed at the interface and induces the a-axis growth throughout the entire YBCO film. Therefore, thermodynamic considerations at the interface seem to determine the overall crystallographic orientation of the film.

The fourth study was of laser-ablated YBCO films doped with Fe. Understanding of the role played by the Cu(2)-O planes and the Cu(1)-O chains is crucial in the high T_c material YBCO. One approach has been to substitute other atoms such as Co, Fe, Ni and Zn for some of the Cu. A linear decrease in the T_c has been observed for several dopants, in particular for Fe substituted bulk samples, where $T_c \rightarrow 0$ at about 15%. Also, Fe-substituted YBCO has been extensively studied in both bulk and thin-film form in order to increase flux pinning. Fe is a potential pinning center in YBCO and several investigations of critical current density in Fe-substituted films have been reported. Thin films of $YBa_2Cu_3O_7$ and $YBa_2(Cu_{1-x}Fe_x)_3O_7$ were prepared on $LaAlO_3$ by laser deposition using a single target of the appropriate composition and using multiple targets which are pulsed the appropriate number of times to yield the desires composition. The latter technique takes advantage of the capabilities of the PolyGun so one can obtain any composition without preparing a new set of targets.

For both deposition procedures, we have achieved substitution of Fe on the Cu sites, as indicated by the x-ray-determined orthorhombic-to-tetragonal transition. Also no other phases are visible in the x-ray spectrum. TEM, however, has observed various types of precipitates. Circular precipitates (platelets) are consistent with cubic Y_2O_3, and are attributed to Ba-deficiency in the target. The platelet density increases with Fe concentration in the samples that we have studied. The platelets are oriented parallel to {100} YBCO planes. Lattice images show that the platelets are coherent precipitates with good match in the direction parallel to the platelet, and a hexagonal-like structure in the normal direction. X-ray energy dispersive analysis of the platelets have shown a significant high density of Fe, an order of magnitude larger that the Fe in the YBCO matrix. The data show that Fe substituted for Cu in YBCO has a tendency to segregate with the production of Fe-rich precipitates.

The most interesting aspect of these studies of YBCO:Fe is the extreme sensitivity of the T_c to cool-down rates. T_c is suppressed as the Fe concentration is increased but the size of the suppression varies widely in the literature. We have varied the parameters over a wide range. A variety of targets and substrate temperatures have been used; however, the most important parameter is the cool-down rate of the films in an O_2 environment immediately after deposition and subsequent anneals. A rapid cool-down, $\approx$ 200°C/min, yields surprisingly high T_c films with $T_c > 60$ K for 13% of the Cu replaced by Fe. A slow cool-down of 10°C/min results in low T_c films with $T_c \Rightarrow 0$ at 10% Fe, a greater suppression than reported for bulk materials. We have also carried our a series of post-deposition anneals in O_2 and find that T_c is significantly changed for anneal temperatures as low as 370°C. This extreme sensitivity of T_c to the cool-down rate and oxygen anneals in Fe-doped YBCO may account for many of the discrepancies reported in the literature and may be related to the Fe-rich precipitates observed in the TEM.

3) Written Publications in Technical Journals

Ajimine, E. M.; Pagaduan, F. E.; Rahman, M. M.; Yang, C. Y.; Inokawa, H.; Fork, D. K.; Geballe, T. H.; Electrical Characterization of metal-insulator-semiconductor diodes fabricated from laser-ablated YBCO/yttria-stabilized zirconia films on Si substrates. Applied Physics Letters. 1991 November; 59(22); 2889-2891.

Boyce, J. B.; Connell, G. A. N.; Fork, D. K.; Fenner, D. B.; Char, K.; Ponce, F. A.; Bridges, F.; Tramontana, J. C.; Viano, A. M.; Laderman, S. S.; Taber, R. C.; Tahara, S.; Geballe, T. H. In-situ growth of superconducting $YBa_2Cu_3O_y$ films by pulsed laser deposition. Society for Photo Optical Instrumentation Engineers Proceedings,

Processing of Films for High T_c Superconducting Electronics, Vol. 1187, 1990; 136–147.

Bridges, F.; Truher, J.; Fork, D. K.; Boyce, J. B.; Fenner, D. B.; Connell, G. A. N.; Geballe, T. H.; Johnson, S.; Liu, L.; Fe Substituted Laser Ablated $YBa_2Cu_3O_7$ Films Using Off-Stoichiometric Targets, Eds. D. C. Paine and J. C. Bravman; Materials Research Society Symposium Proceedings on Laser Ablation for Materials Synthesis; 1990 April 16–20; San Francisco, CA. Pittsburg: Materials Research Society; Vol. 191, 159–164.

Bridges, F.; Boyce, J. B.; Johnson, R. I.; Effect of Thermal History on the Transport Properties and the Location of Fe in YBCO Thin Films, to be published in Appl.Phys. Lett.

Char, K.; Fork, D. K.; Geballe, T. H.; Laderman, S. S.; Taber, R. C.; Jacowitz, R. D.; Bridges, F.; Connell, G. A. N; and Boyce, J. B. Properties of Epitaxial $YBa_2Cu_3O_7$ Films on Al_2O_3 {1012}. Appl. Phys. Lett. 56 (8), 785–787, 19 Feb 1990.

Connell, G. A. N.; Fenner, D. B.; Fork, D. K.; Boyce, J. B.; Ponce, F. A.; Bridges, F.; Geballe, T. H. YBCO films and buffer layers grown in-situ by pulsed laser deposition. D. Christen, J. Narayan and L. Schneemeyer, Eds.; Symposium on High Temperature Superconductors: Fundamental Properties and Novel Materials Processing. 1989 November 27–December 2; Boston, MA. Materials Research Society 169: 485–488.

Fenner, D. B.; Fork, D. K.; Boyce, J. B.: and Connell, G. A. N. Deposition and characterization of Y-Ba-Cu-O thin films on silicon substrates Materials and Mechanisms of Superconductivity: High-Temperature Superconductors. 1989, July 23–28; Stanford, CA. in Physica C 162–164, 141–142 (1989).

Fenner, D. B.; Fork, D. K.; Connell, G. A. N.; Boyce, J. B.; Ponce, F. A.; Tramontana, J. C.; Viano, A. M.; Geballe, T. H. Heteroepitaxial Metal Oxides on Silicon by Laser Ablation; Eds. D. C. Paine and J. C. Bravman. Materials Research Society Symposium Proceedings on Laser Ablation for Materials Synthesis; San Francisco, CA; 1990 April 16–20; Pittsburg, Materials Research Society: 1990; Vol. 191, 187–192.

Fenner, D. B.; Viano, A. M.; Connell, G. A. N.; Boyce, J. B.; Fork, D. K.; Ponce, F. A.; Tramontana, J. C.; XPS analysis of Y-Ba-Cu-O and Zr-O thin films and interfaces with silicon substrates. D. Christen, J. Narayan and L. Schneemeyer, Eds.; Symposium on High Temperature Superconductors: Fundamental Properties and Novel Materials Processing, 1989 November 27–December 2; Boston, MA. Pittsburg, Materials Research Society: 1990; Vol. 169: 1005–1008.

Fenner, D. B.; Viano, A. M.; Fork, D. K.; Connell, G. A. N.; Boyce, J. B.; Ponce, F. A.; Tramontana, J. C. Reactions at the interfaces of thin films of Y-Ba-Cu- and Zr-oxides with Si substrates. Journal of Applied Physics. 1991 February 15; 69 (4): 2176–2182.

Fenner, D. B.; Fork, D. K.; Connell, G. A. N.; Boyce, J. C.; Viano, A. M.; Geballe, T. H. High critical currents in Y-Ba-Cu-O films on silicon using YSZ buffer layers. IEEE Transactions on Magnetics. 1991 March; 27 (2): 958–965.

Fenner, D. B.; Fork, D. K.; Connell, G. A. N.; Boyce, J. B.; Ponce, F. A.; Tramontana, J. C.; Viano, A. M.; Geballe, T. H. Heteroepitaxial metal oxides on silicon by laser ablation. Paine, D. C.; Bravman. J. C., eds. Proceedings of Materials Research Society;

1990 December 3; Boston. Pittsburgh: Materials Research Society; 1990; 191: 187–192.

Fork, D. K.; Char, K.; Bridges, F.; Tahara, S.; Lairson, B.; Boyce, J. B.: Connell, G. A. N; and Geballe, T. H. YBCO Films on YSZ and Al_2O_3 by Pulsed Laser Deposition. Materials and Mechanisms of Superconductivity: High–Temperature Superconductors. 1989, July 23–28; Stanford, CA.in Physica C 162–164, 121–122 (1989).

Fork, D. K.; Fenner, D. B.; Barton, R. W.; Phillips, J. M.; Connell, G. A. N.; Boyce, J. B.; Geballe, T. H. High Critical Currents in Strained Epitaxial $YBa_2Cu_3O_7$ on Si, Appl. Phys. Lett. 57, No. 11, 10 September 1990; 1161, 1161–1163.

Fork, D. K.; Geballe, T. H; Char, K.; Laderman, S. S.; Taber, R. C.; Bridges, F.; Ponce, F. A.; Boyce, J. B.; Connell, G. A. N. Growth and Properties of Epitaxial $YBa_2Cu_3O_y$ Thin Films on {1102] Al_2O_3. D. Christen, J. Narayan and L. Schneemeyer, Eds.; Materials Research Society Symposium on High Temperature Superconductors. 1989 November 27–December 2; Boston, MA. Pittsburg, Materials Research Society: 1990; Vol. 169: 473–476.

D. K. Fork, F. A. Ponce, J. C. Tramontana, and T. H. Geballe. Epitaxial MgO on Si(100) for Y–Ba–Cu–O thin film growth by pulsed laser deposition. Applied Physics Letters, 1991 May 20; Vol.58 (20): 2294–2296.

D. K. Fork, F. A. Ponce, J. C. Tramontana, N. Newman, Julia M. Phillips, and T. H. Geballe. High critical currents in $YBa_2Cu_3O_{7-x}$ thin films on silicon on sapphire. Applied Physics Letters, 1991 May 27; Vol. 58 (21): 2432–2434.

Fork, D. K.; Fenner, D. B.; Barrera, A.; Phillips, Julia; Geballe, T. H.; Connell, G. A. N.; Boyce, J. B. Buffer layers for high quality YBCO films on Si. IEEE Transactions on Applied Superconductivity. 1991 March; 1 (1): 67–73.

Fork, D. K.; Barrera, A.; Phillips, J. M.; Newman, N.; Fenner, D. B.; Geballe, T. H.; Connell, G. A. N.; Boyce, J. B. Structural and electrical properties of epitaxial YBCO films on Si. Singh, R.; Narayan, J.; Shaw, D. T., eds. Proceedings of Society of Photo–Optical Instrumentation Engineers Conference; 1990 October 4–5; Santa Clara, CA. Bellingham, WA: SPIE; 1991; 1394: 202.

Fork, D. K.; Connell, G. A. N.; Fenner, D. B.; Boyce, J. B.; Phillips, J.; Geballe, T. H. YBCO films and YSZ buffer layers grown in–situ on silicon by pulsed laser deposition. In: McConnell, R. D.; Noufi, R., eds. Science and Technology of Thin Film Superconductors, Vol. 2. New York: Plenum Press; 1991:187–196.

Fork, D. K.; Connell, G. A. N.; Boyce, J. B.; Geballe, T. H.; Growth, properties and applications of epitaxial YBCO thin films on Si (100). Proceedings of the conference on Materials and Mechanisms of High–Tc Superconductivity; 1991 July 22–26, Kanazawa, Japan.

Fork, D. K.; Connell, G. A. N.; Ponce, F. A.; Geballe, T. H.; Buffer layers on silicon for growth of YBCO films. Proceedings of the European Materials Research Society Meeting, Strausbourg, France.

Fork, D. K.; The heteroepitaxial growth of YBCO and other metal oxides on silicon

and gallium arsenide by pulsed laser deposition. Ph.D. Thesis; Stanford University, August 1991, 203 pp.

Fork, D. K., Nashimoto, K., and Geballe, T. H., "Superconducting epitaxial Y–Ba–Cu–O thin films on GaAs (001) substrates using buffer layers," submitted to Appl. Phys. Lett.

Fork, D. K., Garrison, S. M., Hawley, Marilyn, and Geballe, T. H., "Effects of homoepitaxial surfaces and interface compounds on the in–plane epitaxy of YBCO films on yttria–stabilized zirconia," submitted to J. Mater. Res.

Nashimoto, K.; Fork, D. K.; Ponce, F. A.; Geballe, T. H.; Epitaxial growth of ferroelectric thin films on GaAs with MgO buffer layers by pulsed laser deposition. Proceedings of the Materials Research Society Meeting; 1991 December 4, Boston MA.

Nashimoto, K., Fork, D. K., and Geballe, T. H., "Epitaxial growth of MgO on GaAs (001) for growing epitaxial $BaTiO_3$ thin films by pulsed laser deposition," to be submitted to Appl. Phys. Lett.

Ponce, F. A.; Boyce, J. B.; Bridges, F.; Tramontana, J. C. Segregation in Fe substituted $YBa_2Cu_3O_7$ films. Bailey, G. W., ed. Proceedings of 49th Annual Meeting of the Electron Microscopy Society of America; 1991 August 4–9; San Jose, CA. San Francisco: San Francisco Press; 1991: 1078–1079.

Ramesh, R.; Inam, A.; Wilkins, B.; Chan, W. K.; Sands, T.; Tarascon, J. M.; Fork, D. K.; Geballe, T. H.; Evans, J.; Bullington, J.; Ferroelectric bismuth titanate/superconductor thin–film heterostructures on silicon. Applied Physics Letters. 1991 September; 59(14): 1782–1784.

Ramesh, R.; Chan, W. K..; Wilkins, B.; Sands, T.; Tarascon, J. M.; Keramides, V. G.; Fork, D. K.; Lee, J. J.; and Safari, A.; Fatigue and Aging of Ferroelectric YBCO/PZT/YBCO Heterostructures. Submitted to J. Applied Physics.

Verghese, S.; Richards, P. L.; Char, K.; Fork, D. K.; and Geballe, T. H. Feasibility of Infrared Imaging Arrays Using High–Tc Superconducting Bolometers. J. Applied Physics 1992 March; 71 (6); 2491–2498.

4) Professional Personnel Associated with Research Effort

J. B. Boyce and G. A. N. Connell, principle investigators;

D. K. Fork, Stanford PhD student of T. H. Geballe and, as of 9/91, an employee at Xerox PARC;

Larc Troger, student from the Freie University Berlin, visiting for 4 months;

F. Bridges, UC Santa Cruz professor working with us one day per week;

F. A. Ponce and J. Tramontana, members of the technical staff at Xerox;

T. H. Geballe, professor at Stanford.

5) Interactions

a) Talks

Many papers have been presented on this work at national and international conferences. In particular, these achievements were recognized by invited papers at the following conferences:

SPIE, Processing of Films for High T_c Superconducting Electronics (Santa Clara, 1989);

Science and Technology of Thin Film Superconductors 2 (Denver, 1990);

SPIE, Progress in high-temperature superconducting transistors and others devices (Santa Clara, 1990);

2nd World Congress on Superconductivity in Thin Films I (Houston Texas, 1990);

Thin film buffer layers and overlayers session of the Applied Superconductivity Conference (Snowmass, CO, 1990);

High Temperature Superconducting Thin Films (Strasbourg, 1991);

Fall MRS, High Temperature Superconductors: Materials Research for Emerging Technologies (Boston, 1991);

March American Physical Society Meeting, Symposium of the Division of Condensed Matter Physics: Thin Film Oxide Superconductors - Applications (Cincinnati, 1991).

b) Advisory Functions and Collaborations

NIST, Boulder, CO - superconductor/semiconductor electrical contacts
Stanford University - film growth and applications
Harvard University - film growth and applications
University of California, Santa Cruz- film growth and characterization
University of California, Berkeley - IR detectors and arrays
Santa Clara University - MIS structures
Bellcore - ferroelectric films
Conductus - film growth and characterization

6) Inventions and Patents

Connell, G. A. N.; Fenner, D. B.; Boyce, J. B.; and Fork, D. K., inventors. *Silicon Substrate Having an Epitaxial Superconducting Layer Thereon and Method for Making Same*. Patent Application, 1990 April 18.

PULSED LASER DEPOSITION OF HIGH T_c SUPERCONDUCTING THIN FILMS

APPENDIX

Scientific and Technical Publications

Final Technical Report
15 April 1992

Electrical characterization of metal-insulator-semiconductor diodes fabricated from laser-ablated $YBa_2Cu_3O_{7-\delta}$ /yttria-stabilized zirconia films on Si substrates

Eric M. Ajimine, Felino E. Pagaduan, M. M. Rahman, and Cary Y. Yang
Microelectronics Laboratory, Santa Clara University, Santa Clara, California 95053

Hiroshi Inokawa
NTT LSI Laboratories, 3-1 Morinosata, Wakamiyo, Atsugi, Kanagawa 243-01, Japan

David K. Fork and T. H. Geballe
Department of Applied Physics, Stanford University, Stanford, California 94305 and Xerox Palo Alto Research Center, Palo Alto, California 94304

(Received 2 July 1991; accepted for publication 29 August 1991)

The purpose of this investigation is to study the electrical properties of the YBCO/YSZ/Si metal-insulator-semiconductor structure and the yttria-stabilized zirconia (YSZ)/Si interface. The YBCO and YSZ layers were epitaxially grown *in situ* on Si by pulsed laser deposition. Current-voltage measurements of devices fabricated on *p*-type Si(100) showed a small leakage current density at 292 K, which decreased further at 80 K. Comparison of capacitance-voltage measurements at 292 K for frequencies between 10 and 400 kHz showed a large variation of capacitance in the accumulation region demonstrating the presence of mobile ions in the YSZ layer. This variation is less pronounced at 80 K. A negative shift of about 5 V in threshold voltage from 292 to 80 K has been attributed to redistribution of charges in the YSZ buffer layer.

The discovery of ceramic materials with superconducting temperatures[1] that overlap the operating temperatures of most silicon devices brought on great efforts to incorporate these materials into silicon technology. In order to deposit epitaxial films of these perovskite-type superconductors on Si, a buffer layer is required.[2] A promising buffer layer is yttria-stabilized zirconia (YSZ), $(Y_2O_3)_{0.09}(ZrO_2)_{0.91}$. It may be grown epitaxially on Si(100) in spite of a -6% lattice mismatch. No deep levels which might affect carrier lifetimes have been found for Zr in Si.[3] YSZ is also an excellent diffusion barrier. $YBa_2Cu_3O_{7-\delta}$ is a well-known high-T_c superconductor and has a $+6\%$ lattice mismatch with YSZ in the commonly observed epitaxial orientation.[4] High-quality films of YSZ and YBCO have been fabricated *in situ* with pulsed laser deposition[5] on a *p*-type Si(100) substrate with a dopant concentration of about 1.5×10^{16} cm^{-3}. Both YSZ and YBCO films are 1500 Å thick. Transmission electron microscopy (TEM) of the YSZ/Si interface reveals a layer of SiO_x approximately 50 Å in thickness.[6] The precise role of this layer is unknown but is probably responsible for the low density of states at the interface. Resistivity measurements for these films yield a critical temperature of 86 K with a transition region of less than 2 K. At 77 K these films typically have a critical current density (J_c) of about 2×10^6 A/cm^2.[5]

The YBCO layer is patterned and etched to produce metal (YBCO)-insulator (YSZ)-semiconductor (Si) diodes. Since direct probing on YBCO results in a contact resistance of a few megaohms, low-resistance ohmic contacts need to be formed for meaningful electrical characterization. Two metals commonly used to make contacts to YBCO are silver and gold.[7] It has been reported that most normal metals other than Ag and Au do not make good electrical contacts to YBCO, due in part to the depletion of oxygen from the YBCO surface.[8] We have therefore employed Au to make contacts to the YBCO electrode. To fabricate these contacts, a kovar stencil mask is used. The kovar sheet is patterned with standard photolithographic techniques. The fabricated mask is placed over the sample in an evaporator. Au is evaporated through the mask at a background pressure of 4×10^{-6} Torr. The YBCO gate and the Au contact diameters are 2 mm and 0.4 mm, respectively. From two-point measurements, total resistance including YBCO and the two contacts at room temperature is less than 200 Ω. This resistance is acceptable for current and capacitance measurements. Gold is also evaporated on the back side of the sample to yield an ohmic contact to the substrate.

Results of room-temperature (292 K) current versus voltage (I-V) measurements are shown in Fig. 1. This plot shows the leakage current of the device (<9 nA/cm^2) as the voltage is swept from -3 to 3 V and then from 3 to -3 V. The large current flow at initial bias, and apparent current flow through the device at 0 V is due to transient effects of ions in YSZ during the voltage sweep. This transient current was eliminated by sweeping the voltage from 0 to 3 V and then from 0 to -3 V. Low-temperature (80 K) I-V measurements reveal even less leakage (<2 nA/cm^2 between -3 and 3 V). Bulk YSZ is an ionic conductor with conductivity that follows an Arrhenius behavior over a wide temperature range with an activation energy of about 1 eV.[9] Pure ZrO_2 is monoclinic, while the cubic phase is stabilized by adding Y_2O_3. Since Y^{3+} substitutes for Zr^{4+}, every two Y^{3+} ions in the YSZ solid solution must induce a mobile oxygen anion vacancy. The

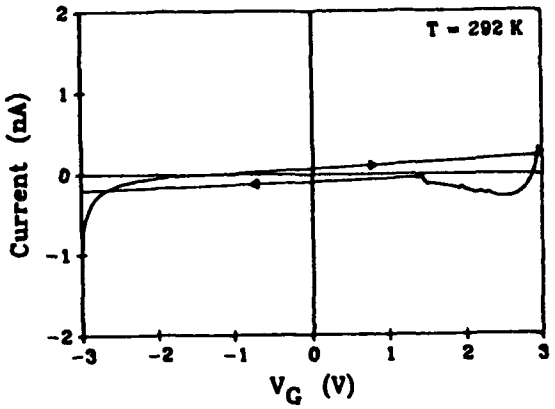

FIG. 1. Room-temperature *I-V* characteristics of a YBCO/YSZ/Si MIS diode swept from − 3 to 3 V and 3 to − 3 V.

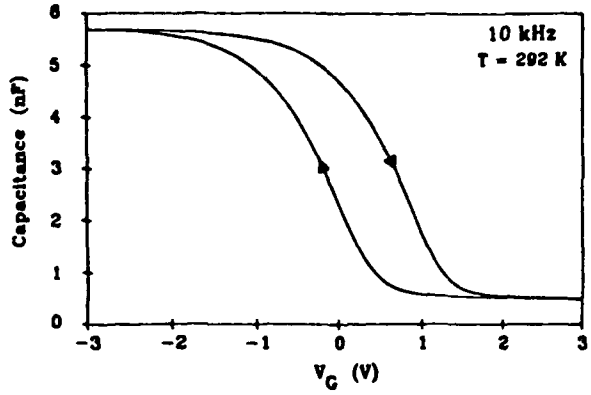

FIG. 3. Room-temperature 10 kHz *C-V* characteristics of a YBCO/YSZ/Si diode swept in the positive and negative gate voltage directions.

resulting conduction by oxygen anions may account in part for the room-temperature leakage and hysteresis, and the decrease thereof at 80 K.

Capacitance versus voltage (*C-V*) measurements at 10, 20, 40, 100, 200, and 400 kHz were performed at 292 K. The gate voltages are swept in the negative direction first and then in the positive direction at a fixed sweep rate and measurement frequency. This procedure helps to restore mobile ions to their original positions so that the true frequency-dependent characteristics can be revealed. As can be seen from Fig. 2, the MIS capacitor shows inversion, depletion, and accumulation regions similar to that of a MOS capacitor. In the accumulation region, there is a decrease in the measured capacitance with increasing frequency. The dielectric constant (K_{ins}) can be estimated from the accumulation capacitance (C_{accum}), assuming that C_{accum} is due to the insulator capacitance only. The dielectric constant of YSZ at 10 kHz is computed to be 31 while that at 400 kHz is 25. This trend of decreasing K_{ins} with increasing frequency is similar to previous reports on bulk YSZ.[10,11] It has been reported[11] that at 200 °C the dielectric constant in bulk YSZ can change by a factor of 2 between 100 Hz and 100 kHz. At room temperature, however, K_{ins} varies only slightly around 30 in the bulk over this frequency range, but is more variable for films, possibly due to defects. In our devices, the C_{accum} decrease with increasing frequency is probably due to anion charge fluctuation in YSZ and in the SiO_x interfacial layer, as well as to K_{ins} variation. In the depletion region, the capacitance curves show a shift in the negative voltage direction with increasing frequency. This behavior is a result of the decrease in C_{accum} with increasing frequency. A comparison of both voltage sweep directions at a single frequency (Fig. 3) reveals considerable hysteresis. This is characteristic of MIS structures with ionic conduction in the dielectric.[12] Hysteresis has also been reported in other MIS structures utilizing YSZ.[13]

C-V measurements were also performed at 80 K, close to the critical temperature of the YBCO film. A dramatic change in the *C-V* characteristics is the negative shift of about 5 V in threshold voltage (Fig. 4). By neglecting interface traps, the flatband voltage V_{fb} is given by[14]

$$V_{fb}=\phi_{ms}-Q_i/C_i, \tag{1}$$

where ϕ_{ms} is the metal-semiconductor work function difference which is presumed temperature independent, C_i is the insulator capacitance, and Q_i is the effective interface charge which is related to the first moment of the insulator charge distribution ρ_i by

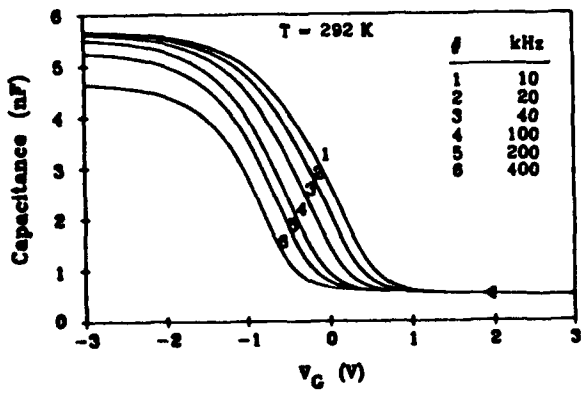

FIG. 2. Room-temperature *C-V* characteristics of a YBCO/YSZ/Si diode swept in the negative gate voltage direction at frequencies between 10 and 400 kHz.

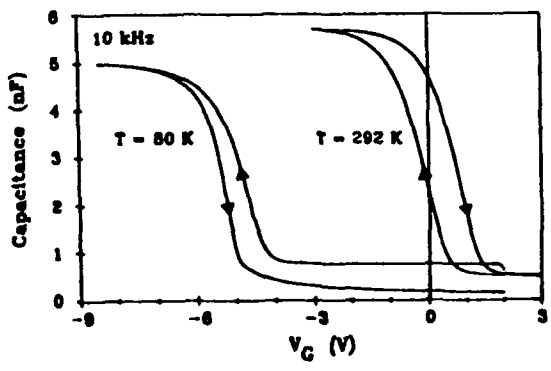

FIG. 4. Comparison of room- and superconducting-temperature 10 kHz *C-V* characteristics of a MIS diode swept in both gate voltage directions. A 5 V shift in the negative direction is observed from room to superconducting temperature.

$$Q_i = \frac{1}{t}\int_0^t \rho_i(x)x\,dx, \qquad (2)$$

where t is the insulator thickness. The germane feature is that Q_i is sensitive to the *distribution* of charges in the insulator. The 5 V shift corresponds to a 5×10^{12} cm^{-2} decrease in effective negative charge. We suggest that this decrease is due to a difference between room- and low-temperature insulator charge distributions as a result of the immobilization of oxygen anions within the YSZ layer. Preliminary measurements on devices cooled down under different bias conditions yield changes in the low-temperature threshold voltage, suggesting a memory effect whereby the charge distribution in YSZ is frozen in with varying amounts of charges concentrated near the YSZ/Si interface.

Also at 80 K, the variation in accumulation capacitance with frequency is smaller, yielding a dielectric constant of 27. This result is consistent with bulk measurements of the dielectric constant of YSZ which converge over a wide frequency range to approximately the same value at low temperature.[11] The effect in the bulk is attributed to anion immobilization, and we suspect the same mechanism is influencing our devices.

Analysis of the C-V stretch-out at high frequency reveals a density of interface traps of about 3×10^{11} eV^{-1} cm^{-2} at midgap. This is about a factor of 3 lower than earlier measurements on ion beam sputtered YSZ/Si films.[13] We conjecture that our lower interface state density is caused by the 5 nm silicon oxide layer which forms at the YSZ/Si interface; the oxide layer may be absent in the prior work[13] because their oxygen growth pressure is ~600 times lower than that in our work.[2] Without an interfacial silicon oxide layer, the -6% lattice mismatch of the YSZ layer would presumably result in an increased number of interface traps.

Figure 4 also shows a comparison of low-temperature curves in the positive and negative voltage sweep directions. The positive sweep curve yields a lower capacitance due to insufficient generation of minority carriers, resulting in partial deep depletion. Variation of sweep rates leads to the conclusion that the inversion capacitance of the negative voltage sweep is overestimated due to the stagnant inversion layer.[15] The true inversion capacitance may be estimated from the positive sweep curves. The resulting value is less than that at room temperature. From computations based on the depletion approximation, and assuming complete dopant ionization at room temperature, we obtain a value of about 10^{16} cm^{-3} for the substrate doping and 70% dopant ionization at 80 K. This is within the range of the estimated doping concentrations in the boron-doped Si substrates.

In summary, a simple MIS structure has been successfully fabricated using a YBCO superconducting gate. The electrical measurements reveal that while the YSZ buffer layer is sufficiently insulating at superconducting temperatures, the effect of ions in this layer and at the insulator/semiconductor interface constitutes the key in understanding the device operation. Our findings do not seem to be dependent on the exact nature of the transition between the normal and superconducting states, nor are they directly influenced by the superconducting property of YBCO. Studies of this transition with capacitance measurements and comparisons between this structure and similar normal-metal gate structures are in progress.

We acknowledge partial support from AFOSR contract No. F49620-89-C-0017 and NSF/RUI grant No. DMR-8822353. D. K. Fork is an AT&T scholar. Helpful comments and suggestions by J. B. Boyce, G. A. N. Connell, and D. B. Fenner are gratefully acknowledged.

[1] J. G. Bednorz and K. A. Muller, Z. Phys. B 64, 189 (1986).
[2] D. K. Fork, D. B. Fenner, A. Barrera, J. M. Phillips, T. H. Geballe, G. A. N. Connell, and J. B. Boyce, IEEE Trans. Appl. Supercond. 1, 67 (1991); A. Mogro-Compero, Supercond. Sci. Tech. 3, 115 (1990).
[3] J. W. Chen and A. G. Milnes, Ann. Rev. Mater. Sci. 10, 157 (1980).
[4] L. A. Tietz, C. B. Carter, D. K. Lathrop, S. E. Russek, R. A. Buhrman, and J. R. Michael, J. Mater. Res. 4, 1072 (1989); S. M. Garrison, N. Newman, R. F. Cole, K. Char, and R. W. Barton, Appl. Phys. Lett. 58, 2168 (1991).
[5] D. K. Fork, D. B. Fenner, R. W. Barton, J. M. Phillips, G. A. N. Connell, J. B. Boyce, T. H. Geballe, Appl. Phys. Lett. 57, 1161 (1990).
[6] D. B. Fenner, A. M. Viano, D. K. Fork, G. A. N. Connell, J. B. Boyce, F. A. Ponce, and J. C. Tramontana, J. Appl. Phys. 69, 2176 (1991).
[7] K. Mizushima, M. Sagoi, T. Miura, and J. Yoshida, Appl. Phys. Lett. 52, 1101 (1988).
[8] J. W. Ekin, T. M. Larson, N. F. Bergen, A. J. Nelson, A. B. Swartzlander, L. L. Kazmerski, A. J. Panson, and B. A. Blankenship, Appl. Phys. Lett. 52, 1819 (1988).
[9] E. C. Subbarao, in *Science and Technology of Zirconia. Advances in Ceramics, Vol. III*, edited by A. H. Heuer and L. W. Hobbs (American Ceramics Society, Columbus, Ohio, 1981), pp. 1–24.
[10] G. A. Samara, J. Appl. Phys. 68, 4241 (1990).
[11] M. T. Lanagan, J. K. Yamamoto, A. Bhalla, and S. G. Sankar, Mater. Lett. 7, 437 (1989).
[12] S. M. Sze, *Physics of Semiconductor Devices*, 2nd ed. (Wiley, New York, 1981), p. 404.
[13] C. Pellet, C. Schwebel, and P. Hesto, Thin Solid Films 175, 23 (1989).
[14] S. M. Sze, *Physics of Semiconductor Devices*, 2nd ed. (Wiley, New York, 1981), p. 395.
[15] A. Goetzberger, IEEE Trans. Electron Devices ED-14, 787 (1967).

In-situ growth of superconducting $YBa_2Cu_3O_y$ films by pulsed laser deposition

J. B. Boyce[1], G. A. N. Connell[1], D. K. Fork[2], D. B. Fenner[1,3], K. Char[4], F. A. Ponce[1], F. Bridges[1,5], J. Tramontana[1], A. M. Viano[3], S. S. Laderman[6], R. C. Taber[6], S. Tahara[2] and T. H. Geballe[2]

[1] Xerox Palo Alto Research Center, 3333 Coyote Hill Road, Palo Alto, CA 94304
[2] Stanford University, Stanford, CA 94305
[3] Santa Clara University, Santa Clara, CA 95053
[4] Conductus, Inc., Sunnyvale, CA 94086
[5] University of California, Santa Cruz, CA 95064
[6] Hewlett-Packard Company, Palo Alto, CA 94304

ABSTRACT

$YBa_2Cu_3O_y$ thin films have been deposited *in-situ* on several substrate materials using pulsed excimer laser deposition. On the substrates, $SrTiO_3$, MgO, $LaAlO_3$, and yttrium-stabilized zirconia (YSZ), excellent films were obtained. These films had high superconducting transition temperatures (91K) with narrow transition widths ($\approx$0.5K), metallic conductivity in the normal state, low room-temperature resistivity ($\approx$250 $\mu\Omega$-cm), high critical currents ($\approx 3 \times 10^7$ A/cm^2 at 4.2K), c-axis orientation perpendicular to the plane of the film, and epitaxial alignment with the substrate. On the more technologically relevant substrates of Al_2O_3 and Si, less optimal results were obtained. The transition temperatures were high (86-88K) and metallic conductivity was obtained in the normal state. However, the room-temperature and microwave surface resistivities were higher and the critical currents were lower than for the above benchmark substrates. These diminished transport properties correlate with the imperfect alignment and epitaxy of the YBCO and substrate. For Al_2O_3 substrates, a narrow substrate-temperature window was found for the best *in-situ* YBCO films. The poorer transport properties correlate with the lack of registry of the YBCO a-b plane with the sapphire r-plane. For Si substrates, a buffer layer is required due to high reactivity even at substrate temperatures as low as 550°C. YSZ provides a good buffer, and our best results were obtained on clean, hydrogen-terminated surfaces rather than oxidized Si. The amount of Y_2O_3 in ZrO_2 was varied, and the best films were obtained with x near 0.1 where $(ZrO_2)_{1-x}(Y_2O_3)_x$ is cubic. Epitaxial alignment of the YBCO with the Si was achieved, but there was a substantial spread in orientations, accounting for the diminished transport properties.

1. INTRODUCTION

Future electronic applications of high-T_c superconductors (HTSC) will require high quality thin films. Currently superconducting films are prepared by a variety of standard thin-film deposition techniques including thermal evaporation, e-beam evaporation,

magnetron sputtering, and ion-beam sputtering. A technique which is comparatively new, yet has been demonstrated for HTSC thin-film deposition and which has a number of advantages over other deposition techniques, is that of laser deposition.[1-6] This deposition technique has produced some of the best $YBa_2Cu_3O_y$ (YBCO) thin films to date. Films with sharp superconducting transitions have been prepared by laser deposition on several substrates, including $SrTiO_3$, MgO, $LaAlO_3$, and yttrium-stabilized zirconia (YSZ). These substrates have the advantage of being relatively unreactive with YBCO at its growth temperature (about 700°C) and also allow for a high degree of epitaxy; however, they also have several undesirable properties for electronic applications, namely, high dielectric constants, low mechanical strengths, and high costs. As a result, efforts have been made to deposit YBCO on substrates such as Al_2O_3 and Si which do not have the above disadvantages and, therefore, will be required for electronic devices. The difficulties in achieving this goal are that both Si and Al_2O_3 react with the superconductor during the high-temperature growth and annealing required to form the superconducting phase. Si, in addition to being more reactive than Al_2O_3, has the added problem that it rapidly forms a thin, poor quality surface oxide thereby preventing epitaxy. Nonetheless, the rewards of good HTSC films on Si make the studies worthwhile and have prompted many attempts.[7]

Here we describe our results on the *in-situ* laser deposition of YBCO thin films. Films have been deposited on the standard substrates, $SrTiO_3$, MgO, $LaAlO_3$, and YSZ, that allow for the growth of films with excellent electrical properties. These results serve as benchmarks for the results of the growth of YBCO films on both Al_2O_3 and Si, the substrates of primary interest here. Comparison of the results on these more reactive substrates is made with those on the benchmark substrate materials. Section 2 presents the experimental details. Section 3 describes the results for the standard substrates and presents some of the experimental details of the characterization techniques used. Sections 4 and 5 present the results for Al_2O_3 and Si substrates, respectively. A summary is provided in the abstract.

2. EXPERIMENTAL METHOD

In all cases, the film deposition was carried out by pulsed laser ablation using a PolyGun [Kurt J. Lesker Co.] system.[6,8] This system has a ten-sided polygon target holder. It holds ten hot-pressed targets, mounted on its faces, and is rotated such as to provide ablation pulses at a frequency between 1 and 10 Hz. A typical rate is 5 Hz. The pulses from a 308 nm XeCl excimer laser [Lambda Physik EMG 103] are synchronized with the target wheel rotation to ablate the target or targets of interest during each revolution. For YBCO on sapphire or the standard substrates, this corresponds to hitting only one or more bulk YBCO targets per revolution. While the target wheel rotation is not necessary for a single-target case, the rotation does significantly reduce the target temperature rise by limiting its exposure to radiation from the hot substrate. The deposited films have better surface morphology as a consequence.[9] Also the target wheel is surrounded by a water-cooled can with a small opening to allow for the laser ablation. This further reduces the heating of the targets and minimizes back-sputtering of one target onto another. The full advantage of the rotating polygon comes into play for multilayer film depositions and for the mixed deposition

of film materials from more than one target. The example, which is described here and which covers both of the two cases, is YBCO on Si where buffer layers are required. The buffer used here is YSZ which contains 9 mole % Y_2O_3 in ZrO_2 to stabilize the cubic, fluorite phase. One could use a single YSZ target, but we used ZrO_2 and Y_2O_3 targets to study the influence of the amount of Y, and thereby the structure of this buffer layer, on the YBCO film. For the YSZ buffer, $(ZrO_2)_{1-x}(Y_2O_3)_x$ is deposited by adjusting the ratio of the number of pulses directed at the ZrO_2 and Y_2O_3 targets. Atomic-scale intermixing of the YSZ is assured, since each pulse only deposits about 0.2 Å of either oxide. Following the deposition of the buffer, the laser firing sequence is changed to deposit the YBCO film from a bulk YBCO target(s).

The output of the excimer laser is defined by an aperture which is imaged by a 25 mm lens into the vacuum chamber and onto the targets. The laser spot size on the target is typically 1.4×3.5 mm^2. The turbo-pumped vacuum system has a base pressure of about 5×10^{-7} Torr. Other typical parameters are the following: a laser pulse energy up to 150 mJ, an energy density of 1 to 2 J/cm^2, and a target-to-substrate distance of 3.5 to 5.5 cm. Most of the depositions were performed with a laser energy density of 1.2 J/cm^2 and a target-to-substrate distance of 5 cm. Deposition rates of about 1-2 Å/sec of YBCO are achieved for these parameters.

The YBCO depositions are carried out at an elevated substrate temperature in an oxygen atmosphere. These are adjusted for *in-situ* growth; no post anneals of the films are performed. The oxygen ambient during YBCO deposition is approximately 200 mTorr with a flow rate of about 50 sccm. Use of a 2.45 GHz atomic oxygen source does not appear to substantially improve the YBCO film quality at the optimum oxygen pressure and substrate temperature. After YBCO deposition, the oxygen pressure is increased to about 400 Torr and the sample is cooled by turning off the heater. If the oxygen pressure is not increased but rather is kept at 200 mTorr during cool down, then poor-quality films are obtained. The substrate temperature is the most important parameter for *in-situ* deposition: ideally, high enough for film growth but not high enough for significant reaction of the YBCO with the substrate. This point is discussed further below for each of the substrate systems studied. The substrates are heated by a quartz lamp. The lamp housing temperature is measured and controlled by a nearby thermocouple and the substrate temperature is measured using an optical pyrometer.

For YBCO/Al_2O_3 good films are obtained only in a narrow substrate-temperature window of 650-670°C.[10,11] For substrate temperatures too high, reaction occurs and the resulting films are transparent and insulating. For substrate temperatures too low, poor epitaxy and film orientation occur, resulting in lowered critical current densities.

For deposition on silicon substrates,[8,12,13] three configurations were studied: (1) YBCO/SiO_2/Si, (2) YBCO/Si, and (3) YBCO/YSZ/Si. In case (1) the SiO_2 is a 150Å-thick, MOS-grade thermal oxide. The clean Si surfaces used for (2) and (3) are spin-etched free of oxide and hydrogen-terminated in a nitrogen-purged hood[14], then immediately introduced into the deposition chamber through a load lock. Their surfaces have been demonstrated to be atomically clean and devoid of oxide prior to the start of a deposition, conditions that are

usually necessary for successful epitaxial growth. For (1) and (2), depositions at several substrate temperatures in the vicinity of 700°C were performed.[8,12] For (3) a two-substrate-temperature deposition was used. First, the substrate temperature was increased to 550°C. This temperature was chosen to minimize the reaction between Si and YSZ during growth. At these temperatures the hydrogen was driven off, and then the YSZ deposited on a clean Si surface (the vacuum is 5×10^{-7} Torr). After depositing about 10–20 Å of YSZ, oxygen is introduced to a pressure of 50 mTorr and the remainder of the film (thickness about 500 Å) is deposited. Second, the substrate temperature was increased to 725°C, the oxygen pressure to 200 mTorr, and about 2000 Å of YBCO deposited. The run was completed by cooling the film in 400 Torr of oxygen.

3. EXPERIMENTAL RESULTS: YBCO on $SrTiO_3$, MgO, $LaAlO_3$, and YSZ

The general procedure in the investigation of film growth was to deposit films under different deposition conditions. The resulting films were characterized electrically by measuring the resistivity versus temperature (ρ versus T) in all cases. For some films the microwave surface resistance, R_s, and the critical current density, J_c, were measured at selected temperatures up to the superconducting transition temperature, T_c. The films were also characterized structurally using x-ray diffraction and, in some cases, transmission electron microscopy (TEM). The compositions of selected films were checked using electron microprobe analysis. In some cases, the deposited-film/substrate interface was investigated using photoelectron spectroscopy. The results of these measurements feed back to the deposition conditions to arrive at the best quality *in-situ* films with parameters as given in Section 2.

Depositions of YBCO on the standard oxide substrates, $SrTiO_3$, MgO, $LaAlO_3$, and YSZ, generally produced good quality films. Typically the superconducting transition temperature increased with substrate temperature, T_s, until significant reaction occurred. The optimal T_s for these substrates was about 700°C, as measured with an optical pyrometer. The resulting zero resistance temperature, T_{c0}, ranged from 87K to 91K. The superconducting transitions were sharp with 90%-to-10% transition widths ranging between 0.5K and 1K. The room temperature resistivities fell between 200 and 300 μΩ-cm and have resistivity ratios, $R=\rho(300K)/\rho(100K)$, between 2.8 and 3.0. The ρ versus T curve for 1000 Å of YBCO deposited on a $LaAlO_3$ substrate is shown in Fig. 1. It has $T_{c0}=91K$, a transition width $\leq 0.5K$, and $R=3$. This curve is typical of those for YBCO on these substrates[15] prepared with $T_s\approx 700°C$.

The surface impedance was measured using a parallel-plate resonator technique. In this method, two rectangular samples of superconductor are pressed together with a dielectric spacer in between. From the Q factor of this resonator in the 10 GHz frequency region, a surface impedance can be calculated. This method yields a value of 24 μΩ for Nb thin films at 11 GHz and 4.2K, consistent with values from cavity measurements[16]. For sputtered films of YBCO on MgO and $LaAlO_3$, values of R_s is as low as 50 μΩ at 11 GHz and 4.2K were obtained. Thus the surface impedance of good YBCO films is comparable to that of Nb.

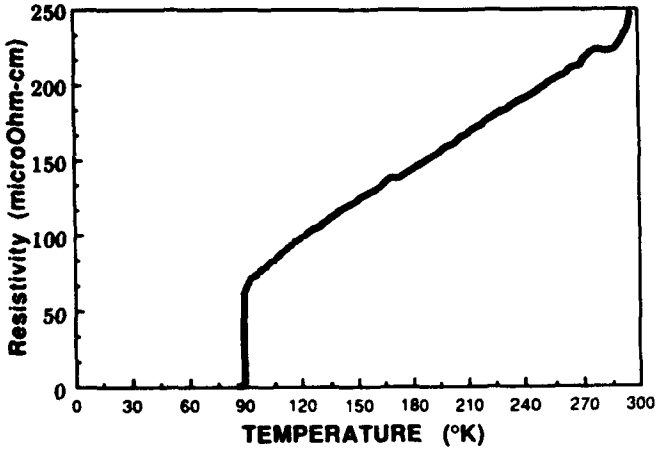

Fig. 1. Resistivity versus temperature for 1000 Å of YBCO deposited on $LaAlO_3$.

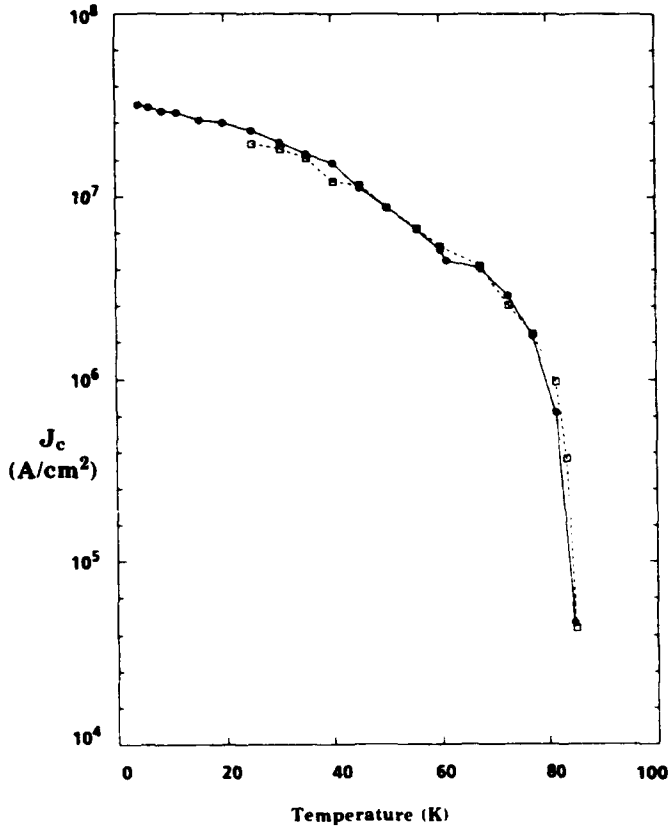

Fig. 2. Critical current density versus temperature for 1200 Å of YBCO on $SrTiO_3$ that had been patterned into lines of width 1.4 μm (solid circles) and 4.3 μm (open squares).

Transport critical current densities were determined in two ways: (1) by measuring the magnetization hysteresis loops and analyzing them in accordance with Bean's critical state model[17], and (2) by measuring the resistivity of films patterned into fine lines of widths ranging from 1 to 7 μm. The two techniques gave comparable values for J_c. For the second technique, the patterning was done by wet chemical etching using dilute nitric acid, and a voltage drop of 0.4 μV was used to define the critical current. An example of the results of this technique is shown in Fig. 2, which displays J_c versus temperature for 1200 Å of YBCO on $SrTiO_3$ that had been patterned into lines of width 1.4 and 4.3μm. The two different line widths yield the same J_c as does scanning either up or down in temperature. J_c is seen to be proportional to $(1-T/T_c)$ and to equal 3.2×10^7 A/cm^2 at 4.2K. Comparable values of J_c are obtained for YBCO films on the other substrates.

The structures of the films were investigated using x-ray diffraction. Diffractometer scans show preferential c-axis orientation for all the films, as shown in Fig. 3 for 1000 Å of YBCO on (100) YSZ. Only the (00n) YBCO diffraction lines are observed and their intensity is high, consistent with a high degree of c-axis orientation. That the c-axis tilt misalignment

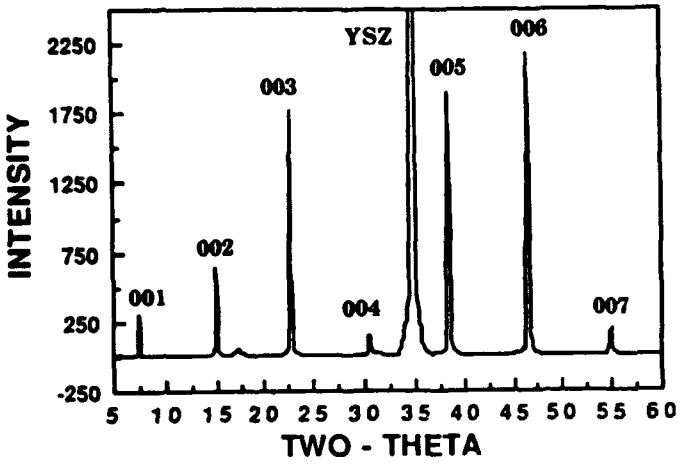

Fig. 3. X-ray diffraction scan for 1000 Å of YBCO on (100) YSZ.

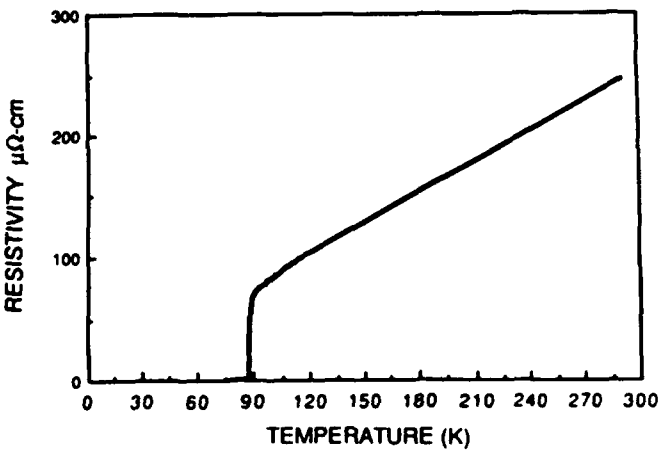

Fig. 4. Resistivity versus temperature for 2000 Å of YBCO deposited on Al_2O_3 for $T_s = 670^\circ C$.

of the grains is small is confirmed by the narrowness of the omega rocking curves. For the strong (005) YBCO peak, this width is only a few tenths of a degree.[18]

There is also substantial alignment in the a–b plane. A scan in phi of the (103) YBCO diffraction peak shows a high degree of in-plane orientation. Large peaks of equal intensity every 90° in phi indicate that the [100] and [010] directions are aligned with the <110> directions of YSZ. Since the lattice constant of YSZ is 5.2 Å and a = 3.823 Å and b = 3.886 Å for YBCO, the lattice mismatch is 4% and 6% for the two possible orientations. Thus, we observe heteroepitaxial growth of YBCO on YSZ, and also for YBCO on $SrTiO_3$. This high degree of orientation accounts, in large part, for the high critical current densities and low surface impedance obtained for these films.

4. EXPERIMENTAL RESULTS: YBCO on Al_2O_3

Due to the high reactivity of sapphire with YBCO, the substrate temperature is an even more critical parameter than for depositions on the substrates of Section 3, where the usual growth temperature is about 700°C. Above $T_s = 700^\circ C$, severe reaction between YBCO and Al_2O_3 occurs.[19,20] For YBCO/Al_2O_3 good films were obtained only in a narrow substrate–temperature window of 650C–670°C.[10,11] However, this lower temperature and the severe lattice mismatch between the sapphire r-plane, $(1\underline{1}02)$, and the YBCO a–b plane degraded the YBCO properties. This is illustrated in Fig. 4 which shows the resistivity versus temperature for a 2000Å–thick film deposited at $T_s = 670^\circ C$. Comparing Figs. 1 and 4 we see that the room temperature resistivity and R are comparable for sapphire and $LaAlO_3$ substrates. However, T_{c0} is lower (88 versus 91K) and the transition width is larger (1 versus 0.5K). The surface impedance at 13 GHz and 4.2K is 1 mΩ, 20 times larger than for the best reported values for YBCO/$LaAlO_3$. In addition the critical current density, as determined from the magnetization hysteresis loop, is only 5.4×10^6 A/cm^2 at 4.2K and 3kG, 6 times lower than that for YBCO/$SrTiO_3$ and YBCO/$LaAlO_3$. Nonetheless, these electrical

parameters for YBCO/Al_2O_3 are the best reported to date. They are somewhat poorer than films on our benchmark substrates, and the reasons can be found in the structural results.

The structures of the films were investigated using x-ray diffraction and cross-section TEM (XTEM). A four-circle diffractometer in the Bragg-Brentano geometry with Cu K_α radiation was used for the x-ray studies. Fig. 5 shows the diffraction scan for the YBCO/Al_2O_3 film of Fig. 4. As in Fig. 3 for YBCO/YSZ only the (00n) YBCO diffraction peaks are observed indicating that the film is oriented, with the c-axis nearly perpendicular to the substrate surface. For this film, however, the omega rocking curve of the (005) peak is large with a full width at half maximum of 2.5 degrees. This is to be compared with values of a few tenths of a degree obtained for YBCO films on $SrTiO_3$ or MgO. This indicates that, unlike YBCO films on the standard substrates, the c-axis tilt misalignment of the grains for YBCO/Al_2O_3 is substantial.

There is also substantial misalignment in the a-b plane. A scan in phi of the (103) YBCO diffraction peak, Fig. 6, shows in-plane orientation. Large peaks of equal intensity every 90° in phi indicate that the [100] and [010] directions of YBCO are aligned with the $<2\underline{2}01>$ directions in the r-plane of Al_2O_3. The peak widths and broad tails, however, show that there is a considerable distribution in this in-plane orientation. This misalignment in the a-b plane is due to the lattice mismatch as seen by considering the structure of the r-plane of sapphire, Fig. 7. The atomic spacing in the r-plane along the $<2\underline{2}01>$ directions is 3.48Å compared with a=3.823Å and b=3.886Å for YBCO. The lattice mismatch is about 10% and the [2$\underline{2}$01] and [02$\underline{2}$1] directions are not orthogonal, but about 2° off. The misalignment is evident also in the XTEM micrograph shown in Fig. 8. Epitaxial growth is seen since the YBCO planes are aligned with the sapphire planes. There is a tilt of about 4° of the c-axis of YBCO with respect to the sapphire [1$\underline{1}$02] direction. This sort of misalignment can account in part for the width of the omega rocking curve. So heteroepitaxial growth does

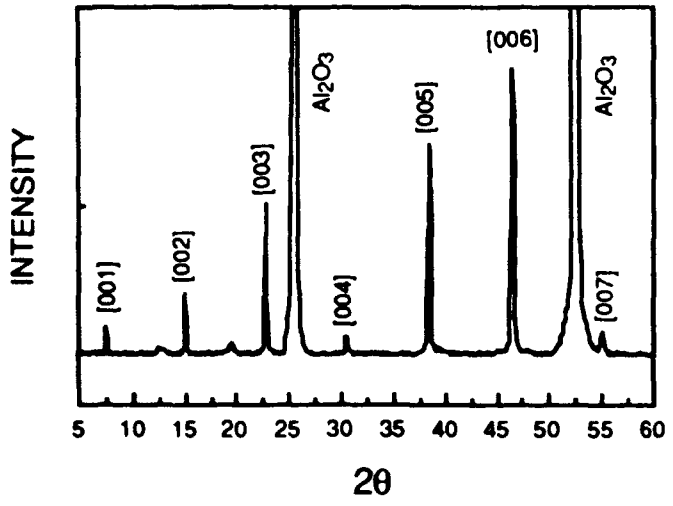

Fig. 5. Diffraction scan for a 2000Å-thick film of YBCO deposited on Al_2O_3 at T_s=670°C.

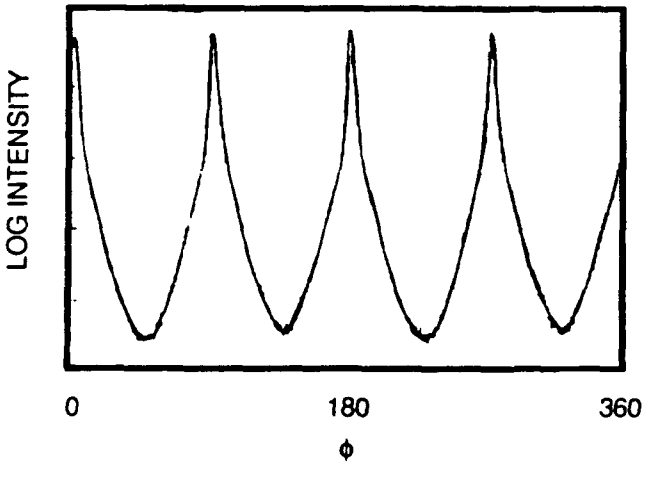

Fig. 6. A scan in phi of the (103) YBCO diffraction peak for a 2000Å-thick film of YBCO deposited on Al_2O_3 at T_s=670°C.

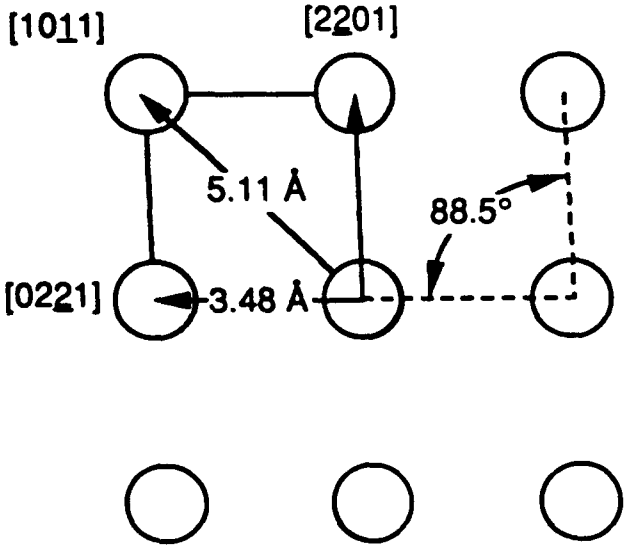

Fig.7. Sapphire r-plane surface perpendicular to <1$\bar{1}$02>.

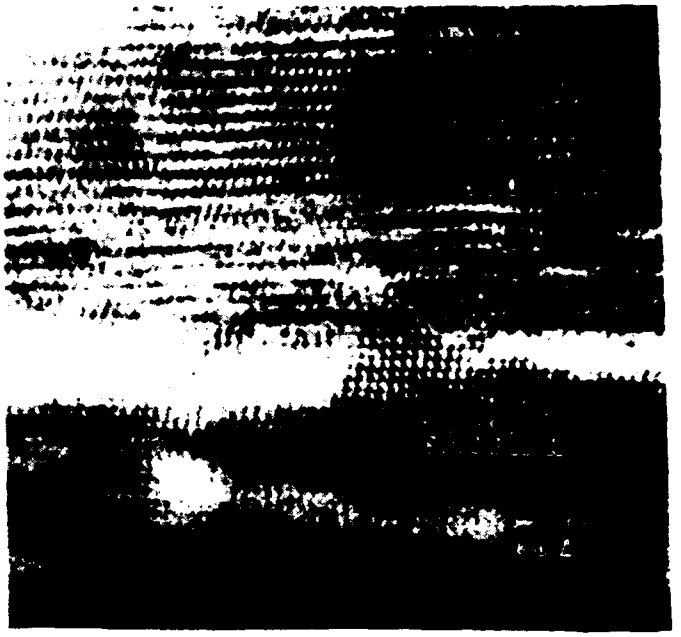

Fig.8. Cross sectional TEM micrograph of a 2000Å-thick film of YBCO deposited on Al_2O_3 at T_s=670°C.

occur for YBCO on Al_2O_3, but there is substantial misalignment. This misorientation accounts, in large part, for the reduced critical current densities and increased surface impedance obtained for these films.

5. EXPERIMENTAL RESULTS: YBCO on Si

YBCO is substantially more reactive with Si than with Al_2O_3. Even at temperatures as low as 550C, substantial reaction occurs. This is evident in Fig. 9 which displays the x-ray photoemission spectra (XPS)[8,12] of a thin layer (20 Å) of YBCO on 150Å-thick, MOS-grade SiO_2 on Si and on clean Si (hydrogen terminated). The bottom four curves in the figure are from films prepared at three different substrate temperatures. The top three curves are reference spectra from Y_2O_3 powder, bulk YBCO[21] and thick (1000 Å) YBCO on SiO_2 on Si. The binding energy region shown includes both the Y 3d and Si 2s core levels. Two aspects of these spectra are to be noted. First, there is a shift of the the Y 3d peak for the thin YBCO films, which is largest for the highest T_s. Second, a Si 2s peak is visible in all the thin (20 Å) film spectra and its intensity increases with T_s. This Si peak is visible not only in the normal emission but also in glancing emission (very surface sensitive), showing that the Si is present throughout the films. Clearly the Si is reacting with the YBCO even at the lowest T_s of 550C. A similar conclusion can be drawn from the Ba 3d XPS. The presence of this much Si renders the film insulating and charging in the XPS beam causes the Y 3d and Ba 3d lines to shift. These observations explain why YBCO films grown on Si or SiO_2 have poor electrical characteristics and only approach good DC electrical properties for very thick (~1 μm) films.[22]

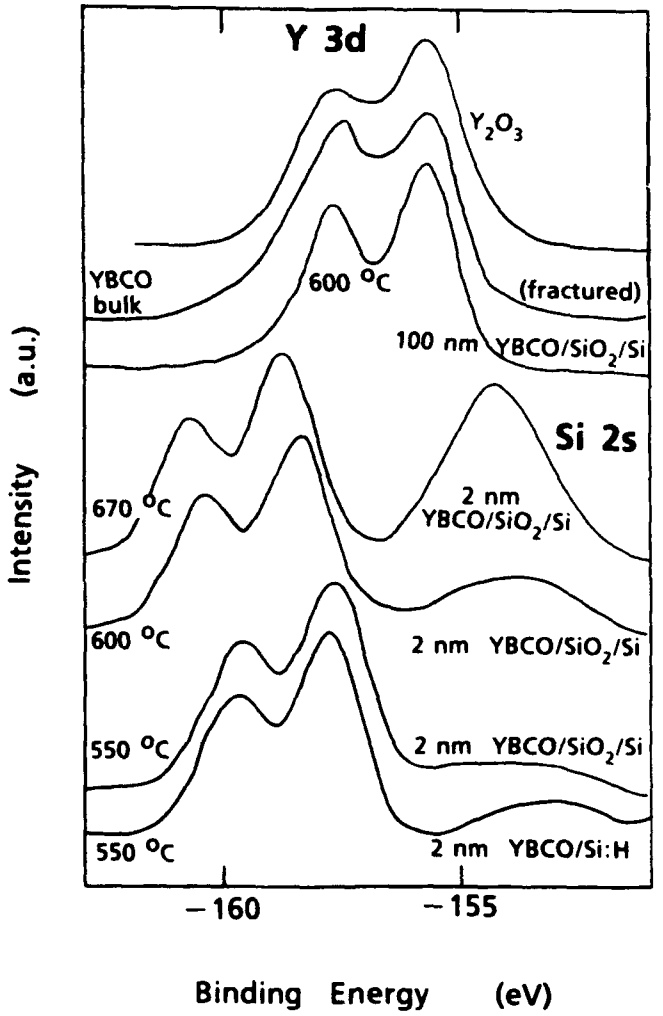

Fig.9. X-ray photoemission spectra of the Y 3d and Si 2s core level region for three reference compounds and four 20Å-thick YBCO films on Si.

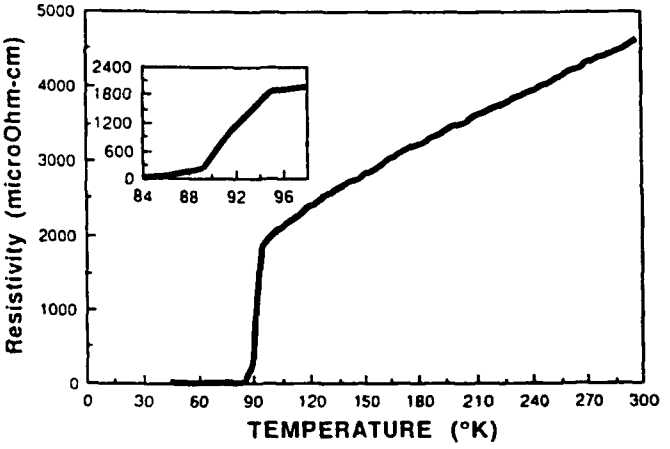

Fig.10. The resistivity of a multilayer of 2500Å-YBCO/200Å-YSZ/150Å-MOS-grade SiO_2/Si, prepared as described in the text.

From these results and others, it appears that high quality films on Si will only be possible with suitable buffer layers that provide chemical stability and also allow for sharp, epitaxial interfaces. A promising candidate, in this regard, is YSZ since it apparently satisfies both criteria. First, YSZ can provide the necessary chemical reaction barrier. In a similar XPS study[8,12] to that described above, 20 Å of YSZ or zirconia deposited on Si at $T_s = 670^{\circ}C$ showed essentially a fully buried, unreacted interface. This, plus the fact that excellent YBCO/YSZ films exist, indicate that YSZ probably has the necessary chemical inertness with both Si and YBCO, even though some reaction with YBCO has been noted.[23] Second, YSZ lattice matches both Si (100) and the a-b plane of YBCO, so the potential exists for sharp, epitaxial interfaces in YBCO/YSZ/Si systems.[24]

The resistivity of a YBCO film on Si with an intervening YSZ buffer layer is shown in Fig. 10. The Si substrate was thermally oxidized Si (100). The YSZ was deposited at 580°C,

as described in Section 2. This particular 200Å–thick buffer did not have the ideal Y_2O_3 content of 9% but rather 4–5%. The 2500Å YBCO film was deposited at 725°C. These results are reasonably good, with $T_{c0} = 86K$ and metallic conductivity in the normal state. Nonetheless, the conductivity results are poorer than for the benchmark films: T_{c0} is 5K lower and ρ(300K) 20 times larger. Also the x–ray diffraction pattern shows c–axis orientation but the peaks have large omega–rocking–curve widths, indicating a substantial distribution in the c–axis alignment.

In an attempt to achieve better epitaxy, comparison was made between multilayer films grown on hydrogen–terminated Si with those grown on thermally oxidized Si surfaces. No improvements in the transport properties were noted initially. However, better quality films appear to be possible with hydrogen–terminated Si as seen in the XTEM images of Figs. 11 and 12. Inspection of Fig. 11 reveals a rough interface between the YSZ buffer and the substrate for the multilayers grown on the oxidized Si. The YSZ is epitaxial and oriented to the Si lattice, but small–grain polycrystalline. For the clean Si surface (Fig. 12), however, the two interfaces are atomically abrupt and smooth. Also the the YSZ is polycrystalline with a bias toward a discrete set of possible orientations with the Si planes. Here an SiO_2 layer has regrown at the interface of the YSZ and Si because of the high temperatures and high oxygen–ion mobility through the YSZ. Nonetheless, the sharp interface and epitaxy for this case indicates that the clean, hydrogen–terminated Si surface should provide a better surface for buffer layer and YBCO growth.

To further improve the YBCO/YSZ/Si interface, films were grown on hydrogen–terminated Si and the composition of the $(ZrO_2)_{1-x}(Y_2O_3)_x$ varied in the polygun process, as described in Section 2. The film quality is best at $x \approx 0.1$. The film's surface morphology, interface, crystal structure and conductivity deteriorate dramatically as x goes to 0 where the resulting $(ZrO_2)_{1-x}(Y_2O_3)_x$ is no longer cubic. This suggests that the cubic phase is forming near $x = 0.1$, lattice matching to Si and providing for epitaxial YBCO growth. The XTEM results of Figs. 13 support this conjecture. The YSZ/Si interface is smooth and sharp.

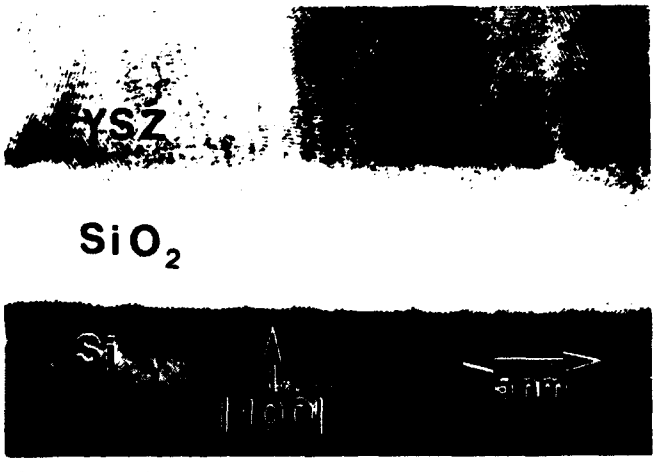

Fig.11. XTEM lattice image of YSZ on Si (100), which has an 150Å–MOS–grade SiO_2 on the surface.

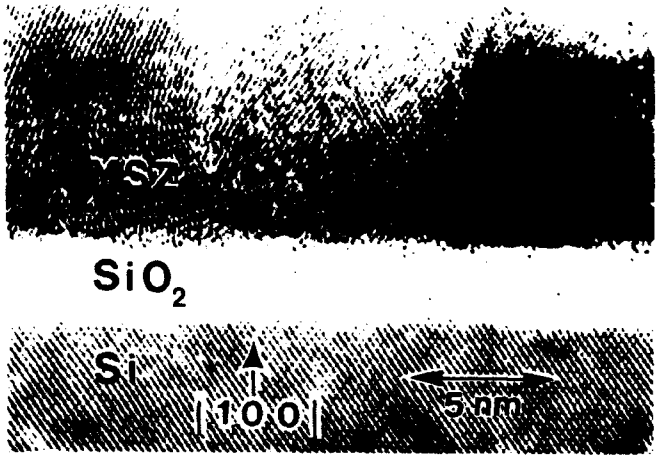

Fig.12. XTEM lattice image of YSZ on Si (100), which has been stripped of oxide using a spin–etch process.

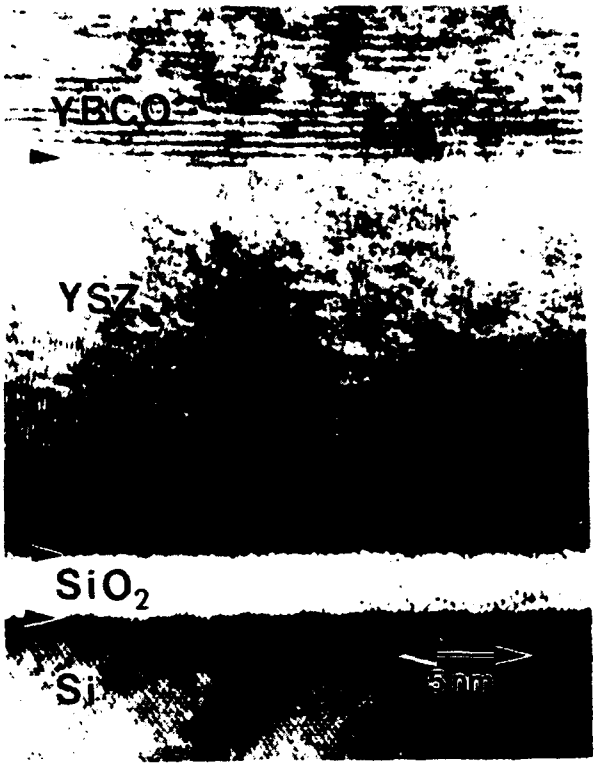

Fig.13. XTEM lattice image of the interface regions of YBCO/YSZ/Si for x = 0.1.

The YSZ film shows a polycrystalline structure with grains of both the cubic and tetragonal phases of about 100 Å in diameter. The YBCO is oriented with the c-axis normal to the substrate. Also an x-ray diffraction scan in phi about the (103) YBCO diffraction peak indicates orientation of the YBCO a- and b-axes with Si <110>. The peaks are broad, however, showing that the there is still substantial misorientation. Also the ρ versus T is similar to that of Fig. 10. Further improvements in epitaxial growth on Si are required to achieve transport properties comparable to those of our benchmark materials.

6. ACKNOWLEDGMENTS

The work is partially supported by AFOSR F49620-89-C-0017. DBF and AMV received support from NSF DMR-8822313. DKF acknowledges the support provided by an AT&T scholarship.

7. REFERENCES

1. D. Dijkkamp, T. Venkatesan, X. D. Wu, S. A. Shaheen, N. Jisrawi, Y. H. Min-Lee, W. L. McLean, and M. Croft, Appl. Phys. Lett. **51**, 619 (1987); T. Venkatesan, X. D. Wu, A. Inam, and J. B. Wachtman, Appl. Phys. Lett. **52**, 1193 (1988).
2. T. Venkatesan, Solid State Technology **30**, 39 (1987).
3. J. Narayan, N. Biunno, R. Singh, O. W. Holland, and O. Auciello, Appl. Phys. Lett. **51**, 1845 (1987).

4. S. Witanachchi, H. S. Kwok, X. W. Wang, and T. D. Shaw, Appl. Phys. Lett. **53**, 327 (1988).
5. D. K. Fork, J. B. Boyce, F. A. Ponce, R. I. Johnson, G. B. Anderson, G. A. N. Connell, C. B. Eom, and T. H. Geballe, Appl. Phys. Lett. **53**, 337 (1988); D. K. Fork, T. H. Geballe, J. B. Boyce, F. A. Ponce, and R. I. Johnson, IEEE Trans. Mag. **25**, 2426 (1989).
6. D. K. Fork, K. Char, F. Bridges, S. Tahara, B. Lairson, J. B. Boyce, G. A. N. Connell, and T. H. Geballe, Int. Conf. Materials and Mechanisms of Superconductivity, Stanford, July 1989, in Physica C, edited by N. E. Phillips, R. N. Shelton, and W. A. Harrison, in press.
7. T. Venkatesan, E. W. Chase, X. D. Wu, A. Inam, C. C. Chang, and F. K. Shokoohi, Appl. Phys. Lett. **53**, 243 (1988); and references therein.
8. D. B. Fenner, D. K. Fork, J. B. Boyce, G. A. N. Connell, and A. M. Viano, Int. Conf. Materials and Mechanisms of Superconductivity, Stanford, July 1989, in Physica C, edited by N. E. Phillips, R. N. Shelton, and W. A. Harrison, in press.
9. F. Bridges, D. K. Fork, J. B. Boyce, K. Char, G. A. N. Connell, D. B. Fenner, T. H. Geballe, and R. C. Taber, unpublished.
10. K. Char, D. K. Fork, T. H. Geballe, S. S. Laderman, R. C. Taber, R. D. Jacowitz, F. Bridges, G. A. N. Connell, and J. B. Boyce, unpublished.
11. D. K. Fork, T. H. Geballe, K. Char, S. S. Laderman, R. C. Taber, F. Bridges, F. Bridges, J. B. Boyce, and G. A. N. Connell, Materials Research Society Symposium Proceedings on *High-Temperature Superconductors: Fundamental Properties and Novel Materials Processing*, Nov. 1989, to be published
12. D. B. Fenner, A. M. Viano, G. A. N. Connell, J. B. Boyce, D. K. Fork, F. A. Ponce, and J. Tramontana, Materials Research Society Symposium Proceedings on *High-Temperature Superconductors: Fundamental Properties and Novel Materials Processing*, Nov. 1989, to be published; D. B. Fenner, A. M. Viano, J. B. Boyce, G. A. N. Connell, F. A. Ponce, and J. Tramontana, unpublished.
13. G. A. N. Connell, D. B. Fenner, D. K. Fork, J. B. Boyce, F. A. Ponce, F. Bridges and T. H. Geballe, Materials Research Society Symposium Proceedings on *High-Temperature Superconductors: Fundamental Properties and Novel Materials Processing*, Nov. 1989, to be published.
14. D. B. Fenner, D. K. Biegelsen, and R. D. Bringans, J. Appl. Phys. **66**, 419 (1989).
15. S. J. Hagen, T. W. Jing, Z. Z. Wang, J. Hovarth, and N. P. Ong, Phys. Rev. B **37**, 2928 (1988).
16. J. P. Turneaure and I. Weisman, J. Appl. Phys. **39**, 4417 (1968).
17. C. P. Bean, Phys. Rev. Lett. **8**, 250 (1962).
18. S. S. Laderman, K. Char, M. Lee, M. R. Hahn, R. H. Hammond, M. R. Beasley, T. H. Geballe, A. Kapitulnik, and R. Barton, Phys. Rev. B **39**, 11648 (1989).
19. X. D. Wu, A. Inman, M. S. Hedges, B. Wilkens, C. C. Chang, D. M. Hwang, L. Nazar, T. Venkatesan, S. Miura, S. Matsubara, Y. Miyasaka, and N. Shohata, Appl. Phys. Lett. **54**, 754 (1989).
20. S. Witanachchi, S. Patel, D. T. Shaw, and H. S. Kwok, Appl. Phys. Lett. **55**, 295 (1989).
21. Z. Shen, J. W. Allen, J. J. Yeh, J. -S. Kang, W. Ellis, W. Spicer, I. Lindau, M. B. Maple, Y. D. Dalichaouch, M. S. Torikachvili, J. Z. Sun, and T. H. Geballe, Phys. Rev. **36**, 8414 (1987).
22. P. Berberich, J. Tate, W. Dietsche, and H. Kinder, Appl. Phys. Lett. **53**, 925 (1988).
23. L. A. Tietz, C. B. Carter, D. K. Lathrop, S. E. Russek, R. A. Buhrman, and J. R. Michael, J. Mater. Res. **4**, 1072 (1989).
24. H. Fukumoto, T. Imura, and Y. Osaka, Jpn. J. Appl. Phys. **27**, L1404 (1988).

Fe SUBSTITUTED, LASER ABLATED $YBa_2Cu_3O_7$ FILMS USING OFF-STOICHIOMETRIC TARGETS

Frank Bridges[1,2], J. Truher[1], D. K. Fork[2,3], J. B. Boyce[2], D. B. Fenner[2,4], G. A. N. Connell[2], T. H. Geballe[3], S. Johnson[5], and L. Liu[5].

1. Physics Department, University of California, Santa Cruz, CA 95064.
2. Xerox Palo Alto Research Center, Palo Alto, CA 94304.
3. Stanford University, Stanford, CA 94305.
4. Physics Department, Santa Clara University, CA 95053.
5. Stanford Research Institute, Stanford CA 94305.

ABSTRACT

We present data on thin films of $YBa_2Cu_3O_7$ (YBCO) and $YBa_2(Cu_{1-x}Fe_x)_3O_7$ prepared by laser ablation using a sequence of targets, including Cu-deficient $YBa_2Cu_{2.4}O_7$, CuO, and $(CuO)_{1-y}(FeO)_y$. This technique achieves mixing on an atomic scale. We find that stochiometric films, made using a combination of the Cu-deficient target and CuO, have a sharp transition (width < 1K) near 90K although the Cu-deficient material alone has a broad transition at a lower T_c. We have achieved substitution of Fe on the Cu sites, using a sequence of the three targets for a range of Fe concentrations. T_c decreases nearly linearly with concentration and $T_c \rightarrow 0$ near 15% Fe. The T_c suppression for the films is slightly less than the corresponding value obtained for bulk samples.

INTRODUCTION

Many experimental investigations have been directed towards a better understanding of the role that the Cu(2)-O planes and the Cu(1)-O chains play in the high T_c material $YBa_2Cu_3O_7$ (YBCO). One approach to probe these layered materials is to substitute[1-4] other atoms such as Co, Fe, Ni, and Zn for some of the Cu. In all cases of Cu substitution in YBCO, using both magnetic and non-magnetic atoms, T_c is significantly decreased at relatively low concentrations ~5%. For several dopants, T_c decreases linearly with concentration, with the largest suppression[3] occurring for Zn. For Fe substituted bulk samples[1], $T_c \rightarrow 0$ at 14–15%. Several investigations indicate that the Fe replaces Cu(1) in the chain sites at low concentrations (<10%) but that some Fe(2) exists at higher concentrations[1,4,5]. In general, bulk sample studies show some variation in the amount of T_c suppression with concentration, likely the result of different sample preparation procedures. However, small amounts of other phases (for example, considerable NiO is present in some Ni substituted samples[6,7], and ZnO in Zn substituted samples) or concentration gradients can vary the observed T_c suppression significantly.

To extend such investigations, we have prepared thin films of Fe substituted YBCO using the laser ablation technique[8-10], by successively ablating from a series of targets. In principle this method should achieve *mixing on an atomic scale* as each laser pulse ablates less than 0.5Å. Consequently, the problems of impurity phases or concentration gradients should be minimized unless there is a tendency for

precipitates to form. In this paper we present our results on stochiometric and Fe substituted YBCO films made using a sequence of targets.

DEPOSITION TECHNIQUE

The laser deposition system uses a computer controlled rotating target holder (POLYGUN) enclosed in a water-cooled shroud. The holder, containing 10 targets, rotates at speeds up to 10 Hz and the laser is fired each time a desired target is correctly oriented. The XeCl excimer laser pulse has a wavelength of 308 nm, a pulse width of 17 μsec, and an energy density on the target of 1-2 J/cm^2. Deposition is carried out under 200 mTorr O_2 pressure, with substrate temperatures in the range 650-700°C. As soon as the deposition is completed, the O_2 pressure is increased to 200 Torr and the sample cooled to 200 C in 20 minutes. For YBCO the deposition rate for a substrate-target distance of 5.5 cm, is about 0.35 Å/pulse, while for CuO and CuO-FeO mixtures, the rate is roughly 0.1 Å/pulse. The targets were made of pressed fine powders of Cu-deficient YBCO ($YBa_2Cu_{2.4}O_7$), CuO, and two mixtures of CuO and FeO — $(CuO)_{1-x}(FeO)_x$, with $x=0.33$ and 0.67. The Cu-deficient YBCO target was made using the freeze dried technique. Substrates were polished MgO or $LaAlO_3$ crystals, 6mm x 6mm in size. They were attached to the heater using Ag paste to achieve good thermal contact; the surface temperature was measured using an optical pyrometer. Deposition temperatures were from 680 to 740 C.

YBCO FILMS FROM $YBa_2Cu_{2.4}O_7$ AND CuO

The first step in this investigation was to verify that high quality YBCO films could be prepared from two targets, the Cu depleted target and CuO. In Fig. 1 we

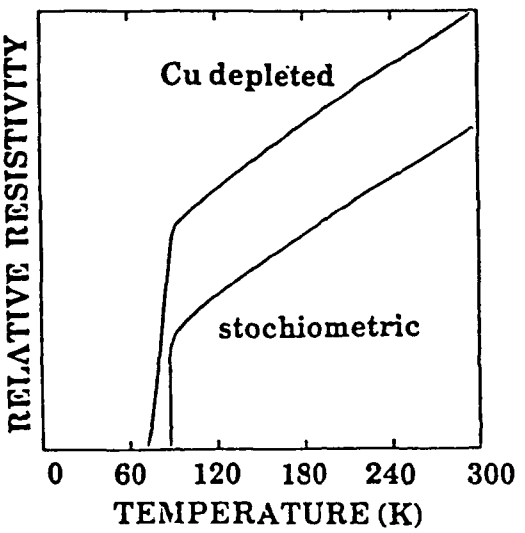

Fig. 1. The relative resistivity versus temperature for the Cu-depleted film and a stochiometric film deposited as described in the text.

compare the resistivity of two ablated films as a function of temperature; a film made from the Cu-deficient target alone and a stochiometric sample made by ablating $YBa_2Cu_{2.4}O_7$ and CuO together such that the Cu content was increased to 3. The relative number of pulses on each target, required to achieve stoichiometry.

was determined approximately by first measuring the thickness of YBCO and CuO films after 10000 pulses. The deposition rate for CuO and CuO/FeO mixtures is about 18-20% that for YBCO. Fine tuning was achieved by checking thick (7000Å) composite films using the microprobe technique. Most of our good samples were slightly (0.5 to 3 %) Cu-rich, and were made using three pulses of $YBa_2Cu_{2.4}O_7$ to one pulse of CuO. The Cu-deficient film has a broad transition with δT_c (10-90%) ≈ 14 K and a midpoint transition temperature T_c = 80 K (ρ=0 at 69 K). This broad transition with a slightly suppressed T_c is typical of a number of Cu-poor samples we have made. In contrast, the composite film made using the two targets, has a transition midpoint of 87.3 K, a 10-90% transition width of 0.5 K and the resistivity goes to zero at T = 87 K. This is only slightly worse than our best films on $LaAlO_3$ made using a single optimized YBCO target. Several of the Cu-deficient and stochiometric composite films were made to check on consistency. The values for T_c and δT_c are very similar to the results presented here.

Fe SUBSTITUTED YBCO FILMS

Fe substituted films of various concentrations were prepared by sequential ablation of three different targets, with part of the CuO required for stoichiometry (as determined above) replaced by a mixture of CuO and FeO. For Fe concentrations up to 7% a $(CuO)_{0.67}(FeO)_{0.33}$ mixture was used; different Fe concentrations were obtained by changing the relative number of pulses on the pure CuO and mixed targets. For concentrations between 7 and 15 %, two mixed CuO-FeO targets, with 33% and 67% FeO, were used. Most films were 1000 Å thick, but two films, 7000Å thick, were made for concentration determinations using microprobe.

We show the x-ray diffraction for a 3.7% Fe substituted film in Fig. 2. Note the

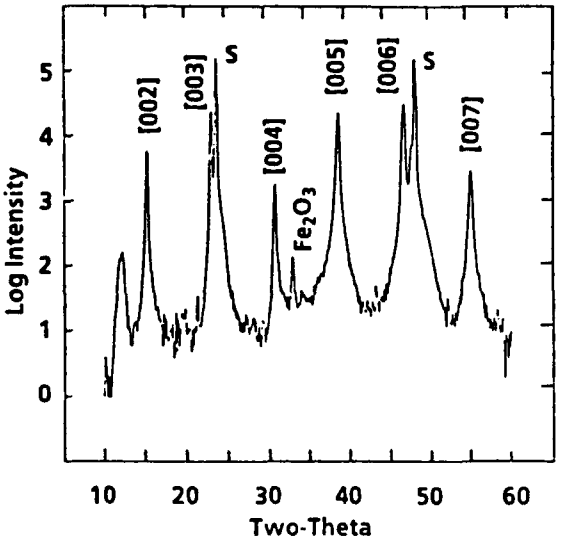

Fig. 2. X-ray difraction of the 3.7% Fe substituted film prepared using the Cu-deficient and CuO/FeO targets. The peaks marked S are $LaAlO_3$ substrate peaks. The small peak at 33° is at the position of the strongest peak in Fe_2O_3 and indicates a small amount of this impurity. The peak near 12° has not been identified.

logarithmic intensity scale. Only the [00n] peaks of YBCO are observed, indicating that the c-axis is perpendicular to the substrate surface and that very little of the film is orientated with the a- or b-axes perpendicular to the surface. These results

show that high quality substituted films can be made by ablating several targets sequentially. In Fig. 3 the resistivity as a function of temperature is shown for films

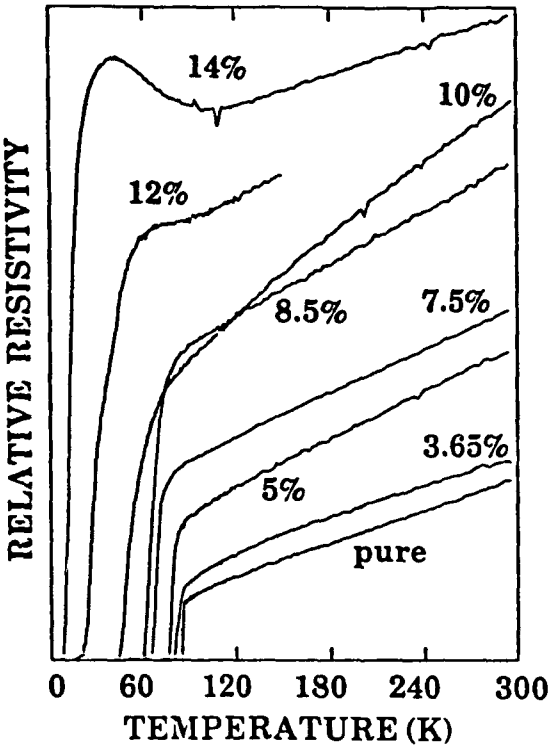

Fig. 3. .The resistivity as a function of temperature for the Fe substituted samples on $LaAlO_3$ substrates. The Fe concentration is relative to Cu.

of different Fe concentrations. Note that all the transitions are quite sharp. A relative resistivity scale is used to separate the different curves; however it correctly reflects the general trends with increasing concentration. The slope of the resistivity curve above T_c gradually decreases with increasing concentration while the magnitude of the resistivity increases with increasing Fe concentration. For the highest concentration sample, the resistivity curve has some semiconductor-like character. Thus Fe substitution likely decreases the number of carriers as well as decreasing T_c. Consequently the suppression of T_c is a combination of mechanisms -- a lowered carrier concentration, lattice distortions[4] and possibly some magnetic interactions. In Fig 4 we plot T_c as a function of concentration, (filled squares) with T_c for this plot defined as the midpoint in the resistivity curve. For comparison, the corresponding values, obtained for bulk samples, are shown as X's. T_c decreases linearly with concentration but the suppression of T_c for the laser ablated films is slightly smaller than for bulk samples. The scatter in T_c as a function of concentration for the laser ablated films is less than ± 5K. Because the laser ablated films are mixed on a unit cell level, the distribution of Fe should be uniform throughout the sample. It is therefore tempting to speculate that the difference between the present results and the bulk results is in part due to concentration gradient effects in the bulk samples. If the Fe substituted bulk material has a slightly higher concentration at the surface of the powder grains (uniform diffusion

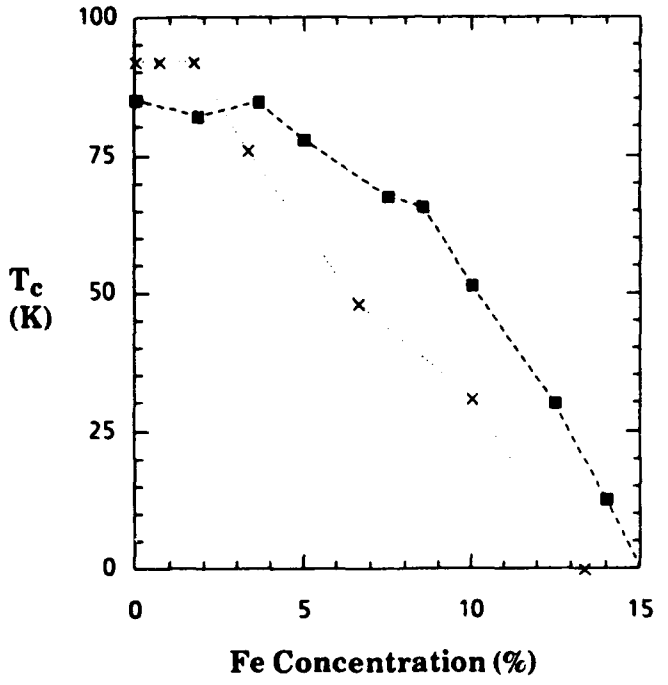

Fig. 4. The midpoint transition temperature T_c as a function of the Fe concentration. The crosses are the data on bulk samples from Tarascon, et al[1].

has not occurred), the measured T_c could be lower than the value for a uniform distribution.

In Fig.5 the 10-90% width of the resistive transition is plotted as a function of the Fe concentration. The width is approximately proportional to the concentration and becomes broad at high concentrations -- 25K -- near 12%. The increasing width may indicate an inhomogeneous distribution of Fe in the films; if so this would suggest that Fe has a tendency to clump as atomic scale mixing is expected with laser ablation. The rather narrow width for 14% Fe is surprising and unexplained at this point.

SUMMARY

We have made high quality YBCO films from off-stoichiometric YBCO using two targets; a Cu-deficient YBCO material and CuO. When the correct amount of CuO is added during deposition by ablating the two targets in a particular ratio, T_c for the film is high and δT_c is small. In general we find that Cu-poor films have broad transitions while slightly Cu-rich films have a sharp transition. Fe substituted films have been made using a sequence of laser ablations of three targets. The resistive transitions remain reasonably sharp but broaden linearly with concentration. T_c in the films is not suppressed by Fe substitution quite as rapidly as found in bulk material.

ACKNOWLEDGEMENT. The work is partially supported by AFOSR (FB, THG), AT&T (DKF), and NSF (DBF).

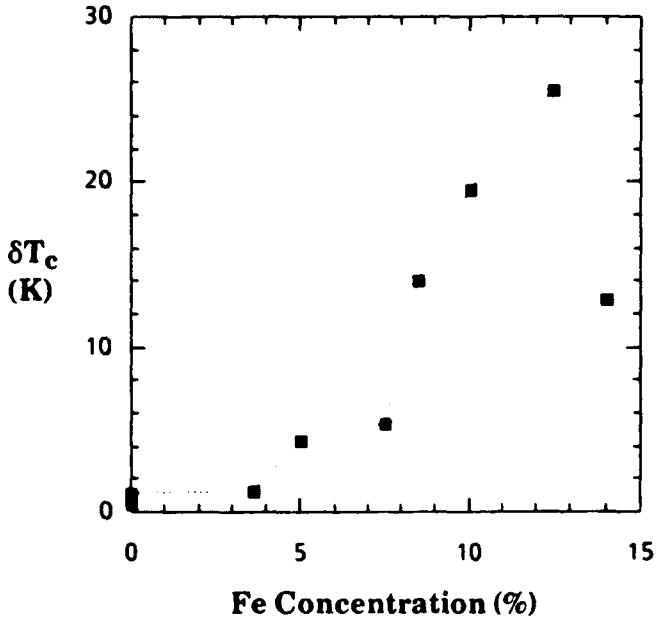

Fig. 5. The 10%-90% width of the resistive transition as a function of the Fe concentration.

REFERENCES

1. J. M. Tarascon, P. Barboux, P. F. Miceli, L. H. Greene, G. W. Hull, M. Eibschutz and S. A. Sunshine, Phys. Rev. **37**, 7458 (1988).
2. Y. Maeno, M. Kato, Y. Aoki and T. Fujita, Jpn. J. Appl. Phys. **26**, L1982 (1987).
3. B. Jayaram, S. K. Agarwal, C. V. Rao, and A. V. Narlikar, Phys. Rev. B **38**, 2903, (1988).
4. F. Bridges, J. B. Boyce, T. Claeson, T. H. Geballe and J. M. Tarascon, Phys. Rev. B **39**, 11603 (1989).
5. R. S. Howland, T. H. Geballe, S. S. Laderman, A. Fischer-Colbrie, M. Scott, J. M. Tarascon and P. Barboux, Phys. Rev. B **39**, 9017 (1989).
6. F. Bridges, J. B. Boyce, T. Claeson, T. H. Geballe *and* J. M. Tarascon, submitted to Phys. Rev. (1990).
7. M. Qian, E. A. Stern, Y. Ma, R. Ingalls, M. Sarikaya, B. Thiel, R. Kurosky, C. Han, L. Hutter, and I. Aksay, Phys. Rev. B **39**, 9192 (1989).
8. T. Venkatesan, E.W. Chase, X.D. Wu, A. Inam, C.C. Chang, and F. K. Shokoohi, Appl. Phys. Lett. 53, 243 (1988); and references therein.
9. D. K. Fork, K. Char, F. Bridges, S. Tahara, B. Lairson, J. B. Boyce, G. A. N. Connell, and T. H. Geballe, *Int. Conf. Materials and Mechanisms of* Superconductivity, Stanford, July 1989, in Physica C, edited by N. E. Phillips, R. N. Shelton, and W. A. Harrison, in press.
10. J. B. Boyce, G. A. N. Connell, D. K. Fork, D. B. Fenner, K. Char, F. A. Ponce, F. Bridges, J. Tramontana, A. M. Viano, S. S. Laderman, R. C. Taber, S. Tahara and T. H. Geballe, SPIE, **1187**, 136 (1989).

APL 4/92

Effect of Thermal History on the Transport Properties and the Location of Fe in $YBa_2Cu_3O_7$ Thin Films

Frank Bridges

UCSC, Santa Cruz, CA 95064 and

Xerox Palo Alto Research Center, Palo Alto, CA 94304

J. B. Boyce and R. I. Johnson

Xerox Palo Alto Research Center, Palo Alto, CA 94304

ABSTRACT

Epitaxial Fe–substituted $YBa_2Cu_3O_7$ films on $LaAlO_3$ substrates prepared by pulsed laser deposition exhibit a large variation in T_c with changes in the cool–down rate of the films in an O_2 environment immediately after deposition. A rapid cool–down rate (200°C/min) yields surprisingly high–T_c films with $T_c > 75K$ for 13% of the Cu replaced by Fe, while a slow cool–down of 10°C/min results in low–T_c films with $T_c \rightarrow 0$ at 11% Fe, a greater suppression than reported for bulk materials. In addition, post–deposition anneals in O_2 affect T_c significantly, even for anneal temperatures as low as 370°C. These results are interpreted in terms of isolated and clustered Fe atoms substituted on the Cu chains sites.

Substitution of Fe, Co, Ni, Zn, and Ga on the copper sites[1-3] in the high temperature superconductor $YBa_2Cu_3O_7$ (YBCO) has served as an important probe of the Cu–O layers, both the chains and planes. Some recent investigations[4-6] have suggested that Fe and Co dopants, which normally reside on the Cu(1) chain site, can be moved to the Cu(2) plane site by a series of vacuum and oxygen anneals. These annealing procedures lead to an orthorhombic structure and, in some cases, to a higher T_c (less T_c suppression). There is, however, considerable disagreement[4-9] as to whether a significant amount of Fe or Co is transferred to the Cu(2) site by this thermal treatment. In addition, recent investigations have considered dopants, such as, Fe, to be potential flux pinning centers, and measurements of the critical current density, J_c, is found to be higher in Fe–doped YBCO than in the pure material at low temperature and moderate magnetic fields.[10] The superconducting transition temperature, T_c, on the other hand, is lowered by the substitutions. For Fe dopants, $T_c \rightarrow 0$ at 15 atomic % Fe in bulk materials[1], while the T_c's for thin films are generally higher[11,12] and can be increased even further by annealing. There is now a wide range in T_c suppression reported, with no obvious explanation available.

We have made an investigation of thin films of Fe–substituted YBCO on $LaAlO_3$ substrates produced by pulsed laser deposition. The T_c suppression is less than that for bulk samples and can be lessened even further with a faster cool–down rate. A wide range in T_c can be obtained for a given Fe concentration by varying two primary parameters: (1) the substrate temperature and (2) the cool–down rate, either in the deposition chamber or in a post–deposition anneal. The cool–down rate has a very large effect for the Fe–substituted films but no effect on pure YBCO films.

The samples were prepared by pulsed laser deposition[13] using a XeCl excimer laser (308 nm) with an energy density at the target of about 3 J/cm^2. The $LaAlO_3$ substrates were attached to a thin wafer of Si or to an inconel holder using silver

epoxy and radiatively back heated with a quartz lamp.The surface temperature of the substrate was monitored using a pyrometer. Depositions were made with 200 mT of O_2 present. The films were cooled in 400 T of O_2 at rates from over 200°C/min (fast–cooled) to 10°C/min (slow–cooled). The Fe substitution in the films was achieved by using substituted targets or by using a combination of targets with an appropriate sequence of laser pulses on the different targets, set to achieve the desired concentration. The Fe concentrations ranged from 1 to 17%.

Fig. 1 shows a resistivity, ρ, versus T plot for the fast–cooled films deposited at a substrate temperature, T_s, of 750°C for several Fe concentrations. In this manner, the superconducting transition temperatures were obtained as a function of the substrate temperature, T_s, Fe concentration, x, and cool–down rate in the chamber after deposition.The variation in T_c with cool–down rate is surprisingly large. For example, with 9% Fe, T_c can range from 18 to 80 K. However, for a fixed set of parameters, T_c is both consistent and reproducible. We now describe the effects of (1) substrate temperature, and (2) cool–down rate (and Fe concentration) on T_c.

The results for T_c as a function of T_s for a series of fast–cooled, YBCO samples containing 9% Fe is shown in Fig. 2. A plateau region with a high T_c clearly exists above T_s = 750°C, with a rapid fall off in T_c in the range 675–725°C. In contrast, T_c for pure YBCO, drops off only slightly at the lower temperatures and is > 65 K for this substrate temperature range.

Fig. 3 displays the concentration dependence of T_c for samples fast cooled from T_s of 700 and 750°C; the latter corresponds to the data of Fig. 1. A small T_c–suppression at low concentration, x, and a flattening out of the curve above 10% Fe is observed. We attribute the independence of T_c on x to the formation of small precipitates of other phases at high concentrations (x > 10%). The presence of those

other phases appears to have little effect on the superconductivity of the film; it is the concentration of Fe in the film plus local atomic arrangements that determine the T_c suppression.

The most striking dependence of T_c on deposition parameter is with the cool–down rate after deposition. Fig. 4 shows T_c as a function of Fe concentration for a slow cool–down rate in the deposition chamber of 10°C/min, starting at T_s = 700°C. For these films, $T_c \rightarrow 0$ near 11% Fe, in contrast to the fast cool–down films where T_c is 60K at 9% Fe (see Fig. 3). This is the most dramatic variation of T_c we have observed for *in situ* deposition. Similar results are obtained for samples cooled slowly from 700°C in a furnace after deposition.

These results indicate that high T_c's can be obtained in Fe–doped films using high substrate temperatures and very fast cool–down rates. This may be very important for increasing flux pinning and possibly for increasing J_c in thin films.

How can one understand such a large variation in T_c suppression and the wide range of results reported in the literature? We propose the following model. The rapidly–cooled samples should have the Fe atoms widely dispersed throughout the film. Since such films have high T_c's, it is unlikely that a large fraction of the Fe atoms are in the conducting Cu(2)–O planes. Zn and Ni, which do occupy the Cu(2) sites[1,2,3,14,15], both suppress T_c strongly. This hypothesis is consistent with the recent measurements that show that Fe diffuses well in the a–b plane but not along the c–axis[16]. If the Cu(2) site were significantly occupied, then diffusion along the c–axis should be larger, as observed for Zn and Ni substituted samples. Thus, the rapidly–cooled samples have well–dispersed, isolated Fe atoms on the Cu(1) sites; the *isolated* Fe(1) atom has little influence on the carrier concentration in the Cu(2)

conducting layers or on the crystal structure, the crystal remains orthorhombic, and T_c remains high.

For slowly cooled samples, clustering occurs, perhaps because of a tendency to form short Fe–O bonds. These clusters likely induce new grain or twin boundaries, but do not result in precipitates of another phase. For example, if the clusters form as chains along the <110> directions[17], they could lead to microtwinning and an average tetragonal crystal structure, as observed in diffraction measurements.The resultant distortions in the lattice, induced by the clusters, are now of much longer range and extend into the Cu(2) layers. We suggest that it is this distortion of the lattice that destroys superconductivity, possibly by partial localization of carriers.

The vacuum/oxygen annealing experiments[4–6] that lead to an orthorhombic crystal structure might be explained within such a model as follows. In a vacuum anneal at 600–700°C, some of the O in the Cu(1) layer is removed and the Fe atoms become partially dispersed because there is not enough O present to promote the clustering. This requires that the Fe atoms are reasonably mobile above 600°C. In a lower temperature anneal in oxygen (typically about 400°C), the O atoms move easily throughout the crystal but the Fe atoms probably do not. This would lead to a orthorhombic structure for the re–oxygenated sample and possibly to higher T_c's if our assumption above, that isolated Fe(1) atoms have little effect on T_c, is correct. However, if only a fraction of the Fe ends up as isolated atoms, the width of the transition will likely broaden significantly.

In summary, T_c for YBCO:Fe thin films is found to be very sensitive to the substrate temperature during deposition and the cool–down rate in O_2 immediately after deposition is completed, in contrast to results for pure YBCO. T_c as high as 75 K can be achieved for 13% Fe YBCO films when using a high value of T_s and a fast cool–

down. There is a critical substrate temperature near 700°C for a high T_c in YBCO:Fe films. One must cool through this critical temperature rapidly; otherwise some phase or cluster of Fe defects, detrimental to superconductivity, forms.

This work was supported in part by AFOSR and by NSF Grant No. DMR-90-04325.

REFERENCES

1. J. M. Tarascon, P. Barboux, P. F. Miceli. L. H. Greene, G. W. Hull, M. Eibschutz and S. A. Sunshine, Phys. Rev. B **37**, 7458 (1988).
2. Y. Maeno, M. Kato, Y. Aoki and T. Fujita, Jpn. J. Appl. Phys. **26**, L1982 (1987); Y. Maeno, T. Tomita, M. Kyogoku, S. Awaji, Y. Aoki, K. Hoshino, A. Minami, and T. Fujita, Nature **328**, 512 (1987).
3. L. W. Song, E. Narumi, F. Yang, H. M. Shao, D. T. Shaw, and Y. H. Kao, Physica C **174**, 303 (1991).
4. E. Takayama-Muromachi, Y. Uchida, and K. Kato, Jpn. J. Appl. Phys. **26**, L2087 (1987).
5. S. Katsuyama, Y. Ueda, and K. Kosuge, Mater. Res. Bull. **24**, 603 (1989).
6. M. G. Smith, R. D. Taylor, H. Oesterreicher, Phys. Rev. B **42**, 4202 (1990).
7. Z. Q. Qui, Y. W. Du, H. Tang, and J. C. Walker, J. Appl. Phvs. **67**, 5458 (1990).
8. L. J. Swartzendruber, L. H. Bennett, M. Z. Harford, and M. Rubinstein, J. Supercond. **1**, 219 (1988).
9. A. Moodenbaugh, C. Y. Yang, Y. Zhu, R. L. Sabatini, Phys. Rev. B **44**, 6991 (1991).
10. M. D. Lan, J. Z. Liu and R. N. Shelton, Phys. Rev. B **43**, 12,989 (1991).
11. *F. Bridges, J. Truher, D. K. Fork, J. B. Boyce, D. B. Fenner, G. A. N. Connell, T. H.* Geballe, S. Johnson, and L. Liu, Mat. Res. Symp.Proc. **191**, 159 (1990).
12. S. B. Ogale, S. T. Bendre, P. Guptasarma and M. Multani, Solid State Commun. **78**, 285 (1991).
13. J. B. Boyce, G. A. N. Connell, D. K. Fork, D. B. Fenner, K. Char, F. A. Ponce, F. Bridges, J. C. Tramontana, A. M. Viano, S. S. Laderman, R. C. Taber, S. Tahara, T.

H. Geballe, SPIE Proceedings, Processing of Films for High T_c Superconducting Electronics, **1187**, 136 (1990).

14. F. Bridges, J. B. Boyce, T. Claeson, T. H. Geballe, and J. M. Tarascon, Phys. Rev. B **42**, 2137 (1990).

15. F. Bridges, G. G. Li, J. B. Boyce, and T. Claeson, Proceedings of the SPIE, to be published.

16. J. Routbort, S. J. Rothman, N. Chen, J. Mundy, and J. E. Baker, Phys. Rev. B **43**, 5489 (1991).

17. F. Bridges, J. B. Boyce, T. Claeson, T. H. Geballe, and J. M. Tarascon, Phys. Rev. B **39**, 11603 (1989).

FIGURE CAPTIONS

Fig. 1. Resistivity versus temperature of YBCO:Fe films for several Fe concentrations, fast cooled (200°C/min) from $T_s = 750$°C. The vertical scale has been adjusted to separate the curves but the order of increasing resistivity is retained.

Fig. 2. Superconducting transition temperature versus substrate temperature for fast–cooled (200°C/min) YBCO films containing 9% Fe.

Fig. 3. T_c versus Fe concentration for films fast cooled (200°C/min) from two different substrate temperatures.

Fig. 4. T_c versus Fe concentration for films slow–cooled (10°C/min) from 700°C.

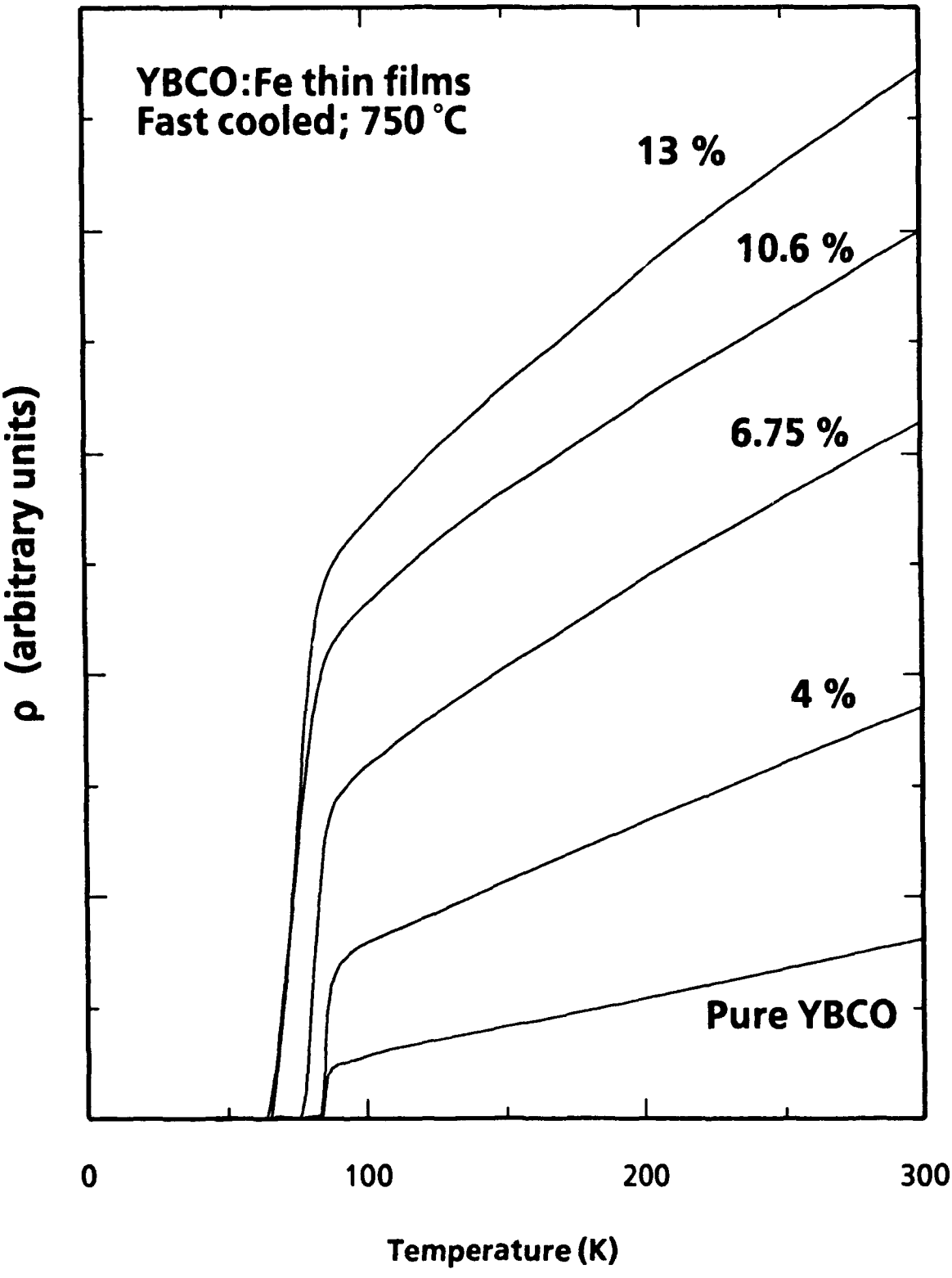
YBCO:Fe thin films
Fast cooled; 750 °C
13 %
10.6 %
6.75 %
4 %
Pure YBCO
ρ (arbitrary units)
0
100
200
300
Temperature (K)

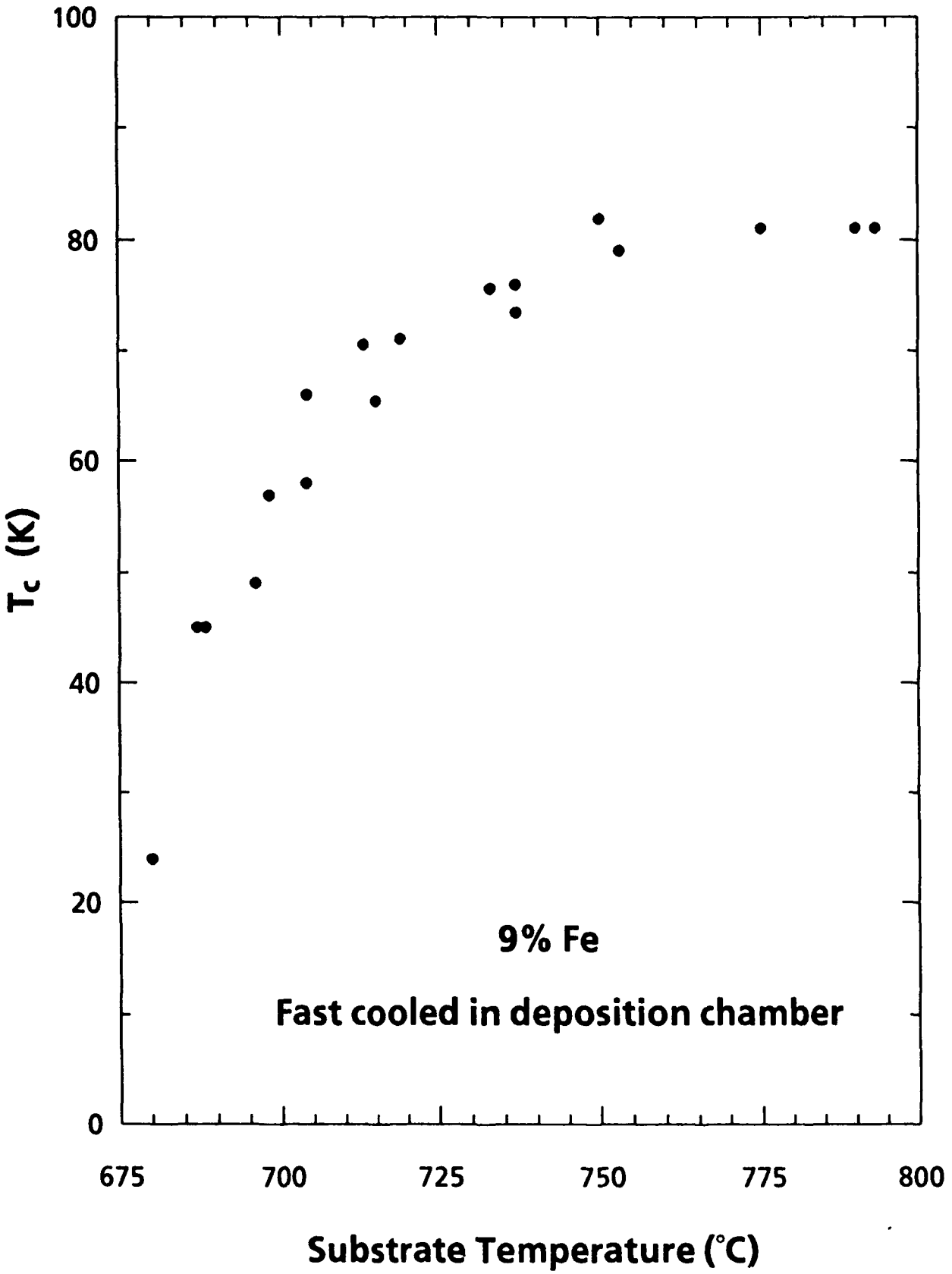
100
80
60
40
20
0
T_c (K)
9% Fe
Fast cooled in deposition chamber
675
700
725
750
775
800
Substrate Temperature (°C)

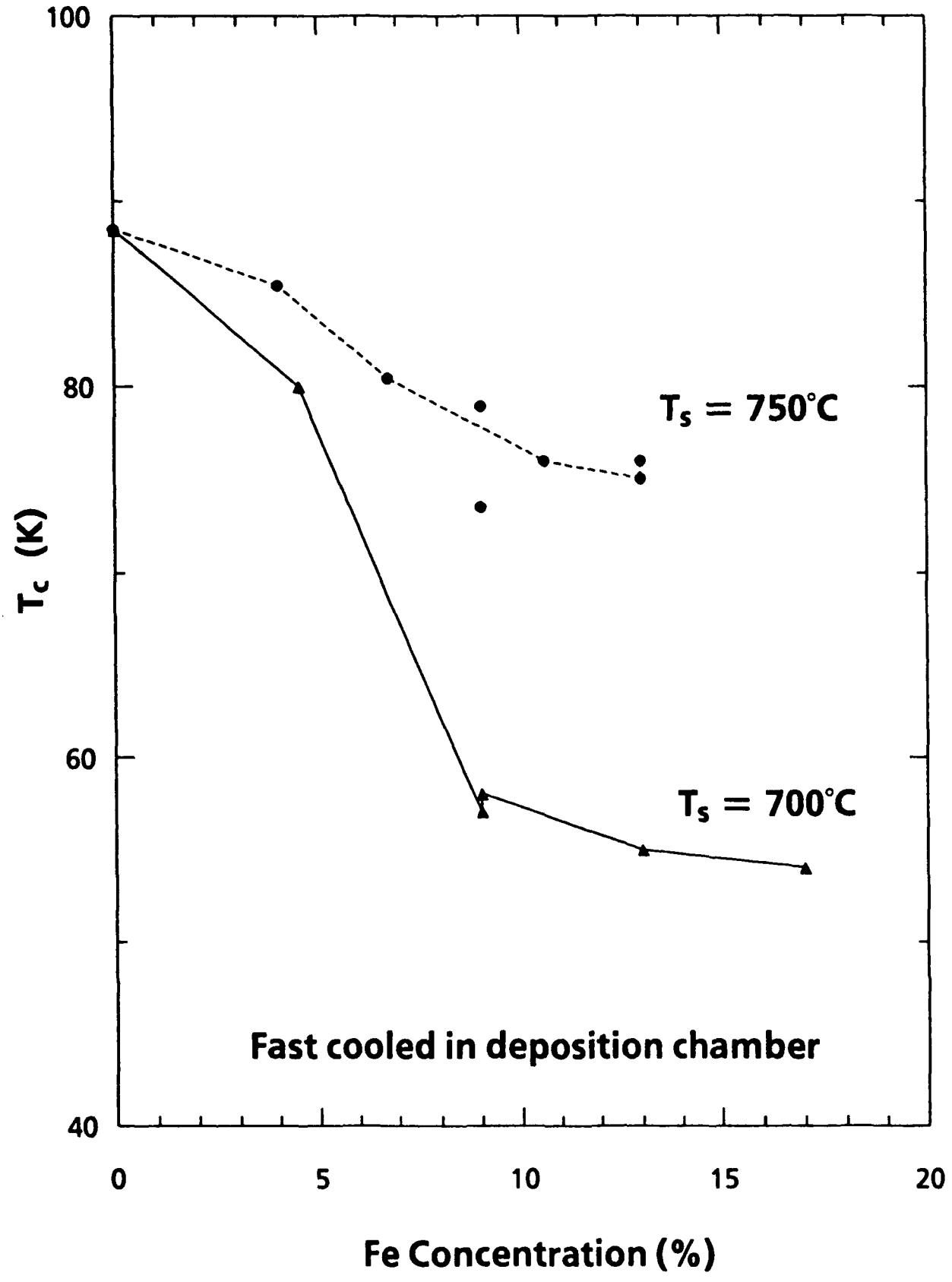
100
80
60
40
T_c (K)
T_s = 750°C
T_s = 700°C
Fast cooled in deposition chamber
0
5
10
15
20
Fe Concentration (%)

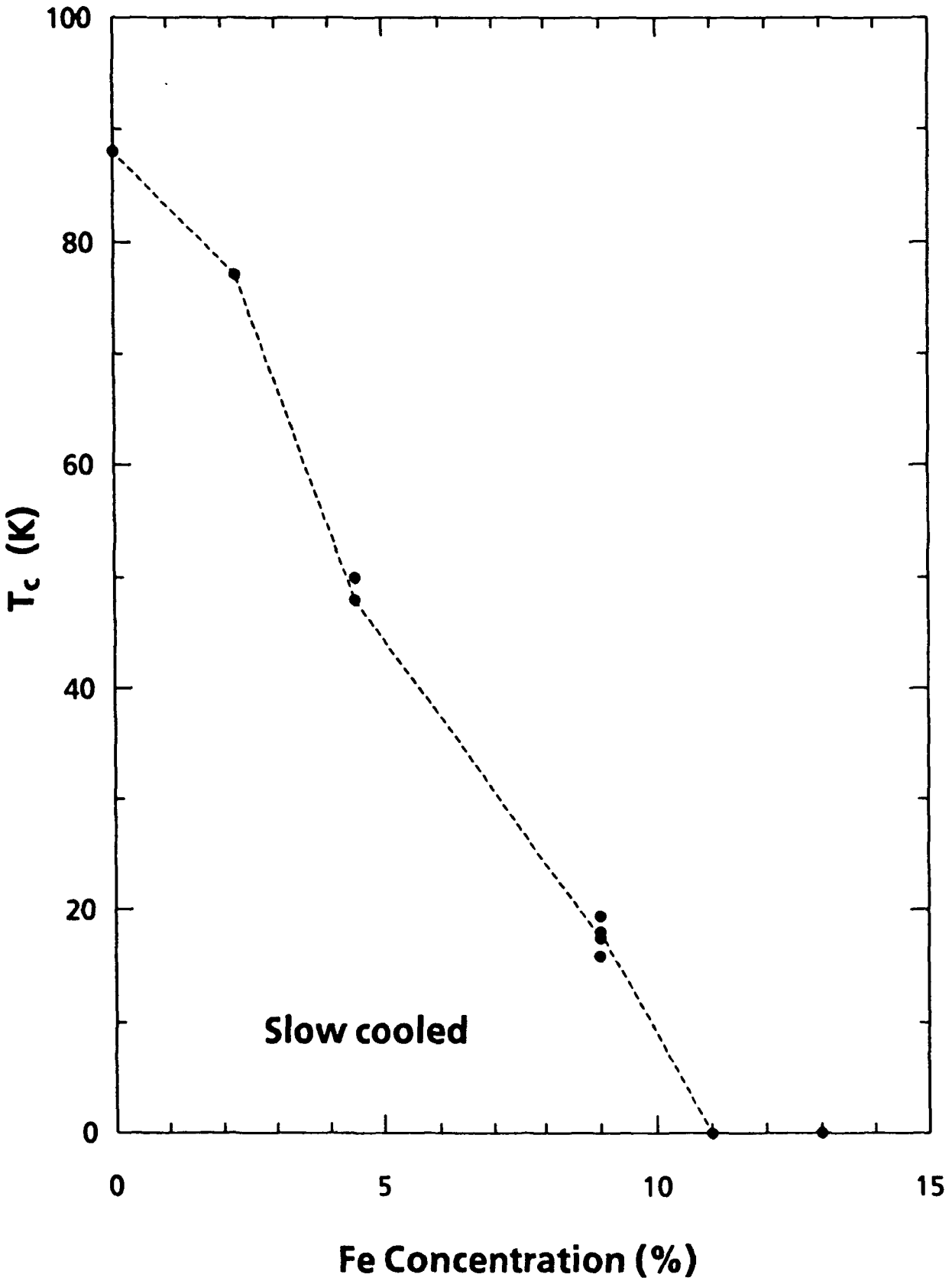
100
80
60
40
20
0
T_c (K)
Slow cooled
0
5
10
15
Fe Concentration (%)

Properties of epitaxial $YBa_2Cu_3O_7$ thin films on Al_2O_3 $\{\bar{1}012\}$

K. Char
Conductus, Inc., Sunnyvale, California 94086

D. K. Fork and T. H. Geballe
Department of Applied Physics, Stanford University, Stanford, California 94305

S. S. Laderman, R. C. Taber, and R. D. Jacowitz
Hewlett–Packard Company, Palo Alto, California 94304

F. Bridges
Department of Physics, University of California, Sante Cruz, California 95064

G. A. N. Connell and J. B. Boyce
Xerox Palo Alto Research Center, Palo Alto, California 94304

(Received 9 November 1989; accepted for publication 18 December 1989)

Epitaxial $YBa_2Cu_3O_7$ films were grown on Al_2O_3 $\{\bar{1}012\}$ by a laser ablation technique. X-ray diffraction shows that films are epitaxial with the c axis perpendicular to the substrate surface and "123" [110] aligned with sapphire [$10\bar{1}1$], although the full width at half maximum of the rocking curve is larger than those of epitaxial films on $SrTiO_3$. Typical T_c's are between 85 and 88 K with transition widths between 0.5 and 3 K. The normal-state resistivity is 270 $\mu\Omega$ cm at 300 K and extrapolates to zero at zero temperature while the magnetization J_c is as high as 5×10^6 A/cm^2 at 4.2 K. High-frequency loss measurements show that 2000-Å-thick epitaxial films on Al_2O_3 $\{\bar{1}012\}$ have a surface impedance about 1 mΩ at 13 GHz at 4.2 K.

Epitaxial thin films of $YBa_2Cu_3O_7$ ("123") have been grown successfully on substrates such as $SrTiO_3$, MgO, yttria-stablized zirconia (YSZ), and $LaAlO_3$ by various deposition techniques.[1] Even though the "123" films on these substrates have excellent properties, the high dielectric constants and losses, low mechanical strengths, size limits, or high costs of some of these substrates have led to efforts to deposit "123" thin films on other substrates like Si and Al_2O_3. The reaction of Si and Al in Al_2O_3 with the "123" at high temperature has been the main obstacle to these efforts. Various buffer layers have been tried to minimize the reaction between the film and the substrates and some successes have been reported.[2] With an *in situ* technique, the growth temperature of the "123" comes down to about 650 °C, making it possible to grow thin films of "123" directly on Al_2O_3, because the Al_2O_3 does not react seriously with the film until 700 °C.[3] Epitaxial thin films of "123" on Al_2O_3 could be very useful in applications such as high Q resonators, delay lines, and infrared bolometers because of the high debye temperature, high thermal conductivity, low microwave loss, high mechanical strength, and easy availability of Al_2O_3. Especially for infrared bolometers, the mechanical strength of Al_2O_3, enabling the substrate to be as thin as 25 μm, and its high thermal conductivity result in a short relaxation time $\tau = C/G$.[4] In this letter we report the successful synthesis of epitaxial "123" films on r-plane $\{\bar{1}012\}$ Al_2O_3 by laser ablation. We also report their structural characteristics, transport properties, and high-frequency loss.

As described in earlier publications,[5] "123" pellets were ablated by a Lambda Physik excimer laser model EM6-103. The pulse energy was 150 mJ and the pulse duration was 15 nS. The beam was focused and imaged by a 25 cm focal length lens onto the pellets. The spot size was approximately 1.2 mm $\times$ 2.5 mm, which corresponds to beam energy density of 1.2 J/cm^2. A unique aspect of the deposition system was that several pellets were mounted on a rotating wheel and a shaft encoder synchronized the laser pulse with the position of each target. The distance of the target and the substrate was varied between 3.5 and 5.5 cm. However, except for the deposition rate and the density of surface particulates, we did not see any significant dependence of sample characteristics on the distance. Oxygen pressure of 200 mTorr was maintained during the deposition and the chamber was backfilled with oxygen up to 400 Torr after the deposition.

Substrate temperature has been the most critical deposition parameter in growing epitaxial "123" films on sapphire. If the temperature was too high, the films came out clear, probably a result of reaction with the substrate. If the temperature was too low, the epitaxy and orientation were not as good as the films grown at higher temperature, resulting in poor transport properties. Therefore, there is a narrow temperature window in which one can grow good epitaxial "123" thin film without severe reaction with the sapphire substrate. The substrates were glued on a Inconel substrate block with silver paste and cured on a hot plate around 150 °C for 30 min. The substrate temperature of 650 to 670 °C was read by an optical pyrometer. The temperature of the cavity, which was heated by a quartz lamp, was controlled with a thermocouple.

Figure 1 shows a resistive transition of an epitaxial "123" thin film on sapphire. The transition temperature was 88 K and the transition width was less than 1 K. The room-temperature resistivity of 270 $\mu\Omega$ cm and the resistivity extrapolating to nearly zero at 0 K are similar to those of single crystals and high quality c-axis oriented epitaxial films on $SrTiO_3$.[6]

Figure 2 shows two x-ray diffraction scans from an epi-

 0003-6951/90/080785-03$02.00

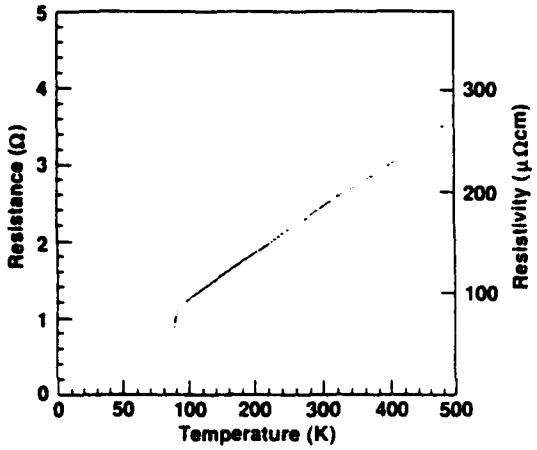

FIG. 1. Resistivity vs temperature data of a "123" film on sapphire {$\bar{1}012$}.

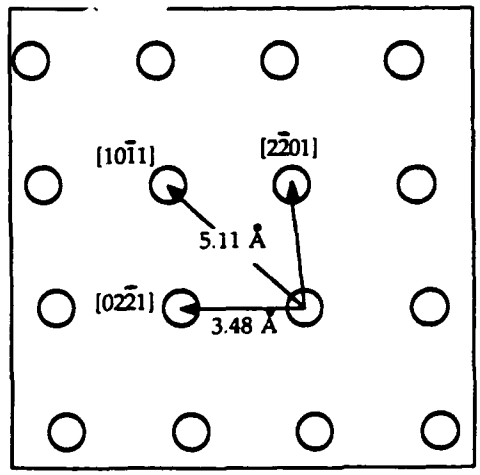

FIG. 3. Sapphire *r*-plane surface perpendicular to [$\bar{1}012$].

taxial "123" thin film on sapphire [$\bar{1}012$]. Figure 2(a) is a *c*-axis scan, showing that the film is highly oriented with the *c* axis nearly perpendicular to the substrate surface. For this sample, the sample orientations at the centers of the "123" [005] and sapphire [$\bar{1}012$] reflections differed by about 1°, but the full width at half maximum of the [005] rocking curve was 2.5°. In comparison, good post-annealed films of "123" on $SrTiO_3$ show rocking curve widths of 0.3°–0.4°[7] and those of *in situ* grown "123" on MgO are as narrow as 0.2°.[8] Figure 2(b) is a φ scan of the "123" [103] peak, where the φ axis is nearly parallel to the "123" *c* axis. The peaks correspond to the *a* and *b* axes of the "123" aligned close to the sapphire [2$\bar{2}$01] directions. The peak widths and broad tails indicate considerable dispersion in the "123" in-plane orientation.

Figure 3 depicts the sapphire [$\bar{1}012$] surface showing selected crystal axes and repeat distances. The "123" epitaxy is somewhat analagous to epitaxial Si grown on sapphire [$\bar{1}012$], where the Si [100] is aligned with the sapphire [10$\bar{1}$1].[9] In the case of "123", it is the [110] directions which are close to the sapphire [10$\bar{1}$1], as the relative lattice spacings would suggest. The relatively wide dispersions in *c* axis and in-plane alignments of the "123" on sapphire are likely due to a combination of the large lattice mismatch and the nonorthogonal axes in the sapphire surface.

The critical current density was measured by a magnetization hysteresis loop according to Bean's critical-state model.[10] Figure 4 shows a magnetization hysteresis loop of an epitaxial "123" film on sapphire. The Bean formula gives $J_c = 5.4 \times 10^6$ A/cm^2 at 4.2 K in 3 kG. This value is not as large as that for epitaxial films on $SrTiO_3$ or $LaAlO_3$, which is about a few times 10^7 A/cm^2, but is the highest so far reported on sapphire substrates. This lower value is probably due to the higher degree of orientational disorder.

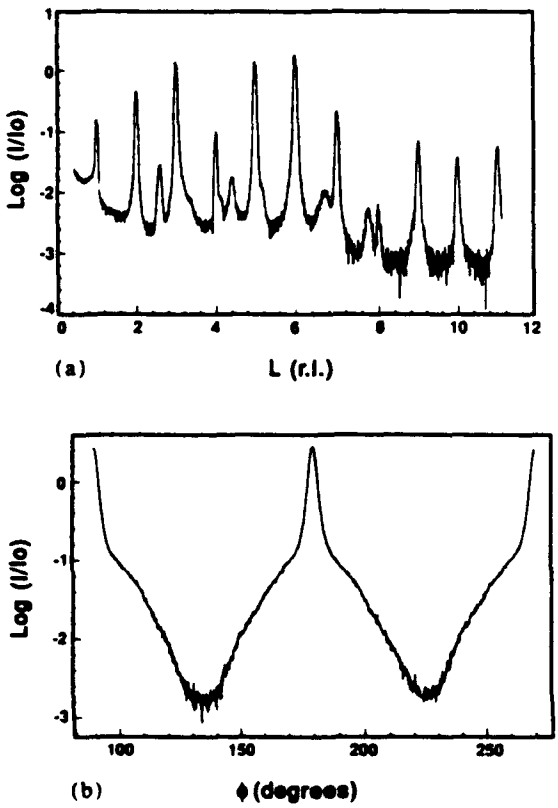

FIG. 2. (a) *c*-axis scan of a "123" film on sapphire {$\bar{1}012$}; (b) φ scan of [103] peak of a "123" film on sapphire {$\bar{1}012$}.

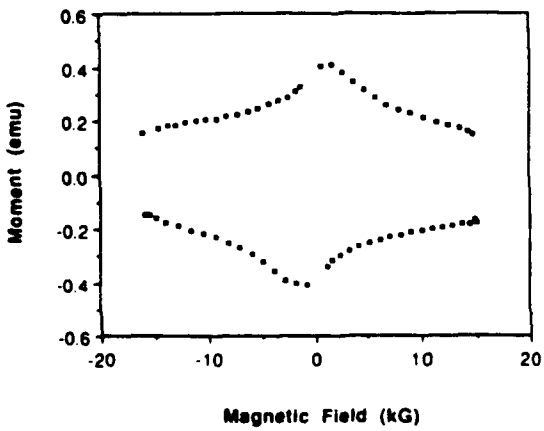

FIG. 4. Magnetization hysteresis loop of a 6 mm × 6 mm × 2000 Å "123" film on sapphire {$\bar{1}012$} at 4.2 K.

The rf surface resistance of these films was measured by use of a parallel-plate resonator technique. In this method, two rectangular samples of superconductor with similar dimensions are pressed face to face with a thin sheet of dielectric material serving as a spacer. This configuration provides a family of transverse electromagnetic modes. For a suitable choice of dimensions and materials, the bandwidths of these modes can be used to calculate the average surface resistance of the two superconducting materials in a straightforward fashion. When this method is used to measure thin films of Nb, a value of 24 $\mu\Omega$ is obtained at 11 GHz and 4.2 K. This value is consistent with cavity-based measurements of solid Nb at 4.2 K.[11]

For the "123" film on sapphire, a resonator Q factor of approximately 6000 was obtained at 4.2 K and 13 GHz with a 250-μm-thick dielectric spacer. This corresponds to a surface resistance $R_s = 1$ mΩ. It is clear that this value cannot be attributed to resistive loss alone. Uncertainties in the detailed structure of the film leave open the possibility that rf leakage through the films may be a substantial contributor to the width of the resonances. For sputtered "123" on other substrates, R_s values as low as 50 $\mu\Omega$ at 11 GHz have been obtained. This value has been achieved on both MgO and $LaAlO_3$ substrates with films that were 2500 and 3000 Å thick, respectively.[12] The fact that the R_s of epitaxial "123" films on sapphire is about 20 times higher than that of epitaxial "123" films on MgO, in spite of their comparable normal-state dc resistivity, suggests that the microstructural disorder might play a major role in generating microwave loss.[13]

In summary, it is encouraging that the epitaxial "123" films can grow on sapphire $\{\bar{1}012\}$ planes and have sharp transtions, low dc resistivities, and high J_c. However, the higher R_s of these epitaxial "123" films on sapphire is a current obstacle to microwave application of these films. Whether the large lattice mismatch necessarily leads to disorder that causes such loss is currently under study. Even if true, it may be possible to overcome this problem by growing a buffer layer with better lattice match to "123."

[1]See a recent review paper by M. R. Beasley, Proc. IEEE 7, 1155 (1989).
[2]X. D. Wu, A. Inam, M. S. Hedge, B. Wilkens, C. C. Chang, D. M. Hwang, L. Nazar, T. Venkatesan, S. Miura, S. Matsubara, Y. Miyasaka, and N. Shohata, Appl. Phys. Lett. **54**, 754 (1989); S. Witanachchi, S. Patel, D. T. Shaw, and H. S. Kwok, Appl. Phys. Lett. **55**, 295 (1989).
[3]M. Naito, R. H. Hammond, B. Oh, M. R. Hahn, J. W. P. Hsu, P. Rosenthal, A. F. Marshall, M. R. Beasley, T. H. Geballe, and A. Kapitulnik, J. Mater. Res. **2**, 713 (1987).
[4]P. L. Richards, J. Clarke, R. Leoni, Ph. Lerch, S. Verghese, M. R. Beasley, T. H. Geballe, R. H. Hammond, P. Rosenthal, and S. R. Spielman, Appl. Phys. Lett. **54**, 283 (1989).
[5]D. K. Fork, K. Char, F. Bridges, S. Tahara, B. Lairson, J. B. Boyce, G. A. N. Connell, and T. H. Geballe, Materials and Mechanisms of Superconductivity Conference, Stanford, CA, 1989 (unpublished).
[6]S. J. Hagen, T. W. Jing, Z. Z. Wang, J. Hovarth, and N. P. Ong, Phys. Rev. B **37**, 2928 (1988).
[7]S. S. Laderman, K. Char, M. Lee, M. R. Hahn, R. H. Hammond, M. R. Beasley, T. H. Geballe, A. Kapitulnik, and R. Barton, Phys. Rev. B **39**, 11648 (1989).
[8]C. B. Eom, J. Z. Sun, K. Yamamoto, A. F. Marshall, K. E. Luther, and T. H. Geballe, Appl. Phys. Lett. **55**, 595 (1989).
[9]F. Ponce and J. Aranovich, Appl. Phys. Lett. **38**, 439 (1981).
[10]C. P. Bean, Phys. Rev. Lett. **8**, 250 (1962).
[11]P. Turneaure and I. Weisman, J. Appl. Phys. **39**, 4417 (1968).
[12]R. C. Tabor and S. S. Laderman (private communication).
[13]T. L. Hylton, A. Kapitulnik, M. R. Beasley, J. P. Carini, L. Drabeck, and G. Gruner, Appl. Phys. Lett. **53**, 1343 (1988); T. L. Hylton and M. R. Beasley, Phys. Rev. B **39**, 9042 (1989).

YBCO FILMS AND BUFFER-LAYERS GROWN IN-SITU BY PULSED LASER DEPOSITION

G. A. N. CONNELL*, D. B. FENNER**, D. K. FORK***, J.B. BOYCE*, F.A. PONCE*, F. BRIDGES****, AND T.H. GEBALLE***
*Xerox Palo Alto Research Center, 3333 Coyote Hill Road, Palo Alto, CA 94304
**Santa Clara University, Santa Clara, CA 95053
***Stanford University, Stanford, CA 94305
****University of California, Santa Cruz, CA 95064

ABSTRACT

YSZ [$(Y_2O_3)_x (ZrO_2)_{1-x}$] buffer-layers for various compositions, x, and YBCO ($Y_1Ba_2Cu_3O_{7-\delta}$) films were grown on hydrogen-terminated Si(100) substrates by laser ablation. The structural and electrical properties of the YBCO are found to depend strongly on x, and to be optimized near $x=0.1$.

INTRODUCTION

There have been many attempts to grow YBCO ($Y_1Ba_2Cu_3O_{7-\delta}$) films directly on Si substrates [1] but in all cases the superconducting properties were severely degraded or destroyed throughout a considerable thickness of the film by the reaction of YBCO with Si during growth. With the possible exception of very thick films [2], it therefore appears that high quality YBCO films will only become available on Si through the use of buffer-layers that do not react at elevated temperatures either with YBCO or Si, that grow epitaxially on Si, and that allow for the subsequent epitaxial growth of YBCO. A number of possibilities exist for epitaxial growth on the Si(100) surface, including YSZ [$(Y_2O_3)_x (ZrO_2)_{1-x}$], the subject of this work[3]. It has two ideal properties: first, at temperatures below 720C, the maximum growth temperature used here, reaction with Si and YBCO is minimal [4]; second, for compositions in the range $0.08<x<0.4$, YSZ grows in the cubic fluorite structure with a lattice constant that closely matches both the near neighbor distance between Si atoms on the (100) surface and the basal plane dimensions in YBCO [5]. We report here a preliminary investigation of this system. We have deposited YSZ buffer-layers as a function of composition, x, followed by YBCO films on hydrogen-terminated Si(100) substrates [6] by laser ablation. We have then correlated the resistivity versus temperature results for YBCO with X-ray diffraction (XRD) and transmission electron microscopy (TEM) measurements on both the superconducting and buffer-layers.

EXPERIMENTAL METHODS

Film deposition is carried out by laser ablation in a PolyGun system[7] in which ten hot-pressed targets are mounted on a rapidly spinning wheel. By synchronizing the pulses from a 308nm XeCl excimer laser with the target wheel rotation, a different sequence of targets may be programmed on each wheel revolution. This feature is used to prepare $(Y_2O_3)_x (ZrO_2)_{1-x}$ by adjusting the ratio of pulses directed at zirconia and yttria targets. Samples with $0<x<0.2$ have been prepared in this way. The YBCO films are deposited from a single target on the target wheel. While the target wheel rotation is not strictly necessary in this case,

Mat. Res. Soc. Symp. Proc. Vol. 169. ©1990 Materials Research Society

the rotation does significantly reduce the target temperature rise by limiting its exposure to radiation from the substrate. The deposited films have better surface morphology as a consequence[8].

The silicon substrates are hydrogen-terminated in a nitrogen-purged hood and immediately introduced into the deposition chamber through a load lock. Their surfaces have been demonstrated to be atomically clean and devoid of oxide prior to the start of a deposition, conditions that are usually necessary for successful epitaxial growth. The substrate temperature is then elevated to 550C (chosen to minimize the reaction between Si and YSZ during growth[3]), driving off the hydrogen, and the YSZ deposition commenced. After depositing the first 1-2 nm of the film (the base pressure is about 5.10^{-7} Torr), oxygen is introduced at 50 mTorr and the remainder of the film is deposited. Upon completion, the substrate temperature is increased to 725C, the oxygen pressure to 200 mTorr, and about 200 nm of YBCO deposited. The run is completed by cooling the layers in 400 Torr of oxygen. Both the YSZ and YBCO depositions use a laser energy of 1-2 J / cm^2 to achieve a deposition rate of about 0.1-0.2 nm / sec at a 5 cm target-substrate distance.

EXPERIMENTAL RESULTS

Figure 1 shows optical micrographs of the surface of the films. The number of asperities changes dramatically with x, particulary for $0.05 < x < 0.1$. The smoother films ($x \geq 0.1$), however, still exhibit more asperities than similar YBCO films prepared directly on YSZ substrates, implying that the asperities are generated primarily during YSZ, rather than YBCO, growth.

Figure 1. Optical micrographs of the surface of the films for x = (a) 0; (b) 0.05; (c) 0.1; and (d) 0.2

The Si-YSZ and YSZ-YBCO interfaces have been examined by cross-sectional transmission electron microscopy (XTEM). In each case, a thin oxide layer about 3 nm thick is present at the Si-YSZ interface although it becomes smoother and less diffuse as x increases. This oxide has regrown as the result of high $O_2^=$ ion mobility in YSZ during the YSZ film deposition. The YSZ-YBCO interface also becomes smoother but less markedly. The most dramatic change, however, is in the structure of the YBCO film. At $x = 0$ the film is highly polycrystalline with minimal preferred orientation, but above $x = 0.05$, there is both an increase in grain size and in the degree of c-axis orientation. Figure 3 shows results for $x = 0.1$. The YSZ film shows a polycrystalline structure with grains of both the cubic and tetragonal

Figure 4 shows the dramatic dependence on x of the conductivity of the YBCO. At x=0, the YBCO is insulating and no measurements could be obtained. But with increasing x, the superconducting properties at first rapidly improve and then slowly deteriorate again. The best results are obtained for the x=0.1 film. At this composition, the superconducting properties of the YBCO are still inferior to those of similar films deposited directly on YSZ substrates[7].

DISCUSSION

The data, summarized in Table 1, on surface morphology, interface and crystal structure, and conductivity all demonstrate that the value of x plays a critical role in preparing the YSZ buffer layer for the subsequent growth of YBCO. That many

x	0	0.05	0.1	0.2
Relative Roughness	10	2	1	1
Relative [005]-Peak	1	90	100	110
T_{c_0} [K]	Insulating	62	77	70
ΔT_c [K]	Insulating	28	13	20
ρ_{300} [μΩ.cm]	Insulating	24,000	6,300	13,000
ρ_{ratio}	Insulating	1.8	2.2	1.85

Table 1. Variation of structural and electrical parameters with x

of the properties are optimized near x=0.1 is suggestive that the cubic YSZ phase is forming here, lattice matched to Si[3]. The XTEM results support this conjecture, albeit under the current deposition conditions, the cubic and tetragonal phases are intermixed with little preferred orientation. At x=0.1, the properties in Table 1 are comparable to the best results reported for YBCO on buffered Si-substrates[1]. The next step toward the growth of high quality YBCO must therefore be to find conditions under which cubic YSZ with x=0.1 can be grown as a single phase with its <100> direction normal to the substrate.

The work is partially supported by AFOSR (FB, THG), AT&T (DKF), and NSF (DBF).

REFERENCES

1. T. Venkatesan, E.W. Chase, X.D. Wu, A. Inam, C.C. Chang, and F. K. Shokoohi, Appl. Phys. Letts. 53, 243 (1988); and references therein.
2. P. Berberich, J. Tate, W. Dietsche, and H. Kinder, Appl. Phys. Letts. 53, 925 (1988)
3. H. Fukumoto, T. Imura, and Y. Osaka, Jpn. J. Appl. Phys. 27, L1404 (1988)
4. D.B. Fenner, A.M. Viano, J.B. Boyce, G.A.N. Connell, F.A. Ponce, and J.C. Tramontana, (to be published)
5. L.A. Tietz, C B. Carter, D.K. Lathrop, S.E. Russek, R.A. Buhrman, and J.R. Michael, J. Mater. Res. 4, 1072 (1989)
6. D.B. Fenner, D.K. Biegelsen, and R.D. Bringans, J. Appl. Phys. 66, 419 (1989)
7. D.B. Fenner, D.K. Fork, J.B. Boyce, G.A.N. Connell, and A.M. Viano, Int. Conf. Materials and Mechanisms of Superconductivity, Stanford, July 1989, in Physica C, edited by N.E. Phillips, R.N. Shelton, and W.A. Harrison (in press)
8. F. Bridges, D.K. Fork, J.B. Boyce, K. Char, G.A.N. Connell, D.B. Fenner, T.H. Geballe, and R.C. Taber (to be published)

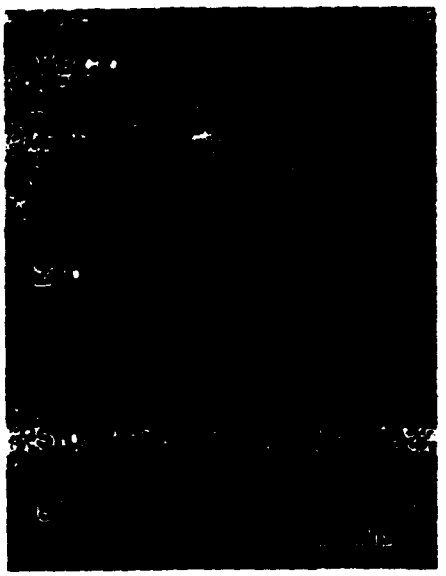

Figure 2. XTEM of film with x = 0.1

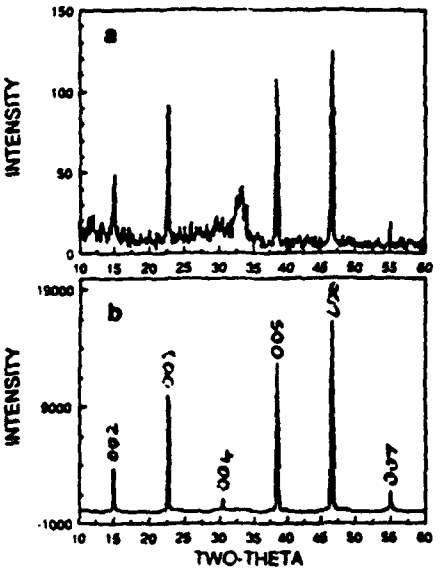

Figure 3. XRD of films with x = (a) 0 and (b) 0.2.

phases of about 10 nm in diameter. The YBCO film above the YSZ is oriented with the c-axis normal to the substrate interface. The YBCO is polycrystalline with grain diameters of order 0.2 μm.

X-ray diffraction (XRD) from the films in the Bragg-Brentano geometry is dominated by the (00n) peaks, typical of preferential c-axis orientation. The most striking feature is a one-hundred-fold decrease in the scattering intensity of the YBCO for x = 0. The variation in the (00n) intensity among the other films was small in comparison. Figure 3 shows 2θ-scans aligned to the Si (004) peak at $2\theta = 69.3^{\circ}$ (outside of plot) for x = 0 and 0.2.

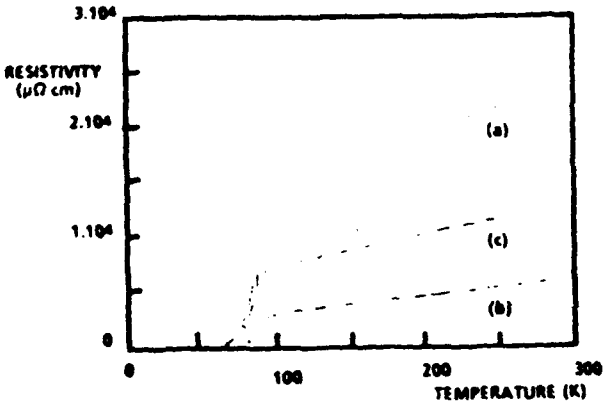

Figure 4. Conductivity versus temperature for x = (a) 0.05; (b) 0.1; and (c) 0.2

HETEROEPITAXIAL METAL OXIDES ON SILICON BY LASER ABLATION

D.B. Fenner,[*+] D.K. Fork,[#] G.A.N. Connell,[*] J.B. Boyce,[*]
F.A. Ponce,[*] J.C. Tramontana,[*] A.M. Viano,[+] and T.H. Geballe[#]

[*]*Xerox Palo Alto Research Center, Palo Alto, CA 94304.*
[+]*Physics Department, Santa Clara University, Santa Clara, CA 95053.*
[#]*Applied Physics Department, Stanford University, Stanford, CA 94305.*

ABSTRACT

Thin epitaxial films of cubic-fluorite structured PrO_2 and YSZ (yttria-stabilized zirconia) were grown on single crystal silicon substrates using the laser ablation-deposition technique. X-ray diffraction theta two-theta, omega rocking and phi scans indicate a high degree of epitaxial orientation of the films to the Si lattice. The highest quality of epitaxy was obtained with the PrO_2 [111] oriented normal to Si(111) surfaces and the cubic YSZ [100] normal to Si(100) surfaces. For both PrO_2 and YSZ, high epitaxial quality required the removal of the Si native oxide prior to deposition and careful control of the deposition environment. It was further found that the YSZ films on Si(100) were an excellent surface for subsequent laser ablation of YBCO films by the usual *in situ* process. The resistivity of this YBCO was ≈250 micro-ohm-cm at 300 K, extrapolated to the resistivity-temperature origin, showed a sharp transition to zero resistance at ≈85 K and was nearly identical to high quality YBCO films deposited on (bulk) YSZ substrates.

INTRODUCTION

The synthesis of high-temperature superconductor films on silicon substrates has failed to keep pace with the rapidly improving films on other substrates, such as $SrTiO_3$, MgO, YSZ, and sapphire.[1,2] This unfortunate situation has occurred despite the efforts of many research groups and the obvious technological importance of combining high-Tc superconducting materials with semiconductors. What is called for is a process for heteroepitaxy, not simply deposition, of metal oxide films on Si. Although many of the growth concepts are expected to be similar to those for compound semiconductors on Si, it is clear that metal oxides present a new set of challenges.

There are two central difficulties with Si as an epitaxial substrate: 1) It causes the copper oxide compounds to undergo a decomposition reaction even at temperatures as much as 200 °C below that normally considered necessary to form good quality films by *in situ* processes, such as laser ablation. We previously characterized this reaction using x-ray photoelectron spectroscopy (XPS) of 2-3 nm films of YBCO deposited directly on Si and SiO_2 surfaces at 550-650 °C. The Si

Mat. Res. Soc. Symp. Proc. Vol. 191. ©1990 Materials Research Society

primarily formed metal silicate compounds.[3] 2) The surface usually formed is unsatisfactory for epitaxial growth of crystalline YBCO since the reaction products and most buffer films are either randomly oriented granular materials or amorphous, as is the silica (SiO_2) film that nearly always forms on Si surfaces exposed to oxygen. YBCO films do tend to self orient their c-axis normal to a freshly growing surface even if deposited on an amorphous base, but the crystalline quality of such films is quite limited (random in plane orientation)

We propose that in order to form high quality metal oxides on Si, it is essential to first remove the native silica film and then execute the deposition of a buffer layer in such a fashion as to limit the formation of nonepitaxial layers and under thermodynamic conditions that stabilize the desired crystal phase of the films. Here we illustrate this process with PrO_2 and YSZ films epitaxially on Si and further demonstrate the considerable value of this process by using it to synthesize a YBCO/YSZ/Si structure with excellent superconducting properties.

SYNTHESIS METHODS

All of our successful film growths on Si have used the spin etch process to clean and terminate the surface with hydrogen. Such surfaces are very passive to reoxidation or contamination even with exposure to an atmosphere of moist air for a few minutes. This passivation is especially useful with the laser ablation process since the surface remains protected by the H termination until it is heated above $\approx 550\ ^{o}C$ just prior to initiating the deposition process. Briefly, the spin etch is a process whereby the Si wafer is first degreased, then rotated under a flow of nitrogen while a few drops of etchant are pipetted onto the surface. Drying occurs immediately and the wafer is ready for transfer to the growth chamber. We have found that[4] a 1:1:10 solution of HF, water, and ethanol all of HPLC-grade (ultrapure) works very well. A detailed study of these surfaces by XPS showed that residual contamination is less than 0.01 ML (monolayer) of C, O, and F while the low energy electron diffraction (LEED) patterns were sharp, unreconstructed Si(100) 1x1.

We use a XeCl laser (308 nm) with pulses of 100-150 mJ focused onto the targets at an energy density of $\approx 1\ J/cm^2$. The substrates are held only by the edges and heated radiantly from behind. An optical pyrometer is used to estimate their true surface temperature (T). The targets are pressed sintered powders of the various metal oxides mounted on a rotating polygon. The polygon motor position is encoded and used to trigger the laser via computer control. This system has considerable flexibility for depositing from multiple targets to synthesize multilayers or mixed oxide films.[5] We have prepared the YSZ films either from separate yttria and zirconia targets, which allowed observations of the effects of varying the fractional Y and Zr content,[6] and from a single target made by mixing the two powders. The latter method produced smoother films, since ablation of the yttria target included

some fragmentary material. Molecular oxygen is introduced into the chamber through a quartz tube exhausting near the substrate surface. Pressure is measured with an ion gauge in a more remote region of the chamber.

EPITAXIAL BUFFER LAYER FILMS

Since PrO_2 forms a cubic fluorite structure with a close lattice match to Si and is unreactive, it would seem to be a good candidate for a buffer layer with YBCO. However the PrO_2 grows best on the (111) surface of Si which in turn is a poor surface for growth of YBCO. These films may have other uses since they are easy to form and of surprisingly high epitaxial quality despite the complete absence of literature references to them.[7] X-ray diffraction (XRD) analysis showed that the PrO_2 [111] was normal to the Si(111) surface, and phi scans of the [200] reflection showed the *in plane* orientation was almost pure b-type phase if the Si was spin etched and the deposition was done at 550 °C in vacuum ($\approx 10^{-6}$ Torr). The type b is that found for CaF_2/Si and consists of an in-plane rotation of the film by 120° from the Si lattice and is threefold rotationally symmetric.

Films of YSZ (9 mole% yttria) deposited on thermally oxidized Si surfaces showed considerable interface roughness in cross-sectional transmission electron microscopy (XTEM). Those made using the spin etch to prepare the Si surface were atomically abrupt despite the presence of an SiO_2 layer regrown at the Si interface.[3,8] These YSZ films showed a high degree of crystallization in the XTEM micrographs but they were polycrystalline. XRD indicated that these films were a mixture of monoclinic, tetragonal and a limited amount of cubic YSZ. These depositions were made in ≈50 mTorr of O_2 and could not be done above ≈550 °C without degrading their quality.

We have considerably improved the quality of these YSZ films on Si by a combined use of spin-etch Si preparation and depositions in lower oxygen partial pressure, $P(O_2)$, and at higher T. Optimum values are in the range of 0.1 – 1.0 mTorr and 750–800 °C. In order to limit regrowth of SiO_2 at the Si interface during the critical period of initial film growth, we begin depositing our YSZ in the $\approx 10^{-6}$ Torr vacuum of our turbo-pumped system until about 2 – 5 nm of film have accumulated, whereupon the $P(O_2)$ is raised to the value used for the remainder of the YSZ deposition.

Figure 1 shows XRD scans of our high quality YSZ epitaxial films on Si(100). These two-theta results show a sharp, single, symmetric [200] reflection at an angle corresponding to cubic YSZ with a lattice constant of 0.516 nm. No monoclinic or tetragonal components were observed, although a small strain-induced peak for the forbidden Si[200] was observed. The [220] peaks of the Si substrate and the cubic YSZ film occurred at different 2θ angles, as seen in Fig. 1, indicating a 5% mismatch in the lattices. This film was nominally 140 nm thick, and has clearly strain relaxed, it being well beyond the critical thickness limit for pseudomorphic strain. Omega

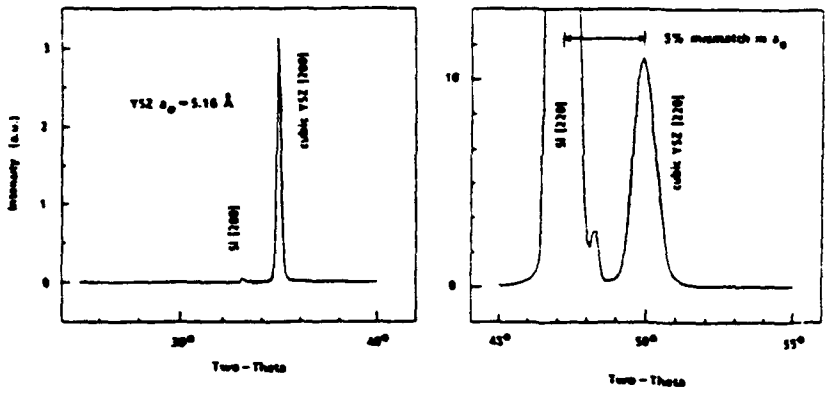

FIG. 1. X – ray diffraction of YSZ on Si(100).

rocking curves about the YSZ [200] peak were $0.7-0.9^{o}$ in width (FWHM). Phi scans of the YSZ[220] peak indicated the presence of only a single in plane orientation of the film, the peak being $\approx 1.2^{o}$ wide (FWHM), and that the YSZ [220] was parallel to the Si [220]. This parallelism of all the major axes of film and substrate is in contrast to the results of Fukimoto *et al.*[9] who reported e – beam deposited YSZ epitaxial on Si rotated in plane by 45^{o}.

In Fig. 2 we propose a simple model for the epitaxial structure of our YSZ films on Si. Shown is a cross – sectional view of the (100) interface viewed from the (011) direction, as in the commonly used view in XTEM micrographs such as in Ref. 3 and 6. The half – length of the diagonal of a face of the Si diamond – structure lattice is indicated as 0.384 nm, and the YSZ is shown lattice matched to this, for simplicity. We note that it is this dimension that is a near match for the *ab* basal plane of the YBCO lattice. The interface is shown in a silicide configuration, as is believed to be the case for CaF_2/Si, without the intrusion of an SiO_2 regrowth, i.e., at an early stage

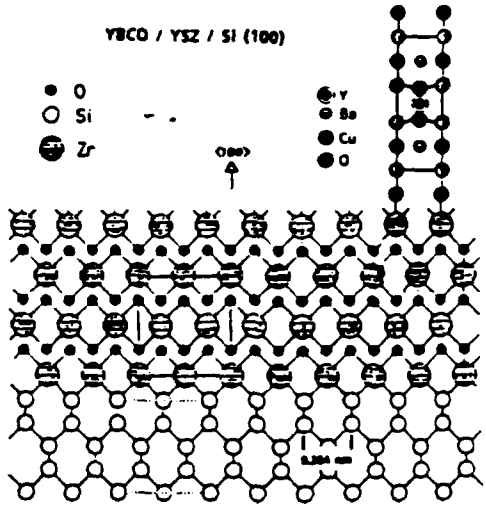

FIG. 2. Structure model for YBCO / YSZ / Si interfaces

in the deposition. Our data so far cannot confirm the apparent natural match of the two structures by a translational displacement of one quarter of the unit-cell face diagonal, as shown in Fig. 2.

YBCO FILMS ON SILICON

Immediately after completion of the YSZ deposition on Si, the T and $P(O_2)$ can be adjusted to 700 - 750 °C and 0.1 - 0.2 Torr, respectively, and deposition of YBCO commenced. Cooling in $P(O_2)$ of 200 - 500 Torr results in films that are superconducting as seen in Fig. 3. Results for two films are shown there. The upper curve is a YBCO film grown on the polycrystalline YSZ/Si, and the lower curve shows the dramatic improvement that occurs for YBCO deposited under the same conditions but now on our improved epitaxial YSZ/Si. The films are quite thin, 15 and 55 nm respectively for the YSZ and YBCO, which provides a stringent test of the film epitaxy. The inset is an expanded view of the transition region for both films, where about a 4 °C improvement in the zero-resistance T_c can be seen. The second film had a 300 K resistivity of about 250 micro-ohm-cm, metallic normal-state resistivity which extrapolates to the origin, and is virtually indistinguishable from resistivity curves for YBCO deposited on single crystal (bulk) cubic YSZ(100) substrates. The latter films were well optimized and fully characterized (including critical current density J_c) and considered to be of very high quality.[5,6] The YBCO films on YSZ/Si reported here have not had their deposition process optimized, but were simply made by repeating the recipe for YBCO on YSZ substrates. Excellent resistivity curves, of course, do not ensure truly high quality YBCO films, but such curves have not previously been reported for fully *in situ* laser-ablated films on Si. Further optimization and characterization is presently underway for our improved YBCO/YSZ/Si materials and will be reported soon.

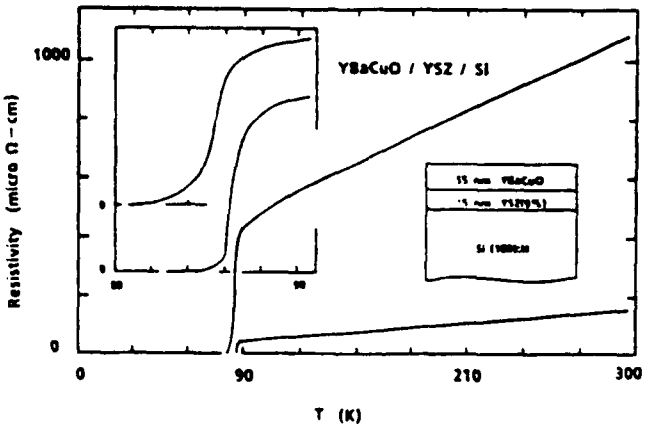

FIG. 3. Resistivity of YBCO films on YSZ/Si.

CONCLUSIONS

Epitaxial films of PrO_2 and YSZ have been grown on Si substrates by laser ablation under conditions that have allowed the beginning of a systematic understanding and control of film crystal quality. The requirements for high quality YSZ/Si are that SiO_2 at the Si interface be limited both by an oxide strip and surface passivation prior to deposition and that the deposition be carried out in as low an oxygen pressure as is consistent with thermodynamic and chemical stability of the growing film. YBCO films deposited on the epitaxial YSZ/Si were excellent superconductors, in that their resistivity curves were very similar to those for YBCO deposited on YSZ substrates. Further improvements in YBCO films are likely to come from devising an extension of the present work to the growth of perovskite structured buffer films on Si, e.g. $SrTiO_3$ or $LaAlO_3$.

DBF and AMV acknowledge support from the NSF (DMR – 8822353), and DKF an AT&T scholarship. Additional support came from the Air Force OSR (F49620 – 89 – C – 0017).

1 S Witanachchi, S. Patel, H.S.Kwok, and D.T. Shaw, Appl. Phys. Lett. 54, 578 (1989).

2 X.D. Wu, A. Inam, M.S. Hegde, B. Wilkens, C.C. Chang, D.M. Hwang, L. Nazar, T. Venkatesan, S. Miura, S. Matsubara, Y. Miyasaka, and N. Shohata, Appl. Phys. Lett. 54, 754 (1989). E.W. Chase, T. Venkatesan, C.C. Chang, B. Wilkens, W.L. Feldmann, P.Barboux, J.M. Tarascon, and D.L. Hart, J. Mater. Res. 4, 1326 (1989).

3 D.B. Fenner, D.K. Fork, J.B. Boyce, G.A.N. Connell, and A.M. Viano, Inter. Conf. Materials and Mechanisms of Superconductivity, Stanford, July 1989, in Physica C, edited by N.E. Phillips, R.N. Shelton, and W.A. Harrison, 162, 141 (1989). D.B. Fenner, A.M. Viano, G.A.N. Connell, J.B. Boyce, D.K. Fork, F.A. Ponce, and J.C. Tramontana, in Materials Research Society Symp. Proc., edited by J. Narayan, P. Chu, L. Schneemeyer, and D. Christen, Vol. 169 (in press).

4 D.B. Fenner, D.K. Biegelsen, and R.D. Bringans, J. Appl. Phys. 66, 419 (1989). D.B. Fenner, D.K. Biegelsen, R.D. Bringans, and B.S. Krusor, Materials Research Soc. Symp. Proc., edited by M. Kawabe, T.D. Sands, E.R. Weber, and R.S. Williams, 148, 279 (1989).

5 J.B. Boyce, G.A.N. Connell, D.K. Fork, D.B. Fenner, K. Char, F.A. Ponce, F. Bridges, J.C. Tramontana, A.M. Viano, S.S. Laderman, R.C. Taber, S. Tahara, and T.H. Geballe, Symp. on *Processing of films for High T_c Superconducting Electronics*, Soc. Photo – Opt. Instru. Eng. Proc., edited by T. Venkatesan, Vol. 1187 (1990).

6 G.A.N. Connell, D.B. Fenner, D.K. Fork, J.B. Boyce, F.A. Ponce, F. Bridges, and T.H. Geballe, in Materials Research Society Symp. Proc., edited by J. Narayan, P. Chu, L. Schneemeyer, and D. Christen, Vol. 169 (in press).

7 D.K. Fork, D.B. Fenner, and T.H. Geballe, submitted for publication.

8 D.B. Fenner, G.A.N. Connell, D.K. Fork, J.B. Boyce, A.M. Viano, F.A. Ponce, and J.C. Tramontana, Bulletin Amer. Phys. Soc. 35, 328 (1990).

9 H. Fukumoto, T. Imura, and Y. Osaka, Jpn. J. Appl. Phys. 27, L1404 (1988).

XPS ANALYSIS OF Y–Ba–Cu–O AND Zr–O THIN FILMS AND INTERFACES WITH SILICON SUBSTRATES

D.B. FENNER*+, A.M. VIANO,+* G.A.N. CONNELL,* J.B. BOYCE,* D.K. FORK,#* F.A. PONCE,* and J.C. TRAMONTANA*

*Xerox Palo Alto Research Center, Palo Alto, CA 94304.
+Physics Department, Santa Clara University, Santa Clara, CA 95053.
#Applied Physics Department, Stanford University, Stanford, CA 94305.

Thin films of $YBa_2Cu_3O_x$, ZrO_2, and yttria–stabilized zirconia (YSZ) have been deposited on Si(100) by the UV–laser ablation technique, and characterized by several techniques including x–ray photoemission spectroscopy (XPS) and cross–sectional transmission electron microscopy (XTEM). Si substrates were prepared by several techniques including thermal oxidation, and oxide etching and passivation by hydrogen termination. Certain of these YBCO films (≈250 nm thick) deposited on YSZ buffer layers have excellent superconducting properties. Other YBCO and zirconia films, deposited to 2–5 nm thickness and transferred under dry N_2 into UHV, allowed XPS evaluation of the thermal and chemical stability of the interfaces and nearby regions. 2–nm films of YBCO on 15–nm films of SiO_2 / Si, deposited at 550–670 °C, showed Cu 2*p* core–level XPS lines similar to those of bulk YBCO (i.e., Cu II) but with two components due to reactions. The Si 2*p* line showed formation of silica on the YBCO surface at 670 °C and of silicate at 550 °C. XTEM lattice images showed that use of H–terminated Si produced superior interfaces with the zirconia films.

It has become increasingly clear that thin films of YBCO on semiconductor substrates present a substantial challenge to those who desire superconductor films of the highest quality.[1, 2] The average *a* and *b* lattice dimensions of the YBCO match within a few percent the Si(100) surface–net [011] dimension, and yet chemical reactions between these two have so far prevented good epitaxy.[3, 4] Films of YSZ may have the necessary material properties to facilitate their use as buffer layers between the Si substrate and the YBCO film. It has been shown that YSZ with about 9 mol% of Y_2O_3 in ZrO_2 will grow in the cubic phase with a lattice that allows a match within ≈0.2% of Si(100).[5] In addition YBCO also matches YSZ closely, although some reactions at this interface were noted.[6]

Si surfaces under normal handling conditions always have a thin (native) oxide known to be of poor structural and electrical quality. Thus, we have prepared our substrates with a high–quality (MOS–grade) thermal oxide, or with the spin–etching method, which leaves the Si surface H terminated, i.e., without oxide or other residue. The latter surface is known to be very passive to reoxidation and was recently demonstrated to be produced by simple and reliable wet–chemistry techniques: etching with an HF in ethanol solution while spinning.[7]

All our multilayer films are deposited during a single sequence of *in situ* exposure to a UV–laser ablation plume from various targets. Up to ten targets are mounted on a rapidly rotating polygon in synchrony with the pulsed laser and under on–line computer control. Targets were pressed YBCO, ZrO_2, and Y_2O_3 which allowed YSZ growth by interleaving various numbers of pulses of the ZrO_2 and Y_2O_3 targets. The pure ZrO_2 and YSZ films were deposited in 50 mTorr of O_2 and the YBCO in 200 mTorr. The substrates were heated directly by a lamp and their temperature *T* monitored with a pyrometer.

A film of YBCO ≈250 nm thick deposited at 725 °C on a 20–nm buffer layer of YSZ (4–5 mol%) which was, in turn, deposited at 580 °C on thermally oxidized Si(100), was found to be superconducting with a transition to zero resistance T_{co}≈88 K. A similar multilayered film was deposited at 670 °C on a nearly identical YSZ buffer layer on H–terminated Si, and was found to have T_{co}≈84 K. Both of these samples were cross sectioned and TEM lattice images of the interfacial regions obtained, and are shown in Fig. 1. Inspection of these images reveals that in (a) the zirconia has a rough interface with the thermal oxide and the original SiO_2 / Si interface also became rough. In (b), however, the two interfaces are atomically abrupt and very flat indicating excellent quality. Also, in (b) it can be seen that an SiO_2 layer has regrown at the lower interface, undoubtedly because of the elevated *T* and high $O_2^=$ ion mobility through the zirconia.

Mat. Res. Soc. Symp. Proc. Vol. 169. ©1990 Materials Research Society

(a) (b)

Fig. 1. Cross-sectional TEM lattice images of zirconia films on Si(100). In (a) the Si surface was prepared with the spin-etch process, and in (b) the Si was initially oxidized thermally to 15 nm thickness. Size scale bars are indicated.

The surfaces of these thin films have also been evaluated by XPS and compared with a fractured bulk YBCO surface, reported in Ref. 8, and various calibration oxides and materials. Thin films were 100 nm of YBCO on SiO_2 / Si, and a sequence of films at various deposition T, but thin enough (~2 nm) so that photoelectrons were able to escape from the interfacial region.[4] Figure 2 shows the core-level spectra for the Y 3d line of various samples, where the ~2 eV spin-orbit split can be seen. The thin (2 nm) samples all show an Y 3d line very similar to the reference spectra but shifted due primarily to surface charging effects. The peaks at lower binding energy are the Si 2s line, and by their relative peak areas clearly indicate that substantially more Si has entered the films deposited at higher T. As seen in Fig. 3, the Ba $3d_{5/2}$ has two components for the reference YBCO sample[8] but only one (shifted) component for the very thin films, indicating reaction of the Ba.

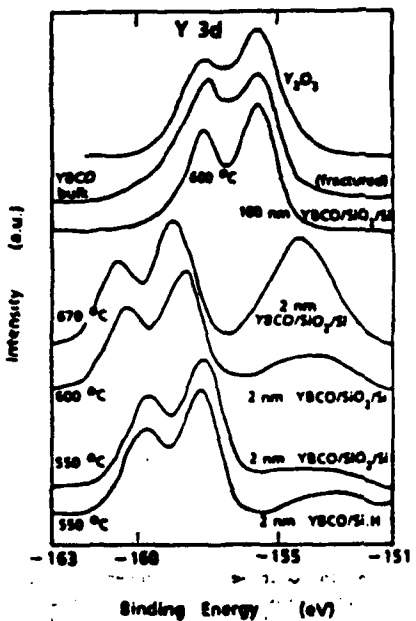

Fig. 2. Y 3d core-level spectra for various samples as labeled.

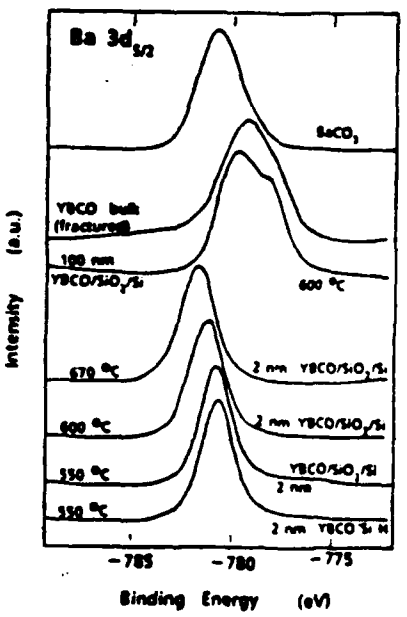

Fig. 3. Ba 3d core-level spectra for various samples as labeled.

The Cu 2*p* spectra have been similarly compared[4] and it was found that all of the YBCO films had a line shape that was primarily Cu II oxidation state and very similar to the spectra of CuO and the bulk YBCO of Ref. 8. The very thin films, especially at 670 °C deposition temperature, show two components to the line, with one shifted substantially to higher binding energy as a consequence of surface charging. Likewise the Si 2*p* have been discussed[4] and their line shapes and shifts indicate considerable reaction of the films with the Si. Comparison of these spectra with reference samples of silica and silicate compounds (especially $ZrSiO_4$) allowed the identification of a large amount of SiO_2 in the surface region of the 670 °C deposited film, and silicate bonding for the Si in the interface region. No silicides were identified in these spectra.[2, 4]

The quantity of Si found in the YBCO and zirconia thin films was calculated from the spectral peak areas. By calibration with various standard materials, the relative concentration was determined and is shown in Fig. 4 with an Arrhenius fit. Both Si 2*p* emission normal to the sample surface (called bulk) and emission at a glancing angle (called surface) are indicated. The activation energies determined by a least squares fit are 1.3±0.4 and 1.8±0.6 eV respectively.

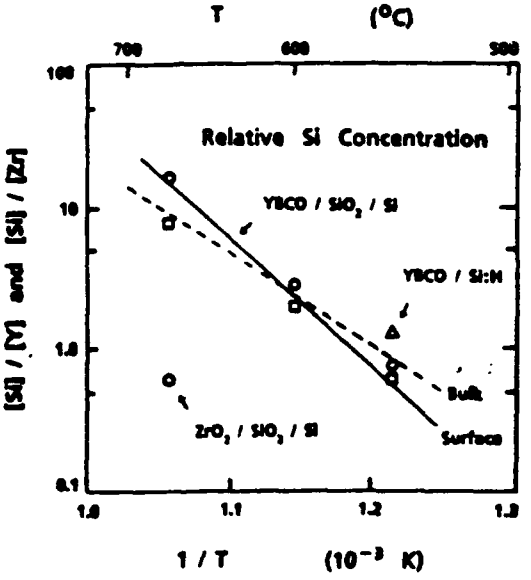

Fig. 4. Relative Si concentrations in various films as calculated from XPS core-level line areas. Data for films at various deposition *T* are cast as an Arrhenius plot and least squares fits to these data sets are indicated by the lines: solid, for normal emission (bulk) from YBCO films; and dashed, for glancing emission (surface).

All our XPS measurements of core levels for the various samples just discussed are summarized in Table I. Here are tabulated the stoichiometries for the films in relation to the Y content of each. The glancing emission, surface sensitive, data are given where available. The thicker YBCO film is near the expected stoichiometry but the thin films are all Cu and O rich (or Y and Ba poor), which is qualitatively similar to recently reported results of very thin YBCO films on $SrTiO_3$ substrates.[9]

Thin films of YBCO deposited on Si substrates, with or without an SiO_2 buffer layer, all reacted substantially with the Si in the temperature range of 550 °C and above. This precludes the growth of high-quality YBCO on Si even at the modest *T* required for the laser ablation process, as currently practiced. Thin films of zirconia and YSZ showed much less reaction with Si in this *T* range, and thus show promise as chemical reaction barrier layers for YBCO. The H-termination of

the Si surface prior to YSZ deposition was used and compared with thermally oxidized surfaces. The former had quite superior interfaces with the zirconia layer in XTEM lattice images.

We greatly appreciate helpful conversations with Kookrin Char, David Biegelsen, Jeongsoo Kang, and Professors T.H. Geballe and F. Bridges. DBF and AMV received support from the National Science Foundation (DMR-8822353), and the project was supported by the Air Force OSR (F49620-89-C-0017). DKF acknowledges an AT&T scholarship.

Table I. THIN-FILM STOICHIOMETRY from XPS
Stoichiometry (relative atomic concentration) of YBCO films measured by XPS. The film thickness and deposition T are indicated. The bulk values are for photoelectron emission normal to the surface, and the surface values are for a 15° takeoff angle. * Estimated sensitivity limit.

Sample		[Ba]/[Y]	[Cu]/[Y]	[O]/[Y]	[Si]/[Y]
YBCO/SiO_2/Si 100 nm, 800 °C	(bulk)	2.0	2.3	6.4	<0.01 *
YBCO/SiO_2/Si	(bulk)	2.4	5.1	29	7.9
2.0 nm, 672 °C	(surface)	–	–	–	16
YBCO/SiO_2/Si	(bulk)	2.4	6.2	17	2.9
2.0 nm, 600 °C	(surface)	–	–	–	2.0
YBCO/SiO_2/Si	(bulk)	1.0	9.8	12	0.76
2.0 nm, 550 °C	(surface)	0.12	1.1	0.63	0.62
YBCO/Si:H	(bulk)	1.7	7.9	13	1.3
2.0 nm, 550 °C	(surface)	–	–	–	1.3
		[Y]/[Zr]	[O]/[Zr]	[Si]/[Zr]	
ZrO_2/SiO_2/Si 50 nm, 560 °C	(bulk)	0	2.6	<0.01 *	
ZrO_2/SiO_2/Si	(bulk)	0	3.0	0.77	
3.8 nm, 670 °C	(surface)	0	2.7	0.62	
ZrO_2/SiO_2/Si	(bulk)	0.04	3.7	0.68	
2.8 nm, 560 °C	(surface)	–	–	0.32	

1. T. Venkatesan, E.W. Chase, X.D. Wu, A. Inam, C.C. Chang, and F.K. Shokoohi, Appl. Phys. Lett. 53, 243 (1988).
2. P. Berberich, J. Tate, W. Dietsche, and H. Kinder, Appl. Phys. Lett. 53, 925 (1988).
3. D.B. Fenner, D.K. Fork, J.B. Boyce, G.A.N. Connell, and A.M. Viano, Int. Conf. Materials and Mechanisms of Superconductivity, Stanford, July 1989, in Physica C, edited by N.E. Phillips, R.N. Shelton, and W.A. Harrison (in press).
4. D.B. Fenner, A.M. Viano, J.B. Boyce, G.A.N. Connell, F.A. Ponce, and J.C. Tramontana, (to be published).
5. H. Fukumoto, T. Imura, and Y. Osaka, Jap. J. Appl. Phys. 27, L1404 (1988).
6. L.A. Tietz, C.B. Carter, D.K. Lathrop, S.E. Russek, R.A. Buhrman, J.R. Michael, J. Mater. Res. 4, 1072 (1989).
7. D.B. Fenner, D.K. Biegelsen, and R.D. Bringans, J. Appl. Phys. 66, 419 (1989).
8. Z. Shen, J.W. Allen, J.J. Yeh, J.-S. Kang, W. Ellis, W. Spicer, I. Lindau, M.B. Maple, Y.D. Dalichaouch, M.S. Torikachvili, J.Z. Sun, and T.H. Geballe, Phys. Rev. 36, 8414 (1987).
9. C.C. Chang, M.S. Hegde, X.D. Wu, B. Dutta, A. Inam, T. Venkatesan, B.J. Wilkens, and J.B. Wachtman, Jr., Appl. Phys. Lett. 55, 1680 (1989).

Reactions at the interfaces of thin films of Y-Ba-Cu- and Zr-oxides with Si substrates

D. B. Fenner[a] and A. M. Viano[b]
Xerox Palo Alto Research Center, Palo Alto, California 94304 and Physics Department, Santa Clara University, Santa Clara, California 95053

D. K. Fork
Xerox Palo Alto Research Center, Palo Alto, California 94304 and Applied Physics Department, Stanford University, Stanford, California 94305

G. A. N. Connell, J. B. Boyce, F. A. Ponce, and J. C. Tramontana
Xerox Palo Alto Research Center, Palo Alto, California 94304

(Received 29 January 1990; accepted for publication 22 October 1990)

Thin films were deposited by pulsed uv-laser (ablation) deposition of $Y_1Ba_2Cu_3O_{7-x}$ (YBCO), and composite zirconia and yttria targets onto silicon wafers. These films were analyzed to ascertain the chemical and physical structure of the film interfaces and further the development of Si substrates for superconducting YBCO films. Substrates were Si(100) with either a high-quality, thermal oxide (SiO_2) film, or a spin-etch processed, oxide-free, hydrogen-terminated surface (Si:H). X-ray photoelectron spectroscopy (XPS) of Y, Ba, Cu, and Si core levels revealed adverse reactions for thin (nominally 2 nm) YBCO films deposited directly onto either substrate surface. The surfaces of thicker YBCO films (50–100 nm) and various oxide powders were compared with XPS results from these thin films. The thicker-film surfaces are similar to those of fractured bulk YBCO, while the thin YBCO films decomposed, as evidenced by changes in the Ba and Cu XPS. The Si XPS on these films showed the formation of metal-silicate compounds, even at deposition substrate temperatures of 550 °C, and silica (SiO_2), especially for 670 °C deposition. A direct consequence of these reactions is that growth of high-quality epitaxial YBCO on Si will require the use of a buffer film. Yttria-stabilized zirconia (YSZ) shows considerable promise for use as a buffer, and XPS of thin films (4 and 8 nm thick) of ZrO_2 on SiO_2/Si and YSZ on Si:H substrates did not show any indication of decomposition, even at deposition temperatures near 800 °C. Transmission electron microscopy of cross-sectioned samples of YBCO/YSZ/Si showed that the lower YSZ interface is rough on the preoxidized (SiO_2/Si) substrates but atomically sharp on the spin-etched Si wafers (Si:H). These sharp YSZ interfaces showed the presence of 3–5 nm of regrown oxide (SiO_x) next to the crystalline Si substrate. This regrown oxide was observed in samples deposited under a variety of conditions.

I. INTRODUCTION

Since the discovery of high-temperature superconducting oxides, it has been anticipated that thin films of these materials on semiconductor substrates would have a wide range of important applications. Heteroepitaxy of semiconductors depends on having a close match of the lattice constants and thermal expansion coefficients, and negligible chemical reaction and interdiffusion at the process temperatures (deposition, growth, and anneal). The advent of pulsed laser deposition (PLD) for *in situ* thin-film deposition of the cupric oxides has accelerated the expectation of high-quality films on semiconductor substrates, since relatively low process temperatures are possible.[1] Mixed results have been reported for films of $YBa_2Cu_3O_{7-x}$ (YBCO) directly on crystalline silicon substrates. These films were found to be structurally and electrically inferior to those on single-crystal oxide substrates (e.g., yttria-stabilized zirconia [YSZ] and $SrTiO_3$).[2,3] Chemical reactions between the YBCO films and the Si surface and its oxides (i.e., SiO_2/Si) have been identified as an important factor contributing to poor film quality, especially for the portion of the film nearest the substrate.[1,4–11] Typically, it was reported that Si substrates required rather thick YBCO films (of order 1 μm) in order to obtain even moderate superconducting quality. Cubic YSZ has been reported as forming an epitaxial film on Si(100),[12] and we have recently shown that such a film can be formed with a high degree of *c*-axis and in-plane epitaxial orientation[13,14] and that it can serve as an excellent buffer layer for high critical-current ($> 2\times 10^6$ A/cm^2 at 77 K) YBCO thin films.[13,15] Here we report an analytical study of the adverse reactions of YBCO, and the lack thereof for YSZ films, with silicon in the near-interfacial regions.

II. RESULTS AND DISCUSSION

A. Experiment

Substrates were 2×2 cm^2 cleaved from Si(100) wafers. Their surfaces, prior to film deposition, were either a 15-nm-thick, device-gate quality thermal oxide (SiO_2/Si), or an oxide-free, hydrogen-terminated Si (Si:H) processed by the

[a] Present address: Advanced Fuel Research, East Hartford, CT 06108.
[b] Present address: Physics Department, Washington University, St. Louis, MO 63130.

 0021-8979/91/042176-07$03.00

spin-etch method.[16] The latter surfaces have been shown to be remarkably ideal (i.e., atomically clean, and unreconstructed) and very passive to reoxidation in air at room temperature. The H is fully evaporated by about 550 °C in vacuum, just prior to epitaxy.[17]

Thin films of YBCO and zirconia compounds were deposited by ablation of composite-YBCO, ZrO_2, and mixed ZrO_2/Y_2O_3 sintered powder targets. The XeCl uv laser was operated at 308 nm and focused to produce pulses of 1–2 J/cm^2 on the targets which were mounted on a motor-driven polygon. Target positioning and laser pulsing were under computer control, providing considerable flexibility. This PLD system has been described elsewhere.[18] Just prior to and during deposition, the Si substrates were heated by direct radiation from an incandescent lamp. The housing temperature (T) was regulated by a nearby thermocouple and the substrate T monitored by an optical pyrometer. Ablation and deposition of YBCO were carried out in an O_2 ambient of 200 mTorr, followed by a cool down in 400 Torr. The ZrO_2 was deposited and cooled in 50 mTorr of O_2, and the 9 mole% YSZ was deposited at 4×10^{-4} Torr of O_2.[13,14]

As we have recently demonstrated, epitaxial YBCO films with critical currents in excess of 2×10^6 A/cm^2 at 77 K can be fabricated on Si wafer substrates by using YSZ buffers deposited on spin-etched Si.[13,15] An essentially single-step PLD *in situ* process was used. These YBCO films required deposition at about 750 °C. Prior to this work, several efforts had been made to improve the, then somewhat limited, YBCO film quality by reducing the deposition T for both the YBCO and the buffer layer.[18,19] The results presented here indicate that lowering deposition temperatures (to 550 °C) does not necessarily improve film quality (by limiting reactions with the Si).[1] This understanding is an important part of our successful effort to obtain high-quality YBCO films on Si wafers.[13,14]

Films of YBCO formed by PLD on Si substrates were evaluated by core-level x-ray photoelectron spectroscopy (XPS) to determine the chemical bonding and hence the presence of decomposition reactions.[8,9] Samples were transferred via dry-N_2 glove boxes on both the deposition and XPS systems. A Mg $K\alpha$ x-ray source and hemispherical energy analyzer were operated with a combined instrumental resolution of 0.85 eV (full width at half maximum).[16] Comparisons with freshly sputtered surfaces of Ag and Cu metals were used to estimate electron binding energies, assuming -368.0 and -932.7 eV for the Ag $3d_{5/2}$ and Cu $2p_{3/2}$ lines, respectively. Electrostatic charging of insulating surfaces during XPS analysis was detected by partially discharging with a low kinetic-energy electron flood gun. Powdered reference samples were mounted by evaporating off a high-purity alcohol from the finely ground powder held in a small stainless-steel cup. The Si wafer samples were frictionally mounted by stainless-steel wire tabs to a small stainless-steel stub.

B. XPS of YBCO/Si

Figure 1 shows XPS Cu $2p$, Ba $3d_{5/2}$, and Y $3d$ spectra (corrected for secondary-electron background and nonmonochromatic x-ray source radiation) for a variety of samples. For reference purposes, spectra are included for Cu metal, CuO (Cu II), $BaCO_3$, Y_2O_3, the fracture surface of bulk YBCO (taken from Ref. 20), and a 100-nm-thick YBCO film deposited at 600 °C on SiO_2/Si. The bulk and thicker film samples of YBCO yielded similar Cu $2p$, Ba $3d_{5/2}$, and Y $3d$ spectra, at least qualitatively similar to those

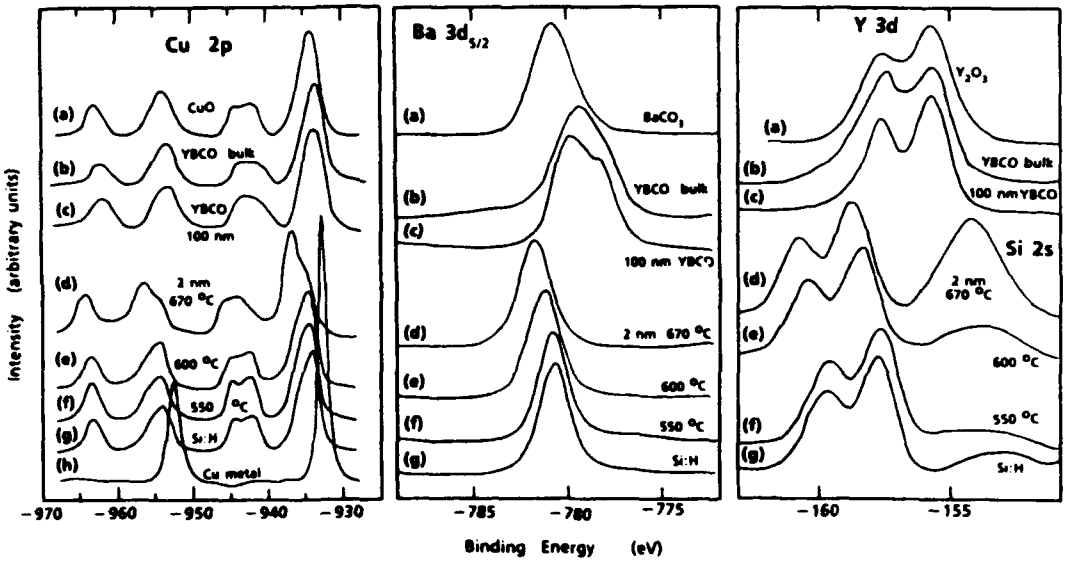

FIG. 1. Cu $2p$, Ba $3d_{5/2}$, and Y $3d$ core-level spectra for various samples: (a) CuO, $BaCO_3$, Y_2O_3 powders, respectively, (b) bulk YBCO from Ref. 20. The remaining curves, (c)–(g), are from YBCO films on Si wafers. For these samples the Si $2s$ can be seen at a binding energy of about -154 eV, near the Y $3d$ lines. The thick YBCO film in (c) was 100 nm thick and deposited at a substrate T of 600 °C. Curves (d)–(g) were from thin films, nominally 2 nm thick, deposited at (d) 670, (e) 600, (f) 550, and (g) 550 °C. The substrates for the films in (c)–(f) were 15 nm of thermal oxide on Si (SiO_2/Si), while (g) was an H-terminated Si wafer (Si:H), prepared as in Ref. 16. Curve (h) is the Cu $2p$ spectra from a freshly sputtered Cu metal surface. Peak heights have been normalized. The typical counting noise limit is about 2% of the indicated intensity (peak height) of the principal lines, and the estimated binding energy accuracy is ±0.1 eV.

reported by others.[3,20-22] Linewidths for the bulk YBCO are somewhat greater due to electron-analyzer operating parameters, and this leads to reduced resolution of the chemical component and spin-orbit splitting for the Ba $3d_{5/2}$ and Y $3d$, respectively.

Next, in Fig. 1, are shown three spectra for very thin YBCO films deposited on SiO_2/Si at 670, 600, and 550 °C and one spectra for a 550 °C film on Si:H.[8,9] These samples were deposited by PLD under 200 mTorr of O_2. The film thickness was limited to 2–4 nm, comparable to the core-level photoelectron escape length. The line shape distortions, evident for these four thin films, indicate that the Cu and Ba near the interface have reacted, thereby decomposing YBCO. Distortion of the Y $3d$ peak shapes was not observed, but the presence of Si near the sample surfaces is clear from the large Si $2s$ peaks seen in Fig. 1 near the Y $3d$. The thin-film spectra in Fig. 1 for all four elements also show, what we have assumed to be, electrostatic surface charging (lines shifted to lower kinetic energy). The electron flood gun failed to significantly shift the kinetic energies of these lines. These films were found to be macroscopically insulating (high resistivity), and since all the lines were observed to shift by the same energy interval, charging of insulating (i.e., reacted) regions is the most likely explanation.[21] The Cu $2p$ line shape improves considerably as the deposition T is reduced: the principal lines are more like Cu II as in Fig. 1(a) for CuO. However, even at 550 °C the Cu $2p$ lines are still asymmetric, and the Ba $3d_{5/2}$ line never recovers when compared with the 100-nm film spectrum.

Si $2p$ core levels for a variety of samples are shown in Fig. 2. For reference, a fresh Si:H surface gave the spectral line of curve (a), which is just narrow enough to resolve the spin-orbit splitting (0.6 eV) as a shoulder on the line.[16] Also for reference is curve (b), the Si $2p$ spectra for the 15 nm of thermal oxide, i.e., the SiO_2/Si substrate surface. The thicker (100 nm) YBCO film sample had no XPS-detectable surface Si. Empirical and calculated cross sections for the elements and core levels in Figs. 1 and 2, indicate that the sensitivity to Si is at least a factor of ten less than that for the other elements, so the presence of a trace of Si near the surface of the thick YBCO film cannot be excluded.

The remaining spectra in Fig. 2 are the Si $2p$ lines for the same thin YBCO samples in Fig. 1, as described above. Spectrum (c), for the 670 °C YBCO thin film, is similar to that of (b), for the SiO_2/Si surface, while the 600 and 550 °C samples (d) and (e) show increasing peak weight at an energy intermediate between to pure silica (SiO_2) and the clean Si surface (Si:H). Curve (g) for the 550 °C deposition onto Si:H shows little or no SiO_2 component and a strong substrate Si line, indicating that oxide has not substantially regrown at this interface.

To obtain qualitative depth-distribution information, the samples were tilted in the spectrometer away from the normal emission angle to a 15° takeoff angle, thus greatly increasing the surface sensitivity. Spectra (f) and (h) in Fig. 2 indicate that the near surface regions of the 550 °C samples are mainly the intermediate binding energy Si species, discussed in more detail below.

Measured intensities of XPS core-level spectra for various oxides (Y_2O_3, $BaCO_3$, CuO, SiO_2/Si, and ZrO_2) provided empirical cross-section calibrations using the common-anion rule. The thicker (100 nm) YBCO film sample was found to be near the expected stoichiometry of 1:2:3:7. The thin films were all Cu and O rich (or equivalently Y and Ba poor). Recent reports of XPS core-level intensities of very thin films of YBCO on $SrTiO_3$ and Auger depth profiles of thicker films on YSZ also described significant deviations from 1:2:3 stoichiometry (at the interface and surface, respectively).[3,23] Since the detailed morphologies of these thin reacted films are largely unknown, quantitative measures by XPS of the Si concentration may not be reliable, but the general trend of more extensive reactions at higher T is clear from the Si $2s$ peak heights in Fig. 1.

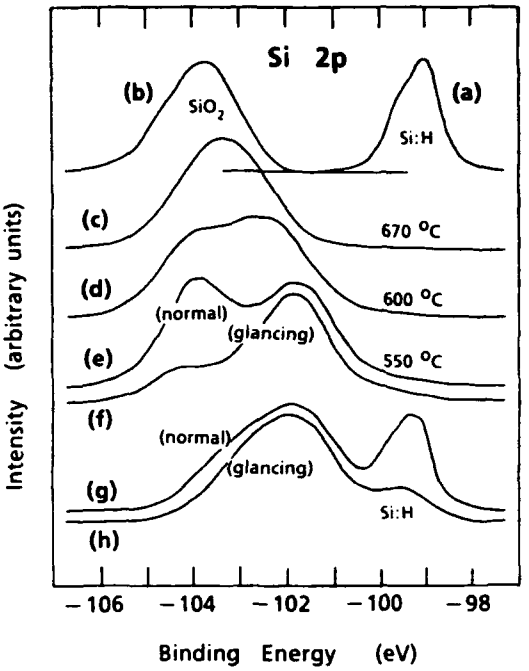

FIG. 2. Si $2p$ core-level spectra for various samples: (a) H-terminated Si (Si:H), prepared as in Ref. 16, and (b) thermal oxide on Si (SiO_2/Si). Curves (c)–(h) are from the same samples as (d)–(g) in Fig. 1, i.e., they are from films of YBCO, nominally 2 nm thick, on Si deposited at (c) 670, (d) 600, and (e)–(h) 550 °C. Curves (c)–(f) are with SiO_2/Si, and (g) and (h) are with Si:H substrates. All spectra were measured with photoelectrons emitted normal to the sample surface except for (f) and (h) which were for a 15° takeoff angle. Peak heights have been normalized. The typical counting noise limit is about 2% of the indicated intensity (peak height) of the principal lines, and the estimated binding-energy accuracy is ± 0.1 eV.

C. XPS of zirconia/Si

Next, we report on thin zirconia-compound films on Si wafers. In Figs. 3 and 4 are Zr $3d$ and Si $2p$ spectra measured for two reference materials and various thin films. Most of these materials and films are insulators, and surface charging was observed. In order to facilitate spectral shape comparisons, the spectra in Figs. 3 and 4 have had their binding energies normalized (shifted) so as to align the principal peaks in the Zr $3d$. The 4-nm-thick YSZ film showed the least charging shift (little or none, ± 0.5 eV) and hence the other spectra were aligned with it. The Si $2p$ spectra in Fig. 4 were shifted by corresponding amounts.

The thin zirconia films are: 3 nm of ZrO_2 deposited by

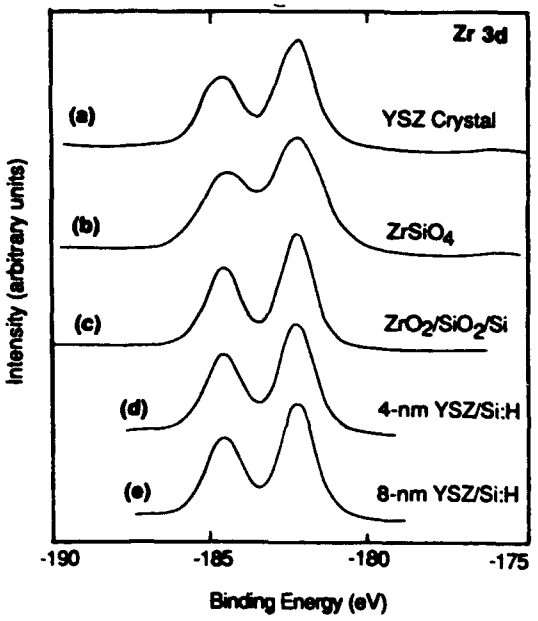

FIG. 3. Zr 3*d* core-level spectra for various samples: (a) a YSZ crystal, (b) $ZrSiO_4$ powder, and three films (c)–(e). Spectrum (c) is from a ZrO_2 film, nominally 4 nm thick, deposited at 670 °C on an SiO_2/Si substrate. Spectra (d) and (e) are YSZ films, nominally 4 and 8 nm thick, respectively, deposited at 790 °C on Si:H, prepared as in Ref. 16. The indicated binding energies of spectra (a)–(c) and (e) have been empirically corrected for electrostatic charging by aligning their principal maxima with that of spectrum (d). Peak heights have been normalized, and the estimated binding energy accuracy is ± 0.5 eV.

PLD on SiO_2/Si at 670 °C, and 4 and 8 nm of YSZ on Si:H at 790 °C. The deposition conditions for these two YSZ films were identical to our process for forming the highly epitaxial 150-nm-thick YSZ films[13,14] and the 50-nm-thick buffer films upon which the high critical-current YBCO films were deposited.[13,15]

The very thin YSZ film samples were also tilted in the spectrometer, and representative spectra are shown in Fig. 4 (there was no change in the Zr 3*d* line shapes). For both the 4- and 8-nm samples, the peak height of the lower binding-energy peak component was reduced at glancing emission angle. This, together with this peak's narrower linewidth and approximate binding-energy value, indicate that the peak is from photoelectrons emitted from deeper regions in the samples, perhaps 1–2 escape lengths. In addition, the relative proportion of the two line components in each of the normal emission-angle spectra, shows less of the lower binding-energy component for the thicker (8 nm) film, as would be qualitatively expected. Hence, this peak is identified as Si at the interface and first few atomic layers below, i.e., substrate Si.

In contrast to the YBCO films on Si wafers, the ZrO_2 and YSZ films deposited on SiO_2/Si and Si:H were found to be chemically unreactive, as we now discuss. First, a thicker (50 nm) ZrO_2 film was deposited at 560 °C on SiO_2/Si, and no Si was detectable by XPS with normal-emission geometry. Second, the qualitative Zr 3*d* line shapes in Fig. 3 indicate that to this resolution the Zr binding configurations are quite similar. More detailed information on chemical shifts cannot be clearly established from the data shown in Figs. 3 and 4, due to the large corrections for electrostatic charging. Thus, in Table I we have numerically tabulated the relative kinetic energies of the XPS lines from representative samples. Kinetic energy differences (ΔE_k) eliminate the need to correct for electrostatic charging in the spectrometer. In the case of SiO_2, ΔE_k values have been reported in the literature for several bulk and film, structures and morphologies.[24,25] Reported values of ΔE_k for the Si 2*p* and O 1*s* lines of various forms of SiO_2, are consistently 429.7 eV except for very thin (less than 1 or 2 nm) oxide films, where ΔE_k drops by a few tenths of an eV. The first three sample entries in Table I are in agreement with these reports. The oxide residue (third entry in Table I) was the submonolayer quantity left on an Si wafer after HF etching in a dipping process.[16] There it was at the crystalline Si free surface and could be clearly distinguished from other oxides since its Si 2*p* peak intensity was very small, compared with the substrate Si 2*p*, due to the relatively few Si atoms involved in the submonolayer. The suboxide chemical shift is substantially less than that for SiO_2, since the Si oxidation state is not + IV as it is in a high-quality SiO_2 (silica).

D. XPS of silica and silicates

Distinguishing the XPS spectra of various compounds of metals, silicon and oxygen requires care. These compounds are numerous and plentiful in nature (they compose most of the earth's crust), and $ZrSiO_4$, in particular, occurs commonly in nature as the mineral zircon.[26] It is one of the few simple silicate compounds (an orthosilicate) having each silicon atom bonded tetrahedrally to four oxygen atoms, and these SiO_4^{4-} ligands are in turn bonded primarily

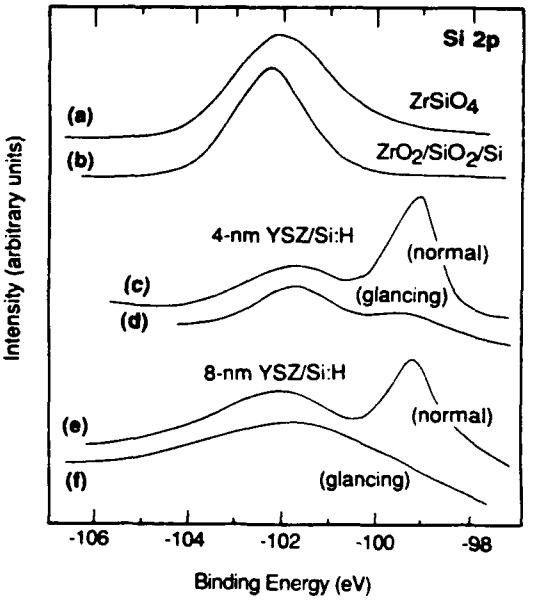

FIG. 4. Si 2*p* core-level spectra for various samples, the same as those in Fig. 3 (b)–(e), i.e., (a) is the $ZrSiO_4$ powder, (b) the ZrO_2 film on SiO_2/Si, (c)–(f) the YSZ films on Si:H. For the YSZ films spectra are shown for both normal and glancing photoelectron emission angles. Peak heights are normalized and the reported binding energies for all but (c) and (d) have been adjusted by the corresponding amounts which were used to align the Zr 3*d* peaks in Fig. 3. Peak heights have been normalized, and the estimated binding energy accuracy is ± 0.5 eV.

TABLE I. Photoelectron kinetic energy differences ΔE_k between components of the Si 2*p*, O 1*s*, and Zr $3d_{5/2}$ core-level lines from XPS measurements on various samples. The first two ΔE_k columns report energy differences between components of the same line, while the second two columns are differences between specific components of lines from different elements. An entry of zero indicates that only one line component was observed, while a dash entry indicates that a line(s) was not present in that sample. The experimental resolution was ± 0.1 eV.

Sample	ΔE_k (eV) Si 2*p*	ΔE_k (eV) O 1*s*	ΔE_k (eV) Si2*p*—O1*s*	ΔE_k (eV) Zr$3d_{5/2}$—O1*s*
15 nm SiO_2 on Si	4.6	0	429.7	···
2 nm native oxide	4.2	0	429.3	···
SiO_x residue on Si[a]	3.2	0	429.2	···
$ZrSiO_4$ powder	0	1.9	429.0	347.1
ZrO_2 powder	···	0	···	348.2
YSZ crystal	···	0	···	347.8
2 nm YBCO/Si:H	2.7	2.3	428.6	···
3 nm ZrO_2/SiO_2/Si	0	1.7	429.6	347.8
4 nm YSZ/Si:H	2.9	1.6	429.8	347.9
8 nm YSZ/Si:H	2.8	1.5[b]	429.5	347.8

[a] Residue of 0.15 monolayer of total oxygen on Si(100) after etching in HF solution by a dipping process, as described in Ref. 16.
[b] Weak line with ± 0.5-eV resolution in ΔE_k.

ionically to Zr^{4+} ions. Each Zr is eight-fold coordinated to O that are members of six distinct SiO_4 tetrahedra. Thus, not all Zr—O distances are equal, which may lead to the slight broadening of the Zr 3*d* line of Fig. 3(b). Spectra for the $ZrSiO_4$ powder had two components in its O 1*s* line, consistent with two types of oxygen bonding. One line component clearly originated from the Zr—O bond, as can be seen by comparison with the entries in Table I for ΔE_k (Zr$3d_{5/2}$—O1*s*) of ZrO_2 and YSZ. The other O 1*s* component of the $ZrSiO_4$ sample was identified as the Si—O bond in this compound, i.e., silicate SiO_4.

The Si 2*p* binding energy in silica and silicate compounds may be understood in the following way. In SiO_2 each O is bonded to two Si and the electronegativity difference between O and Si pulls the bonding electron density toward each O and away from the oxidation state + IV Si atoms. This ionic contribution to the Si—O bond increases the binding energy of the Si, leading to the observed 4.6 eV chemical shift from Si in crystalline silicon to that in silica (first entry in Table I). To the extent that the silicate ligand SiO_4 is ionically bonded to the counter ion (e.g., Ba, Cu, or Zr ions) electron charge density is transferred from the cation onto the silicate ion where it resides in the O 2*p* orbitals away from the central Si. This has the effect of reducing the polarity in the Si—O bond and hence decreasing the Si 2*p* chemical shift. This scheme is consistent with the 0.7 eV reduction in ΔE_k (Si2*p*—O1*s*) we have observed for $ZrSiO_4$ relative to SiO_2, as seen in Table I.

Table I next lists ΔE_k values measured for four thin films. The 2-nm YBCO film on Si:H had two components to both the Si 2*p* and O 1*s*, and eliminating the Si—Si and metal—O components identifies the Si—O bond as having too small a ΔE_k to be silica. Thus, we establish the presence of silicate compounds (most likely Ba, based on its low electronegativity) in this film.[11,27] Extending this analysis to the other YBCO films on Si wafers, spectra (c–h) in Fig. 2, the intermediate binding-energy peaks seen there are also indicators of silicate compounds. Clearly then, the 550, 600, and possibly 670 °C YBCO thin films contained Si in both silica and silicate forms, the latter necessarily indicative of YBCO decomposition and deterioration of the potential for superconductivity. Higher deposition *T* apparently causes a larger proportion of silica over silicate, but this may just signify the sequential decomposition by thermal activation (in the presence of excess oxygen) of YBCO into metal-silicate and then into a mixed phase of silica plus a multitude of other oxides.

For additional reference, we have obtained XPS data from another sample likely to contain silicates: a thin Cu film, vacuum evaporated onto Si:H at 400 °C, and later exposed to air. This Cu—Si—O film showed both a substrate Si 2*p* line (Si—Si bonding) and a component with about 3.3 eV higher binding energy (Si—O). The Cu 2*p* spectrum had the shape of Cu II as in Fig. 1(a) for CuO. Cu—Si—O compounds, including copper silicates and silicides, are not common, so for comparison we have measured the ΔE_k between the principal Cu 2*p* and O 1*s* in the just mentioned film and in CuO (Cu II oxidation state) and in Cu_2O (Cu I) powders. These ΔE_k were: 404.4 eV (CuO), 402.5 eV (Cu_2O), and 401.3 eV (Cu—Si—O film on Si), lending further evidence to the presence of a copper silicate in the film. It is not surprising to find the Cu here in the II oxidation state, since the I and III states are much less stable in general. None of our various film samples showed any indication of containing copper silicides, as has been reported by others in YBCO films on Si.[4,5] Such silicides are rarely stable compounds in the presence of oxygen, and would have a relatively small shift in the Si 2*p* binding energy, due to the small electronegativity difference.

In contradistinction to the YBCO films on Si, we conclude from the ΔE_k (Si2*p*—O1*s*) in Table I that the zirconia-compound films contain Si in a silica and suboxide form without any detectable amounts of silicate or silicide material, i.e., no decomposition of the ZrO_2 and YSZ films. The relatively small values for ΔE_k of the two Si 2*p* components observed for the YSZ samples (Table I) are indicative of near-interfacial Si no longer exclusively bonded to other Si (chemically shifted) due to the presence of the interface and some suboxide (SiO_x).

E. TEM of YSZ/Si

To elucidate buffer film evolution from very thin YSZ on Si:H to thicker films, used in turn for supporting YBCO films, we have made cross-sectional transmission electron microscopy (XTEM) evaluations.[18,19] In Fig. 5 is an XTEM micrograph of the region just above the Si substrate interface of a complete multilayer sample of YBCO/YSZ/Si. The 4-nm-thick amorphous layer seen immediately above the substrate Si is not a purposefully deposited layer. The substrate was prepared by the spin-etch method which initially H-terminates the Si surface. These Si:H surfaces are free of oxide prior to film deposition, but were always observed to regrow an amorphous SiO_2 layer, as can be seen in Fig. 5, during the depositions. We have postulated that this is due to the well-known high O^{2-}-ion conductivity of YSZ (and other oxide ceramics including YBCO)[28] while at elevated T and under ambient O_2 gas exposure, i.e., during film depositions.[29] The XTEM micrographs of a series of films, deposited in 50 mTorr of O_2, showed that the regrown oxide thickness is independent of the YSZ deposition T (550–650 °C), the yttria concentration (0–20 mole%), and even the YSZ film thickness (50–250 nm). This saturation of the oxide thickness is qualitatively what is commonly observed with native oxide films on Si.[30] The appearance of an amorphous SiO_x layer at the Si interface of rf-sputtered buffer layers of $BaTiO_3/MgAl_2O_3$ on Si substrates was recently reported,[31] and oxide regrowth under chemical vapor deposition of silica films has also been reported.[30]

The oxide regrowth need not interfere with epitaxy of these films, as is well known from recrystallization of Si on thin SiO_2/Si. Since little or no oxide is present when the epitaxial growth is initiated (i.e., Si:H), the substrate crystalline template is available to reduce the film free energy for epitaxial orientations. As the film thickens, the substrate epitaxial influence is quickly lost anyway, so oxide regrowth (or even removal of the substrate) can occur as long as the regrown oxide does not exceed the strain limit of the film. Thermal expansion mismatch with the film and phase transformations in the regrown oxide would be expected to present a problem, but only if the oxide is thick enough. Cracking or void formation was not observed in the XTEM work on these YSZ films on Si.[14]

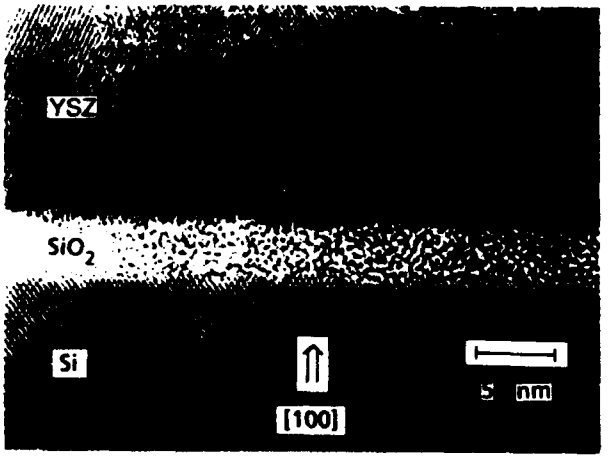

FIG. 5. Cross-sectional transmission electron micrograph (XTEM) of the interfacial region between a deposited zirconia (YSZ) film and the Si(100) substrate. The intermediate layer is (amorphous) SiO_2. The substrate orientation and a size scale bar are indicated.

In fact, as seen in Fig. 5, XTEM lattice images of the interfacial regions near the substrate clearly indicate[9] that both the YSZ/SiO_2 and SiO_2/Si interfaces are atomically flat and sharp for this Si:H substrate. XTEM of a similar sample of films deposited on the thermal oxide coated wafers (SiO_2/Si) showed distinctly poorer quality interfaces with regions of interdiffusion at the YSZ/SiO_2 and roughening at the SiO_2/Si interface.[9,19,32] Despite the presence of the amorphous SiO_2 layer, the zirconia grains in the film on Si:H (Fig. 5) are nearly all oriented to the substrate [011] over relatively large distances, at least 100 nm along the interface. By contrast the film on SiO_2/Si showed more nonaligned regions. More recent x-ray diffraction analysis of YSZ films on Si:H indicates that granularity can be dramatically reduced and epitaxial orientation to the substrate Si greatly improved by deposition under optimized conditions.[13,14]

III. CONCLUSIONS

XPS evaluations of the interfaces of YBCO films on SiO_2 and Si:H substrates indicate that considerable reaction occurs at deposition temperatures of 550–670 °C. The Si primarily formed metal-silicate and silica compounds, and the usual Cu and Ba line shapes were badly distorted compared with spectra from good-quality YBCO. Our results indicate that the growth of YBCO films having sharp interfaces with Si substrates will require buffer layers that can prevent reactions, if the depositions are to be done at temperatures generally considered necessary for high-quality *in situ* YBCO films.

Very-thin zirconia (ZrO_2 and YSZ) films were found by XPS to be chemically stable on SiO_2 and Si:H substrates. In particular, YSZ films deposited by PLD on Si:H substrates were unreactive and found to have interface regions with only a small amount of silica when the film was thin (4–8 nm). XTEM micrographs of thicker films showed the presence of a regrown SiO_2, which did not disrupt the abruptness of the interfaces and the film epitaxial quality if Si:H substrates were used. Together, these XPS and XTEM studies of YSZ interfaces with Si substrates indicate the suitability of YSZ as a buffer layer on Si which has been prepared by hydrogen termination. These results provide an important background of understanding upon which we have developed a process to fabricate very high-quality YBCO film materials on Si wafer substrates.

ACKNOWLEDGMENTS

We would like to acknowledge many stimulating and useful conversations with Jeongsoo Kang, Ross Bringans, John Northrup, David Biegelsen, and Professors T. H. Geballe and F. Bridges. D. B. F. and A. M. V. received support from the NSF (DMR-8822353), and D. K. F. an AT&T scholarship. Additional support for the project came from the Air Force OSR (F49620-89-C-0017).

[1] T. Venkatesan, E. W. Chase, X. D. Wu, A. Inam, C. C. Chang, and F. K. Shokoohi, Appl. Phys. Lett. **53**, 243 (1988); X. D. Wu, A. Inam, M. S. Hegde, B. Wilkens, C. C. Chang, D. M. Hwang, L. Nazar, T. Venkatesan, S. Miura, S. Matsubara, Y. Miyasaka, and N. Shohata, Appl. Phys. Lett. **54**, 754 (1989).
[2] A. Mogro-Campero, Appl. Phys. Lett. **52**, 1185 (1988); A. Mogro-Campero, L. G. Turner, and G. Kendall, *ibid* **53**, 2566 (1988); A. Mogro-Campero, Supercond. Sci. Technol. **3**, 155 (1990).
[3] C. C. Chang, M. S. Hegde, X. D. Wu, B. Dutta, A. Inam, T. Venkatesan, B. J. Wilkens, and J. B. Wachtman, Jr., Appl. Phys. Lett. **55**, 1680 (1989).
[4] P. Berberich, J. Tate, W. Dietsche, and H. Kinder, Appl. Phys. Lett. **53**, 925 (1988).
[5] T. Asano, K. Tran, A. S. Byrne, M. M. Rahman, C. Y. Yang, and J. D. Reardon, Appl. Phys. Lett. **54**, 1275 (1989).
[6] G. Koren, E. Polturak, B. Fisher, D. Cohen, and G. Kimel, Appl. Phys. Lett. **53**, 2330 (1988).
[7] S. Witanachchi, S. Patel, H. S. Kwok, and D. T. Shaw, Appl. Phys. Lett. **54**, 578 (1989).
[8] D. B. Fenner, D. K. Fork, J. B. Boyce, G. A. N. Connell, and A. M. Viano, Physica C **162**, 141 (1989).
[9] D. B. Fenner, A. M. Viano, G. A. N. Connell, J. B. Boyce, D. K. Fork, F. A. Ponce, and J. C. Tramontana, in Mater. Res. Soc. Symp. Proc. **169**, 1005 (1990).
[10] Q. Y. Ma, E. S. Yang, and C-A. Chang, J. Appl. Phys. **66**, 1866 (1989).
[11] C. T. Cheung and E. Ruckenstein, J. Mater. Res. **4**, 1 (1989).
[12] H. Fukumoto, T. Imura, and Y. Osaka, Jpn. J. Appl. Phys. **27**, L1404 (1988).
[13] D. B. Fenner, D. K. Fork, G. A. N. Connell, J. B. Boyce, F. A. Ponce, J. C. Tramontana, A. M. Viano, and T. H. Geballe, Mater. Res. Soc. Symp. Proc. **191**, 187 (1990).
[14] D. K. Fork, D. B. Fenner, G. A. N. Connell, J. M. Phillips, and T. H. Geballe, Appl. Phys. Lett. **57**, 1137 (1990).
[15] D. K. Fork, D. B. Fenner, R. W. Barton, J. M. Phillips, G. A. N. Connell, J. B. Boyce, and T. H. Geballe, Appl. Phys. Lett. **57**, 1161 (1990).
[16] D. B. Fenner, D. K. Biegelsen, and R. D. Bringans, J. Appl. Phys. **66**, 419 (1989); D. B. Fenner, D. K. Biegelsen, R. D. Bringans, and B. S. Krusor, Mater. Res. Soc. Symp. Proc., edited by M. Kawabe, T. D. Sands, E. R. Weber, and R. S. Williams, **148**, 279 (1989).
[17] S. H. Wolff, S. Wagner, J. C. Bean, R. Hull, and J. M. Gibson, Appl. Phys. Lett. **55**, 2017 (1989).
[18] D. K. Fork, G. A. N. Connell, D. B. Fenner, J. B. Boyce, J. M. Phillips, and T. H. Geballe, *Proc. SERI Conf. Sci. Technol. Thin-Film Superconductors* (Plenum, New York, in press).
[19] J. B. Boyce, G. A. N. Connell, D. K. Fork, D. B. Fenner, K. Char, F. A. Ponce, F. Bridges, J. C. Tramontana, A. M. Viano, S. S. Laderman, R. C. Taber, S. Tahara, and T. H. Geballe, Soc. Photo-Opt. Instrum. Eng. Proc. **1187**, 136 (1990).
[20] Z. Shen, J. W. Allen, J. J. Yeh, J.-S. Kang, W. Ellis, W. Spicer, I. Lindau, M. B. Maple, Y. D. Dalichaouch, M. S. Torikachvili, J. Z. Sun, and T. H. Geballe, Phys. Rev. B **36**, 8414 (1987).
[21] A. Fujimori, E. Takayama-Muromachi, Y. Uchida, and B. Okai, Phys. Rev. B **35**, 8814 (1987); W. Herzog, M. Schwarz, H. Sixl, and R. Hoppe, Z. Phys. B **71**, 19 (1988).
[22] R. P. Vasquez, M. C. Foote, and B. D. Hunt, Appl. Phys. Lett. **55**, 1801 (1989); R. P. Vasquez, B. D. Hunt, and M. C. Foote, *ibid* **54**, 2373 (1989); *ibid* **53**, 2692 (1988).
[23] O. M. Bakunin, S. M. Klotsman, S. A. Matveev, and K. A. Stepanov, Appl. Phys. Lett. **55**, 78 (1989).
[24] A. Iqbal, C. W. Bates, and J. W. Allen, Appl. Phys. Lett. **47**, 1064 (1985).
[25] F. J. Grunthaner and P. J. Grunthaner, Mat. Sci. Rep. **1**, 65 (1986).
[26] C. S. Hurlbut and C. Klein, *Manual of Mineralogy*, 19th ed. (Wiley, New York, 1977), p. 349.
[27] P. Kulkarni, S. Mahamuni, M. Chandrachood, I. S. Mulla, A. P. B. Sinha, A. S. Nigavekar, and S. K. Kulharni, J. Appl. Phys. **67**, 3438 (1990).
[28] W. Carrillo-Cabrera, H-D. Wiemhofer, and W. Gopel, Solid State Ionics **32/33**, 1172 (1989).
[29] D. B. Fenner, G. A. N. Connell, D. K. Fork, J. B. Boyce, A. M. Viano, F. A. Ponce, and J. C. Tramontana, Bull. Am. Phys. Soc. **35**, 328 (1990).
[30] G. Lucovsky, S. S. Kim, D. V. Tsu, G. G. Fountain, and R. J. Markunas, J. Vac. Sci. Technol. B **7**, 861 (1989).
[31] D. M. Hwang, R. Ramesh, C. Y. Chen, X. D. Wu, A. Inam, M. S. Hegde, B. Wilkens, C. C. Chang, L. Nazar, T. Venkatesan, S. Miura, S. Matsubara, Y. Miyasaka, and N. Shohata, J. Appl. Phys. **68**, 1772 (1990).
[32] L. A. Tietz, C. B. Carter, D. K. Lathrop, S. E. Russek, R. A. Buhrman, and J. R. Michael, J. Mater. Res. **4**, 1072 (1989).

HIGH CRITICAL CURRENTS IN Y-Ba-Cu-O FILMS ON SILICON USING YSZ BUFFER LAYERS

D.B. FENNER *
XEROX, Palo Alto Research Center, Palo Alto, California 94304
Physics Dept., Santa Clara University, California 95053
D.K. FORK
XEROX, Palo Alto Research Center, Palo Alto, California 94304
Dept. of Applied Physics, Stanford University, Stanford, California 94305
G.A.N. CONNELL J.B. BOYCE
XEROX, Palo Alto Research Center, Palo Alto, California 94304
A.M. VIANO **
XEROX, Palo Alto Research Center, Palo Alto, California 94304
Physics Dept., Santa Clara University, California 95053
T.H. GEBALLE
Dept. of Applied Physics, Stanford University, Stanford, California 94305

Abstract

Exceptionally high quality films of $Y_1Ba_2Cu_3O_{7-x}$ (YBCO) were successfully grown epitaxially on Si(100) wafers with a buffer layer of yttria-stabilized zirconia (YSZ) using a fully *in-situ* pulsed laser deposition (PLD) process. Critical current densities of a 30-nm thick film are $2x10^7$ at 4.2 K and $2.2x10^6$ at 77 K. Zero-resistance critical temperatures are about 87 K, the transition width is 1 K, and normal-state resistivity is 0.28 mOhm-cm at 300 K. X-ray diffraction phi scans indicate in-plane epitaxial alignment within 1.0 and 2.0°, for the YSZ and YBCO respectively. Lattice constant and thermal expansion mismatches occur at both subsurface interfaces. This causes strain cracks to occur in YBCO films thicker than about 50 nm. The Si surface preparation utilizes an oxide etch and hydrogen termination that is an essential step in the process, as is careful control of the deposition environment temperature and oxygen pressure. Here we describe the crystallographic and chemical structure of the interfaces and their role in film formation. The crystal quality of YSZ buffer layers on Si is not degraded by decomposition reactions, as is YBCO directly on Si or SiO_2, and cube-on-cube orientation of the YSZ cubic fluorite on Si(100) surfaces can be made to occur very effectively.

* Present address: Advanced Fuel Research, East Hartford, Connecticut 06118.

** Present address: Physics Department, Washington University, St. Louis, Missouri 63130.

Manuscript received September 24, 1990.

Introduction

Since the discovery of superconductivity in copper oxide compounds there has been considerable speculation and many design proposals have been advanced for electronic devices that would combine conventional semiconductor materials with the new high-temperature superconductors (HTSC), especially in thin film form. Such proposed devices run the gamut of integration from mere bonding after formation of the materials, to monolithic integration of HTSC film devices onto semiconductor wafers containing conventional microelectronic circuits (e.g., VLSI CMOS), up to hybrid superconducting-semiconducting devices potentially capable of new functionalities. For the 92-K transition materials, such as $Y_1Ba_2Cu_3O_{7-x}$ (YBCO), it has been pointed out that operation at about 45 K is optimal for many applications of the superconductivity and at the same time would improve the performance of some important semiconducting devices and materials (e.g., GaAs).[1-3]

The synthesis of thin films of the HTSC materials on silicon, and occasionally gallium arsenide, wafers has been attempted by many research groups.[4-8] The (110) dimension of the Si(100) surface is well matched to the average ab-axis dimension of YBCO. Unfortunately, the superconducting performance of these films was invariably inferior to that of films on crystalline metal-oxide substrates, e.g., $SrTiO_3$, yttria-stabilized zirconia (YSZ), MgO, and even sapphire. Decomposition reactions of the YBCO in the presence of Si was identified as a prime problem,[6,9,10] however it was found that thicker films tend to out run the reacted region and form a moderate quality superconducting film nearer the surface.[11] Alternatively, buffer layers (e.g., YSZ)

0018-9464/91/0300-0958$01.00 © 1991 IEEE

can be used to prevent the reaction.[7,8] In the latter case, however, the superconducting quality of the (unreacted) film was still not exceptional (somewhat limited critical current density J_c).

We have recently reported substantial improvements in the quality of YBCO films formed on Si wafers as judged by the usual figures of merit, especially x-ray diffraction (XRD) and J_c.[12-15] The importance of crystalline microstructure in determining the superconducting quality of the new HTSC materials cannot be overemphasized, and indeed we believe this to be the central issue with YBCO and buffer-layer films on Si substrates.

Experimental

Pulsed laser deposition (PLD) was used exclusively to synthesize the thin films reported here. This technique, whereby composite stoichiometric oxide targets are ablated by a pulsed laser beam and allowed to deposit on a substrate, has rapidly gained recognition as one of the most effective methods of forming stoichiometric HTSC thin films *in-situ*, i.e., without a post-deposition annealing.[6,16] We have described our PLD system and methods of deposition in several previous publications.[9,10,12-15] The 308-nm excimer laser beam is focused to about 1 J/cm^2 on composite targets. For the buffer layer we have found that targets of pressed and sintered mixtures of yttria and zirconia powders, at 9 mole% yttria, produced the best films.

In order to obtain epitaxy on Si, the amorphous surface oxide film (SiO_2) must be removed and prevented from reforming. Here, the Si substrates were prepared by the little known, but simple and effective, technique of spin etching.[17] This process strips the surface oxide and hydrogen terminates the surface (i.e., Si:H). With this method, the commercial wafers are degreased with solvents, and etched with a solution of HF in ethanol while the wafer is spinning under a free flowing nitrogen stream. The Si surface is then exceptionally clean and passive to reoxidation and/or contamination. It is moved into the deposition chamber, evacuated, heated to 250°C for a few minutes to outgas, and then heated quickly to the desired temperature T for the first film (e.g., YSZ) deposition. By about 550°C all the H has evaporated from the surface.

Our best quality YBCO/YSZ/Si material is formed on the Si:H substrates using the following procedures. After the substrate reaches 800°C, laser pulsing is commenced immediately, about 100 pulses of YSZ film is deposited (0.02 nm per pulse), and then oxygen is introduced into the chamber to a pressure of 4×10^{-4} Torr. Deposition is continued until 50 nm of YSZ has accumulated. The substrate is allowed to cool to 750°C, the oxygen pressure is increased to 0.2 Torr, and the YBCO film deposited (typically 13 to 150 nm thick). The film is then cooled at its natural rate in 200-400 Torr of oxygen.

Results

Interface Chemistry

For information on interface chemistry we have deposited very thin YBCO films directly onto the Si:H substrates, and, for comparison, onto wafers prepared with a high quality (thermal) gate oxide film 15 nm thick (SiO_2/Si). Serious decomposition reactions of all these films were observed by x-ray photoelectron spectroscopy (XPS), as seen in Fig. 1.[18] By comparing with the various reference material spectra there, one can see that the Cu 2*p* and Ba $3d_{5/2}$ lines are substantially distorted for the thin films. The Cu, Ba and Y lines are all shifted to lower kinetic energy due to electrostatic charging of the decomposed and insulating films. Near the Y 3*d* line can be seen the Si 2*s* line with increasing intensity at higher deposition T, indicating increasing amounts of Si near the film surface.

In Fig. 2 are the Si 2*p* lines for the YBCO films of Fig. 1. For two of these films the samples were tilted in the spectrometer, which increases sensitivity to near-surface material. An intermediate-oxidation state Si, identified as a silicate, has formed in the decomposed material.[9,10,18] Very thin films of ZrO_2 and YSZ were deposited on SiO_2/Si and Si:H and the XPS spectra of Fig. 3 indicate no decomposition of these films. A detailed chemical analysis of all the very thin decomposed YBCO films found the presence of metal-silicate compounds and silica, but no silicides. These assignments were made primarily on the basis of observed photoelectron kinetic energy differences, which are summarized in Tab. 1.

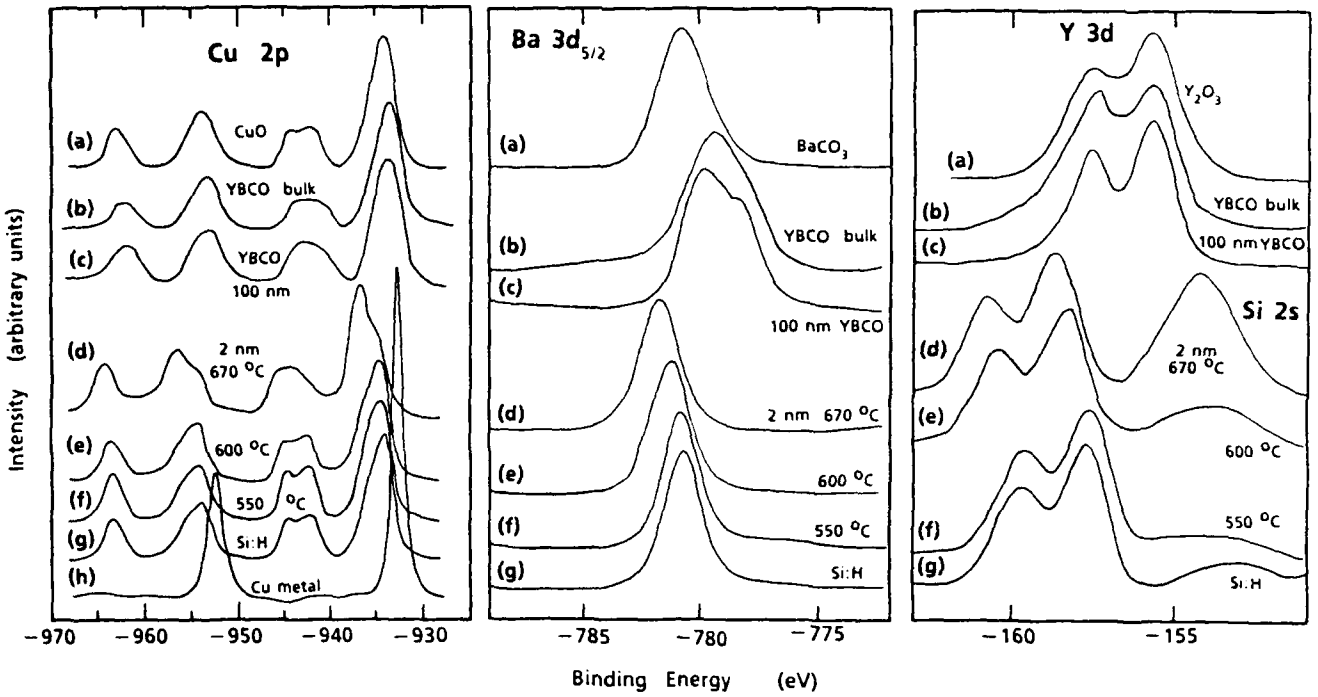

Figure 1. Core-level XPS data for Cu, Ba, Y, and Si. Spectra (a) and (b) in each panel are bulk reference samples, as described in Refs. 9, 10 and 18. Spectra (c)-(g) are from several thin YBCO films on Si wafers. The film thicknesses and deposition T are indicated. All Si substrates had the SiO_2 thermal oxide except the curves (g), labeled Si:H, which was H terminated.

Table 1. Photoelectron kinetic energy differences ΔE_k between components of the Si $2p$, O $1s$, and Zr $3d_{5/2}$ core-level lines from XPS measurements on various samples. A dash indicates the line was not present. The resolution was ± 0.1 eV.

Sample	ΔE_k (eV) Si$2p$-O$1s$	ΔE_k (eV) Zr$3d_{5/2}$-O$1s$
15 nm SiO_2 on Si	429.7	-
$ZrSiO_4$ powder	429.0	347.1
ZrO_2 powder	-	348.2
YSZ crystal	-	347.8
2 nm YBCO/Si:H	428.6	-
3 nm $ZrO_2/SiO_2/Si$	429.6	347.8
4 nm YSZ/Si:H	429.8	347.9
8 nm YSZ/Si:H	429.5[a]	347.8

[a] Weak O $1s$ line component with ± 0.5 eV resolution.

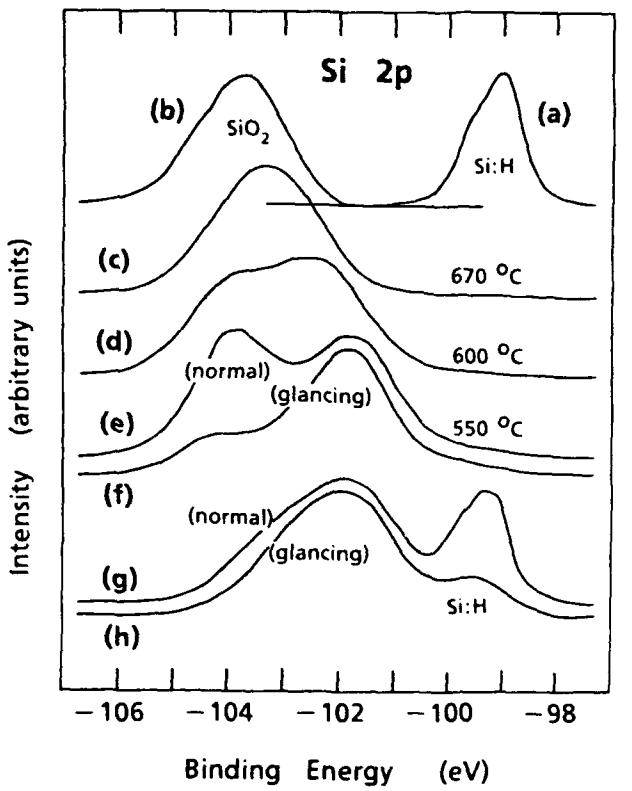

Figure 2. Silicon core level $2p$ spectra. Curves (a) and (b) are the surfaces of H-terminated Si and thermal oxide (SiO_2) film on Si. Spectra (c)-(h) are from the thin YBCO films, as in Fig. 1.

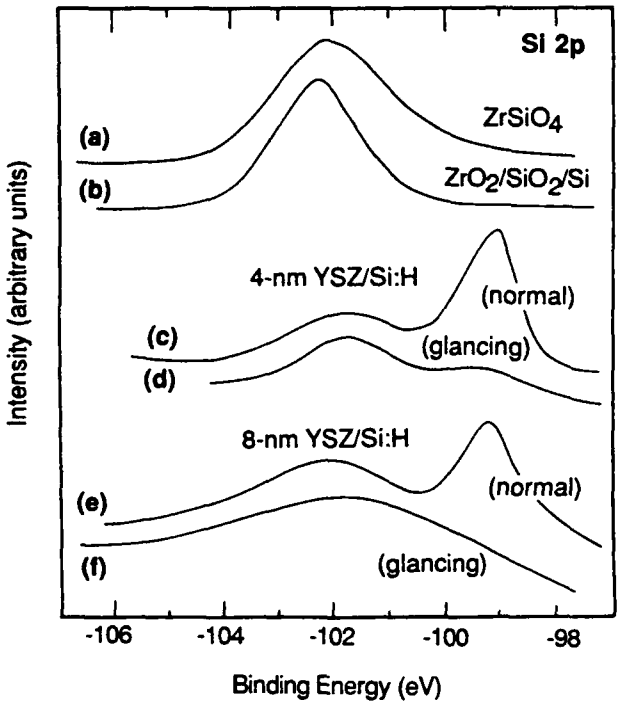

Figure 3. Silicon core level 2*p* spectra. Curve (a) is bulk material for reference, and (b)-(f) are thin films. The ZrO_2 film, curve (b), was 4 nm thick and deposited at 670°C on SiO_2/Si. The two YSZ films were deposited on Si:H at 800°C in $4x10^{-4}$ Torr of O_2.

Transmission electron microscopy (TEM) of cross sections of 50-nm thick YSZ films on the Si:H substrates showed nearly atomically abrupt interfaces with the Si and YSZ, as can be seen in Fig. 4. However, YSZ films on SiO_2/Si substrates were roughened, indicating degradation.[9,10] In addition, all of these cross-sectioned samples showed an amorphous silica layer between the YSZ and crystalline Si substrate. We have reported that this oxide regrows at the (subsurface) YSZ/Si interface during film deposition, due to the high $O^=$ ion conductivity of YSZ and YBCO at elevated T.[18,19] Interestingly, its growth saturates (at about 4-5 nm thickness), and since it is absent at the initiation of YSZ film growth, the deposited YSZ can grow epitaxially based on the initially available substrate template.

Figure 4. TEM cross section micrograph of a YSZ film deposited on Si(100) which had been prepared by H termination. From Refs. 10 and 18.

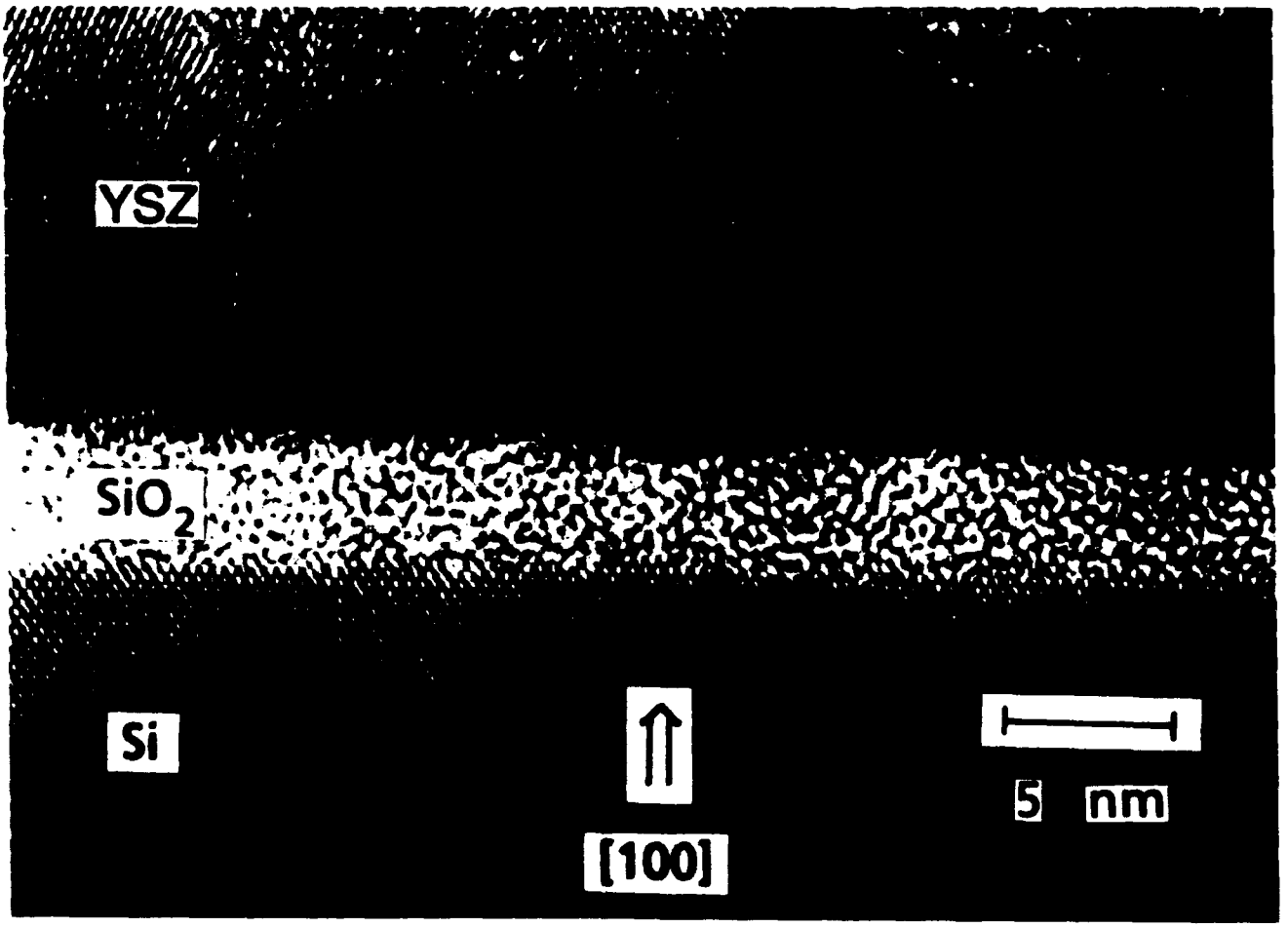

Interface Structure

Zirconia (ZrO_2) is polymorphic, but with 4-40 mole% yttria content the cubic fluorite structure is stabilized (YSZ). Two epitaxial orientations on Si have been demonstrated with thin films.[14,20] Our (9 mole%) YSZ films have the fully parallel (cube-on-cube) orientation with 5-6% lattice mismatch (YSZ smaller) to the (100) oriented Si substrate. Crystallographic compatibility of the (100) faces of the Si diamond lattice and the YSZ fluorite lattice is possible. We suggest that initially the interface Zr and Y atoms deviate from their usual 8-fold coordination to 6-fold with a silicide-like interface bond to the Si. This ideal scheme is illustrated by the model in Fig. 5. There the YBCO is shown epitaxially on the YSZ with a 45° rotation in the interface plane. In reality, this interface is also mismatched: by 5%, with the YSZ smaller.

XRD analysis of our YSZ films on Si:H and YBCO films on YSZ/Si:H indicate a high degree of epitaxial orientation with the directions shown in the model of Fig. 5. The two-theta scan for a typical YSZ film is shown in Fig. 6, where the 140-nm thick film has clearly relaxed to its bulk lattice constant.[12] The omega rocking curves for the YSZ[200] peak were about 0.7° FWHM. The deposition T and oxygen pressure were varied systematically and subsequent XRD indicated that the best conditions are those described above. An especially sensitive test of epitaxial quality for these films was XRD phi scans of the YSZ [202] peak. Clearly, from Fig. 7 these films show excellent in-plane epitaxial alignment with the Si substrate. The scattered intensity is shown on a log scale, and the flatness of the regions between the 4-fold rotationally symmetric peaks and near absence of side wings on the

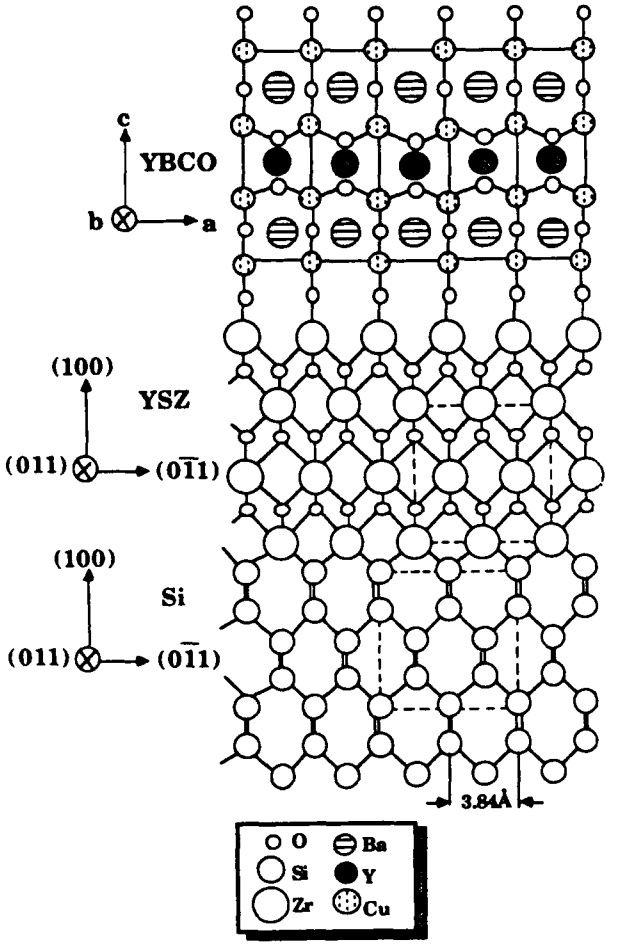

Figure 5. Ball and stick model for the ideal epitaxial YBCO film on YSZ film on a Si crystal. A cross section, through an (011) plane, is shown with the original Si free surface (100) direction upward, as indicated. The diamond and cubic-fluorite unit cells are indicated by dotted lines within the Si and YSZ lattice.

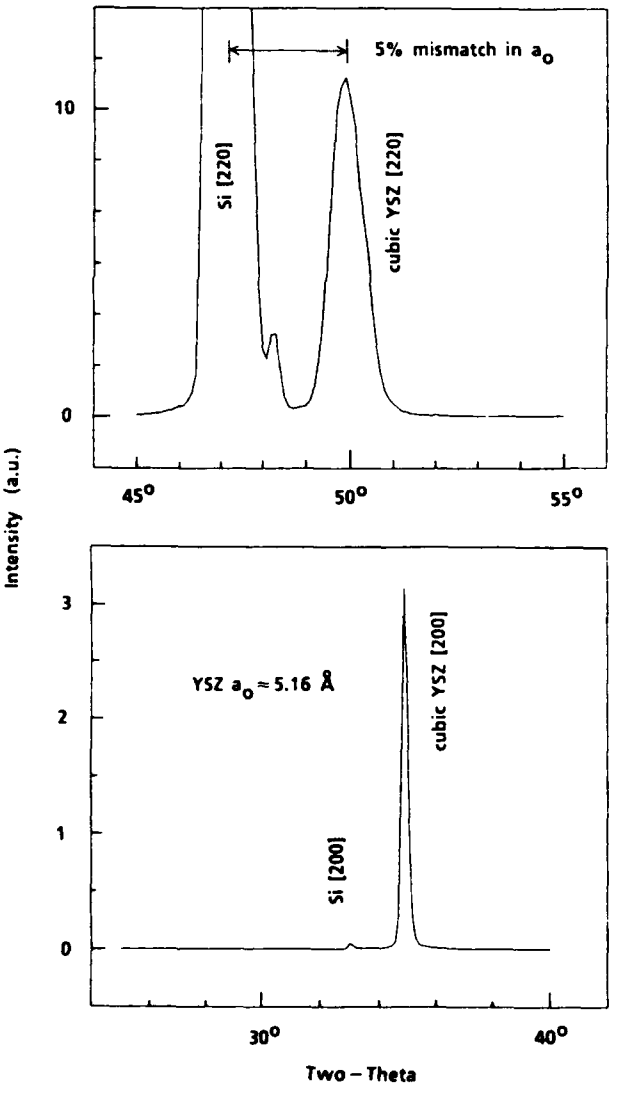

Figure 6. XRD two-theta scans of a YSZ film on Si:H. The YSZ was deposited under optimized conditions. Peak identifications are noted.

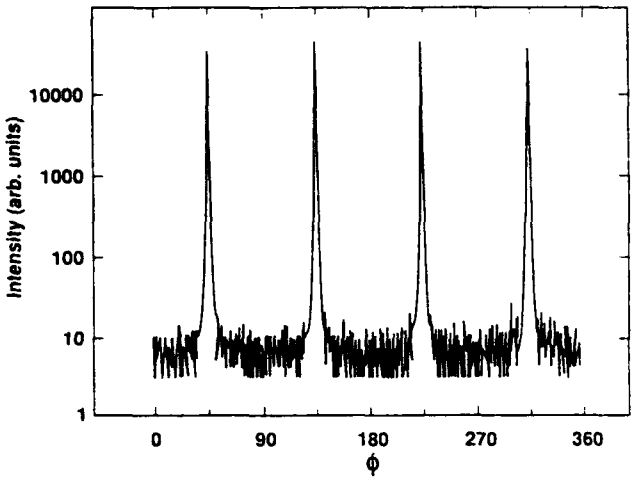

Figure 7. XRD phi scan of the YSZ (202) peak for an optimized YSZ film on Si:H. The phi (in-plane) orientation of 45° corresponds with the substrate Si [101] direction.

peaks indicates nearly single-crystal quality. We have also reported Rutherford backscattering spectroscopy (RBS) of these YSZ films which indicated channeling minimum yields of about 5% for the (Zr,Y) peak.[14]

Optimized films of YBCO on YSZ buffered Si:H were analyzed by XRD and RBS, and the YBCO films were found to be of excellent structural quality.[15] This has occurred despite the crystallographic and dimensional mismatches of the YBCO and YSZ. As in Fig. 6, the YSZ buffer films are relaxed to their bulk lattice dimensions since they are intrinsically materials of high yield strength (and elastic modulus). Indeed, for very thin (13 nm), high J_c YBCO films on YSZ/Si, we found the c-axis length shortened by 0.4%, indicating (unrelaxed) tensional strain. The YBCO films begin to relax at about 50 nm thickness causing cracks, which are visible after weak etching in a solution of Br in methanol.[15] The data are consistent with the following scenario: during deposition at 750°C, the growing YBCO lattice accommodates its mismatch to the YSZ by interface misfit dislocations, then during the cool down after growth the fully-formed thicker films are unable to accommodate the induced mismatch due to the differences in thermal expansion coefficients between the YBCO, YSZ, and Si. This scenario is also consistent with recent reports on interfaces between YBCO and MgO, an epitaxial system with even greater mismatch, that can nevertheless be controlled to produce high J_c YBCO films.[21]

Discussion

As with all forms of epitaxy, the growth of high quality YSZ buffer films on Si requires control of, and at least a conceptual understanding of, the mechanisms and synthesis conditions for both the heteroepitaxial nucleation and the subsequent homoepitaxial film thickening growth regimes. Growing a crystallized oxide compound onto a Si wafer presents special challenges, especially the need to deposit at elevated T (to have film crystallization) and to have oxygen available (for incorporation into the film oxide) but executed in such a fashion as to not excessively oxidize the Si (since that oxide [SiO_2] is amorphous).

Our nucleation tactic has been to initiate deposition on the hot Si surface (freshly relieved of its H termination) in the base pressure of the vacuum system, i.e., in a reducing atmosphere. Fortunately the heats of formation (per cation) of ZrO_2 and Y_2O_3, and hence YSZ, are somewhat larger than that of SiO_2. Thus, the regrowth of SiO_2 on the Si can be limited, even at equilibrium, during the early stages of growth, as the XPS data of very thin YSZ films indicate, Fig. 3. This is sufficient to allow epitaxy to initiate, as indicated by the XRD, Figs. 6 and 7. Growth of YSZ films thicker than a few unit cells cannot occur in the reducing environment without forming an oxygen deficient material that is highly defective.[22] Likewise too oxidizing a deposition environment is detrimental to the YSZ film, as we have empirically determined.[14] The need for careful and systematic optimization of thermodynamic and chemical growth conditions is evident.

Conclusions

Epitaxial films of YSZ have been grown on Si substrates using PLD. These films have served as excellent buffer layers for subsequent films of YBCO. The requirements for epitaxy of the YSZ are: (1) SiO_2 at the Si interface be limited by both an oxide strip and surface passivation with H prior to film deposition, (2) film nucleation be done in high vacuum, (3) followed by deposition of the YSZ in as low an oxygen pressure as is consistent with stability of the growing film. The YBCO films were also expitaxial and carried high current densities.

Improvements in film quality and potential for applicability will occur when solutions are found to the lattice and thermal expansion mismatch problems. This will allow thicker films without cracking and raising the T_c and J_c figures of merit. Further improvement is needed in the film surface morphology, reduction in density of near-micron sized fragment asperities and pinholes. The latter occur at low, but worrysome, density in the YSZ films. At present, the pinholes cause localized reaction of the Si with the YBCO leaving small insulating spots. The pinholes will also allow Cu to enter the Si substrate where it will diffuse over large distances deteriorating the semiconductor device quality. Other buffer layer materials, in addition to YSZ, together with procedures from their synthesis into high quality crystalline films, are also needed. Despite these current problems, the YBCO/YSZ/Si system we have demonstrated opens the door for many envisioned applications of HTSC thin films on semiconductor substrates or films.

Acknowledgments

DBF and AMV were supported by NSF (DMR-8822353), DKF is an AT&T scholar, additional support came from Air Force OSR (F49620-89-C-0017).

References

1. T. Van Duzer, "Superconductor-Semiconductor Hybrid Devices, Circuits and Systems", *Cryogenics*, 28, 527-531, 1988.

2. H. Kroger, C. Hilbert, D.A. Gibson, U. Ghoshal, and L.N. Smith, "Superconductor-Semiconductor Hybrid Devices, Circuits, and Systems", *Proc. IEEE*, 77, 1287-1301, 1989.

3. J.P. Krusius and W.E. Pence, "Potential of Low Temperature CMOS With Normal and Superconductive Interconnect", *Proc. Sixth IEEE VLSI Multilevel Interconnection Conf.*, 233-240, 1989.

4. A. Mogro-Campero, L.G. Turner, E.L. Hall, and M.C. Burrell, "Characterization of Thin Films of Y-Ba-Cu-O on Oxidized Silicon With a Zirconia Buffer Film", *Appl. Phys. Lett.*, 52, 2068-2070, 1988.

5. A. Mogro-Campero, L.G. Turner and G. Kendall, "Thickness and Annealing Dependence of the Superconducting Transition Temperature of Y1Ba2Cu3O7-x Thin Films On Oxidized Silicon and Polycrystalline Alumina Substrates", *Appl. Phys. Lett.*, 53, 2566-2568, 1988.

6. T. Venkatesan, E.W. Chase, X.D. Wu, A. Inam, C.C. Chang, and F.K. Shokoohi, "Superconducting $Y_1Ba_2Cu_3O_{7-x}$ Films on Si", *Appl. Phys. Lett.*, 53, 243-245 1988.

7. X.D. Wu, A. Inam, M.S. Hegde, B. Wilkens, C.C. Chang, D.M. Hwang, L. Nazar, T. Venkatesan, S. Miura, S. Matsubara, Y. Miyasaka, and N. Shohata, "High Critical Currents In Epitaxial $YBa_2Cu_3O_{7-x}$ Thin Films On Silicon With Buffer Layers", *Appl. Phys. Lett.*, 54, 754-756, 1989.

8. D.M. Hwang, R. Ramesh, C.Y. Chen, X.D. Wu, A. Inam, M.S. Hegde, B. Wilkens, C.C. Chang, L. Nazar, T. Venkatesan, S. Miura, S. Matsubara, Y. Miyasaka, and N. Shohata, "Epitaxial Relations Between In Situ Superconducting $Y_1Ba_2Cu_3O_{7-x}$ Thin Films and $BaTiO_3/MgAl_2O_4/Si$ Substrates", *J. Appl. Phys.*, 68, 1772-1786, 1990.

9. D.B. Fenner, D.K. Fork, J.B. Boyce, G.A.N. Connell, and A.M. Viano, "Deposition and Characterization of Y-Ba-Cu-O Thin Films on Silicon Substrates: Interface Analysis", Inter. Conf. Materials and Mechanisms of Superconductivity, in *Physica C*, edited by N.E. Phillips, R.N. Shelton, and W.A. Harrison, 162, 141-142, 1989.

10. D.B. Fenner, A.M. Viano, G.A.N. Connell, J.B. Boyce, D.K. Fork, F.A. Ponce, and J.C. Tramontana, "XPS Analysis of Y-Ba-Cu-O and Zr-O Thin Films and Interfaces With Silicon Substrates", in *Mater. Res. Soc. Symp. Proc.*, edited by J. Narayan, P. Chu, L. Schneemeyer, and D. Christen, Vol. 169 (in press).

11. P. Berberich, J. Tate, W. Dietsche, and H. Kinder, "Low Temperature Preparation of Superconducting $Y_1Ba_2Cu_3O_{7-x}$ Films On Si, MgO, and $SrTiO_3$ By Thermal Coevaporation", *Appl. Phys. Lett.*, 53, 925-926, 1988.

12. D.B. Fenner, D.K. Fork, G.A.N. Connell, J.B. Boyce, F.A. Ponce, J.C. Tramontana, A.M. Viano, and T.H. Geballe, "Heteroepitaxial Metal Oxides On Silicon By Laser Ablation", in *Mater. Res. Soc. Symp. Proc.*, edited by D.C. Paine and J.C.Bravman, Vol 191 (in press).

13. D.K. Fork, G.A.N. Connell, D.B. Fenner, J.B. Boyce, J.M. Phillips, and T.H. Geballe, "YBCO Films and YSZ Buffer Layers Grown In Situ on Silicon By Pulsed Laser Deposition", *Conf. on Sci. Technol. Thin-Film Superconductors* (SERI), Denver, 1990 (in press).

14. D.K. Fork, D.B. Fenner, G.A.N. Connell, J.M. Phillips, and T.H. Geballe, "Epitaxial Yttria-Stabilized Zirconia on Hydrogen Terminated Si By Pulsed Laser Deposition", *Appl. Phys. Lett.*, 57, 1137-1139 (1990).

15. D.K. Fork, D.B. Fenner, R.W. Barton, J.M. Phillips, G.A.N. Connell, J.B. Boyce, and T.H. Geballe, "High Critical Currents in Strained Epitaxial $Y_1Ba_2Cu_3O_{7-x}$ On Si", *Appl. Phys. Lett.*, 57, 1161-1163 (1990).

16. R.K. Singh, O.W. Holland, and J. Narayan, "Theoretical Model For Deposition of Superconducting Thin Films Using Pulsed Laser Evaporation Technique", *J. Appl. Phys.*, 68, 233-247, 1990.

17. D.B. Fenner, D.K. Biegelsen, and R.D. Bringans, "Silicon Surface Passivation By Hydrogen Termination: A Comparative Study Of Preparation Methods", *J. Appl.*

Phys., 66, 419-424, 1989. D.B. Fenner, D.K. Biegelsen, R.D. Bringans, and B.S. Krusor, "Silicon Surface Passivation For Heteroepitaxy By Hydrogen Termination", *Mater. Res. Soc. Symp. Proc.*, edited by M. Kawabe, T.D. Sands, E.R. Weber, and R.S. Williams, 148, 279-284, 1989.

18. D.B. Fenner, A.M. Viano, D.K. Fork, G.A.N. Connell, J.B. Boyce, F.A. Ponce and J.C. Tramontana, "Reactions At The Interfaces of Thin Films of Y-Ba-Cu- and Zr-Oxides With Si Substrates", submitted for publication.

19. D.B. Fenner, G.A.N. Connell, D.K. Fork, J.B. Boyce, A.M. Viano, F.A. Ponce and J.C. Tramontana, "Reoxidation At The Interfaces of Thin Films of ZrO_2 With Hydrogen-Terminated Si Surfaces", *Bull. Amer. Phys. Soc.*, 35, 328, 1990.

20. H. Fukumoto, T. Imura, and Y. Osaka, "Heteroepitaxial Growth of Yttria-Stabilized Zirconia (YSZ) on Silicon", *Jpn. J. Appl. Phys.*, 27, L1404-1405, 1988.

21. R. Ramesh, D.M. Hwang, T.S. Ravi, A. Inam, J.B. Barner, L. Nazar, S.W. Chan, C.Y. Chen, B. Dutta, T. Venkatesan, and X.D. Wu, "Epitaxy of Y-Ba-Cu-O Thin Films Grown On Single-Crystal MgO", *Appl. Phys. Lett.*, 56, 2243-2245, 1990.

22. A.S. Kao and C. Hwang, "Microstructure of Yttria-Stabilized Zirconia Overcoats For Thin Film Recording Media", *J. Vac. Sci. Technol.* A8, 3289-3294 (1990).

High critical currents in strained epitaxial $YBa_2Cu_3O_{7-\delta}$ on Si

D. K. Fork
Xerox Palo Alto Research Center, Palo Alto, California 94304 and Department of Applied Physics, Stanford University, Stanford, California 94305

D. B. Fenner[a)]
Xerox Palo Alto Research Center, Palo Alto, California 94304 and Physics Department, Santa Clara University, Santa Clara, California 95053

R. W. Barton
Conductus, Inc., Sunnyvale, California 94086

Julia M. Phillips
AT&T Bell Laboratories, Murray Hill, New Jersey 07974

G. A. N. Connell and J. B. Boyce
Xerox Palo Alto Research Center, Palo Alto, California 94304

T. H. Geballe
Department of Applied Physics, Stanford University, Stanford, California 94305

(Received 21 May 1990; accepted for publication 11 July 1990)

Epitaxial $YBa_2Cu_3O_{7-\delta}$ (YBCO) films were grown on Si (100) using an intermediate buffer layer of yttria-stabilized zirconia. Both layers are grown via an entirely *in situ* process by pulsed laser deposition. All films consist of *c*-axis oriented grains as measured by x-ray diffraction. Strain results from the large difference in thermal expansion coefficients between Si and YBCO. Thin (<500 Å) YBCO films are unrelaxed and under tensile strain with a distorted unit cell. Rutherford backscattering spectroscopy indicates a high degree of crystalline perfection with a channeling minimum yield for Ba as low as 12%. The normal-state resistivity is 280 $\mu\Omega$ cm at 300 K; the critical temperature T_c ($R=0$) is 86–88 K with a transition width (ΔT_c) of 1 K. Critical current densities of 2×10^7 A/cm^2 at 4.2 K and 2.2×10^6 A/cm^2 at 77 K have been achieved.

Successful growth of the high-temperature superconductors (HTSCs) on Si has been slowed by several fundamental problems. A feature precluding the growth of HTSC directly on Si is the substrate reaction,[1] which is damaging even at temperatures as low as 550 °C.[2] This problem has been addressed with little success by growing thick films, and with improved success by introducing buffer layers. A recent review of past efforts to grow HTSC films on Si is contained in Ref. 3. The necessity of epitaxy for high quality films[4] has made it essential to develop techniques for growing epitaxial buffer layers. Epitaxial oxides appear currently to have the advantage over fluorides, silicides, and metals. A desirable feature of buffer layer growth is compatibility with techniques already developed for HTSC film growth, hence the ability to fabricate high quality films on Si in a single process step. In this letter we report a technique which incorporates all of these features for the first time; we have chosen yttria-stabilized zirconia (YSZ) as our epitaxial buffer layer. Finally, the problem of thermal mismatch must be assessed; the thermal expansion constants of Si, YSZ, and $YBa_2Cu_3O_{7-\delta}$ (YBCO) are 3.8×10^{-6} °C^{-1}, 11.4×10^{-6} °C^{-1}, and 13×10^{-6} °C^{-1}, respectively, indicating that an ~0.7% strain is incorporated at room temperature after growth. Our preliminary results on the elastic limits of YBCO films on YSZ/Si will be presented.

Our laser deposition technique appears in Ref. 5. Hydrogen-terminated Si wafers enter our chamber through a N_2 purged glove box. YSZ and YBCO targets, mounted on a rotating polygon within a water-cooled shroud, are ablated at an energy density of 1.3 J/cm^2 using 130 mJ, 308 nm wavelength pulses. The Si substrates are heated radiantly and temperature is determined by pyrometry. At a target-substrate distance of 5 cm, each 17 ns laser pulse deposits about 0.2 Å of either YBCO or YSZ. The laser is fired at 8–10 Hz.

The Si wafers undergo degreasing followed by spin etching in a flowing N_2 hood; this technique is a variation of Ref. 6. The Si wafer is rotated, flushed with high-purity alcohol, and etched with several drops of a 1:10:1 mixture of HF, ethanol, and water, all of high purity. This process produces an oxide-free wafer covered by one monolayer of hydrogen which is passive to the effects of brief exposure to room air.[7] Using a recently developed procedure[8] we deposit a 500 Å epitaxial YSZ layer at 800 °C in 4×10^{-4} Torr O_2 followed immediately by a variable thickness YBCO film grown at 750 °C in 200 mTorr O_2.

All films were characterized by x-ray diffraction on a four-circle diffractometer with a Cu K_α source. Figure 1 shows a 2θ scan of a 1350-Å-thick film with a 500-Å-thick YSZ buffer layer. One observes only *c*-axis YBCO peaks, and the YSZ (002) and Si (004) peaks. The ω-rocking curve widths of the YBCO (005) peak, which characterize the tilt of the *c*-axis grains, fall in the range from 0.6° to

[a)]Now at Advanced Fuel Research, East Hartford, CT 06118.

 0003-6951/90/371161-03$02.00

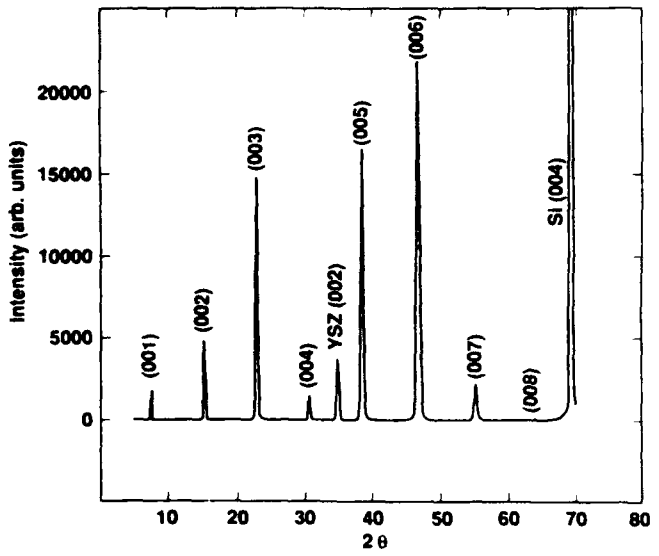

FIG. 1. c-axis scan of a 1350 Å YBCO film with a 500 Å YSZ buffer layer grown on Si (100). The YBCO (005) peak has a rocking curve full width at half maximum of 0.6°.

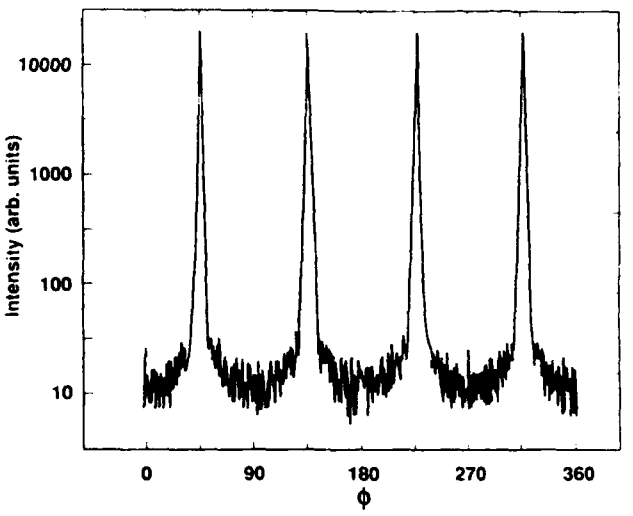

FIG. 2. ϕ scan of the {103} family of peaks of a 1350-Å-thick YBCO film with a 500 Å YSZ buffer layer on Si (100). The peaks every 90° reveal in-plane epitaxial alignment of the YBCO to ~2.0°.

1.0°. This compares favorably to the value of $<0.65°$ obtained for epitaxial YBCO films grown by pulsed laser deposition (PLD) on $SrTiO_3$.[9]

To determine the thermally induced strain on these films, least-squares refinement was performed on diffraction data gathered from an automated search of 25 *hkl* reflections. This allowed us to accurately determine the *c* lattice constant, and the *ab* average lattice constant. Our results have an uncertainty of less than 0.015 Å. Films more than 1300 Å thick have lattice constants typical[10] of bulk YBCO at room temperature, whereas thinner, unrelaxed films, exhibit the effect of tensile strain in the *ab* plane. In such films, the *c* axis is contracted, while the *a* and *b* axes are expanded. Data for two films, as well as parameters of bulk YBCO, are listed in Table I. A strain ϵ_{ab} of $(0.41 \pm 0.20)\%$ is indicated with respect to the bulk value for the 130 Å film, which has an unusually short *c* axis (compare Ref. 11). The relaxation of these films begins to occur at ~500 Å, as evidenced by cracks occurring at ~1 μm intervals along ⟨100⟩ directions. These cracks are visible by scanning electron microscopy after etching in 0.5% Br in methanol. These features can be completely obscured prior to etching.

In-plane film texturing and twist misalignment was determined from phi scans of the YBCO {103} peaks with the phi rotation axis parallel to the YBCO *c* axis. Figure 2 shows a log-linear plot of the phi scan obtained for a 1300 Å YBCO film grown on a 500 Å YSZ buffer layer. Zero degrees phi in this figure was obtained by aligning the Si (101) reflection, which clearly shows that the YBCO unit cell is rotated 45° in plane with respect to the Si. Peaks occur every 90°, showing that no additional in-plane YBCO orientations occur, unlike films we produced earlier on single-crystal YSZ substrates.[12] Multiple in-plane orientations are undesirable due to the potential disruption of current flow. The (103) peak widths in phi across a sampling of ten films fell between 2.0 and 2.5°; this is only slightly larger than the texturing observed for our YSZ films on Si.[8] Our resolution in ϕ as measured on the Si (202) peak is 0.57°.

TABLE I. Lattice parameters for strained and relaxed YBCO films and bulk YBCO.

Thickness (Å)	*ab* average (Å)	*c* (Å)	Cell volume (Å^3)
130	3.872 ± 0.005	11.629 ± 0.011	174.3 ± 0.5
1400	3.859 ± 0.006	11.664 ± 0.014	173.7 ± 0.6
Bulk powder[a]	3.856	11.678	173.6

[a]Data taken from Ref. 10.

Rutherford backscatter spectra along aligned ⟨001⟩ and random directions were taken using 1.8 MeV $^4He^+$ ions to determine crystalline quality, and characterize strain relaxation. Figure 3 shows aligned and random backscatter spectra for a 1350 Å YBCO film grown on a 500 Å YSZ buffer layer. The ratio of the backscattered yield along ⟨001⟩ to that in a random direction (χ_{min}) for Ba is 12%. This is substantially better than the best previously published value for YBCO on Si of 50%.[4] The best YBCO films on more conventional substrates[13] have χ_{min} as low as 2–3%, equal to that for single crystals.[14] The values of χ_{min} for YSZ and Si change dramatically with YBCO thickness.[15] For the elastically strained 130 Å YBCO film in Table I, the χ_{min} values for YSZ and Si were 22 and 46%. In contrast, the 1350 Å YBCO film in Fig. 3 had χ_{min} of 67 and 77% for YSZ and Si. It appears that the strain relaxation we see by x-ray diffraction in thicker films produces a channeling discontinuity in the epitaxy at the interface.

Figure 4 shows a resistivity versus temperature plot for a YBCO film grown on Si. The transition temperature (zero resistance) is 86 K, and the transition width is 1 K. The transition is somewhat lower and broader than our films on single crystal $LaAlO_3$, however, the normal-state resistance is ~280 $\mu\Omega$ cm at 300 K, which is typical of films grown on conventional substrates. The extrapolated

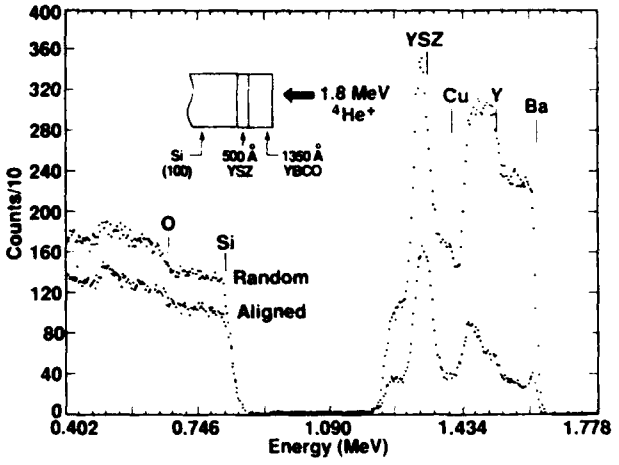

FIG. 3. Energy spectra of ⟨001⟩ aligned and random 1.8 MeV $^4He+$ ions backscattered from a 1400 Å YBCO film with a 500-Å-thick buffer layer on Si. The channeling minimum yield is 12%. The YSZ and Cu peaks overlap.

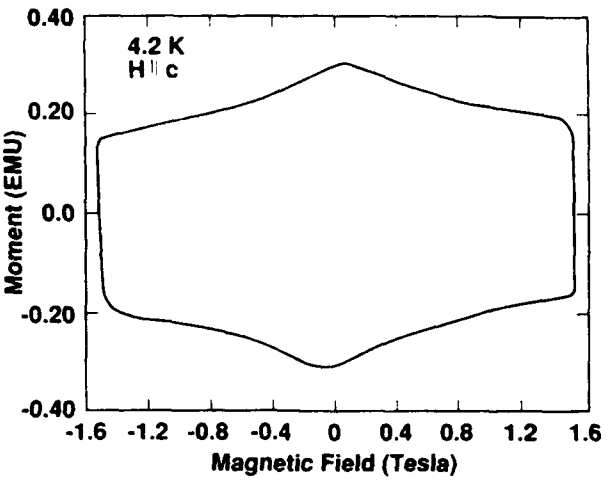

FIG. 5. Magnetization hysteresis loop of a 6 mm × 6 mm × 400 Å YBCO/YSZ/Si film at 4.2 K indicating J_c of 2×10^7 A/cm^2.

resistance curve crosses the positive side of the temperature axis, which is not typically observed in the 1-2-3 system. We conjecture that this may be the influence of strain on the normal-state properties.

Critical currents (J_c) in these films were measured by transport and vibrating sample magnetometry. A magnetization hysteresis loop for a 400 Å film is shown in Fig. 5. The J_c at 4.2 K in zero field as determined using the Bean critical state model[16] is 2×10^7 A/cm^2. The field dependence is similar to that of films of $LaAlO_3$; J_c is reduced by a factor of 1.7 at 1.5 T. Transport J_c at 77 K was measured on a 60-μm-wide excimer-laser-patterned strip. The J_c of a 305 Å film was 2.2×10^6 A/cm^2 based on a voltage criterion of 1 μV/mm. These values are $\sim2\times$ lower than those for epitaxial films on $LaAlO_3$, but are the highest currently reported on Si substrates. The development of cracks in films thicker than 500 Å degrades J_c; at 1300 Å J_c drops to 1.0×10^5 A/cm^2 at 77K.

In summary, epitaxial YBCO films have been grown on Si (100) by PLD via a single *in situ* process. This work has brought the YBCO film quality on Si close to that of YBCO films grown on other, more conventional substrates. These films are suitable for a variety of device applications, including infrared bolometers, and this development enjoys compatibility with Si processing technology. Continued work and aimed at concentrating strain relief in the buffer layer should extend the thickness limitation.

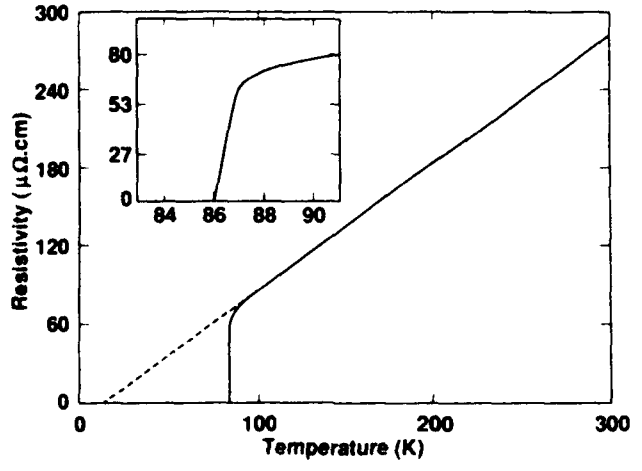

FIG. 4. Resistivity vs temperature data for a 500 Å YBCO film on YSZ on Si.

We thank Bruce Lairson for help obtaining J_c data, Richard Johnson, Steve Ready, and Lars-Erik Schwartz for technical assistance, and Don Beard and Robert Sparks of Sieman's Analytical X-ray Inc. for the single-crystal data acquisition capability. This work benefits from AFOSR (F49620-89-C-0017). DBF received support from NSF (DMR-8822353). DKF is an AT&T scholar.

[1] T. Komatsu, O. Tanaka, K. Matusita, M. Takata, and T. Yamashita, Jpn. J. Appl. Phys. **27**, L1025 (1988).
[2] D. B. Fenner, A. M. Viano, G. A. N. Connell, D. K. Fork, J. B. Boyce, F. A. Ponce, and J. C. Tramontana (unpublished).
[3] A. Mogro-Campero, Supercond. Sci. Technol. **3**, 155 (1990).
[4] X. D. Wu, A. Inam, M. S. Hegde, B. Wilkins, C. C. Chang, D. M. Hwang, L. Nazar, T. Venkatesan, S. Miura, S. Matsubara, Y. Miyasaka, and N. Shohata, Appl. Phys. Lett. **54**, 754 (1989).
[5] D. K. Fork, J. B. Boyce, F. A. Ponce, R. I. Johnson, G. B. Anderson, G. A. N. Connell, C. B. Eom, and T. H. Geballe, Appl. Phys. Lett. **53**, 337 (1988).
[6] F. J. Grunthaner and P. J. Grunthaner, Mater. Sci. Rep. **1**, 65 (1986).
[7] D. B. Fenner, D. K. Biegelsen, and R. D. Bringans, J. Appl. Phys. **66**, 419 (1989).
[8] D. K. Fork, D. B. Fenner, G. A. N. Connell, Julia M. Phillips, and T. H. Geballe, Appl. Phys. Lett. **57**, 1137 (1990).
[9] B. Roas, G. Endres, and L. Shultz, Appl. Phys. Lett. **53**, 1557 (1988).
[10] J. D. Jorgensen, M. A. Beno, D. G. Hinks, L. Soderholm, K. J. Volin, R. L. Hitterman, J. D. Grace, Ivan K. Schuller, C. U. Segre, K. Zhang, and M. S. Kleefisch, Phys. Rev. B **36**, 3608 (1987).
[11] C. B. Eom, J. Z. Sun, K. Yamamoto, A. F. Marshall, K. E. Luther, T. H. Geballe, and S. S. Laderman, Appl. Phys. Lett. **55**, 595 (1989).
[12] D. K. Fork, K. Char, F. Bridges, S. Tahara, B. Lairson, J. B. Boyce, G. A. N. Connell, and T. H. Geballe, Physica C **162–164**, 121 (1989).
[13] X. D. Wu, R. E. Muenchausen, S. Foltyn, R. C. Estler, R. C. Dye, C. Flamme, N. S. Nogar, A. R. Garcia, J. Martin, and J. Tesner, Appl. Phys. Lett. **56**, 1481 (1990).
[14] N. G. Stoffel, P. A. Morris, W. A. Bonner, and B. J. Wilkins, Phys. Rev. B **37**, 2297 (1988).
[15] We ordinarily expect a χ_{min} of 5–6% for YSZ films on Si with no epitaxial overlayer.
[16] C. P. Bean, Phys. Rev. Lett. **8**, 250 (1962).

1989 Fall Meeting-Symposium M
High Temperature Superconductors
GROWTH AND PROPERTIES OF EPITAXIAL $YBa_2Cu_3O_7$ THIN FILMS ON $\{1\underline{1}02\}Al_2O_3$

D. K. Fork*, T. H. Geballe*, K. Char**, S. S. Laderman*** and R. Taber***,
F. Bridges****, F. Ponce*****, J. B. Boyce*****, and G. A. N. Connel*****

* Dept. of Applied Physics, Stanford University, Stanford, CA 94305
** Conductus, Inc., Sunnyvale, CA 94086
*** Circuit Technology R&D, Hewlett-Packard Company, Palo Alto, CA 94304
**** Dept. of Physics, University of California, Santa Cruz, CA
***** Xerox Palo Alto Research Center, Palo Alto, CA 94304

ABSTRACT

Epitaxial $YBa_2Cu_3O_7$ (YBCO) films were grown on r-plane Al_2O_3 $\{1\underline{1}02\}$ by laser ablation. X-ray diffraction shows that films are epitaxial with the c-axis perpendicular to the substrate and the a or b axes parallel to $(2\underline{2}01)$, although the full width at half maximum of the rocking curve is larger compared to those of epitaxial films on $SrTiO_3$. The critical temperatures (zero resistance) are between 85 K and 88 K with transition widths between 0.5 K and 3 K. The 300 K resistivity of 250 $\mu\Omega$cm extrapolates to zero at zero temperature and the critical current is as high as 5×10^6 A/cm^2 at 4.2 K according to magnetization hysteresis measurements. Surface resistance data shows that 2000 Å thick epitaxial films on $\{1\underline{1}02\}$ have about 1 mΩ at 13 GHz at 4.2 K.

INTRODUCTION

The physical properties of sapphire make it a highly attractive material for thin films of the high temperature superconductors, particularly yittrium barium copper oxide (YBCO). Its low loss tangent makes sapphire an ideal choice as a dielectric for microwave applications such as transmission lines, delay lines and high-Q resonators. Sapphire has high internal optical transmittance from 150nm (vacuum ultraviolet) to 6000 nm (mid IR). Its high mechanical strength makes it possible to produce wafers that are less than 25 μm thick. For application to infared bolometers, this property is essential in reducing the heat capacity, since the relaxation time $\tau = C/G$[1]. The high Debye temperature, hence high thermal conductivity G, of Al_2O_3 is also clearly advantageous. Since it may be produced as large wafers, Al_2O_3 is comparatively less expensive than the perovskite materials which are proven to promote good epitaxial growth of the high temperature superconductors. Efforts to grow high quality epitaxial YBCO films on Al_2O_3 with properties comparable to films grown on $SrTiO_3$, MgO, Yttria-stabilized-zirconia (YSZ) and $LaAlO_3$ have been rendered difficult due to the reaction of YBCO with Al. Attempts to overcome this problem using buffer layers have been reported[2]. Substrate reaction is a more severe problem on silicon, where buffer layers may be unavoidable[3]. In this paper we report the sucessful growth of epitaxial YBCO films directly on r-plane sapphire $\{1\underline{1}02\}$ along with

structural and transport properties.

DEPOSITION TECHNIQUE

Reference 4 details the laser ablation technique. Briefly, pellets of the bulk YBCO material are ablated by focussed pulses from a 308 nm Lambda Physik EMG 103 excimer laser. The beam is passed through a defining aperture and imaged through a 25 mm lens onto the pellet. The pulse energy is 150 mJ, and the energy density is 1.2 J/cm^2. The deposition is carried out in 200 mT of oxygen. Immediatly following deposition, the oxgen pressure is raised to 100 T, and the films cool as the pressure was allowed to rise to 400 T. The most sensitive deposition parameter is substrate temperature. If the temperature is above a critical value, the substrate reaction occurs rapidly, and the result is a transparent, insulating film. At temperatures a few degrees lower, the films are black and conducting yet lack ideal properties. If the temperature is allowed to fall more than twenty degrees below the critical reaction temperature, poor epitaxy and orientation results. When this occurs, the critical current is typically a factor of ten lower.

EXPERIMENTAL RESULTS

Figure 1 shows the resistance vs. temperature for a sample which was grown at optimized temperature. The normal state resistivity is observed to extrapolate to zero, and the resistance at room temperature is 250 $\mu\Omega$-cm. The zero resistance temperature is 88 K and the transition width is 1 K. The transition is somewhat lower and broader than on similarly prepared films on $LaAlO_3$, which have zero resistance at 91 K and <.5 K wide transitions.

Thin film samples were analyzed with a four circle diffractometer in the Bragg-Brentano geometry using a Cu Kα source. Firgure 2a shows the predominance of the [00n] peaks in the θ-2θ scan indicating that the film is highly oriented with the c-axis perpendicular to the substrate. Omega rocking curves show that the [005] YBCO is aligned to within 1 degree of the [$\underline{1}$012] sapphire peak, however, the width of the [005] peak is 2.5 degrees, indicating that there is substantial tilt misalignment of the grains. Good post annealed films on SrTiO3 have widths of 0.3 to 0.4 degrees[5], and in-situ grown films on MgO have rocking curves as narrow as 0.2 degrees[6]. FIgure 2b is a ϕ-scan of the YBCO [103] peak, with the ϕ axis nearly parallel to the c-axis direction of the film. The peaks occurring every 90 degrees correspond to the a and b axes of the YBCO aligned near to the sapphire <2$\underline{2}$01> directions. There is considerable spead in the film's in plane orientaion indicated by the width of the peaks.

Figure 3 depicts selected spacings and crystal axes on the r-plane surface. The YBCO [110] direction lies along sapphire [10$\underline{1}$1] as the spacing would suggest. Both the non-orthogonality and lattice mismatch are thought to contribute to the in-plane texturing of the YBCO films. Epitaxy of YBCO on sapphire is much like Si on sapphire[7], where the Si [100] lies along sapphire [10$\underline{1}$1].

The critical current density was measured by a magnetization hysteresis loop according to Bean's critical state model [8]. The Bean formula gives $J_c = 5.4 \times 10^6$ A/cm^2 at 4.2 K in 3 kG. This value is less than for our epitaxial films on $SrTiO_3$ or $LaAlO_3$, which is several times 10^7 A/cm^2, but is the highest currently reported on sapphire substrates.

Surface resistance of these films were measured inside a Cu cavity by sandwiching two films with dielectric material in between. The Quality (Q) factor of this structure was

measured by finding the resonance peak around 13 GHz. The Q value was around 6000 with dielectric thickness of 250 μm. This corresponds to the surface resistance of R_s = 1 mW at 4.2 K. The lowest R_s that has been measured with the same setup was R_s = 20 mW at 4.2 K around 13 GHz measured on sputtered films on MgO substrates.

SUMMARY

In summary, successful epitaxial growth of YBCO thin films on sapphire with low dc resistivity, sharp resistive transitions and high Jc by pulsed laser ablation has been demonstrated. Although the results are promising, the surface resistance remains too high for practical microwave applications. Further improvements will most certainly require overcoming the lattice mismatch and misorientation, possibly through the use of appropriate intermediate layers.

REFERENCES

1. P. L. Richards, J. Clarke, R. Leoni, P. Lerch, S. Verhese, M. R. Beasley, T. H. Geballe, R. H. Hammond, P. Rosenthal and S. R. Spielman, Appl. Phys. Lett. 54, 283 (1989).
2. T. L. Hylton, A. Kapitulnik, M. R. Beasley, J. P. Carini, L. Drabeck, and G. Gruner, Appl. Phy. Lett., 53, (1988).
3. S. Witanachchi, S. Patel, D. T. Shaw and H. S. Kwok, Appl. Phys. Lett. 55,295 (1989). and also bellcore....
4. D. K. Fork, K. Char, F. Bridges, S. Tahara, B. Lairson, J. B. Boyce, G. A. N. Connell and T. H. Geballe, Proceedings of the Materials and Mechanisms of Superconductivity Conference, Physica C, North Holland.
5. S. S. Laderman, K. Char, Mark Lee, M. R. Hahn, R. H. Hammond, M. R. Beasley, T. H. Geballe, A. Kapitulnik and R. Barton, Phys. Rev. B 39, 11648 (1989).
6. C. B. Eom, J. Z. Sun, K. Yamamoto, A. F. Marshall, K. E. Luther, T. H. Geballe, and S. S. Laderman, Appl. Phys. Lett. 55, 595 (1989).
7. F. A. Ponce, Appl. Phys. Lett. 41, 371 (1982).
8. C. P. Bean, Phys. Rev. Lett. 8, 250 (1962).
9.
10.
11.

M. Naito, R. H. Hammond, B. Oh, M. R. Hahn, J. W. P. Hsu, P. Rosenthal, A. F. Marshall, M. R. Beasley, T. H. Geballe and A. Kapitulnik, J. Mater. Res. 2, 713 (1987).

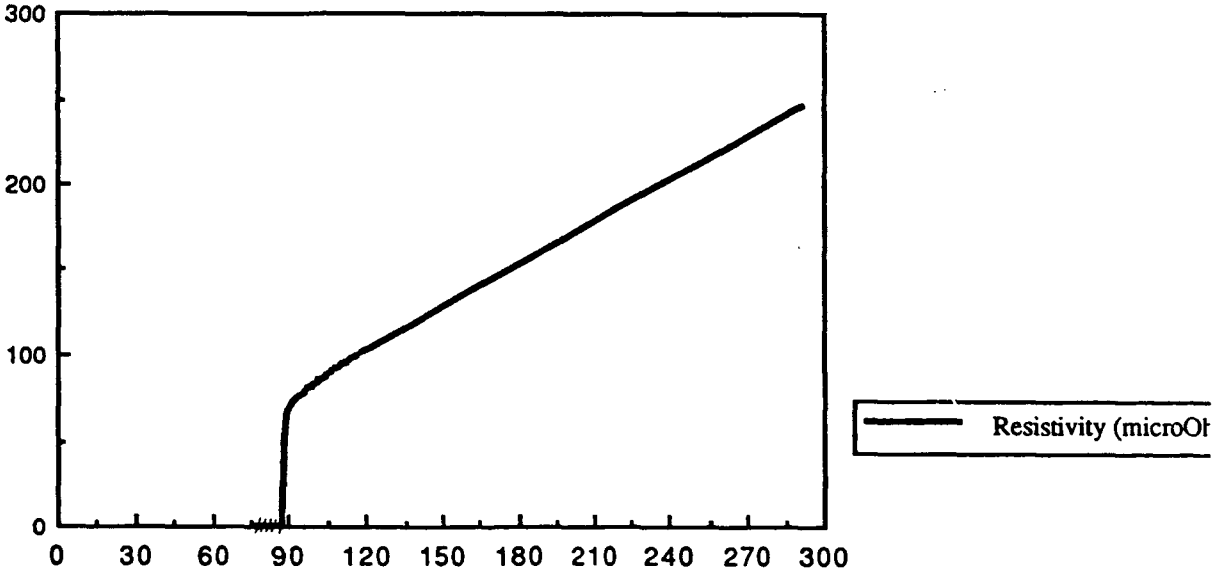
300
200
100
0
0
30
60
90
120
150
180
210
240
270
300
Resistivity (microOh

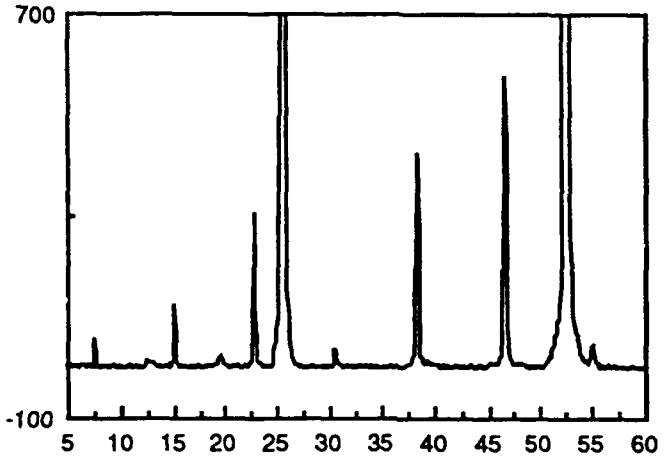
700
-100
5
10
15
20
25
30
35
40
45
50
55
60

Laser Ablation of HTSC at Xerox: an industry/university collaboration

Phi scan for [103] peak of YBCO on Al_2O_3

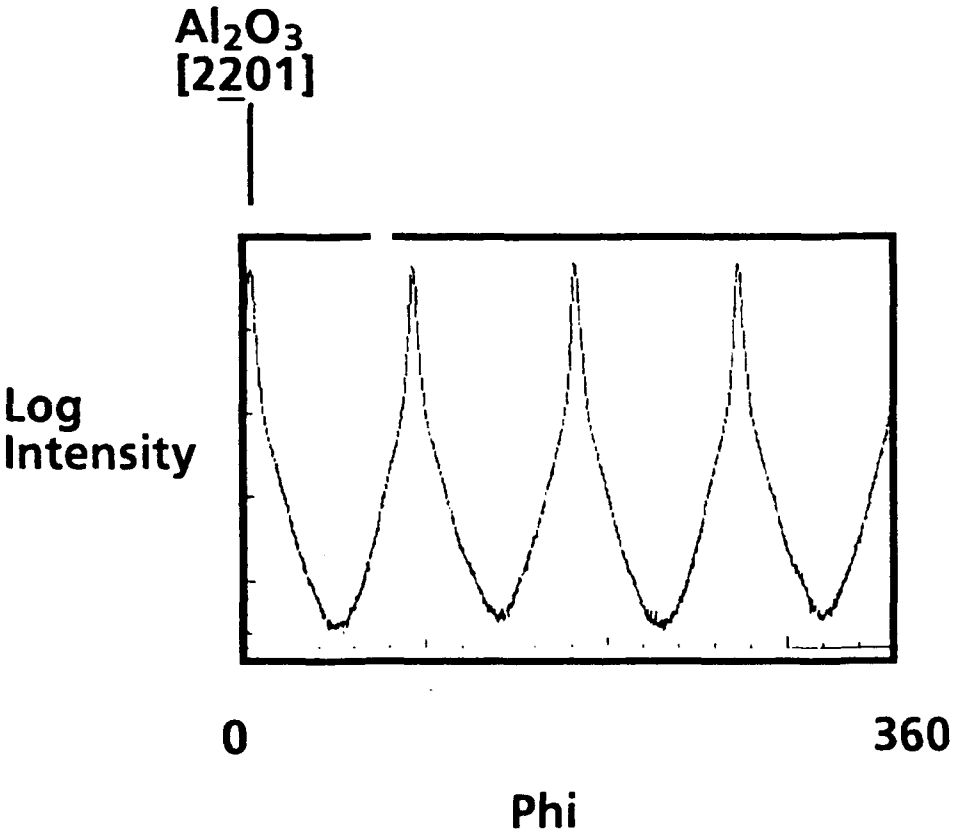

Conclusion

YBCO [100] and [010] directions are aligned with Al_2O_3 [2$\bar{2}$01] direction

2° misalignment produces line broadening

Neville Connell
Xerox PARC
October 10, 1989

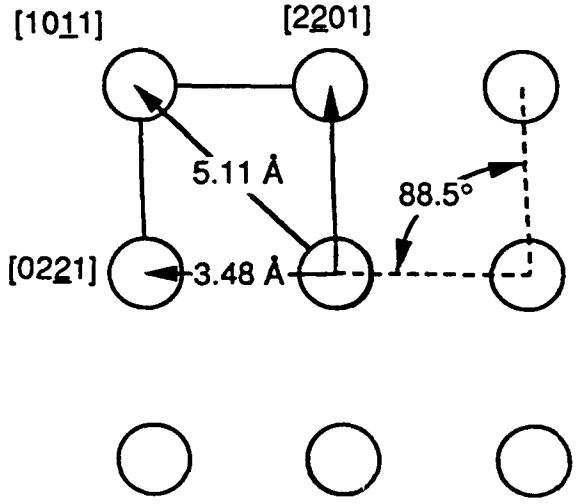
[10$\bar{1}$1]
[2$\bar{2}$01]
5.11 Å
88.5°
[02$\bar{2}$1]
3.48 Å

High critical current densities in epitaxial $YBa_2Cu_3O_{7-\delta}$ thin films on silicon-on-sapphire

D. K. Fork
Department of Applied Physics, Stanford University, Stanford, California 94305 and Xerox Palo Alto Research Center, Palo Alto, California 94304

F. A. Ponce and J. C. Tramontana
Xerox Palo Alto Research Center, Palo Alto, California 94304

N. Newman
Conductus, Inc., Sunnyvale, California 94086

Julia M. Phillips
AT&T Bell Laboratories, Murry Hill, New Jersey 07974

T. H. Geballe
Department of Applied Physics, Stanford University, Stanford, California 94305

(Received 17 December 1990; accepted for publication 28 March 1991)

The use of silicon on sapphire (SOS) as a substrate for $YBa_2Cu_3O_{7-\delta}$ allows the growth of thick ($\sim$4000 Å) films without the thermally induced cracking characteristic of epitaxial films on bulk Si substrate. Epitaxy is sustained and reaction is prevented by an intermediate buffer layer of yttria-stabilized zirconia (YSZ). The transport critical current density is as high as 4.6×10^6 A/cm^2 at 77 K, and surface resistance measurements at 4.2 K are reported. Microtwin propagation from Si into YSZ is shown not to occur.

Recent activity in the growth of high-temperature superconducting films has focused on the development of high quality films on technologically important substrates, two of which are silicon and silicon-on-sapphire (SOS). Methods for high quality films[1,2] on Si have recently increased the critical current density between 50 and 80 times above what was possible a year ago. Si is a favored substrate because advanced processing techniques and numerous device capabilities exist for Si, and are likely to enable on-chip combination of semiconducting and superconducting technologies at cryogenic temperatures. SOS has some advantages over bulk Si such as high mechanical strength, high radiation tolerance and reduction in parasitic capacitance, transistor latchup, and crosstalk. Si-on-insulator devices require less energy and lower voltages. Majority-carrier devices such as microwave integrated circuits, gate arrays and complementary metal-oxide-semiconductors (CMOS) static memories have distinct advantages when implemented in SOS. The disadvantages of SOS for semiconductors devices result from crystal defects; these include low channel mobility, high reverse-bias junction leakage, and short minority-carrier lifetime.

In this letter we show device-quality $YBa_2Cu_3O_{7-\delta}$, herein referred to as YBCO, can be grown on SOS substrates. Our films are grown by pulsed laser deposition as described in Ref. 1, with Si replaced by SOS. For resistivity measurements, the four-point dc transport geometry is defined by excimer laser patterning 1 mm $\times$ 50 μm strips. As in Fig. 1, the temperature dependence of the normal-state resistivity does not extrapolate to positive temperatures at zero resistivity as was observed for elastically strained films on bulk Si.[1] Zero resistance occurs at 88 K, and the transition width (10–90%) is 0.85 K. The critical current density (J_c) measured on a 1300 Å film at 77 K is 4.6×10^6 A/cm^2. This exceeds (J_c) for films of any thickness on bulk Si, a result consistent with the reduction of the strain in YBCO as discussed later.

Microwave surface resistance (R_s) was measured using a resonator formed by sandwiching two 1 cm $\times$ 1 cm thin films face to face separated by a 12.5-μm-thick Teflon dielectric. The current distribution is calculable, hence the relation between the Q and R_s may be determined. The measurement resolution of this method is about 5 $\mu\Omega$ at 10 GHz. A full description of this technique is given in Ref. 3.

R_s was measured at 4.2 K by sandwiching a reference Nb film (20 $\mu\Omega$ at 4.2 K at 10 GHz) with a YBCO film grown on a 1500 Å YSZ (yttria-stabilized zirconia) buffer layer on SOS. The surface resistance of the YBCO film was measured to be 72 $\mu\Omega$ at 11.8 GHz. Temperature dependent R_s measurements were made by sandwiching pairs of

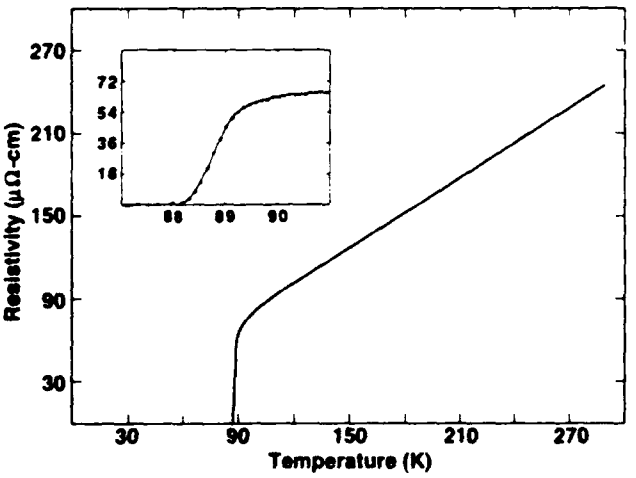

FIG. 1. Resistance vs temperature for a 1300-Å-thick YBCO/YSZ/Si/Al_2O_3 film. The critical current density measured at 77 K is 4.6×10^6 A/cm^2.

 0003-6951/91/212432-03$02.00

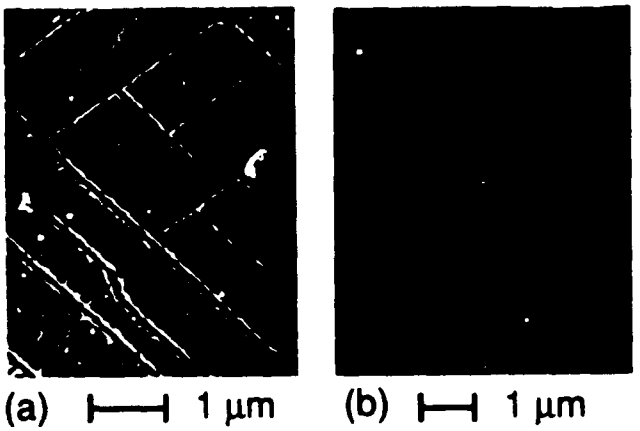

FIG. 2. Scanning electron micrographs of YBCO/YSZ films of comparable thickness on (a) SOS and (b) bulk silicon. Note cracks caused by thermal strain in (b). (Br in methanol used to enhance morphology.)

YBCO films; R_s rose rapidly with temperature to exceed 1 mΩ by 50 K. Model calculations suggest the rapid rise in R_s results primarily from losses in the YBCO film rather than in the Si. The low-temperature R_s is comparable to films grown on sapphire with $SrTiO_3$ buffer layers, however, in the films on SOS, the rise in R_s with temperature is larger.[4] If the increased losses we see at higher temperatures occur in the Si, the obvious solution is to remove the Si and grow on sapphire as in Ref. 4.

One inherent limitation of high quality YBCO growth on bulk Si is thermally induced strain during cooldown. Since YBCO films are grown *in situ* at a substrate temperature of about 700 °C at room temperature, the relative contraction of the YBCO with respect to the Si is about 0.83%; as determined from the average thermal expansion constants between 23 and 700 °C for Si[5] (3.8×10^{-6}/°C) and the *ab* average (1.6×10^{-5}/°C) for YBCO.[6] This thermally induced strain has been shown to decrease the critical current density of films thicker than ~500 Å by causing cracking along ⟨100⟩ directions, and produces elastic deformations in the lattice constants of thinner films.[1] The average thermal expansion coefficient of Al_2O_3 between 23 °C and 700 °C is 8.4×10^{-6}/°C, hence the relative contraction at room temperature is ~0.52%. Our results suggest this is within acceptable limits for producing unfractured YBCO films.

We have grown YBCO films on SOS as thick as 4000 Å; within this range, there are no signs of thermally induced cracking. This is eight times the critical thickness we observe on bulk Si.[1] YBCO films on Si thicker than ~500 Å are required in applications needing larger current carrying capacity (for example interconnects) or in high-frequency applications where the thickness should exceed the penetration depth (λ) of about 2000 Å, or in applications requiring lower kinetic inductance [which scales as λ^2/(film thickness)].

Figure 2 compares scanning electron micrographs of ~1500 Å YBCO films on (a) 500 Å YSZ on Si(100) and (b) 500 Å YSZ on 2500 Å Si(100) on $\{1\bar{1}02\}Al_2O_3$. Both films have been etched with a 0.5% Br in methanol solution to enhance the film morphology. The film on bulk Si (a) appears cracked, but the film grown on SOS (b) shows none of the obvious ⟨100⟩ crack boundaries.

The structural properties of these films produce figures of merit close to what we have reported previously on bulk Si.[1] Rocking curves in ϕ and ω were used to evaluate the epitaxial alignment of the Si, YSZ, and YBCO grains (Table I). ω measures the tilt misalignment; ϕ scans are taken on off-axis peaks, hence reveal twist (in-plane) misalignment. The relative out-of-plane layer alignments is YBCO[001]||YSZ[001]||Si[001]||$Al_2O_3[1\bar{1}02]$; the in-plane alignment is YBCO[100]||YSZ[110]||Si[110]||$Al_2O_3[\bar{2}021]$. Rocking curve widths in ϕ and ω (Table I) are narrower than for films grown on sapphire with $SrTiO_3$ buffer layers;[4] this occurs because the silicon is better aligned to the sapphire than is $SrTiO_3$. Growth of Si on Al_2O_3 is a mature technology, whereas growth techniques for $SrTiO_3$ on Al_2O_3 are new, and may in time yield much better material. The structural evaluation of these films has been done by x-ray diffraction and Rutherford backscattering spectroscopy (RBS). We observe pure *a*-axis growth of the epitaxial YSZ film, and pure *c*-axis growth of the YBCO film. This result contrasts with Ref. 4 where some *a*-axis YBCO material is present.

Rutherford backscattering spectra along aligned ⟨100⟩ and random directions were taken using 1.8 MeV $^4He^+$ ions. Figure 3 shows aligned and random backscatter spectra for a 2300 Å film grown on a 1500 Å YSZ buffer layer on SOS. The ratio of the backscattered yield along ⟨001⟩ to that in a random direction (χ_{min}) for Ba is 12%. The (χ_{min}) for Ba is comparable to what we have obtained on bulk Si,[1] however it is higher than the single-crystal value of 2–3%. Values of χ_{min} for bare (1500 Å) YSZ on SOS and bare (2500 Å) Si on Al_2O_3 appear in Table I. The χ_{min} of YBCO and YSZ are comparable, whereas that for Si is actually higher by about a factor of 2. This value is typical of 0.25-μm-thick silicon on sapphire.

It is known that Si close to the Si/Al_2O_3 interface con-

TABLE I. X-ray diffraction rocking curve figures of merit and RBS χ_{min} for various layers.

Film structure	$\Delta\omega$	ω peak used	$\Delta\phi$	ϕ peak used	Backscattering element	χ_{min}
YBCO/YSZ/Si/Al_2O_3	0.74°	YBCO(005)	1.74°	YBCO(103)	Ba	12%
YBCO/$SrTiO_3$/Al_2O_3[a]	2.4°	YBCO(005)	3.8°	YBCO(103)	...	...
YSZ/Si/Al_2O_3	1.14°	YSZ(002)	1.57	YSZ(202)	Zr&Y	13%
Si/Al_2O_3	0.49°	Si(004)	0.72°	Si(202)	Si	23%

[a]Taken from Ref. 4.

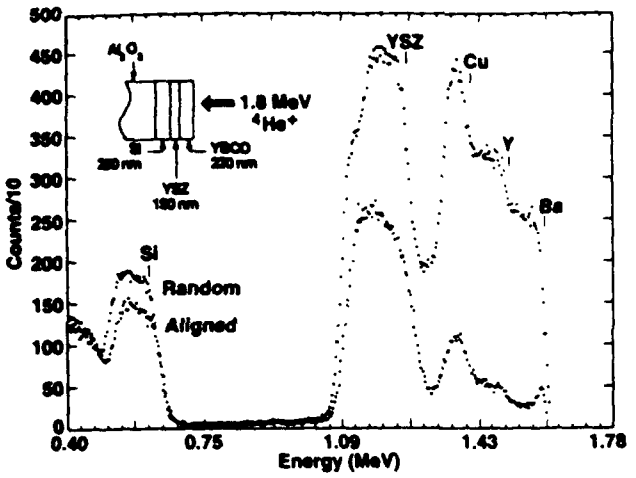

FIG. 3. Energy spectra of ⟨001⟩ aligned and random 1.8 MeV $^4He^+$ ions backscattered from a YBCO/YSZ/Si/Al_2O_3 film. The channeling minimum yield for Ba is 12%.

tains microtwins (Fig. 4) whose density decreases with distance from the interface.[7] Figure 4 shows the interface region between YSZ and Si with an intermediate amorphous oxide layer. Two microtwins lying along the [110] direction and slipping on {111} planes impinge on the interface but do not continue into the YSZ. The Si{111} planes are the planes of lowest bond density, and hence are the easy planes for slip dislocations. We believe the high stacking fault energy of a {111}YSZ slip dislocation explains their absence in the YSZ. YSZ has an oxygen deficient cubic fluorite structure; for an ideal cubic fluorite crystal of YSZ dimensions, the {111} bond density is ~2.2 times higher than for Si. Both YSZ and YBCO thin-film layers channel better than the Si (Table I) consistent with our observation that microtwin defects in the Si do not continue into the overlying layers. The dechanneling in the Si is large because the microtwin defects in the Si are inclined at 54.7° to the substrate (Fig. 4), therefore, a small volume defect can cause dechanneling throughout a large area of the film. The transmission electron microscope (TEM) observations also explain why the YBCO and YSZ layers can have broader rocking curves than the silicon layer but better channeling (Table I).

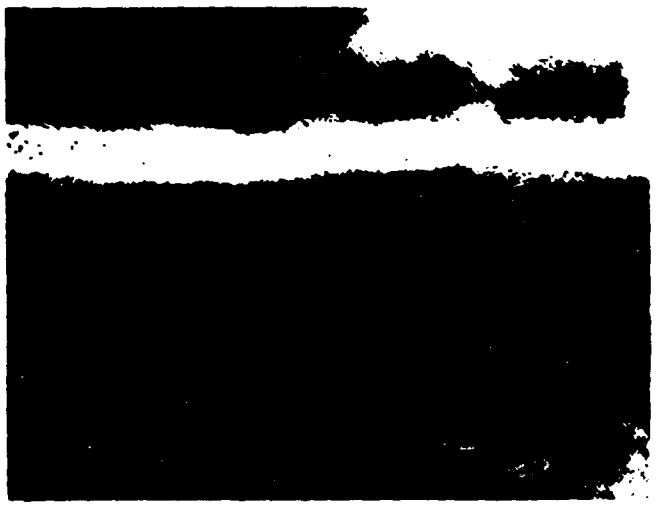

FIG. 4. Lattice image of the YSZ/Si interface region. A 40 Å amorphous oxide is observed. The stacking faults and microtwins in the silicon film terminate at this interface.

About 40 Å of silicon-oxide has formed at the YSZ/Si interface. Since epitaxy is maintained across the interface, this oxide must form after epitaxy is established. This is not surprising since YSZ is an oxygen ion conductor. Additional discussion of this interfacial amorphous oxide layer appears in Ref. 8.

In summary, epitaxial YBCO films have been grown on SOS substrates with a surface resistance as low as 72 $\mu\Omega$ at 4.2 K at 11.8 GHz and a critical current density of 4.6×10^6 A/cm^2 at 77 K using intermediate epitaxial buffer layers of YSZ. The principle advantage afforded by this work is the increased YBCO thickness permissible in comparison to YBCO on bulk Si. In addition it has been demonstrated that the microtwin defects in epitaxial silicon on sapphire do not propagate into the epitaxial YSZ, as characterized by channeling and TEM.

We thank Brian Langley for useful discussions, S. Ready and L.-E. Swartz for technical assistance, and especially Dave Fenner (now at Advanced Fuel Research) for his involvement prior to this work. This work benefits from AFOSR (F49620-89-C-0017). DKF is an AT&T scholar.

[1] D. K. Fork, D. B. Fenner, R. W. Barton, Julia M. Phillips, G. A. N. Connell, J. B. Boyce, and T. H. Geballe, Appl. Phys. Lett 57, 1161 (1990).
[2] H. Myoren, Y. Nishiyama, N. Miyamoto, Y. Kai, Y. Yamanaka, Y Osaka, and F. Nishiyama, Jpn. J. Appl. Phys. 29, L955 (1990).
[3] R. C. Taber, Rev. Sci. Instrum. 61, 2200 (1990).
[4] K. Char, N. Newman, S. M. Garrison, R. W. Barton, R. C. Taber, S S. Laderman, and R. D. Jacowitz, Appl. Phys. Lett. 57, 409 (1990).
[5] Y. S. Touloukian, R. K. Kirby, R. E. Taylor, and T. Y. R. Lee, *Thermophysical Properties of Matter*, Vol. 13 "Thermal Expansion, Nonmetallic Solids" (Plenum, New York, 1977).
[6] J. D. Jorgensen, M. A. Beno, D. G. Hinks, L. Soderholm, K. J. Volin, R. L. Hitterman, J. D. Grace, Ivan K. Schuller, C. U. Segre, K. Zhang, and M. S. Kleefisch, Phys. Rev. B 36, 3608 (1987).
[7] F. A. Ponce, Appl. Phys. Lett. 41, 371 (1982); F. A. Ponce and J Aramovich, Appl. Phys. Lett. 38, 439 (1981).
[8] D. B. Fenner, A. M. Viano, D. K. Fork, G. A. N. Connell, J. B Boyce, F. A. Ponce, and J. C. Tramontana, J. Appl. Phys. 69, 2176 (1991).

Epitaxial MgO on Si(001) for Y-Ba-Cu-O thin-film growth by pulsed laser deposition

D. K. Fork
Department of Applied Physics, Stanford University, Stanford, California 94305 and Xerox Palo Alto Research Center, Palo Alto, California 94304

F. A. Ponce and J. C. Tramontana
Xerox Palo Alto Research Center, Palo Alto, California 94304

T. H. Geballe
Department of Applied Physics, Stanford University, Stanford, California 94305

(Received 11 January 1991; accepted for publication 18 February 1991)

Epitaxial MgO thin films were grown on Si(001) by pulsed laser deposition. In spite of a large (-22.5%) lattice mismatch, epitaxy occurs with alignment of all crystallographic axes. Epitaxial quality and deposition rate are both sensitive to temperature and oxygen pressure. We believe this is the first demonstration of epitaxial MgO on Si. We employ MgO intermediate layers for superconducting epitaxial $YBa_2Cu_3O_{7-\delta}/BaTiO_3$ thin films on Si with a critical current density of 6.7×10^5 A/cm^2 at 77 K.

The growth of epitaxial oxides on Si is an expanding research topic with important technological applications. Possibilities typically cited for insulating layers on Si include metal-insulator-semiconductor structures and three-dimensional integrated circuits. In a somewhat different vein, this work has been carried out with the purpose of finding new buffer layer materials for the high-temperature superconductors. To date, a variety of epitaxial oxides on Si are known; these include yttria-stabilized zirconia (YSZ),[1] $MgAl_2O_4$,[2] Y_2O_3,[3] CeO_2,[4] PrO_2,[5] and Al_2O_3.[6] An expanded set of epitaxial materials on Si is desirable because of the increased design choices for device fabrication. To the authors' knowledge, there are no previous reports of epitaxial MgO thin films on Si.

MgO, mineral name periclase, is a highly ionic insulating crystalline solid with the NaCl structure. Its refractive index and dielectric constant are 1.7 and 10 respectively. It has *fcc* Mg and O sublattices, and low-energy, charge neutral {100} cleavage planes. The lattice constant of MgO is 4.211 Å, whereas that of Si is 5.431 Å, implying a mismatch of -22.5% for the orientation we observe. Epitaxial MgO on Si is an interesting technology because single-crystal MgO is a low dielectric substrate for the high-temperature cuprate superconductor $YBa_2Cu_3O_{7-\delta}$(YBCO). In addition, MgO is a suitable host lattice for a variety of other epitaxial materials, notably perovskites like $BaTiO_3$.

Pulsed laser deposition (PLD) has recently been used to rapidly explore new epitaxial materials on Si. The first epitaxial oxide grown on Si by PLD was PrO_2.[5] Since then, PLD has been used to fabricate high quality epitaxial thin films of yttria-stabilized zirconia (YSZ)[1] and $YBa_2Cu_3O_{7-\delta}$ on YSZ/Si.[7]

The films reported in this letter are grown in a system with a base pressure of 2×10^{-7} Torr. This pressure is high compared to pressures employed for the commonly used Si surface cleaning procedure (Shiraki cleaning) of evaporating the surface oxide at temperatures greater than 1000 °C.[8] Because epitaxy requires removal of the native silicon-oxide, we have adopted a room-temperature technique entitled spin etching[9] for removing the oxide and hydrogen-terminating the surface prior to loading the Si in the growth chamber. The H prevents Si oxidation in air, and remains bonded to Si until the substrate is heated above 400 °C. The source material is Mg metal, ablated 5 cm from the Si substrate. A laser energy of ~130–160 mJ is generated by a Lambda Physik EMG 103 XeCl excimer laser which produces an energy density of 2.0–2.5 J/cm^2 on the target. The Si substrate is heated by radiation from a quartz lamp. The wafer forms one side of an inconel box containing the lamp, and temperature is measured using a thermocouple affixed to an inner wall of the box. Temperatures quoted for the thermocouple are hotter than the Si substrate.

Oxide growth by PLD is ordinarily done using oxide targets. We use a Mg metal target because the absorption of MgO at 308 nm is too low for ablation to occur. Mg metal can be ablated, although its thermal conductivity and reflectance lowers the ablation rate. Mg oxidizes readily, making "reactive" laser deposition feasible; its gettering effect is noticeable while the laser is running. The deposition rate depends strongly on both background O_2 pressure and substrate temperature. For example, at 500 °C the deposition rate dropped from ~0.1 Å/pulse at 10 mTorr to ~0.01 Å/pulse at 0.002 mTorr. Over a temperature range from 300 to 600 °C the deposition rate (i.e., sticking coefficient) dropped by ~6× at the highest temperature. Our results are consistent with experiments by Yadavalli *et al.*,[10] which demonstrate that in zero O_2 flux, Mg atoms desorb from substrate surfaces with a thermal activation energy comparable to the cohesive energy of Mg metal (i.e., sticking coefficient drops with increasing temperature). Reference 10 also shows that in a finite O_2 flux, Mg capture by O_2 decreases the desorption, in agreement with our observations that higher O_2 pressures yield high deposition rates.

Epitaxy has been characterized by four-circle x-ray (Cu K_α) diffraction (XRD) and transmission electron mi-

 0003-6951/91/202294-03$02.00

TABLE I. X-ray diffraction figures of merit for MgO(002) reflection.

Heater temp. (°C)	O_2 pressure (mTorr)	Rocking curve width ($\Delta\omega$)	Peak intensity Counts
600	0.005	2.9°	500
500	10	...	7
500	1	...	11
500	0.01	5.7°	140
500	0.005	2.6°	850
500	0.002	2.9°	500
400	0.005	2.5°	1400
300	0.002	4.0°	275
300	0.001	6.6°	65

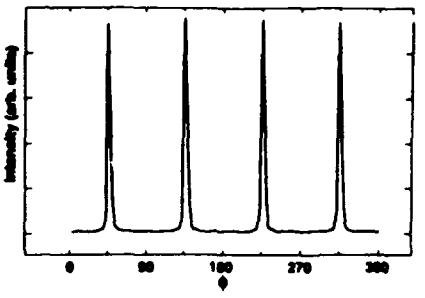

FIG. 1. X-ray diffraction phi scan of the MgO(202) family of reflections.

croscopy (TEM). Coupled on-axis (θ-2θ) x-ray scans gathered reflections from MgO crystal planes parallel to the substrate surface. On Si(001) the desired MgO reflection is (002). Only at the highest pressures, where epitaxy was poorest, could we observe reflections other than MgO(002) and Si reflections.

Table I lists XRD data from on-axis scans of the MgO/Si films grown for this study. ω-rocking curve full widths at half maximum (FWHM) were measured on the MgO(002) reflection to characterize the tilt misalignment of the MgO grains. As expected, films with higher peak intensities had narrower rocking curves; however, we note that the peak intensity is a less reliable measure of epitaxial quality since it is dependent on film thickness. The peak intensity results were taken under identical collection conditions. The rocking curve width, and hence the epitaxial growth, displayed a strong sensitivity to O_2 pressure, much like the growth of YSZ on Si.[1] Films grown at 500 °C (thermocouple temperature) in 1 and 10 mTorr O_2 had rocking curves too broad to measure; epitaxy improved steadily as the pressure was lowered to 0.005 mTorr, then worsened. The narrowest rocking curves obtained were about 2.5° (400 °C, 0.005 mTorr). This is wider than is suitable for many epitaxial semiconductor applications. For the high-temperature superconductors, the epitaxial constraints are less restrictive. Films of good quality have been grown on MgO buffer layers on sapphire which had comparable rocking curves.[11] The ω-resolution of the diffractometer measured on Si(004) is 0.6°.

The on-axis diffraction data is a useful characterization, however, it is not a rigorous demonstration of epitaxy, in fact, preferred MgO(001) growth on Si has been reported previously for nonepitaxial depositions.[12] In the present work, epitaxy has been verified by off-axis phi scans of the MgO(202) reflections with the phi axis normal to the plane of the film. A typical phi scan is shown in Fig. 1. The epitaxial relation is MgO[100]||Si[100], hence the crystallography is cube on cube, with a large mismatch of -22.5%. The width in phi is 3°. The phi resolution of the diffractometer is 0.65° as measured on the Si(202) reflection.

Transmission electron microscopy was performed to examine the MgO-Si interface. Figure 2 is a high-resolution interface lattice image of a film grown at 500 °C in 5×10^{-6} Torr O_2. The lattice spacing and electron diffraction (not shown) corroborate the cube-on-cube crystallography determined by XRD. The interface is abrupt and free from secondary phases or obvious interdiffusion. It is interesting to note that no *regrown* silicon-oxide is observed at the MgO-Si interface. A regrown amorphous oxide is observed for epitaxial YSZ/Si films.[13] The silicon-oxide formation is believed to occur via oxygen ion conduction through the film *after* epitaxy is established. The results are sensible since one expects far more oxygen ion conduction through YSZ (due to its oxygen vacancies) than through MgO.

Epitaxial systems with large lattice mismatch have been observed to nucleate commensurate with the substrate, and undergo an incommensurate (or commensurate at some rational spacing) phase transformation within a small number of monolayers (four monolayers[14] in the

FIG. 2. High-resolution transmission electron micrograph of the MgO/Si interface taken in the [110] zone axis orientation. The film was grown by PLD at 500 °C in 0.005 mTorr O_2. The interface is incommensurate but maintains the ⟨100⟩||⟨100⟩ orientational relationship.

Buffer Layers for High-Quality Epitaxial YBCO Films on Si

David K. Fork, *Member, IEEE*, David B. Fenner, *Member, IEEE*, Adrian Barrera, Julia M. Phillips, Theodore H. Geballe, G. A. N. Connell, and James B. Boyce

Abstract—**Efforts aimed at producing device quality $YBa_2Cu_3O_{7-\delta}$ (YBCO) films on Si have resulted in films with properties comparable to what can be achieved with conventional oxide substrates such as $SrTiO_3$. Epitaxial YBCO films were grown on Si (100) using an intermediate buffer layer of yttria-stabilized zirconia (YSZ). Both layers are grown via an entirely *in situ* process by pulsed laser deposition (PLD). The large difference in thermal expansion coefficients between silicon and YBCO causes strain at room temperature. Thin (< 500 Å) YBCO films are unrelaxed and under tensile strain with a distorted unit cell. Ion channeling reveals a high degree of crystalline perfection with a channeling minimum yield for Ba as low as 12%. The normal state resistivity is 250–300 $\mu\Omega \cdot$ cm at 300 K; the critical temperature, Tc ($R = 0$), is 86–88 K with a transition width (ΔTc) of 1 K. Critical current densities of 2×10^7 at 4.2 K and 2.2×10^6 at 77 K have been achieved. Noise measurements indicate that these films are suitable for use in highly sensitive far infrared bolometers. Applications of this technology to produce *in situ* reaction patterned microstrip lines is discussed.**

I. Introduction

IT HAS been the goal of many research efforts to produce high quality films of the superconductor $Y_1Ba_2Cu_3O_{7-\delta}$ (YBCO) on Si. Efforts in this direction have explored a number of deposition techniques and processes, many of which are summarized in a recent review in [1]. Although a variety of thin-film growth techniques can now routinely produce excellent quality YBCO films with critical current (J_c) at 77 K in excess of 10^6 A/cm^2 on substrates such as $SrTiO_3$ and MgO, only recently has this been achieved on Si substrates [2], [3]. It is too early to estimate what the technological impact of having high J_c films on Si will be; however, it is virtually essential to the substrate level mating of superconducting and semiconducting technologies. A recent review [4] by Van Duzer and Kumar discusses semiconductor-superconductor hybrid electronics with particular attention given to thermal management. A variety of hybrid semiconductor-superconductor applications are discussed in [5]. Many applications are contingent upon the identification of a suitable Josephson element; however, in the past year, significant progress in this area has been made. This paper will focus on the materials issues that have been addressed and in large part solved. The electrical properties and fabrication processes relevant to some device structures will be discussed.

Manuscript received October 19, 1990. This work was supported in part by AFOSR under Grant F49620-889-C-0017, by NSF under Grant DMR-8822353, and by an AT&T scholarship to D. K. Fork.

D. K. Fork is with the Department of Applied Physics, Stanford University, Stanford, CA and the Xerox Palo Alto Research Center, Palo Alto, CA 94304.

D. B. Fenner was with the Xerox Palo Alto Research Center, and with the Physics Department, Santa Clara University, Santa Clara, CA 95053.

A. Barrera and T. H. Geballe are with the Department of Applied Physics, Stanford University, Stanford, CA.

J. M. Phillips is with AT&T Bell Laboratories, Murray Hill, NJ 07974.

G. A. N. Connell and J. B. Boyce are with the Xerox Palo Alto Research Center, Palo Alto, CA 94304.

IEEE Log Number 9042302.

The principal difficulty in obtaining high J_c films on Si has been to prevent the severe reaction between YBCO and Si while maintaining epitaxy from the substrate through to the YBCO. The reaction problem suggests the use of a buffer layer of some type. Metals [6] and silicides as a buffer layer on Si are typically less inert than oxides; hence these are ruled out, leaving a large number of possible oxides, which are then narrowed down by the constraint calling for an epitaxial buffer layer. Several group IIA fluorides [7], [8] have also been studied as substrates and buffer layers; however, the results have generally been less encouraging than for oxides. Without epitaxy, there is virtually no possibility of producing films with high critical currents or low noise or low surface resistance. Some oxides are known to grow epitaxially on Si, hence possible epitaxial buffer layers based on known technology include yttria-stabilized zirconia (YSZ) [9]–[11], $MgAl_2O_4$ [12], Y_2O_3 [13], CeO_2 [14], PrO_2 [15], and Al_2O_3 [16]. Currently, the best YBCO films on Si as determined by their structural and electrical properties have been obtained using YSZ buffer layers [2] or a variation [3] using Y_2O_3/YSZ. This paper will focus on the results obtained using YSZ as a buffer layer.

II. Growth Technique

All of our films are deposited by pulsed laser deposition (PLD) in a system specifically designed to handle the growth process on Si. An excellent review of the PLD technique as applied to a large variety of materials is contained in [17]. Our laser deposition technique is similar in most respects to other systems for making YBCO films; however, unlike most other systems, we use an N_2 purged glove box and a load lock to introduce hydrogen terminated silicon wafers into our deposition chamber. All of our targets are mounted on a rotating polygon surrounded by a water-cooled shroud that reduces heating from the substrate heater. We use an XeCl excimer laser that generates an energy density of 1.3 J/cm^2 on the targets. The Si substrates are heated by radiation from a quartz lamp heater and temperature is determined by optical pyrometry. Although many groups glue their substrates down to a heated block with silver paste, we have avoided this procedure for our work on Si because of the possible surface contamination resulting from the silver paste outgassing. Our procedure also allows the handling of delicate structures and very thin Si. At a target-substrate distance of 5 cm, each 17-ns laser pulse deposits about 0.2 Å of either YBCO or YSZ. Other materials may have somewhat different deposition rates. The laser is fired at between 4 and 10 Hz.

The Si wafers undergo degreasing followed by spin-etching in a flowing-N_2 hood; this technique is a variation of [18]. The Si wafer is rotated, flushed with high purity alcohol, and etched with several drops of a 1:10:1 mixture of HF, ethanol, and water, all of high purity. This process produces an oxide-free wafer covered by one monolayer of hydrogen which is passive

1051-8223/91/0003-0067$01.00

to the effects of brief exposure to room air [19]. We use the N_2 purged load lock to introduce these wafers into the deposition chamber once spin etching is completed. Using a recently developed procedure [2] we deposit a 500-Å epitaxial YSZ layer at 750–800°C in 4×10^{-4} torr O_2 followed immediately by a variable thickness YBCO film grown at 700–750°C in 200 mtorr O_2.

III. Film Crystallography and Structure

The structural observations made by various groups on YBCO films on a host of substrates are varied and complex, and ultimately will provide a comprehensive picture of the growth behavior of these films, and also provide insight into the correlation of microstructure with electrical properties. With systems requiring buffer layers, structural information becomes even more critical.

A large portion of the structural optimization of a heteroepitaxial growth technique can be done by observing X-ray diffraction θ-2θ scans and ω-rocking curve widths or channeling minimum yields. The θ-2θ scans can identify improper phases and orientations, whereas the ω-rocking curve widths provide a figure of merit for the tilt misalignment of the grains. By monitoring both θ-2θ spectra and ω widths, it is possible to close in rapidly on the optimal deposition parameters for a growth process. We have done so for epitaxial YSZ on Si, and the results are discussed in [11]. Briefly, we observed that a critical parameter for the epitaxy of YSZ on Si is the O_2 pressure during growth. In the low pressure regimes, films grown in a base pressure of 10^{-6} torr are reduced, semiconducting, silvery in appearance, and adhere poorly to Si; the cubic fluorite YSZ phase, while present to some degree, is oriented randomly. In the high pressure regime, films deposited on Si(100) in 50 mtorr O_2 have poor epitaxy with only weak preferred [001] orientation. Presumably, at this pressure, silicon oxide regrowth through the growing YSZ film is impeding epitaxy as we observed for the growth of PrO_2 on Si [15]. The optimal pressure lies between these two regimes, and is around 0.4 mtorr [11].

The *in-plane* film texturing and twist misalignment of the grains in an epitaxial film may be determined from X-ray diffraction phi scans of out-of-plane peaks with the phi rotation axis perpendicular to the film. By aligning first to the substrate, and then systematically observing the off-axis peaks of all subsequent epitaxial layers, all of the *in-plane* epitaxial relations many be established. The width of reflections in phi ($\Delta\phi$) also provide a figure of merit for the *twist* misalignment of the epitaxial grains.

We have performed phi scans on our epitaxial YSZ films on Si; the alignment of the YSZ grains is constrained to about 1° to the Si lattice. An interesting additional feature we observed is that not all deposition techniques for YSZ on Si have reported the same *in-plane* orientation. Films grown by electron beam evaporation are reported to grow with YSZ [110] parallel to Si [100]. This epitaxial relation has a lattice mismatch of 0.2% for YSZ/Si heteroepitaxy, requiring Si [010] parallel to YSZ [110] and a ratio of 3:2 in the lattice-match repeat lengths [9]. The lattice mismatch for the orientation we obtain by pulsed laser deposition is larger (−5.8%); however, no material oriented as in [9] appears in our films. The crystallographic relation we observe on Si(100) agrees with what is observed for the growth of epitaxial Si on YSZ [20]. We note that for epitaxy with a 3:2 ratio in the lattice constants, the coalescence of separate nucleation seeds may not be coherent, possibly resulting in antiphase boundaries.

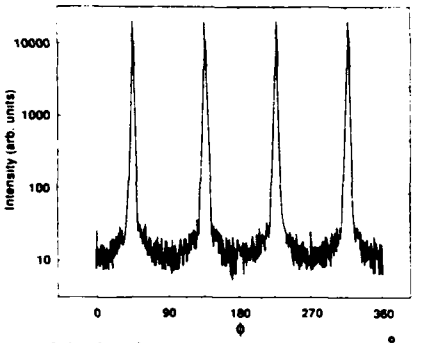

Fig. 1. ϕ-scan of the {103} family of peaks of a 1350-Å thick YBCO film with a 500-Å YSZ buffer layer on Si(100). Peaks every 90° show *in-plane* epitaxial alignment to ~2.0°.

Much attention has been given to the *in-plane* epitaxy of YBCO on various substrates, particularly MgO [21] and YSZ [23], where grain boundaries necessarily develop at the interfaces between *c-axis* grains with a discreet set of distinct *in-plane* orientations. In cases where the epitaxy is both heterostructural and poorly lattice-matched, the variety of possible in-plane orientations appears to increase dramatically; this appears to be true for both MgO or YSZ when used as substrates for YBCO, suggesting that they are members of a category characterized by weak epitaxy, which allows several orientations to compete. In general it is expected that the mating of cubic fluorite or rock salt structures with YBCO differs markedly from the growth of YBCO on $SrTiO_3$. This work has shed light on the in-plane epitaxial behavior of YBCO on YSZ, which is an oxygen deficient cubic fluorite structure compound.

Several groups including ours investigated YSZ as a buffer layer material because of its chemical inertness with Si and YBCO. It is known however that YBCO films on YSZ frequently include many 45° twist grain boundaries, in addition to a small variety of other low angle grain boundaries. In the presence of such mixed epitaxy, the critical current density is lower. Based solely on a knowledge of the epitaxial growth of YBCO on single crystal substrates, there are many other buffer layer choices with potentially better epitaxy; however, either due to chemical reactions or an inability to produce epitaxial thin films of the material on Si, a variety of materials have been ruled out or appear difficult to control. It is a fortunate occurrence that YBCO films grown *in situ* on epitaxial YSZ films on Si have only a *single in-plane orientation* (see Fig. 1) neglecting twinning. This result suggests that the *in situ* prepared YSZ surface is an ideal growth surface for YBCO, and that the YSZ surface is easily disrupted in a fashion that allows other orientations to nucleate and grow. Confirmation of this effect is provided below in the section on reaction patterning of YBCO on Si. It is worth mentioning that the method reported in [2] is currently the only fully *in situ* technique whereby both the epitaxial buffer layer and the YBCO film are deposited by the same process without interruption.

Fig. 1 shows a log-linear plot of a phi scan of the YBCO {103} peaks obtained for a 1300-Å YBCO film grown on a 500 Å YSZ buffer layer. Zero degrees phi in this figure was obtained by aligning the Si (101) reflection. This reveals that the YBCO unit cell is rotated 45° in the plane with respect to the Si. Peaks occur every 90°, showing than no additional *in-plane* YBCO orientations occur, unlike films we produced earlier on single crystal YSZ substrates [13]. From the width of the peaks, it is possible to infer that the YBCO is aligned to with about 1° to the YSZ and about 2° to the Si.

TABLE I
EPITAXIAL RELATIONS OBSERVED IN THE COURSE OF THIS WORK

Film Interface	In-Plane Relation	$\Delta\phi$	Out of Plane Relation	$\Delta\omega$
YBCO/YSZ(100)	[110]‖[100]	1.5–2.5	[001]	0.6–1.0
YSZ/Si(100)	[100]‖[100]	1.1–1.5	[001]	0.7–0.8
YBCO/YSZ(111)	random	∞	[001]	large
YSZ/Si(111)	$[1\bar{1}0]\|\|[10\bar{1}]$	2.6	[111]	2.0
PrO_2/Si(111)	$[1\bar{1}0]\|\|[10\bar{1}]$	0.9–1.0	[111]	0.78–1.0
$CaTiO_3$/Si(100)	random	—	random	—
$SrTiO_3$/Si(100)	random	—	mostly [110]	—
$BaTiO_3$/Si(100)	random	—	mostly [110]	—
$LaAlO_3$/Si(100)	random	—	random	—

Many additional epitaxial relations have been studied in the course of this work. Table I lists the epitaxial relations of a variety of material systems we have investigated to date. We have already discussed the YBCO/YSZ(100) and the YSZ/Si(100) systems. We have also grown epitaxial YSZ films on Si(111), which for many cubic fluorite structure materials is a more hospitable growth surface. One would expect this system to have crystallography similar to CaF_2 on Si(111), which is the most studied cubic fluorite-on-diamond heterostructural epitaxial system [24]. It is indeed the case, that like CaF_2, both YSZ and PrO_2 produce type-b interfaces on Si(111). This implies that with respect to the silicon, the film crystal lattice is rotated 180° about the [111] direction.

Attempts to grow epitaxial YBCO on YSZ(111)/Si(111) resulted in nonepitaxial *c-axis* oriented films. This suggests that the orientation is dominated by growth kinetics rather than by any template provided by the substrate; again, this supports the view that YBCO/YSZ is a system possessing weak epitaxy. Similar observations have been made by Shi *et al.* [25]. The *in-plane* structure of such a film is necessarily random; hence the electrical properties are expected to suffer due to the random network of grain boundary orientations. This is observed as a $\sim 3x$ increase in the YBCO resistivity, a lowering of the critical current density, and a suppression of the critical temperature by several degrees.

Our earliest success growing epitaxial metal oxides on Si occurred during the investigation of PrO_2 on Si(111) [15]. The epitaxial relations of this system are listed in Table I. This material did not make a satisfactory buffer layer for YBCO on Si(100); however, it did elucidate many aspects of the hydrogen termination process and deposition conditions.

Some effort has been directed at the growth of perovskite buffer layers on Si. This has been dictated in large part by the success obtained for YBCO growth on single crystal perovskite family compounds, such as $SrTiO_3$ and $LaAlO_3$. The results on hydrogen-terminated Si have been thus far nonepitaxial for the four perovskite structure compounds listed in the bottom of Table I. It is too early to tell the precise reason why epitaxy does not occur. There do appear to be subtle differences in the preferred orientations of these polycrystalline perovskite films on Si.

Additional microstructural information has been obtained on our films through the use of Rutherford backscatter spectroscopy (RBS.) X-ray diffraction is capable of looking at grains of a particular orientation; random or highly misoriented material is difficult to detect. RBS data are complimentary since by comparing random to channeled spectra, a quantitative figure of merit for the overall crystallinity, the χ_{min}, is obtained. This is simply the ratio of the backscattered yield along [001] to that in a random direction. A typical spectrum for YSZ films on Si has been reported in [11], wherein a minimum yield for Zr of 5.3% was reported. The minimum yield of completely random material is 100%, whereas that for a single crystal would be about 2–3%. This indicates that the YSZ film is close to single crystal quality. Interfacial disorder is also observed in RBS spectra of YSZ/Si, and is discussed in [11].

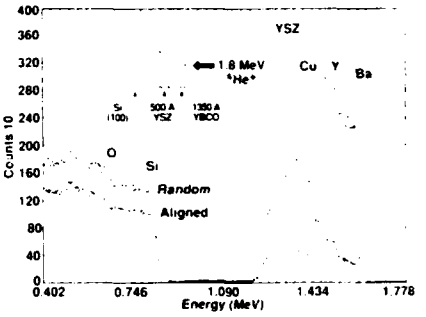

Fig. 2. Energy spectra of ⟨001⟩ aligned and random 1.8 MeV 4He + ions backscattered from a 1400-Å YBCO film with a 500-Å thick buffer layer on Si. The channeling minimum yield for Ba is 12%. The YSZ and Cu peaks overlap.

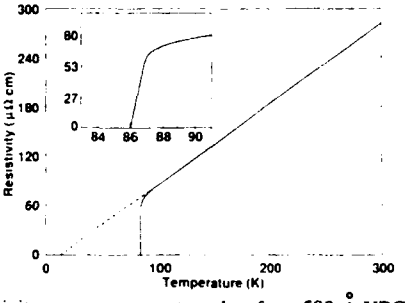

Fig. 3. Resistivity versus temperature data for a 500-Å YBCO film on YSZ on Si.

Some channeling spectra have also been taken on YBCO/YSZ/Si. Fig. 2 shows the backscatter spectrum for one such film. The ratio of the backscattered yield along ⟨001⟩ to that in a random direction (χ_{min}) for Ba is 12%. Although this is an indication of crystalline order, it is still higher than what is observed for single crystals [26]. Disorder, evidenced by a larger χ_{min}, appears to increase near the interface. The values of χ_{min} for YSZ and Si change dramatically with YBCO thickness. For a very thin 130-Å YBCO film, the χ_{min} values for YSZ and Si were 22% and 46%. In contrast, the 1350-Å YBCO film in Fig. 2 had χ_{min} of 67% and 77% for YSZ and Si, respectively. This is not surprising in light of the tensile strain imposed on the epitaxial layers by their thermal contraction; more will be said about thermal strain in a subsequent section.

IV. ELECTRICAL PROPERTIES

The dc electrical properties of these YBCO films produced by the technique described above are comparable to the most favorable values reported for films on $SrTiO_3$ and MgO; this result is expected based on the similarity of crystal quality. In the regime close to zero frequency, state of the art epitaxial YBCO thin films appear to have transport properties that are approaching the intrinsic limits for the material. In addition, it is worth commenting that ideal crystalline perfection is not necessarily desirable due to the likelihood of select defects acting as centers for flux pinning. The intrinsic electrical properties at microwave frequencies remain unknown and incalculable since no reliable model exists for an idealized YBCO crystal, unlike the case of normal metals where skin depth and surface resistance are easily

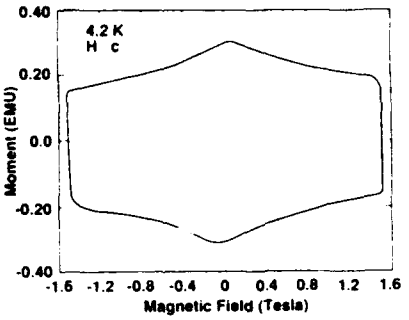

Fig. 4. Magnetization hysteresis loop of a 6 mm × 6 mm × 400 Å YBCO/YSZ/Si film at 4.2 K indicating J_c of 2×10^7 A/cm^2.

estimated. What is generally believed, however, is that the requirements for high dc critical current or weak magnetic field dependence and low microwave loss may be at odds, and may require epitaxial films with different microstructures. With these remarks in mind, some of the electrical properties are discussed below.

Fig. 3 shows a resistivity versus temperature plot for a 500-Å YBCO film grown on YSZ/Si. Many such measurements have been made on these films. The transition temperatures (zero resistance) fall in a range of 86–88 K, and the transition widths are typically 1 K. The transitions are somewhat lower and broader than our films on single crystal $LaAlO_3$; however, the normal state resistivity falls in a range from 250 to 300 $\mu\Omega \cdot$ cm at 300 K, which is typical of films grown on conventional substrates. Numerous groups, including our own, have observed that films on MgO and YSZ single crystal substrates often have critical temperatures that are a few degrees lower than those on $SrTiO_3$ or $LaAlO_3$. The origins of this effect are not understood fully, but may be related to differences in lattice match. The normal state behavior of the YBCO films on Si differs markedly from films on other substrates in that the extrapolated resistance curve crosses the positive side of the temperature axis. This is not typically observed in single crystals or in thin films. We conjecture that this may be the influence of strain on the normal state properties.

Critical currents (J_c) in these films were measured by transport and vibrating sample magnetometry. The transport J_c at 77 K was measured on a 60-μm wide excimer-laser-patterned strip. The strip is generated by removing ~25-μm square portions of the film while translating it on an xy stage until a four-point pattern is isolated within the center of the wafer. The J_c of a 305 Å film was 2.2×10^6 A/cm^2 based on a voltage criterion of 1 μV/mm. Vibrating sample magnetometry was used to measure J_c at 4.2 K and to obtain magnetic field dependence to 1.5 Tesla. A magnetization hysteresis loop for a 400-Å film is shown in Fig. 4. The J_c at 4.2 K in zero field as determined using the Bean critical state model [27] is 2×10^7 A/cm^2. The field dependence is similar to that of films on $LaAlO_3$; J_c is reduced by a factor of 1.7 at 1.5 T. The zero field values of the critical current density are about one-half the highest reported values on $LaAlO_3$ and MgO, but are the highest currently reported on Si substrates.

It is clear that pinning is playing an important role in these films. At low temperature, the critical current density is only about a factor of 10 less than the depairing critical current density estimated in [28]. Well-ordered YBCO single crystals have a J_c about tenfold lower than the measured critical current in our films; however, when damaged by proton irradiation [29], the critical currents become comparable, as does the field dependence. The channeling data provides a quantitative comparison of the crystalline order between the thin films on Si and single crystals, i.e., $\chi_{min,film} \sim 5(\chi_{min,crystal})$. Although the precise nature of the disorder in the film is not clear, it is arguable that some of the crystalline imperfection, whether arising from lattice mismatch, thermal strain or a variety of other defects, is involved in pinning.

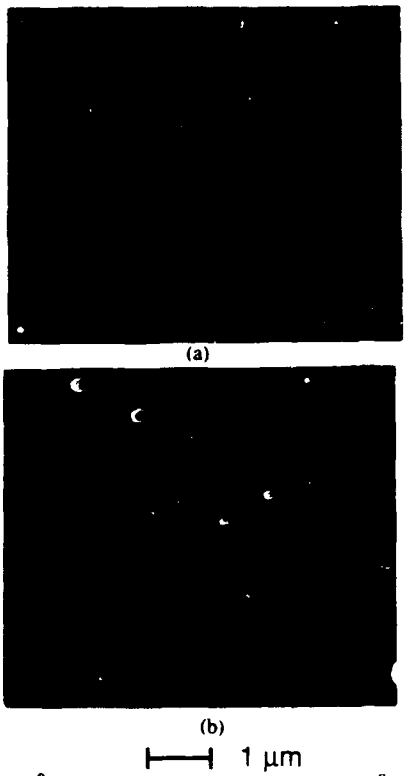

Fig. 5. (a) 130-Å YBCO film on YSZ/Si. (b) 1300-Å YBCO film on YSZ/Si. Note crack boundaries.

V. Effects of Thermal Strain

Thermal strain is perhaps one of the most critical remaining issues that will have important effects on the applicability of YBCO on Si technologies. The thermal contraction of the system consisting of a thick substrate and any number of thin epitaxial layers will invariably be dominated by the substrate. The thermal expansion constants of Si and YBCO are such as to place the YBCO film under tension; this introduces the potential for cracking. Since YBCO films are grown *in situ* at a substrate temperature of about 700°C, the idealized strain of the YBCO with respect to the Si is about 0.83% at room temperature; this value is obtained by taking the average thermal expansion constants between 23°C and 700°C for Si [30] (3.8×10^{-6}/°C) and the *ab* average for YBCO (1.6×10^{-5}/°C) [31]. It is natural to expect that for very thin films, the epitaxial layers will respond elastically to the biaxial stress, without fracturing. This indeed has been observed. In the limit where films are strained and unfractured, the YBCO unit cell is distorted and the critical current is high as reported above. Beyond a critical thickness of about 500 Å, the films begin to fracture, and by 1300 Å, the current path is sufficiently disrupted to lower the critical current by a factor of ~20.

Although X-ray diffraction was used to measure the distortion of the YBCO unit cell, the critical thickness of ~500 Å was determined by performing both scanning electron microscopy and critical current measurements. Fig. 5(a) shows a micrograph

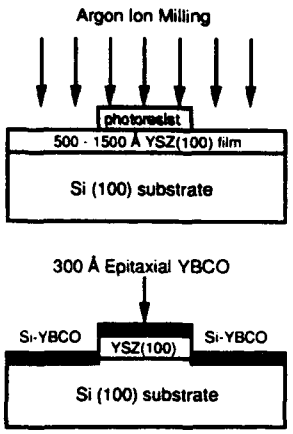

Fig. 6. Scheme of the YBCO reaction patterning process.

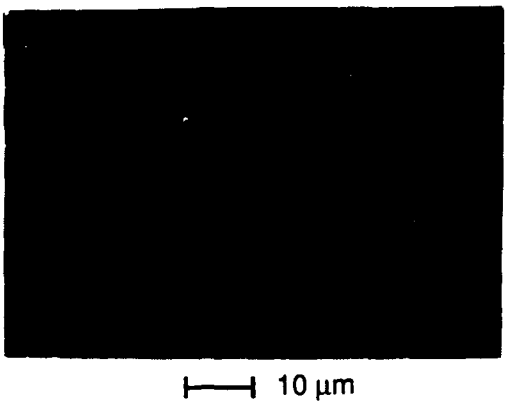

Fig. 7. SEM photo of 3-μm reaction patterned YBCO microstrip.

of a 130-Å thick YBCO film on Si which was elastically strained and had a c-axis lattice constant of 11.63 Å [2]. This lattice spacing is significantly shorter than the bulk value of 11.68 [31]. It must also be borne in mind that the *c*-axis lattice constants of YBCO films are often *longer* than the bulk value [32], and vary depending on the processing conditions. Fig. 5(b) shows a micrograph of a 1300-Å thick YBCO film on Si that shows rather obvious fractures. These fractures run predominantly along [100] and [010] directions and are spaced about 1 μm apart. In this film, the lattice constants were observed to be very close to the bulk YBCO values.

Si has a thermal expansion constant that is smaller than many oxides (one notable exception is SiO_2) and compound semiconductors; hence thermal strain is a frequently encountered problem, having plagued epitaxial systems such as CaF_2 on Si [22], Si on YSZ [20], and GaAs on Si [33]. Since the study of YBCO on Si is in its infancy, many approaches to solving this problem remain untried.

VI. Reaction Patterning of YBCO on Silicon

Although the reaction between YBCO and Si is one of the reasons for avoiding Si as a substrate, this property has been recognized as useful for creating insulating thin film domains, and hence "reaction patterning" microstructures. The first report of such an application was made by Q. Y. Ma *et al.* [34], wherein it was reported that YBCO films could be reaction patterned down to 2.5 μm by patterning Si on MgO substrates prior to the YBCO deposition and a subsequent post anneal treatment at 980°C. The resulting microstrip in that work had a critical current density of 300 A/cm^2 at 75 K.

Our adaptation [35] of [34] consists of growing an epitaxial YSZ film on Si (100) by pulsed laser deposition as described above, removing selected areas of the YSZ film by Ar^+ ion milling, and then *in situ* laser depositing a layer of YBCO (Fig. 6). The desired pattern is defined lithographically in positive photoresist. The Ar^+ ion milling procedures uses a Kaufman ion source operating at 500 V. The substrates are cooled during the milling procedure. The etch rate of YSZ was determined by profilometry to be 20 Å/min. Fig. 7 shows scanning electron micrographs of the final product. An advantage of this process is the formation of a mesa structure isolating the patterned YBCO features from the possibility of lateral Si diffusion. The electrical isolation of separate mesas was > 20 MΩ for all of the films we tested. The J_c of a 3-μm wide reaction patterned microstrip line was 1.6×10^6 A/cm^2 at 77 K, which is very close to the J_c of unpatterned films.

One principal advantage of this technique is that fully operational planar devices such as bolometers, delay lines, and weak link structures such as substrate step edge superconducting quantum interference devices (SQUID's) can be produced without subjecting the YBCO film to wet chemical etchants, photoresist, or solvents. This may be of particular benefit in the case of ultrathin films or structures mounted on thin substrates, such as membrane bolometers [36].

In the course of this work, it was discovered that removing the YSZ film from the growth chamber for processing and reinserting it into the chamber altered the growth surface sufficiently to seriously degrade the epitaxy. Again, this supports the inference that YBCO/YSZ is a weak epitaxial system that is easily disrupted. In this instance, the disruption manifested itself by the presence of 45° angle and low angle grain boundaries in c-axis oriented grains. This effect was easily observed with x-ray diffraction phi scans of the YBCO {103} reflections, and was remedied by growing 20 Å of homoepitaxial YSZ on the surface prior to growth [35]. The 20-Å YSZ was not sufficient to prevent diffusion of the Si in the areas intended to be insulating.

VII. Conclusion

This paper has reviewed some of the current progress and activity aimed at advancing the technology for growing and utilizing epitaxial YBCO films on Si substrates. Although many buffer layer materials have been investigated by a variety of groups, one of the most promising buffer layers is YSZ. In spite of this material's potential for supporting weak epitaxy, films of excellent crystal quality are easy to produce under the proper processing conditions. Residual defects in the YBCO may be responsible for pinning. Thermal strain is a problem in this system; however, a variety of potential solutions exist, and will certainly be reported in the future.

Acknowledgment

The authors thank Don Beard and Robert Sparks of Sieman's Analytical X-ray, Inc. for the single crystal data acquisition capability, Bruce Lairson for help obtaining magnetization data, and Richard Johnson, Steve Ready, and Lars-Erik Swartz for technical assistance.

References

[1] A. Mogro-Campero, "A review of high-temperature superconducting films on silicon," *Supercond. Sci. Tech.*, vol. 3, pp. 115-158, 1990.

[2] D. K. Fork, D. B. Fenner, R. W. Barton, Julia M. Phillips, G.

A. N. Connell, J. B. Boyce, and T. H. Geballe, "High critical currents in strained epitaxial YBCO on Si," *Appl. Phys. Lett*, vol. 57, pp. 1161-1163, 1990.

[3] H. Myoren, Y. Nishiyama, N. Miyamoto, Y. Kai, Y. Yamanaka, Y. Osaka, and F. Nichiyama, "Crystalline quality and critical current densities of as-grown YBCO thin films on silicon with buffer layers," *Jap. J. Appl. Phys*, vol. 29, L955-L957, 1990.

[4] T. Van Duzer and S. Kumar, "Semiconductor-superconductor hybrid electronics," *Conf. Low-T Electronics*, Berkeley, CA, Apr. 1990.

[5] H. Kroger, C. Hilbert, D. A. Gibson, U. Ghoshal, and L. N. Smith, "Superconductor-semiconductor hybrid devices, circuits and systems," *Proc. IEEE*, vol. 77, pp. 1287-1301, 1990.

[6] T. Asano, K. Tran, A. S. Byrne, M. M. Rahman, C. Y. Yang, and J. D. Reardon, "Interface analysis of YBCO films on Al-coated Si substrates," *Appl. Phys. Lett.*, vol. 54, pp. 1275-1277, 1989.

[7] Siu-Wai Chan, E. W. Chase, B. J. Wilkins, and D. L. Hart, "Superconducting YBCO thin films on alkaline earth fluorides," *Appl. Phys. Lett.*, vol. 54, pp. 2032-2034, 1989.

[8] F. Radpour, R. Singh, S. Sinha, A. M. Tulpule, P. Chou, R. P. S. Thakur, M. Rahmati, N. J. Hsu, and A. Kumar, "Preparation of YBCO superconducting thin films using BaF_2 as a buffer layer," *Appl. Phys. Lett.*, vol. 54, pp. 2479-2480, 1989.

[9] H. Fukumoto, T. Imura, and Y. Osaka, "Heteroepitaxial growth of YSZ on silicon," *Jap. J. Appl. Phys.*, vol. 27, pp. L1404-L1405, 1988.

[10] P. Legagneux, G. Gary, D. Dieumegard, C. Schwebel, C. Pellet, G. Gautherin, and J. Siejka, "Epitaxial growth of yttria-stabilized zirconia films on silicon by ultrahigh vacuum ion beam sputter deposition," *Appl. Phys. Lett.*, vol. 53, pp. 1506-1508, 1988.

[11] D. K. Fork, D. B. Fenner, G. A. N. Connell, Julia M. Phillips, and T. H. Geballe, "Epitaxial yttria-stabilized zirconia on hydrogen terminated Si by pulsed laser deposition, *Appl. Phys. Lett*, vol. 57, pp. 1137-1139, 1990.

[12] M. Mikami, Y. Hokari, K. Egami, H. Tsuya, and M. Kanamori, "Formation of Si Epi/MgO · Al_2O_3 Epi/SiO_2 /Si and its epitaxial quality," *Extended Abstracts of the 15th Conf. Solid State Devices and Materials*, pp. 31-34, Tokyo, 1983.

[13] H. Fukumoto, T. Imura, and Y. Osaka, "Heteroepitaxial growth of Y_2O_3 films on silicon," *Appl. Phys. Lett.*, vol. 55, pp. 360-362, 1989.

[14] T. Inoue, Y. Yamamoto, S. Koyama, S. Suzuki, and Y. Ueda, "Epitaxial growth of CeO_2 layers on silicon," *Appl. Phys. Lett.*, vol. 56, pp. 1332-1333, 1990.

[15] D. K. Fork, D. B. Fenner, and T. H. Geballe, "Growth of epitaxial PrO_2 thin films on hydrogen terminated Si (111) by pulsed laser deposition," *J. Appl. Phys.*, vol. 68, pp. 4316-4318, 1990.

[16] M. Ishida, K. Sawada, S. Yamaguchi, T. Nakamura, and T. Suzaki, "Heteroepitaxial Si/Al_2O_3/Si structures," *Appl. Phys. Lett.*, vol. 55, pp. 556-558, 1989.

[17] J. T. Cheung and Haluk Sankur, "Growth of thin films by laser induced evaporation," *CRC Crit. Rev. Solid State Mat. Sci.*, vol. 15, pp. 63-109, 1988.

[18] F. J. Grunthaner and P. J. Grunthaner, "Chemical and electronic structure of the SiO_2 /Si interface," *Mater. Sci. Ret.*, vol. 1, pp. 65-160, 1986.

[19] D. B. Fenner, O. K. Biegelsen, and R. D. Bringans, "Silicon surface passivation by hydrogen termination: A comparative study of preparation methods," *J. Appl. Phys.*, vol. 66, pp. 419-424, 1989.

[20] I. Golecki, H. M. Manasevit, L. A. Moudy, J. J. Yang, and J. E. Mee, "Heteroepitaxial Si films on yttria-stabilized, cubic zirconia substrates," *Appl. Phys. Lett.*, vol. 42, pp. 501-503, 1983.

[21] R. Ramesh, D. Hwang, T. S. Ravi, A. Inam, J. B. Barner, L. Nazar, S. W. Chan, C. Y. Chen, B. Dutta, T. Venkatesan, and X. D. Wu, "Epitaxy of Y-Ba-Cu-O thin films grown on single-crystal MgO," *Appl. Phys. Lett.*, vol. 56, pp. 2243-2245, 1990.

[22] T. S. Ravi, D. M. Hwang, R. Ramesh, S. W. Chan, L. Nazar, C. Y. Chen, A. Inam, and T. Venkatesan, "Grain boundaries and interfaces in Y-Ba-Cu-O films laser deposited on single crystal MgO," *Phys. Rev. B*, vol. 42, pp. 10141-10151, 1990.

[23] D. K. Fork, K. Char, F. Bridges, S. Tahara, B. Lairson, J. B. Boyce, G. A. N. Connell, and T. H. Geballe, "YBCO films on YSZ and Al_2O_3 by pulsed laser deposition," *Physica C*, vol. 162-164, pp. 121-122, 1989.

[24] L. J. Showalter and R. W. Fathauer, "Growth of single crystal insulators on silicon," *CRC Crit. Rev. Solid State Mat. Sci.*, vol. 15, pp 367-421, 1989.

[25] W. Shi, J. Shi, J. Sun, W. Yao, and Zh. Qi, "Influence of substrate temperature on the orientation of YBCO films," *Appl. Phys. Lett.*, vol. 57, pp 822-824, 1990.

[26] N. G. Stoffel, P. A. Morris, W. A. Bonner, and B. J. Wilkins, "Ion-channeling study of single-crystal $YBa_2Cu_3O_x$," *Phys. Rev. B*, vol. 37, pp. 2297-2300, 1988.

[27] C. P. Bean, "Magnetization of hard superconductors," *Phys. Rev. Lett.*, vol. 8, pp. 250-253, 1962.

[28] S. Tahara, S. M. Anlage, J. Halbritter, C. B. Eom, D. K. Fork, T. H. Geballe, and M. R. Beasley, "Critical currents, pinning, and edge barriers in narrow YBCO thin films," *Phys. Rev. B*, vol. 41, pp. 11203-11208, 1990.

[29] R. B. van Dover, E. M. Gyorgy, A. E. White, L. F. Schneemeyer, R. J. Felder, and J. V. Waszczak, "Critical currents in proton-irradiated single-crystal YBCO," *Appl. Phys. Lett.*, vol. 56, pp. 2681-2683, 1990.

[30] Y. S. Touloukian, R. K. Kirby, R. E. Taylor, and T. Y. R. Lee, *Thermophysical Properties of Matter, Vol. 13: Thermal Expansion, Nonmetallic Solids*. New York: Plenum, 1977.

[31] J. D. Jorgensen, M. A. Beno, D. G. Hinks, L. Soderhold, K. J. Volin, R. L. Hitterman, J. D. Grace, Ivan K. Schuller, C. U. Segre, K. Zhang, and M.S. Kleefisch, "Oxygen ordering and the orthorhombic-to-tetragonal phase transition in YBCO," *Phys. Rev. B*, vol. 36, pp. 3608-3616, 1987.

[32] C. B. Eom, J. Z. Sun, K. Yamamoto, A. F. Marshall, K. E. Luther, T. H. Geballe, and S. S. Laderman, "In situ grown YBCO thin films from single-target magnetron sputtering," *Appl. Phys. Lett.*, vol. 55, pp. 595-597, 1989.

[33] Masami Tachikawa and Hidefumi Mori, "Dislocation generation of GaAs on Si in the cooling stage," *Appl. Phys. Lett.*, vol. 56, pp. 2225-2227, 1990.

[34] Q. Y. Ma, E. S. Yang, G. V. Treyz, and Chin-an Chang, "Novel method of patterning YBaCuO superconducting thin films," *Appl. Phys. Lett.*, vol. 55, pp. 896-898, 1989.

[35] D. K. Fork, A. Barrera, T. H. Geballe, A. M. Viano, and D. B. Fenner, *Appl. Phys. Lett.*, vol. 57, pp. 2504-2506, 1990.

[36] P. L. Richards, J. Clarke, R. Leoni, Ph. Lerch, S. Verghese, M. R. Beasley, T. H. Geballe, R. H. Hammond, P. Rosenthal, and S. R. Speilman, "Feasibility of the high Tc superconducting bolometer," *Appl. Phys. Lett.*, vol. 54, pp. 283-285, 1989.

David K. Fork (M'90) received the B.S. degree in physics and the M.S. degree in electrical engineering from the University of Rochester in 1987 and is currently working toward the Ph.D. degree in applied physics at Stanford University. During his doctoral thesis work, he has had a joint appointment at Stanford University and Xerox, Palo Alto Research Center. His thesis work incorporates pulsed laser deposition growth of epitaxial dielectric ferroelectric, optoelectronic and superconducting materials on Si.

He is author or co-author of 27 publications and is inventor or co-inventor on six patent filings.

Dr. Fork is a member of APS and MRS.

David B. Fenner (M'90) received the Ph.D. in physics from Washington University, St. Louis, in 1976.

He was an Associate Professor of Physics at Santa Clara University in Santa Clara, CA, where for the past three years he collaborated at the Xerox Palo Alto Research Center in the Electronic Materials Laboratory. At PARC he developed a simplified method of spin etching Si wafer surfaces for hydrogen termination and was a co-inventor of epitaxial YBCO films on YSZ buffered Si wafers. In June 1990 he joined Advanced Fuel Re-

search, Inc., East Hartford, CT, where he is Manager of the Superconductivity Group. He is the author of about 50 journal and conference publications.

Dr. Fenner is a member of APS and MRS.

Adrian S. Barrera Roldán received the B.Sc., M.Sc., and Ph.D. degrees in physics from the National Autonomous University of Mexico in 1981, 1983, and 1989, respectively.

From 1984 to 1987, he was a visiting scholar in the Department of Applied Physics at Stanford University. He was an associate professor in the Physics Department of the Autonomous Metropolitan University and the National Institute of Technology, in Mexico City from 1988 to 1989. In 1989 he joined the National Institute of Petroleum in Mexico City as a specialized researcher. Since January 1990, he has been a postdoctoral research affiliate in the Department of Applied Physics at Stanford University. His professional interests include superconducting electronic devices made of both low and high T_c materials.

Julia M. Phillips received the B.S. degree in physics from the College of William & Mary in 1976 and the Ph.D. in applied physics from Yale University in 1981.

In 1981, she joined AT&T Bell Laboratories as a member of the Technical Staff. In 1988 she became the supervisor of the Thin Film Research Group. Her interests include the growth and properties of epitaxial thin films and the relationships between film structure and other properties. She has authored or co-authored about 75 publications.

Theodore H. Geballe received the Ph.D. from the University of California, Berkeley, in 1949.

In 1952 he joined the staff of Bell Laboratories, where he specialized in semiconductor research, superconductivity, and the properties of materials at low temperatures. He is currently the Theodore and Sydney Rosenberg Professor of Applied Physics at Stanford University, where he has been since 1986. His most recent activities have been concerned with high temperature superconducting films. In 1970 he received the Oliver E. Buckley Solid State Physics Prize of the American Physical Society "for experimental investigations of superconductivity which challenged theoretical understanding and opened up the technology of high field superconductors." He is a member of the National Academy of Sciences and the American Academy of Arts and Sciences. In 1989 he was recipient of the first Bernd Matthias Memorial Award sponsored by AT&T Bell Laboratories.

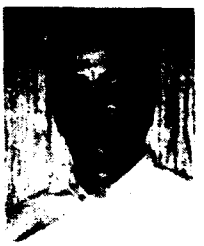

G. A. Neville Connell received the B.A. degree in natural sciences and the M.A. and Ph.D. degrees in physics from Cambridge University.

He spent six years in the Department of Engineering and Applied Science at Harvard University, where he started work on sputtered amorphous germanium and silicon thin films, and introduced the use of hydrogen to control the effects of dangling bonds on their electronic properties. In 1976, he came to Xerox PARC where he investigated materials for write-once optical recording by laser ablation, work which led to the formation of Optimem for product development. He is Manager of the Electronic Materials Laboratory at Xerox PARC. His most recent activities have been directed to thin-film materials and systems for magneto-optic recording, activities that have now also been incorporated in product.

James B. Boyce received the B.S. degree in engineering physics and the M.S. and Ph.D. degrees in physics from the University of Illinois, Champaign-Urbana.

After graduating, he spent one year as an IBM Post-Doctoral Fellow at the University of Illinois where he worked on NMR studies of the Kondo effect. In 1973 he joined the Xerox Palo Alto Research Center where he has worked on the characterization of defects and imperfectons in crystals, atomic motion in solids and liquids, magnetism, supercondictivity, amorphous materials, and the structure and dynamics of compounds and alloys. He was manager of the Complex Interactive Systems Area before assuming his current position as Manager of the Thin Film Semiconductor Area. His recent research has focused on the preparation and characterization of thin-film semiconductor and superconductor materials.

Epitaxial yttria-stabilized zirconia on hydrogen-terminated Si by pulsed laser deposition

D. K. Fork
Xerox Palo Alto Research Center, Palo Alto, California 94304 and Department of Applied Physics, Stanford University, Stanford, California 94305

D. B. Fenner
Xerox Palo Alto Research Center, Palo Alto, California 94304 and Physics Department, Santa Clara University, Santa Clara, California 95053

G. A. N. Connell
Xerox Palo Alto Research Center, Palo Alto, California 94304

Julia M. Phillips
AT&T Bell Laboratories, Murray Hill, New Jersey 07974

T. H. Geballe
Department of Applied Physics, Stanford University, Stanford, California 94305

(Received 7 May 1990; accepted for publication 12 July 1990)

Epitaxial yttria-stabilized zirconia films were grown on Si (100) and Si (111) by pulsed laser deposition. Rutherford backscattering spectroscopy indicates a high degree of crystalline perfection with a channeling minimum yield of 5.3%. A necessary predeposition process is removal of native silicon oxide from the Si prior to film growth. This is done outside the deposition chamber at 23 °C using a wet-chemical hydrogen-termination procedure. Epitaxial $YBa_2Cu_3O_{7-\delta}$ films have been grown on these films.

Yttria-stabilized zirconia (YSZ) is attractive for applications including storage capacitors in dynamic random access memories, hard disk protective overlayers, and radiation hard devices. YSZ is an ionic conductor[1] and has been used as a solid electrolyte in thin-film oxygen sensors[2] and fuel cells. YSZ has an index of refraction of 1.98 at 6328 Å, and is useful as a high quality facet coating for semiconductor lasers.[3] YSZ has a dielectric constant of 27 at 10 GHz,[4] and a 5 eV band gap. The cubic fluorite structure of $(Y_2O_3)_x(ZrO_2)_{1-x}$ is maintained over the composition range $x \approx 0.04$–0.30.[5] Strong electronic absorption[6] begins around 400 nm, making YSZ a useful source for pulsed laser deposition (PLD) using a XeCl (308 nm) excimer laser. Epitaxial YSZ has been grown by ion beam sputter deposition[7] and electron beam deposition.[5] PLD and sputtering have been used to grown nonepitaxial, polycrystalline films of YSZ on Si.[8] In this letter, we report the first growth of epitaxial YSZ on Si by PLD.

One benefit of developing a PLD technology for epitaxial YSZ is the ease with which films of the high-temperature superconductors may be grown. The $Y_1Ba_2Cu_3O_{7-x}$ (YBCO)-Si decomposition reaction is severe whereas YSZ is comparatively inert with Si.[9] Past work[8] has demonstrated that YBCO films grown on Si with YSZ buffer layers have better properties than films grown directly on Si, principally due to the avoidance of reaction. None of the previously reported films have approached the quality attainable with substrates such as MgO, $SrTiO_3$, $LaAlO_3$, and in particular single-crystal YSZ[10] due to the polycrystalline and multiphase nature of the YSZ buffer film. With the process reported here, we have grown YBCO/YSZ/Si films with T_c ($R=0$) of 86–88 K, critical current of 2.2×10^6 A/cm^2 at 77 K, and a Rutherford backscattering spectroscopy (RBS) channeling minimum yield of 12%.[11]

An obstacle to epitaxial growth on Si is the surface oxide. Recently our group demonstrated the effectiveness of hydrogen-terminated Si surfaces, which allowed the growth of epitaxial PrO_2 on Si for the first time.[12] The technique is an *ex situ*, room-temperature wet-chemical process, effective for both (100) and (111) orientations.

The PLD technique is reviewed in Ref. 13. YSZ targets made by pressing mixtures of ZrO_2 and Y_2O_3 at 50 000 psi and sintering for 36 h at 1000 °C in flowing O_2 produce smoother films than earlier YSZ films made by depositing ZrO_2 and Y_2O_3 separately. The Si substrates are heated radiantly to 800–850 °C, as recorded by an optical pyrometer, and held 5 cm from the target; each 17 ns laser pulse deposits about 0.2 Å per 130 mJ (1.3 J/cm^2) pulse. The laser is fired at 8–10 Hz.

The wafers are degreased and spin etched in a flowing N_2 hood; this is a variation of Ref. 14. The Si wafer is rotated, flushed with high-purity alcohol, and etched with several drops of a 1:10:1 mixture of HF, ethanol, and water, all of high purity. The subtrates are transferred in N_2 to our deposition system via a N_2 purged glove box and load lock. X-ray photoelectron spectroscopy indicates that after spin etching, 0.03 monolayer (ML) of total carbon residue and ~0.005 ML each of oxygen and fluorine remain on the surface.[15] These H-terminated Si surfaces are very passive to reoxidation or contamination even in 1 atm air. The H remains on the surface until the substrates are heated above ~500 °C.

A critical parameter for epitaxy is O_2 pressure during growth. In the low-pressure regime, films grown in a base pressure of 10^{-6} Torr are reduced, semiconducting, silvery in appearance, and adhere poorly to Si; the cubic YSZ

 0003-6951/90/371137-03$02.00

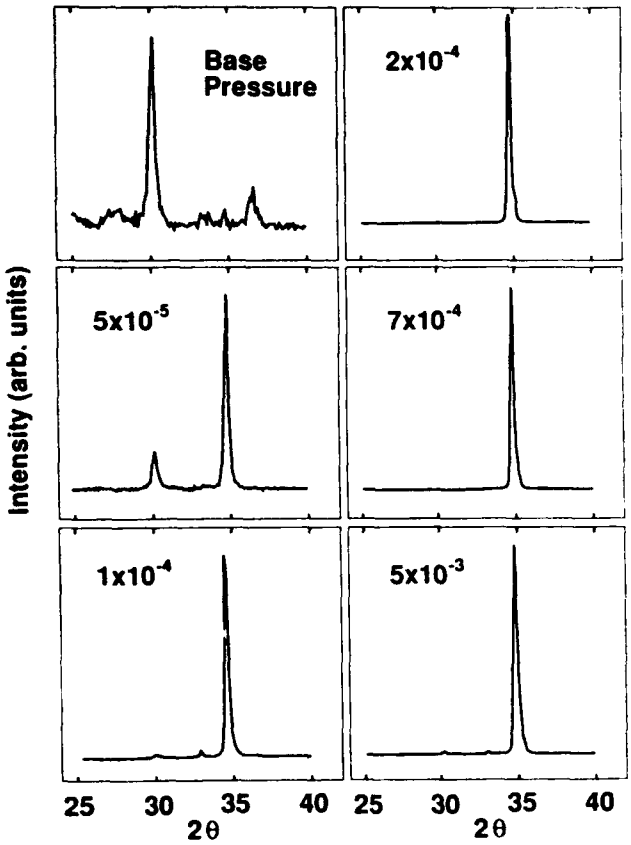

FIG. 1. 2θ scans of YSZ films grown at 800 °C on H-terminated Si (100) over a range of oxygen pressures as indicated in Torr. The base pressure is 10^{-6} Torr. Peaks occurring at 30° are the undesirable (111) orientation of the YSZ. Peaks at 35° correspond to epitaxial YSZ (002).

phase, while present to some degree, is oriented randomly. In the high-pressure regime, films deposited on Si (100) in 50 mTorr O_2 have poor epitaxy with only weakly preferred [001] orientation. Presumably, at this pressure, silicon oxide regrowth through the growing YSZ films is impeding epitaxy as we observed[12] for the growth of PrO_2 on Si. This suggested that an optimized O_2 pressure would minimize both adverse effects, as we have observed. All samples in this experiment were heated in $\sim 10^{-6}$ Torr and O_2 was introduced shortly after the laser pulsing began.

All films were characterized by x-ray diffraction on a four circle diffractometer with a Cu K_α source. Figure 1 shows 2θ scans of a series of $x = 0.05$ YSZ films grown on Si (100) at 800 °C in 10^{-6} Torr to 5 mTorr O_2. One notes the elimination of the undesired YSZ (111) peak as the orientation improves with increasing O_2 pressure. The optimum O_2 pressure lies between 2×10^{-4} and 7×10^{-4} Torr, producing ω-rocking curve full width at half maxima (FWHM) of 0.7° to 0.8° for YSZ (002) (Table I). Our resolution in ω as determined by the Si (004) peak is 0.2°. The YSZ (002) intensities also peak in the optimal pressure range. The small shoulder on the YSZ (002) peak, which is attributable to the tetragonal ZrO_2 phase, is not present in films with $x = 0.09$, indicating that only the cubic fluorite structure is obtained. A film grown on Si (111) was also epitaxial with a rocking curve full width at half maximum (FWHM) also in Table I.

TABLE I. ω-rocking curve FWHM and peak intensity for films grown at 800 °C as a function of O_2 pressure.

Substrate	O_2 (Torr)	YSZ peak	ω FWHM	peak intensity
Si (100)	vacuum	(200)	>5°	12
Si (100)	5×10^{-5}	(200)	4.50°	70
Si (100)	1×10^{-4}	(200)	1.19°	450
Si (100)	2×10^{-4}	(200)	0.82°	1150
Si (100)	4×10^{-4}	(200)	0.71°	1300
Si (100)	7×10^{-4}	(200)	0.86°	1450
Si (100)	1×10^{-3}	(200)	0.88°	800
Si (100)	5×10^{-3}	(200)	1.05°	720
Si (100)	5×10^{-2}	(200)	1.76°	220
Si (111)	1×10^{-4}	(111)	1.47°	140

In plane film texturing was determined from phi scans of the YSZ {202} peaks. The crystallography of all films is cube on cube with the YSZ [110] direction along the Si [110] direction. This epitaxy is rotated by 45° with respect to that in Ref. 5, which reported a lattice match of 0.2% for YSZ/Si heteroepitaxy requiring Si [010] parallel to YSZ [110] and a ratio of 3:2 in the lattice-matched repeat lengths. The lattice mismatch for the orientation we observe is larger (-5.8%), however, no material oriented as in Ref. 5 appeared in our phi scans. In contrast, we have observed multiple in-plane orientations in the PrO_2/Si system, particularly when growth conditions were not optimized. The twist misalignment of the YSZ grains, measured by the phi width, was less than 1° ($\Delta\phi = 1.14°$); our resolution in ϕ as measured on the Si (202) peak is 0.57°.

Rutherford backscattering spectroscopy along aligned ⟨001⟩ and random directions using 1.8 MeV[4] He^+ ions characterized thickness and crystalline quality. Figure 2 shows aligned and random spectra for a YSZ ($x = 0.09$) film grown at 800 °C in 4×10^{-4} Torr O_2. The thickness at center was determined to be 1500 Å. The ratio of the backscattered yield along ⟨001⟩ to that in a random direction (χ_{min}) is 5.3%. This result compares with the best reported[5] value for electron beam deposited films of 5%. χ_{min} would be ~3% for a high quality single crystal.

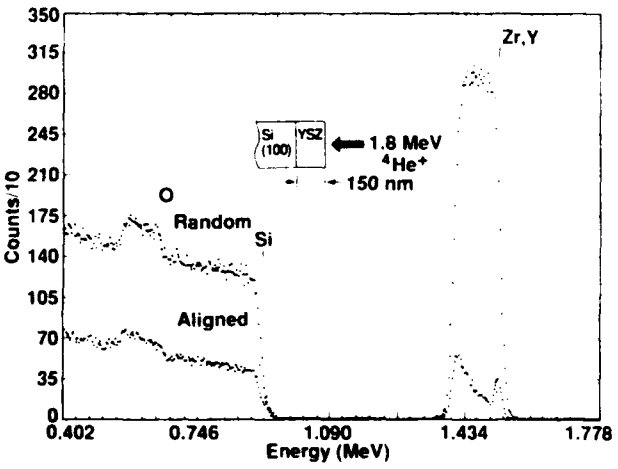

FIG. 2. Energy spectra of ⟨001⟩ aligned and random 1.8 MeV 4He $^+$ ions backscattered from a 1500 Å YSZ film on Si (100).

FIG. 3. Scanning force micrographs of (a) a 1500-Å-thick YSZ film grown at 800 °C. The area shown is 4×4 μm^2. The full grey scale is 40.5 Å. (b) A 1×1 μm^2 area of a 1500-Å-thick YSZ films grown at 850 °C. Note that the grey scale is $10\times$ larger than (a).

There is strong dechanneling in all YSZ films, particularly near the interface, which may contribute to the nonideal χ_{min}. This observation is reminiscent of epitaxial CaF_2 films on Si, which like YSZ films have a large mismatch in the thermal expansion coefficients[16] (α) between substrate and film ($\alpha_{Si} = 3.8\times10^{-6}$/°C, $\alpha_{YSZ} = 11.4\times10^{-6}$/°C, $\alpha_{CaF_2} = 19\times10^{-6}$/°C). Microplasticity has been observed[17] in YSZ at 23 °C, and may be involved in the relaxation; the yield strain (~0.0057) is close to the thermally induced strain (~0.0059). Both lattice match and plasticity should increase with yttria content which may be beneficial.

Characterization of the surface morphology of 1500 Å films grown at 800 °C by scanning electron microscopy and stylus profilometry failed due to the extreme smoothness of the films. Scanning force microscopy using a Park Scientific Instruments model No. SFM-BD2 revealed [Fig. 3 (a)] a surface roughness of ~10 Å over a 4×4 μm^2 area. This is comparable to the ~6 Å roughness of polished Si. The surface features are dominated by extremely shallow valleys $\sim10\,000$ Å long, ~1500 Å wide, and ~10 Å deep. These ⟨110⟩ oriented features provide additional evidence for strain relaxation in these films. Films grown at 850 °C have a seriously degraded surface [Fig. 3(b)] with a roughness of ~350 Å in a 1×1 μm^2 area.

In summary, epitaxial YSZ films have been grown on Si (100) and Si (111) by PLD. O_2 pressure is a critical parameter for epitaxy of the cubic phase. Smooth, epitaxial films consisting only of the cubic YSZ phase were obtained for $x = 0.09$. A critical step prior to epitaxy is the Si oxide removal and passivation with H. Films characterized by RBS channeling have χ_{min} as low as 5.3%. These YSZ films have permitted fabrication of high quality YBCO films on Si via an entirely *in situ* process.

We thank Michael Kirk of Park Scientific Instruments for scanning force microscopy, and R. I. Johnson, S. Ready, and L. E. Schwartz for technical assistance. This work benefits from AFOSR (F49620-89-C-0017). DBF received NSF (DMR-8822353). DKF is an AT&T scholar.

[1] S. Ikeda, O. Sakurai, K. Uematsu, N. Mizutani, and M. Kato, J. Mater. Sci. **20**, 4593 (1985).
[2] Yuji Miyahara, Keiji Tsukada, and Hiroyuki Miyagi, J. Appl. Phys. **63**, 2431 (1988).
[3] A. K. Chin, A. Satyanarayan, J. H. Zarrabi, and W. Vetterling, J. Appl. Phys. **64**, 994 (1988).
[4] M. T. Lanagan, J. K. Yamamoto, A. Bhalla, and S. G. Sankar, Mater. Lett. **7**, 437 (1989).
[5] H. Fukumoto, T. Imura, and Y. Osaka, Jpn. J. Appl. Phys. **27**, L1404 (1988).
[6] D. L. Wood and K. Nassau, Appl. Opt. **21**, 2978 (1982).
[7] P. Legagneux, G. Gary, D. Dieumegard, C. Schwebel, C. Pellet, G. Gautherin, and J. Siejka, Appl. Phys. Lett. **53**, 1506 (1988).
[8] A. Mogro-Campero, Supercond. Sci. Technol. **3**, 155 (1990).
[9] D. B. Fenner, A. M. Viano, G. A. N. Connell, D. K. Fork, J. B. Boyce, F. A. Ponce, and J. C. Tramontana (unpublished).
[10] D. K. Fork, K. Char, F. Bridges, S. Tahara, B. Kairson, J. B. Boyce, G. A. N. Connell, and T. H. Geballe, Physica C **162–164**, 121 (1989).
[11] D. K. Fork, D. B. Fenner, R. W. Barton, Julia M. Phillips, G. A. N. Connell, J. B. Boyce, and T. H. Geballe, Appl. Phys. Lett. **57**, 1161 (1990).
[12] D. K. Fork, D. B. Fenner and T. H. Geballe, J. Appl. Phys. **68**, 15 Oct. (1990).
[13] J. T. Cheung and H. Sankur, CRC Crit. Rev. Solid State Mater. Sci. **15**, 63 (1988).
[14] F. J. Grunthaner and P. J. Grunthaner, Mater. Sci. Rep. **1**, 65 (1986).
[15] D. B. Fenner, D. K. Biegelsen, and R. D. Bringans, J. Appl. Phys. **66**, 419 (1989).
[16] L. J. Schowalter, R. W. Fathauer, R. P. Goehner, L. G. Turner, R. W. DeBlois, S. Hashimoto, J.-L. Peng, W. M. Gibson, and J. P. Krusius, J. Appl. Phys. **58**, 203 (1985).
[17] J. Lankford, J. Mater. Sci. Lett. **8**, 947 (1989).

High T_c Superconductor Thin Films
L. Correra (Editor)

Buffer layers on silicon for growth of YBCO films

D. K. Forka,b, G.A.N. Connella, F.A. Ponce[a], J.B. Boyce[a], and T.H. Gebalb

[a]Xerox Palo Alto Research Center, 3333 Coyote Hill Rd., Palo Alto, CA 94304, USA

[b]Dept. of Applied Physics, Stanford University, Stanford, CA 94305, USA

Abstract

Pulsed laser deposition is a powerful technique for the epitaxial growth of superconducting oxide films on numerous oxide substrates. Until recently, epitaxy on silicon substrates was made impossible by the chemical reactivity and thermal expansion mismatch of silicon and superconducting oxides. By interleaving an epitaxial buffer layer of yttria-stabilized zirconia in a fully *in-situ* laser deposition process, we have addressed both of these problems to grow c-axis oriented, epitaxial $Y_1Ba_2Cu_3O_{7-\delta}$ (YBCO) films on silicon. X-ray diffraction indicates an in-plane, epitaxial alignment within 2°. The films not only have high superconducting transition temperatures of 88 K but also have critical current densities of $2.2x10^6$ A/cm^2 at 77 K. Transition widths are 1 K and normal state resistivities are 0.28 mOhm-cm at 300 K. Additional studies of YBCO on silicon-on-sapphire show that the limit on thickness of about 50 nm, set by thermal strain, for oxide films on bulk silicon can be overcome, and films with thicknesses far beyond this critical thickness have been grown. The surface resistance of these films at 4.2K and 11.8GHz is 72 μΩ cm and the critical current at 77 K is $4.6x10^6$ A/cm^2. The values of the above parameters are now high enough to enable the fabrication of micro-electronic devices with superior performance.

1. OUTLINE

In this extended abstract, we review our work on the epitaxial growth of YBCO on silicon and silicon-on-sapphire using YSZ as an epitaxial buffer layer.

2. PULSED LASER DEPOSITION

All growths in this study were performed by pulsed laser deposition using a rotating polygon target system ('PolyGun') designed to accommodate ten different materials during a single deposition run. By triggering a 308 nm XeCl excimer laser to ablate a particular target with each revolution of the polygon, interfacial monolayers, films formed by atomic level mixing of numerous target materials, and multilayer stacks can all readily be deposited under computer control. We have used all of these growth techniques in the work reported here.

3. WHY CHOOSE YSZ AS A BUFFER LAYER?

YSZ is an attractive buffer layer for numerous reasons: it is chemically inert both with silicon and YBCO at the growth temperature of 750 ^{o}C [1]; its cubic fluorite structure is related to the silicon structure and has a lattice constant that may be controlled by varying the yttria content [2]; and it provides a good silicon diffusion barrier when more than 20 nm thick, such that thicknesses well below the critical thickness for crack propagation from thermally induced strain can be used [3]. But previous work on the deposition of YBCO on single crystal YSZ points to a potential problem: the in-plane epitaxy of YBCO on YSZ is tristable with the YBCO a-axis either parallel to the YSZ<100>, parallel to the YSZ <110>, or broadly distributed about $\pm 9^{o}$ to the YSZ <100> [4]. Such grain boundaries will severely restrict the critical current attainable in the YBCO film [5]. We have shown that the occurrence of grains other than those with the a-axis parallel to the YSZ <110> is minimized by first growing a homoepitaxial YSZ layer on theYSZ and initiating the YBCO growth with a monolayer of CuO or Y_2O_3 [6]. We therefore have an effective process for growing high quality YBCO films on single crystal YSZ and epitaxial YSZ films on silicon.

4. EPITAXIAL GROWTH AND STRUCTURE OF YSZ AND YBCO ON SILICON

An essential step for the epitaxial growth of YSZ on silicon is the preparation of the silicon surface. In our work, the silicon wafers are spin cleaned and etched in flowing nitrogen first using high purity alcohol and then a 1:10:1 mixture of HF, ethanol, and water. This process produces an oxide-free, passivated wafer surface, covered by one monolayer of hydrogen, that remains uncontaminated during the passage of the wafer through the nitrogen-purged load lock into the deposition chamber [7]. Epitaxial growth of a 50 nm thick YSZ film is then achieved using an excimer laser energy density of 1-2 J/cm^2, a substrate temperature of 750 ^{o}C, and background oxygen pressure of 5x10^{-4} Torr. The epitaxial growth of YBCO follows immediately using the same laser energy density and substrate temperature, but with a background oxygen pressure of 200 mTorr [8].

The structural orientation and in-plane texturing of the YSZ and YBCO films have been examined by x-ray diffraction. The YSZ films have [001] perpendicular to the surface to within 0.8^{o} and [100] parallel to silicon [100] to within 1.1^{o}. This cube-on-cube epitaxy occurs with a lattice mismatch to silicon of almost 6%, but the ratio of the Rutherford backscattered yield along <100> to that in a random direction (X_{min}) of 5.3% is little greater than the 3% observed in high quality YSZ single crystals. There is strong dechannelling at the YSZ-silicon interface attributable to the large mismatch in the thermal expansion coefficients [9].

The YBCO films have their c-axes oriented perpendicular to the surface to within 0.8^{o} and [110] parallel to YSZ [100] to within 2^{o}. Thin films are placed under strain by the great difference in the thermal expansion coefficients of silicon and YBCO - the average ab-distance is expanded by 0.41% while the c-distance is contracted by a similar amount in 13 nm thick films. In films thicker than about 50 nm, the strain energy is relaxed by cracks occuring at about 1 μm spacings along <100> directions [10]. Cracking in thicker films can be overcome

by using silicon-on-sapphire as the substrate [11]. In this case, the closer match of the thermal expansion coefficients of sapphire and YBCO allow films with thicknesses of at least 400 nm to be grown before strain relaxation by cracking occurs.

5. ELECTRICAL PROPERTIES OF YBCO ON SILICON AND SILICON-ON-SAPPHIRE

YBCO films grown in this study have a zero resistance at 88 K and a transistion width of less than 1 K. For films on silicon-on-sapphire, the critical current at 77 K is 4.6×10^6 A/cm^2 and the surface resistance at 11.8 GHz and 4.2 K is 72μΩ. For films on silicon, the electrical properties depend strongly on film thickness. When cracking occurs, the critical current at 77 K drops precipitously to 1×10^5 A/cm^2 from a value of 2×10^6 A/cm^2 in thin films.

6. CONCLUSION

Using a straightforward *in-situ* deposition process, we believe that we have taken the first steps in developing the materials technology needed to design electronic circuits in which superconducting and semiconducting elements are integrated. We now plan to address the challenging materials issues associated with circuit delineation, cross-over and via fabrication, and active device design.

7. REFERENCES

1 D.B. Fenner, A.M. Viano, D.K. Fork, G.A.N. Connell, J.B. Boyce, F.A. Ponce, and J.C. Tramontana, J. Appl. Phys., 69 (1991) 2176.
2 I. Golecki, H.M. Manasevit, L.A. Moudy, J.J. Yang, and J.E. Mee, Appl. Phys. Lett., 42 (1983) 501.
3 M.S. Hu, M.D. Thouless, and A.G. Evans, Acta Metall., 36 (1988) 1301.
4 D.K. Fork, A. Barrera, T.H. Geballe, A. M. Viano, and D.B. Fenner, Appl. Phys. Lett., 57 (1990) 2504.
5 D. Dimos, P. Chaudhari, J. Mannhart, and F.K. Legouse, Phys. Rev., B41 (1990) 4038.
6 D.K. Fork, S.M. Garrison, F.A. Ponce, Marlyn Hawley, D.M. Wehner, and T.H. Geballe, J. Mats. Res. (to be published).
7 D.B. Fenner, D.K. Biegelsen, and R.D. Bringans, J. Appl. Phys., 66 (1989) 419.
8 D.K. Fork, D.B. Fenner, A. Barrera, J.M. Phillips, T.H. Geballe, G.A.N. Connell, and J.B. Boyce, IEEE Trans. Appl. Supercond., 1 (1991) 67.
9 L.J. Schowalter, R.W. Fathauer, R.P. Goehner, L.G. Turner, R.W. DeBlois, S. Hashimoto, J.L. Peng, W.M. Gibson, and J.P. Krusius, J. Appl. Phys., 58 (1985) 203.
10 D.K. Fork, D.B. Fenner, R.W. Barton, J.M. Phillips, G.A.N. Connell, J.B. Boyce, and T.H. Geballe, Appl. Phys. Lett., 57 (1990) 1161.
11 D.K. Fork, F.A. Ponce, J.C. Tramontana, N. Newman, J.M. Phillips, and T.H. Geballe, Appl. Phys. Lett., (to be published May 27, 1991).

Physica C 185-189 (1991) 2117-2118
North-Holland

PHYSICA C

SUMMARY ABSTRACT: GROWTH, PROPERTIES AND APPLICATIONS OF EPITAXIAL $YBa_2Cu_3O_{7-\delta}$ THIN FILMS ON Si

David K. Fork,[1,2] G. A. N. Connell,[2] J. B. Boyce,[2] and T. H. Geballe[1]

[1]Stanford University, Department of Applied Physics, W. W. Hansen Laboratories, Stanford, CA 94305, USA
[2]Xerox Palo Alto Research Center, 3333 Coyote Hill Road, Palo Alto, CA 94304, USA

Earlier attempts to produce high quality thin films of $YBa_2Cu_3O_{7-\delta}$ on Si substrates were thwarted by their reactivity and thermal expansion behavior. The collective research or several groups has demonstrated several epitaxial buffer layer systems including yttria-stabilized zirconia and MgO which allow the epitaxial growth of YBCO on Si without chemical reaction. Although direct epitaxy of YBCO on silicon may not be possible, buffer layers permit the growth of device quality YBCO films with critical current densities in excess of 10^6 A/cm^2 at 77 K. Methods have been developed to pattern these films in-situ by removing the buffer layer in selected areas to produce isolated superconducting mesas. The complications of thermally induced tensile stress have been eliminated through the use of silicon-on-sapphire instead of silicon. This work has revealed methods for controlling the in-plane epitaxy of YBCO films on zirconia via homoepitaxy and nucleation-initiating monolayers. A variety of application-oriented measurements and structures will be reported.

1. Introduction

Monolithic combination of the high-temperature superconducting cuprates and silicon semiconducting technology will require thin film structures which prevent interdiffusion and adverse chemical interactions and which also permit the epitaxial growth of these materials. There has been considerable progress recently which has produced thin films of $YBa_2Cu_3O_{7-\delta}$ (YBCO) with dc transport properties close to what are considered intrinsic limits of the material. This paper will review the progress and discuss the related materials and applications issues.

2. Materials

All of the reports of YBCO films on silicon with high critical current densities have employed epitaxial oxide buffer layers. Table 1 lists representative structures.

TABLE 1
Epitaxial Buffer Layer Systems for YBCO on Si

Structure	Group	T_c (K)	J_c (77 K) MA/cm^2	One System	t_{YBCO} (nm)	Ref.
$BaTiO_3$/ $MgAl_2O_4$	Bellcore/ Rutgers	87	0.06	no	100	1
Y_2O_3/YSZ	Hiroshima	84	1.0	no	60	2
YSZ	Stanford/ Xerox	88	2.2	yes	<50	3
$BaTiO_3$/MgO	"	88	0.7	yes	<50	4
YSZ/Si/Al_2O_3	"	88	4.6	no	>400	5
CeO_2	Los Alamos	87	0.2	no	220	6

Critical current density (J_c) is limited by buffer layer quality and effects of thermally induced biaxial tension. This also limits the thickness of the YBCO layer (t_{YBCO}). The highest J_c has been obtained by mitigating thermal stress by using silicon-on-sapphire substrates (α_{YBCO} = 16x10^{-6}/°C, α_{Si} = 8.4x10^{-6}/°C and $\alpha_{Al_2O_3}$ = 3.8x10^{-6}/°C) .[5] This may be the most direct route to obtaining YBCO films thick enough for microwave applications. Stress can also be lowered by techniques which lower the YBCO growth temperature, however, these have not been adequately developed. Crack nucleation appears to be influenced somewhat by the type of buffer layer material accounting for some variation in reported critical thicknesses, typically from 50 to 100 nm on bulk Si for the highest critical currents.

Fabrication of all thin film layers via one integrated process has been demonstrated in two cases[3,4] and it should be possible to integrate many other systems also. The YBCO/YSZ epitaxial system is known to frequently produce several epitaxial orientations,[7] however it has been noted that the in-situ processing of YBCO and YSZ layers renders one orientation singularly stable.[5,8] Additional techniques for controlling the epitaxial relations in this system have been recently discovered. These involve monolayers of Y or Cu oxides, or layers of CeO_2 prior to YBCO deposition.[9]

Three techniques in Table I have a demonstrated potential for producing a-axis oriented YBCO on Si[1,4,6] which may be desirable in tunneling structures requiring vertical access to the long (~1 nm) YBCO coherence length. The $BaTiO_3$ layer described in Ref. 4 has been used as a substrate for off-axis sputter deposition of a 90% a-axis film, and Ref. 6 reports use of [110] oriented CeO_2 on Si (100) to nucleate a-axis material.

Little has been done so far to asses the impact of these buffer layer oxides on the electronic properties of the silicon,

however, there is no evidence for Zr induced deep levels in Si.[11] Time will delineate which buffer layer systems are most practical in applications.

3. Applications

Applications are at the inception stage. Silicon offers some unique patterning capabilities. Self-aligned in-situ patterning may be done by removing the buffer layer in selected areas prior to YBCO deposition to produce electrically isolated superconducting YBCO mesas.[8] Similarly, deeply etched silicon features can define edges of YBCO constrictions.[12]

Well established techniques for producing ~ 1 μm supported silicon membranes[13] make YBCO/Si attractive for transition edge membrane bolometers operating in the far-infrared (≥10 μm).[14] Voltage noise measurements on YBCO/YSZ/Si in the transition indicate approximately Johnson noise limited behavior.[15]

The YBCO/buffer-layer/Si bilayer is readily modified to perform capacitance voltage characterization. C-V data on YBCO/YSZ/Si indicates low leakage and possible usage as a gate or interconnect structure.[16] The density of interface traps at the YSZ/Si interface is about $3x10^{11}$ /eVcm^2 at midgap, and the ionic conduction properties of the YSZ layer are largely frozen out at 77 K.

The normal state conductivity of YBCO/Si may be utilized for lattice matched metallization of epitaxial ferroelectrics on silicon for nonvolatile memories and related applications which operate at room termperature. Recent demonstration of bismuth titanate/YBCO heterostructures on silicon with hysteretic remanence of 0.7 - 1.2 μC/cm^2 and a coercive field of 80 to 100 KV/cm has been reported.[17]

Contact schemes for electrical connection of the YBCO layer to the Si substrate have currently taken two forms. (1) Conducting buffer layers,[18] and (2) metal overlayers contacting the Si through vias opened in the buffer layer. All of the conducting buffer layers (indium tin oxide, RuO_2 and $CoSi_2$) are currently non-epitaxial and therefore do not yield satisfactory Jc and are not listed in Table 1. The second technique should be adaptable from techniques employed for low temperature CMOS designs.

4. Summary

This report has summarized current results germane to the area of YBCO-silicon monolithic structures. We acknowledge support from AFOSR (F49620-89-C-0017). DKF is an AT&T scholar.

5. References

1. X. D. Wu, A. Inam, M. S. Hegde, B. Wilkins, C. C. Chang, D. M. Hwang, L. Nazar, T. Venkatesan, S. Miura, S. Matsubara, Y. Miyasaka and N. Shohata, Appl. Phys. Lett. **54**, 754 (1989).
2. H. Myoren, Y. Nishiyama, N. Miyamoto, Y. Kai, Y. Yamanaka, Y. Osaka and F. Nishiyama, Jap. J. Appl. Phys. **29**, L955 (1990).
3. D. K. Fork, D. B. Fenner, R. W. Barton, Julia M. Phillips, G. A. N. Connell, J. B. Boyce and T. H. Geballe, Appl. Phys. Lett. **57**, 1161 (1990).
4. D. K. Fork, F. A. Ponce, J. C. Tramontana and T. H. Geballe, Appl. Phys. Lett. **58**, 2294 (1991).
5. D. K. Fork, F. A. Ponce, J. C. Tramontana, N. Newman Julia M. Phillips and T. H. Geballe, Appl. Phys. Lett. **58**, 2432 (1991).
6. Li Luo, X. D. Wu, R. C Dye, R. E. Muenchausen, S. R. Foltyn, Y. Coulter, C. J. Maggiore and T. Inoue (unpublished).
7. S. M. Garrison, N. Newman, B. F. Cole, K. Char and R. W. Barton, Appl. Phys. Lett. **58**, 2168 (1991).
8. D. K. Fork, A. Barrera, A. M. Viano, D. B. Fenner and T. H. Geballe, Appl. Phys. Lett. **57**, 2504 (1990).
9. D. K. Fork, S. M. Garrison and T. H. Geballe (unpublished).
10. C. B. Eom, D. K. Fork (unpublished).
11. J. W. Chen and A. G. Milnes, Ann. Rev. Mater. Sci. **10**, 157 (1980).
12. H. Myoren, N. Miyamoto, Y. Osaka, T. Hamasaki, Ext. Abs. 22nd Int. Conf. Sol. State Dev. and Mater. 577 (1990).
13. K. C. Lee, J. Electrochem. Soc. **137**, 2256 (1990).
14. P. L. Richards, J. Clarke, R. Leoni, Ph. Lerch, S. Verghese, M. R. Beasley, T. H. Geballe, R. H. Hammond, P. Rosenthal and S. R. Spielman, Appl. Phys. Lett **54**, 283 (1989).
15. S. Verghese, D. K. Fork (unpublished data).
16. E. Ajimine, F. Pagaduan, M. M. Rahman, C. Y. Yang, H. Inokawa, D. K. Fork, T. H. Geballe (unpublished).
17. R. Ramesh, A. Inam, B. Wilkins, W. K. Chan, J. M. Tarascon, D. K. Fork, T. H. Geballe, J. Evans and J. Bullington, Appl. Phys. Lett. (accepted).
18. B. J. Kellet, J. H. James, A. Gauzzi, B. Dwir, D. Pavuna, F. K. Reinhart, Appl. Phys. Lett **57**, 2588 (1990); Q. X. Jia and W. A. Anderson, Appl. Phys. Lett **57**, 304 (1990); Li Luo, R. E. Muenchausen, C. J. Maggiore, J. R. Jimenez, L. J. Schowalter, Appl. Phys. Lett **58**, 419 (1990).

Reaction patterning of $YBa_2Cu_3O_{7-\delta}$ thin films on Si

D. K. Fork
Xerox Palo Alto Research Center, Palo Alto, California 94304, and Department of Applied Physics, Stanford University, Stanford, California 94305

A. Barrera and T. H. Geballe
Department of Applied Physics, Stanford University, Stanford, California 94305

A. M. Viano[a)] and D. B. Fenner
Xerox Palo Alto Research Center, Palo Alto, California 94304, and Physics Department, Santa Clara University, Santa Clara, California 95053

(Received 7 September 1990; accepted for publication 9 October 1990)

A novel technique exploiting the severe chemical reaction between Si and $YBa_2Cu_3O_{7-\delta}$ (YBCO) has been developed for patterning epitaxial YBCO films *in situ*. Patterning is achieved by etching features in epitaxial YSZ on Si(100), and then depositing a final layer of YBCO; the material which grows on the exposed Si is insulating. Linewidths down to 3 μm have been demonstrated with a zero resistance critical temperature (T_c) of 86 K and a transport critical current density of 1.6×10^6 A/cm^2 at 77 K. 45° and low-angle twist grain boundaries occur under some circumstances but can be eliminated by regrowing 20 Å of homoepitaxial YSZ on the surface prior to YBCO growth. Si diffusion in insulating portions has been characterized by x-ray photoemission spectroscopy, indicating vertical diffusion through the film.

It has been established for over two years[1] that the reaction of Si with $YBa_2Cu_3O_{7-\delta}$ (YBCO) is severe. This causes YBCO/Si thin films to have reacted interfaces[2] and has slowed progress in growing high quality YBCO thin films on silicon substrates.[3] With the growth of high quality YBCO on Si now possible,[4] this reaction can now be exploited to react selected areas of the YBCO film to achieve *in situ* patterning. The reaction of Si with YBCO not only destroys the superconductivity, but renders it insulating as well. The idea for patterning YBCO with Si was originally practiced by Ma *et al.*[5] who used patterned Si on MgO substrates; by using a post-deposition anneal treatment at 980 °C, lines down to 2.5 μm were defined having a transition temperature (T_c) of 76 K and a critical current density (J_c) of 300 A/cm^2 at 75 K.

Recently, we have shown that *in situ* patterning is feasible at a much lower temperature, 750 °C, and results in electrically isolated features on Si substrates with a zero resistance $T_c\sim86$ K and $J_c=1.6\times10^6$ A/cm^2 at 77 K. One principle advantage of this technique is that fully operational planar devices such as bolometers, delay lines, and weak link structures such as substrate step edge superconducting quantum interference devices (SQUIDs) can be produced without subjecting the YBCO film to wet chemical etchants, photoresist, or solvents. This may be of particular benefit in the case of ultrathin films or structures mounted on thin substrates, such as membrance bolometers.

Our process consists of growing an epitaxial yttria-stabilized zirconia (YSZ) film on Si(100) by pulsed laser deposition as described in Ref. 6, removing selected areas of the YSZ film by Ar^+ ion milling, and then laser depositing a layer of YBCO. This process is illustrated in Fig. 1. Figure 2 shows a scanning electron micrograph of a 3-μm-wide line reaction patterned into a 400 Å YBCO film. The desired pattern is defined lithographically in positive photoresist. The Ar^+ ion milling procedure uses a Kaufman ion source operating at 500 V. The substrate holder is water cooled during milling. The etch rates of Si and YSZ were determined by profilometry to be 40 and 20 Å/min, respectively. An advantage of this process is the formation of a mesa structure isolating the patterned YBCO features from the possibility of lateral Si diffusion.

Prior to this work, little effort existed investigating the influence of surface preparation on the epitaxy of YBCO on YSZ. This work reveals that an *in situ* grown YSZ surface is in many respects an ideal growth surface for YBCO. Our first attempts to produce high quality *in situ* patterned YBCO films produced films with the *c* axis normal to the substrate, however, the electrical properties were degraded due to the presence of 45° angle twist grain boundaries and other low-angle twist boundaries. These grain boundaries never developed when YBCO/YSZ/Si bilayer films were processed entirely *in situ* without interruption between the YBCO and YSZ depositions.[4] The homoepitaxial growth of a thin ~20 Å layer of YSZ just prior to YBCO growth removes the unwanted twist boundaries, and greatly improves the critical current density.

Characterization of this effect was performed by taking x-ray diffraction phi scans of the YBCO {103} peaks. This measurement reveals the in-plane epitaxial arrangement of the *c*-axis oriented YBCO grains. Figure 3(a) shows a phi scan of a 300 Å YBCO film grown on a YSZ/Si substrate which had been removed from the deposition system to have features ion milled into the 1500 Å YSZ film. After returning the substrate to the deposition system, a 20 Å YSZ layer was grown *in situ* moments prior to the YBCO deposition. The in-plane orientation is YBCO ⟨110⟩ par-

a)Present address: Physics Department, Washington University, St. Louis, MO 63130.

 0003-6951/90/492504-03$02.00

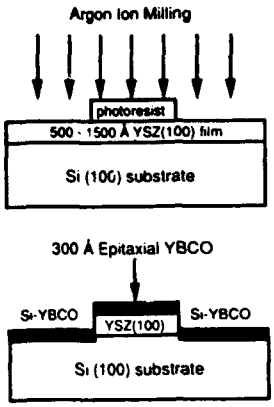

FIG. 1. Scheme of the YBCO reaction patterning process.

allel to YSZ ⟨100⟩. For comparison is curve (b), which shows the same type of scan for a film which lacked the 20 Å YSZ layer, but was otherwise identically prepared. The additional peaks correspond to three additional grain orientations, one rotated by 45° so that YBCO ⟨110⟩ is parallel to YSZ ⟨110⟩ and two low angle grain boundary orientations at $\sim \pm 8.0°$ from the above.

There are several possible causes for the nucleation of multiple in-plane orientations. One influence is thermally induced inelastic strain in the YSZ; the relative thermal expansion of YSZ and Si produces a strain close to the elastic limit of YSZ.[6] Another influence is poisoning by processing chemicals; ~2.5 times more carbon appeared in x-ray photoemission spectroscopy (XPS) spectra of YSZ films which were exposed to photoresist and rinsed with acetone, compared to films taken directly out of the deposition chamber. Twist boundaries with the same orientations reported here also result from YBCO growth on single-crystal YSZ substrates, suggesting a homoepitaxial YSZ layer as a solution in that case as well.

The electrical properties improve substantially with the removal of twist boundaries. Figure 4 shows resistivity versus temperature data for an *in situ* patterned YBCO line 3 μm wide and 1.5 mm long. This film lacked any detectable twist boundaries, and had a resistivity at 300 K of ~230 μΩ cm; this is comparable to the resistivity of laser-deposited films[7] on $SrTiO_3$ and single crystals.[8] The transition width is ~1 K wide, and the normal-state resistivity extrapolates to positive temperatures, as is typical of many of our films on Si. Higher normal-state resistivity (450 μΩ cm at 300 K), and a lower T_c (83 K) for the microstrip containing twist boundaries manifest the disrupted current path. The twist boundaries also had a pronounced effect on the critical current (J_c); using a voltage criterion of 0.75 μV/mm, J_c of the film without twist boundaries was 1.6×10^6 A/cm^2 at 77 K, whereas a comparable film with twist boundaries had a J_c of $\sim1\times10^6$ A/cm^2 at 60 K. The electrical isolation of unconnected $YBa_2Cu_3O_{7-\delta}$ mesas at 23 °C was greater than 20 MΩ for all of the films we tested, however. It is impossible to tell whether the leakage current is occurring across the reacted surface or through the YSZ. Separate measurements indicate that the YSZ isolates the YBCO from the Si by between 5 and 50 MΩ

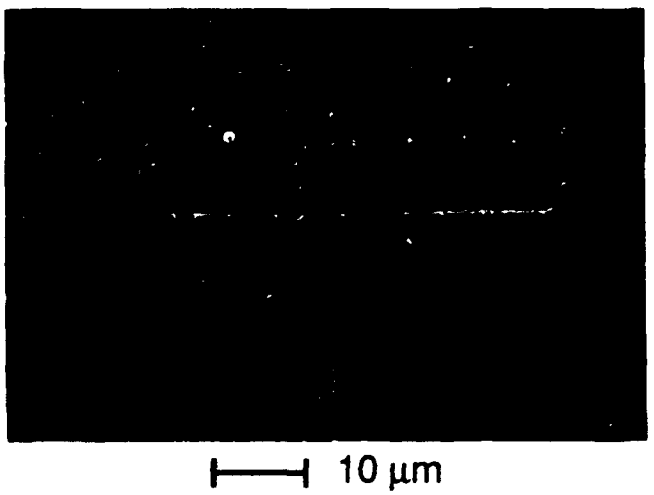

FIG. 2. SEM micrograph of a 3 μm reaction patterned YBCO microstrip.

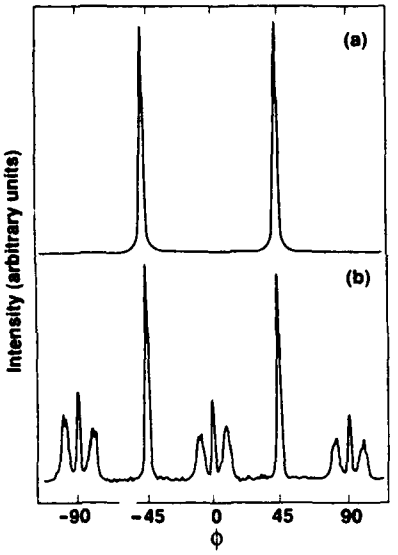

FIG. 3. φ scan of the {103} family of peaks of two 300-Å-thick reaction patterned YBCO films on Si with YSZ buffer layers. For curve (a) deposition included a 20 Å YSZ homoepitaxial layer prior to YBCO deposition whereas the film in curve (b) did not.

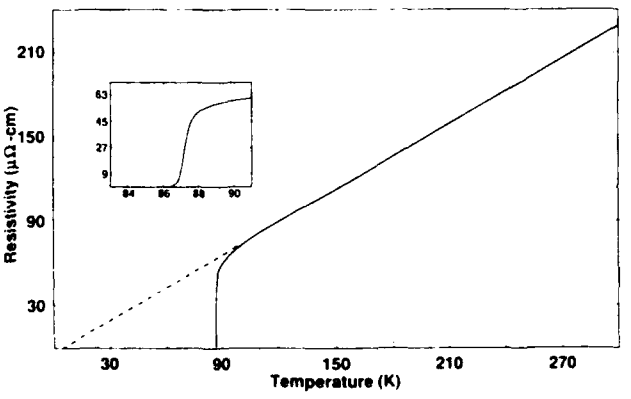

FIG. 4. Resistance vs temperature for a reaction patterned YBCO line on YSZ on Si. The line was 3 μm × 1500 μm × 400 Å.

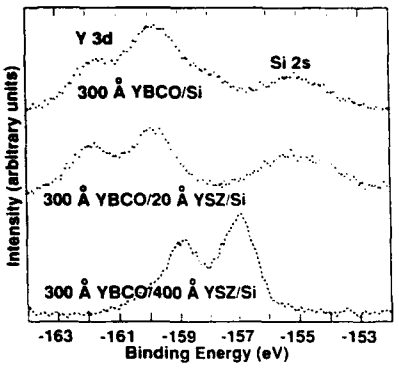

FIG. 5. X-ray photoemission spectra showing Y 3*d* and Si 2*s* lines for 300 Å YBCO films grown on Si, 20 Å YSZ on Si, and 400 Å YSZ on Si by the method in Ref. 4. The upper two spectra are representative of the insulating material which isolates superconducting structures. The bottom curve is typical of a fully superconducting YBCO film on Si.

presumably this leakage is due to pinholes resulting from laser-ablated YSZ fragments. Although this isolation is low compared to what is required for many semiconductor applications, it is well suited to many superconductor applications.

The need to prepare the YSZ surface with an additional 20 Å YSZ raises the question as to how this influences Si diffusion in areas where an insulator is desired. To gain a rudimentary understanding, we performed XPS of Si, Y, Ba, and O for 300 Å YBCO films[9] on Si (100) at 750 °C with and without a 20 Å intermediate YSZ layer. The electron escape depth is much less than 300 Å, hence, assuming uniform coverage, this measurement is sensitive only to diffused Si intermixed with Y, Ba, and Cu. Figure 5 shows the Y 3*d* and Si 2*s* spectra taken for these two films in addition to a spectrum for a typical superconducting 300 Å YBCO film grown on a 400 Å YSZ buffer layer. The reacted films show a substantial Si component, whereas the superconducting film shows no detectable Si.

The Y 3*d* peaks in the two upper curves of Fig. 5 are shifted ~ 2.9 eV to higher binding energy with respect to Y 3*d* in the bottom curve. This shift is attributable at least in part to charging as determined by analysis of the adventitious C 1*s* peak in all three films; the shift to higher binding energy is attributable to the reacted film's insulating rather than metallic nature. These results, combined with the electrical isolation measurements, demonstrate that the 20 Å YSZ layer is too thin to permit coverage, and hence does not prevent the YBCO Si reaction. We have used the splitting of the O 1*s* and Ba $3d_{5/2}$ peaks observed by Chang *et al.*[10] in superconducting YBCO films as a further indication that superconducting material is absent in the reacted films. We note that splittings were observed only for the film in the bottom curve of Fig. 5.

In summary, epitaxial YBCO films have been patterned *in situ* by a novel Si-YBCO reaction process. Isolation of unconnected, unreacted areas of the film is provided by the insulating nature of the reaction products, and by the elevated mesas supporting the superconducting portions of the film. With the proper surface preparation, the dc superconducting properties of these patterned films can rival the best unpatterned films on Si and other substrates.

We thank G. A. N. Connell for useful discussions, and Richard Johnson, Lars-Erik Swartz, and Zan Matsumoto for technical assistance. This work benefits from AFOSR (F49620-89-C-0017). AMV received support from NSF (DMR-8822353). DKF is an AT&T scholar.

Note added in proof. We have used homoepitaxial YSZ on single-crystal YSZ substrates to reduce the number of 45° and low angle twist grain boundaries in YBCO films.

[1] A. Mogro-Campero, B. D. Hunt, L. G. Turner, M. C. Burrell, and W. E. Balz, Appl. Phys. Lett. **52**, 584 (1988); C. T. Cheung and E. Ruckenstein, J. Mater. Res. **4**, 1 (1989).
[2] D. B. Fenner, D. K. Fork, J. B. Boyce, G. A. N. Connell, and A. M. Viano, Physica C **162–164**, 141 (1989).
[3] A. Mogro-Campero, Supercond. Sci. Technol. **3**, 155 (1990).
[4] D. K. Fork, D. B. Fenner, R. W. Barton, Julia M. Phillips, G. A. N. Connell, J. B. Boyce, and T. H. Geballe, Appl. Phys. Lett. **57**, 1161 (1990).
[5] Q. Y. Ma, E. S. Yang, G. V. Treyz, and Chin-An Chang, Appl. Phys. Lett. **55**, 896 (1989).
[6] D. K. Fork, D. B. Fenner, G. A. N. Connell, Julia M. Phillips, and T. H. Geballe, Appl. Phys. Lett. **57**, 1137 (1990).
[7] I. Roas, L. Schultz, and G. Endres, Appl. Phys. Lett. **53**, 1557 (1988).
[8] S. J. Hagen, T. W. Jing, Z. Z. Wang, J. Horvath, and N. P. Ong, Phys. Rev. B **37**, 7928 (1988).
[9] We have not investigated YBCO films thicker than 400 Å due to the thickness limitation imposed by the thermally induced strain in the YBCO, which causes cracking to occur in films thicker than about 500 Å.
[10] C. C. Chang, M. S. Hegde, X. D. Wu, B. Dutta, A. Inam, T. Venkatesan, B. J. Wilkins, and J. B. Wachtman, Jr., Appl. Phys. Lett. **55**, 1680 (1989).

Epitaxial $YBa_2Cu_3O_{7-\delta}$ on GaAs(001) using buffer layers

D. K. Fork and K. Nashimoto[a)]
Xerox Palo Alto Research Center, Palo Alto, California 94304

T. H. Geballe
Department of Applied Physics, Stanford University, Stanford, California 94305

(Received 6 December 1991; accepted for publication 27 January 1992)

Epitaxy of $YBa_2Cu_3O_{7-\delta}$ (YBCO) on GaAs substrates has been demonstrated using epitaxial buffer layers. Recently developed methods for growing epitaxial YBCO thin films on Si have been adapted to achieve similar results on GaAs. MgO thin films were grown epitaxially on GaAs at below 400 °C. This layer provides a suitable template for the growth of YBCO or YBCO on $BaTiO_3$. All materials are deposited *in situ* by pulsed laser deposition in a single growth process. The in-plane crystallography of MgO on GaAs is [100] parallel to [100], accommodating a lattice mismatch of -25.5%. Zero resistance at temperatures as high as 87 K and transition widths as narrow as 1.5 K are reported. Critical current densities as high as 9×10^6 A/cm^2 at 4.2 K and 1.5×10^5 A/cm^2 at 77 K have been measured.

Recent advances in the epitaxial growth of $YBa_2Cu_3O_{7-\delta}$ (YBCO) on silicon substrates[1-4] have been unmatched by progress on other tetrahedral semiconductors. Ironically, the favorable surface resistance of YBCO films in the 10–35-GHz regime may best be exploited in combination with GaAs circuitry, not with silicon. Adaptation of YBCO epitaxy to GaAs substrates may offer the best possibility of millimeter-wave hybrid electronics. This report narrows the gap between progress in growing epitaxial $YBa_2Cu_3O_{7-\delta}$ (YBCO) on silicon and epitaxial YBCO on GaAs.

Si and GaAs both react readily with YBCO to form insulating products. Prior reports of superconducting YBCO on GaAs have employed buffer layers of CaF_2,[5] AlGaAs,[6] indium-tin-oxide,[7] Al_2O_3,[8] yttria-stabilized zirconia (YSZ),[9] or YSZ on Si_3N_4[10] as buffer layers. Where critical currents are reported, they have been low in comparison to typical YBCO films on oxides and silicon, due presumably to lack of epitaxy, but possibly also due to residual interdiffusion and arsenic contamination. Reported zero resistance temperatures were about 85 K and below. As with silicon, high quality YBCO on GaAs requires a suitable *epitaxial* buffer layer material, in addition to the control of interdiffusion and contamination.

Our laser deposition processes for making epitaxial oxides on silicon[1,2] have recently been tested on GaAs substrates with the result that both MgO and YSZ may be grown epitaxially on GaAs under similar growth conditions; process details are reported separately.[11] We believe epitactic growth on the other tetrahedral semiconductors should also occur. These two buffer layers should permit epitaxy of a wide range of superconductor and ferroelectric materials on semiconductors. Laser deposition is a powerful technique for exploring new epitaxial systems, but as noted earlier, other techniques are also expected to work.[2] Recently, the MgO process has been extended to electron-beam evaporation.[12]

One feature of GaAs that is an immediate improvement over silicon is its larger thermal expansion constant. This lowers the thermally induced biaxial stress in the YBCO layer, making thin-film fracture less likely. The thermal expansion constants of Si, GaAs, and YBCO are 3.8×10^{-6}, 8.4×10^{-6}, and 16×10^{-6}/°C, respectively;[13] the YBCO value refers to the *a-b* plane. No evidence of fracture was observed in 100-nm-thick YBCO films on GaAs examined by scanning electron microscopy (Fig. 1), regardless of the type of buffer layer. On silicon, fracture is common for thicknesses above 50 nm.[1] The type of buffer layer impacted the YBCO morphology (Fig. 1). With a YSZ buffer layer, ~500-nm intergrowths roughened the surface, possibly due to interdiffused Ga or As atoms. MgO and $BaTiO_3$/MgO buffer layers produced mirror-like YBCO films. The additional $BaTiO_3$ layer did not improve the YBCO morphology or other properties unlike in YBCO/$BaTiO_3$/$MgAl_2O_4$/Si[3] and YBCO/$BaTiO_3$/MgO/Si.[2] All the YBCO films were grown in 200-mTorr O_2 at about 700 °C.

The volatility of arsenic in GaAs makes it imperative to deposit the initial barrier layer at temperatures below ~600 °C. MgO is particularly suited to this purpose; Yadavalli *et al.*[14] have shown that MgO epitaxy can be carried out down to −133 °C (1/20th the absolute melting point) and our work has shown that MgO homoepitaxy on Si[2] and GaAs[11] can be carried out below 300 °C. Once the MgO layer is in place, it caps the top surface of the wafer, and subsequent layers can be deposited at temperatures above 600 °C. Although YSZ may be grown epitaxially on GaAs, the higher growth temperature and possibly poor barrier effectiveness make it a less suited material than MgO. Other attempts to use YSZ as a buffer layer produced material with zero resistance at 73 K.[9] CeO_2 was similarly ineffective as a diffusion barrier, and reacted visibly with the substrate.[11] The remainder of this paper will concentrate on MgO buffer layers.

Epitaxy has been characterized by four-circle x-ray (Cu K_α) diffraction (XRD). Figure 2 shows a coupled on-axis (θ-2θ) x-ray scan of a YBCO/MgO/GaAs (001) bilayer. Only the (001) reflections of MgO, YBCO, and

[a)]Currently at Materials Research Laboratory, Fuji Xerox Co., Ltd., Kanagawa, Japan.

 0003-6951/92/131621-03$03.00

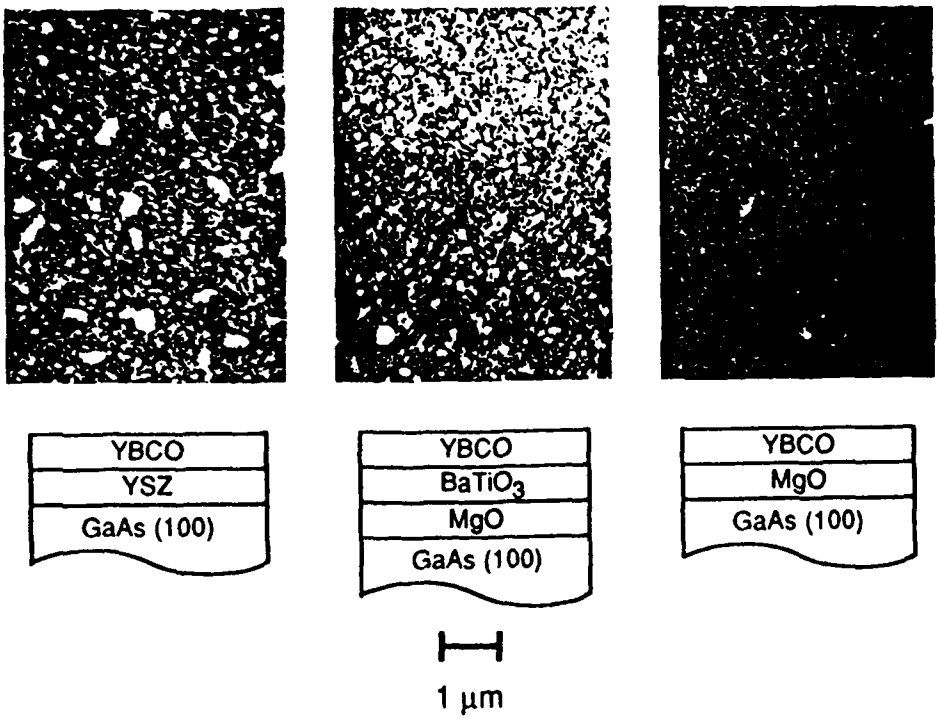

FIG. 1. SEM images of 100-nm-thick YBCO films on YSZ/GaAs, $BaTiO_3$/MgO/GaAs, and MgO/GaAs. The thicknesses of the MgO, YSZ, and $BaTiO_3$ layers are all approximately 50 nm.

GaAs are visible. Rocking curves in omega characterize the tilt of grains away from the substrate normal. An overlay of ω-rocking curves of the YBCO (006), MgO (002), and GaAs (004) reflections appears below in Fig. 2. The ω resolution of the diffractometer is determined from the GaAs (004) reflection to be about 0.2°. The 1.0° rocking curve width (full width at half-maximum) of the MgO film indicates highly oriented material with some residual tilt disorder. Rocking curves as narrow as 0.74° were obtained on GaAs (001) substrates polished 10° off towards [110]. The narrower rocking curve in this case supports the ledge growth mechanism proposed earlier for alkali halides[15] and MgO.[14] The YBCO orientation on vicinal GaAs was shifted toward the surface normal, in agreement with the observations of Streiffer *et al.*[16] The YBCO and MgO rocking curve widths were correlated in a series of films on nonvicinal GaAs indicating that improved crystallinity in the MgO layer is expected to carry into all subsequent layers. An additional buffer layer of $BaTiO_3$ between YBCO and MgO widened the YBCO rocking curve, suggesting that disorder was cumulative.

On-axis x-ray diffraction it is not a rigorous demonstration of epitaxy. In the present work, epitaxy has been verified by off-axis phi scans of the MgO (202), $BaTiO_3$ (202), and YBCO (103) reflections with the phi axis normal to the plane of the film. The in-plane epitaxial relations are YBCO[100]||MgO[100]||GaAs[100] or YBCO[100]||$BaTiO_3$[100]||MgO[100]||GaAs[100], i.e., all interfaces are cube-on-cube. The direct lattice mismatch between MgO and GaAs is -25.5%, however, in a ratio of 4:3, MgO and GaAs are practically commensurate, with a mismatch of only 0.65%. Transmission electron micros-

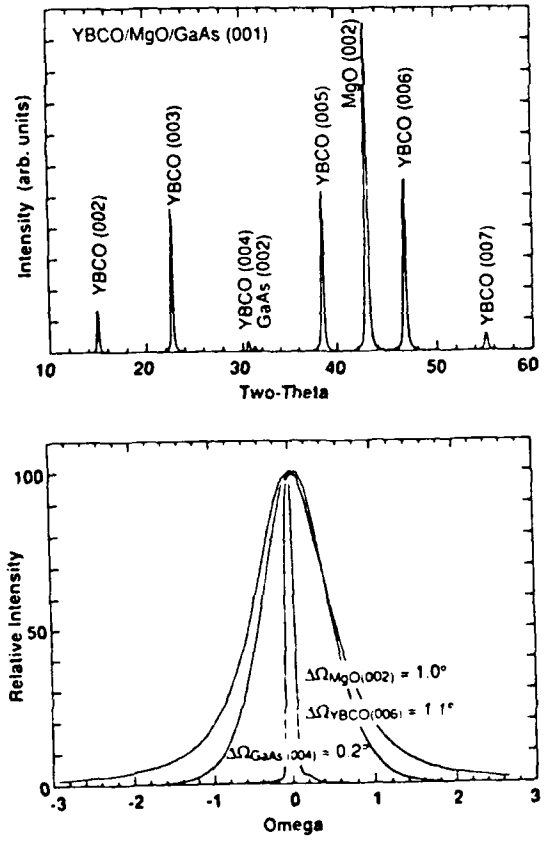

FIG. 2. X-ray diffraction coupled 2θ scan (top) of a 100-nm YBCO film on 50-nm MgO on GaAs (001). The substrate has been tilted slightly to suppress the GaAs (002) reflection. ω-rocking curves (bottom) of the YBCO (006), MgO (002), and GaAs (004) reflections taken on the same film.

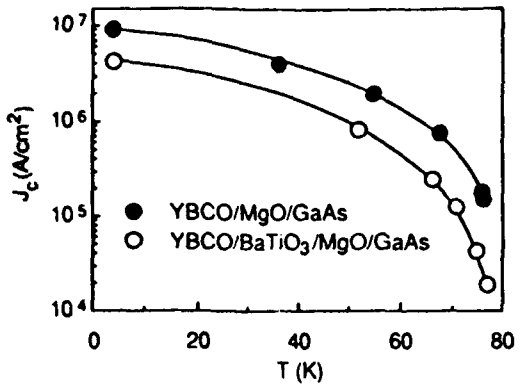

FIG. 3. Critical current density vs temperature for 100-nm YBCO films on MgO/GaAs and $BaTiO_3$/MgO/GaAs.

copy has revealed smooth, unreacted interfaces between MgO and GaAs.[17]

The temperature dependence of resistivity in the normal state is metallic with resistance extrapolating to zero. We have obtained zero resistance at temperatures up to 87 K, and transition widths (10% to 90%) of about 1.5 K. Critical currents has been measured by dc transport on 50-μm-wide excimer laser patterned lines using a voltage criterion of 1 μV/mm. Gold pads were evaporated to provide contact to the sample. The temperature dependence of J_c in two types of films is shown in Fig. 3. The critical current density was higher in the YBCO/MgO bilayers than in the YBCO/$BaTiO_3$/MgO trilayers, in agreement with other figures of merit, such as rocking curves. J_c was about 10^5 A/cm^2 at 77 K and 9×10^6 A/cm^2 at 4.2 K in the best film measured. The magnitude of J_c is slightly lower at all temperatures than what typifies high-quality YBCO films on oxides and silicon. In addition, the room-temperature resistivity is typically a factor of 2 or more higher (500–900 $\mu\Omega$ cm) than optimum values. This is likely to be caused by contamination from As_2O_3 coming off the back and sides of the GaAs chip during YBCO deposition. The edges and backside of all wafers with YBCO films are darkened from As loss, and the surrounding holder accumulates a whitish oxide. At the highest YBCO deposition temperatures, this causes a visible deterioration of the YBCO around the edges where the As_2O_3 flux is presumably highest. There is no indication of As_2O_3 loss where the GaAs is capped by MgO, suggesting that optimum film quality should require at worst, a modification of the GaAs handling to cap the free surfaces of the chip.

In summary, we report a substantial improvement in the crystal quality and transport properties in YBCO films grown on GaAs by using an epitaxial MgO buffer layer. Interdiffusion and arsenic loss are prevented by an epitaxial layer which may be grown at temperatures as low as 300 °C. Modification of the process to cap the entire chip against arsenic loss should produce further improvement in the film properties. The effects of thermally induced stress are significantly reduced in comparison to the effects on silicon. MgO is the first epitaxial oxide demonstrated on GaAs, and should therefore provide a basis for a variety of interesting heterostructures.

We thank Jim Boyce and Neville Connell of Xerox Palo Alto Research Center for useful discussions. We thank Paresh Patel of Santa Clara University for technical assistance. This work benefits from AFOSR (F49620-89-C-0017). DKF acknowledges an AT&T scholarship.

[1] D. K. Fork, D. B. Fenner, R. W. Barton, J. M. Phillips, G. A. N. Connell, J. B. Boyce, and T. H. Geballe, Appl. Phys. Lett. 57, 1161 (1990).
[2] D. K. Fork, F. A. Ponce, J. C. Tramontana, and T. H. Geballe, Appl. Phys. Lett. 58, 2294 (1991).
[3] S. Miura, T. Yoshitake, S. Matsubara, Y. Miyasaka, N. Shohata, and T. Satoh, Appl. Phys. Lett. 53, 1967 (1988); X. D. Wu, A. Inam, M. S. Hegde, B. Wilkins, C. C. Chang, D. M. Hwang, L. Nazar, T. Venkatesan, S. Miura, S. Matsubara, Y. Miyasaka, and N. Shohata, *ibid.* 54, 754 (1989).
[4] H. Myoren, Y. Nishiyama, N. Miyamoto, Y. Kai, Y. Yamanaka, Y. Osaka, and F. Nishiyama, Jpn. J. Appl. Phys. 29, L955 (1990); L. Luo, X. D. Wu, R. C. Dye, R. E. Muenchausen, S. R. Foltyn, Y. Coulter, C. J. Maggiore, and T. Inoue, Appl. Phys. Lett. 59, 2043 (1991).
[5] K. Mizuno, M. Miyauchi, K. Setsune, and K. Wasa, Appl. Phys. Lett. 54, 383 (1989).
[6] M. R. Rao, E. J. Tarsa, L. A. Samoska, J. H. English, A. C. Gossard, H. Kroemer, P. M. Petroff, and E. L. Hu, Appl. Phys. Lett. 56, 1905 (1990); L. D. Chang, M. Z. Tseng, L. A. Samoska, J. J. O'Shea, Y. J. Li, E. J. Cain, E. J. Hu, P. M. Petroff, and H. Kroemer, J. Appl. Phys. 70, 5108 (1991).
[7] B. J. Kellett, A. Gauzzi, J. H. James, B. Dwir, D. Pavuna, and F. K. Reinhart, Appl. Phys. Lett. 57, 2588 (1990).
[8] J. Shewchun, Y. Chen, J. S. Hölder, and C. Uher, Appl. Phys. Lett. 58, 2704 (1991).
[9] P. Tiwari, S. Sharan, and J. Narayan, Appl. Phys. Lett. 59, 357 (1991).
[10] Q. X. Jia, S. Y. Lee, W. A. Anderson, and D. T. Shaw, Appl. Phys. Lett. 59, 1120 (1991).
[11] K. Nashimoto, D. K. Fork, and T. H. Geballe, Appl. Phys. Lett. 60, 1199 (1992).
[12] L. D. Chang, M. Z. Tseng, D. K. Fork, and E. L. Hu, Appl. Phys. Lett. (to be published).
[13] Y. S. Touloukian, R. K. Kirby, R. E. Taylor, and T. Y. R. Lee, *Thermophysical Properties of Matter* (Plenum, New York, 1977), Vol. 13; J. D. Jorgensen, M. A. Beno, D. G. Hinks, L. Soderholm, K. J. Volin, R. L. Hitterman, J. D. Grace, I. K. Schuller, C. U. Segre, K. Zhang, and M. S. Kleefisch, Phys. Rev. B 36, 3608 (1987); the values quoted are the integrated temperature average between 23 °C and the YBCO growth temperature.
[14] S. Yadavalli, M. H. Yang, and C. P. Flynn, Phys. Rev. B 41, 7961 (1990).
[15] M. H. Yang and C. P. Flynn, Phys. Lett. 62, 2476 (1989).
[16] S. K. Streiffer, B. M. Lairson, and J. C. Bravman, Appl. Phys. Lett. 57, 2501 (1990).
[17] K. Nashimoto, D. K. Fork, F. A. Ponce, and T. H. Geballe, Mater. Res. Soc. Proc. (in press).

BG#: 4736
Article#: 91.410
Typesetter: ls

Effects of homoepitaxial surfaces and interface compounds on the in-plane epitaxy of YBCO films on yttria-stabilized zirconia

D.K. Fork
Department of Applied Physics, Stanford University, Stanford, California 94305, and Xerox Palo Alto Research Center, Palo Alto, California 94304

S.M. Garrison
Conductus Inc., Sunnyvale, California 94086

Marilyn Hawley
Los Alamos National Laboratory, Los Alamos, New Mexico 87545

T.H. Geballe
Department of Applied Physics, Stanford University, Stanford, California 94305

(Received 22 November 1991; accepted 21 February 1992)

Control of the in-plane epitaxial alignment of *c*-axis $YBa_2Cu_3O_{7-\delta}$ (YBCO) films on yttria-stabilized zirconia (YSZ) substrates is necessary for achieving optimal transport properties. We have used pulsed laser deposition to grow homoepitaxial YSZ and heteroepitaxial CeO_2 on YSZ single crystal substrates. This procedure dramatically improves the epitaxy of YBCO and reduces the number of low and high angle grain boundaries. We have also studied the effects of preparing the YSZ growth surface with approximately monolayer amounts of CuO, Y_2O_3, BaO, and $BaZrO_3$ to determine the effects these compositional variations have on the subsequent YBCO epitaxy. CuO, Y_2O_3, and $BaZrO_3$ induce an in-plane crystallography of YBCO distinct from that initiated with BaO. Both homoepitaxy and monolayer depositions may be carried out *in situ* and are simple and effective for controlling the epitaxy and electrical properties of YBCO on YSZ. The effects of substrate temperature, oxygen pressure, and yttria content have also been studied.

I. INTRODUCTION

Microelectronic applications require thin films of the high temperature oxide superconductor $YBa_2Cu_3O_{7-\delta}$ (YBCO) to be capable of carrying large critical current densities on readily available substrates. Excellent films with critical current densities (J_c) > 10^6 A/cm^2 at 77 K can be produced on lattice matched substrates such as $SrTiO_3$, $LaAlO_3$, and $LaGaO_3$ over a wide range of growth conditions. These substrates, however, are expensive and are frequently available in diameters no greater than 2 inches. Some are twinned, resulting in dielectric anisotropy, or have unacceptably large losses. Excellent YBCO films have been produced on MgO which is relatively inexpensive but mechanically fragile and difficult to polish. Buffer layers have made sapphire substrates viable for high quality thin film growth[1–3]; however, the small thermal expansion constant of sapphire appears to cause microcracking in multilayer structures,[4] and sapphire has an inherent dielectric anisotropy due to its rhombohedral symmetry.

Due to its mechanical strength, chemical stability, and low cost, yttria-stabilized zirconia (YSZ) has become a popular single crystal substrate for films of YBCO.[5–10] YSZ has also been identified as an effective epitaxial buffer layer for producing YBCO films with high critical current densities on Si[11,12] and on sapphire.[3] Polycrystalline YSZ ceramics are being studied as potential substrates for YBCO tapes, i.e., for power leads.[13] Polycrystalline YSZ thin films have been used as buffer layers for the deposition of YBCO on metallic substrates.[14] YSZ substrates may provide a cost effective alternative in a variety of electronic applications. YSZ is an ionic conductor, hence the dielectric constant and loss tangent increase rapidly above 300 K; at temperatures of interest for high-T_c superconductors, below 100 K, YSZ is a low-loss dielectric.[15] YBCO and YSZ are dissimilar in their crystal structures and in their lattice constants. This appears to explain the feature that epitaxial *c*-axis films grown on YSZ are frequently polycrystalline and have several in-plane orientations. This texturing on YSZ has been observed by several groups.[5,9,10,16] Under some circumstances, it has been possible to produce critical current densities in excess of 10^6 A/cm^2 at 77 K; however, these results have not always been reproducible. This paper reports ways to control and understand the texturing in order to reliably produce films with large J_c.

The reduction of J_c at a tilt or twist grain boundary in YBCO has been studied and reported extensively. Dimos *et al.*[17] grew post-annealed thin films on $SrTiO_3$

bicrystals and showed that the J_c between misoriented grains decreases inversely with the misorientation angle for small angles, saturating at a value of about 1/50 for large angles. Recently, Ivanov *et al.*[18] have shown that in *in situ* processed *c*-axis YBCO films on YSZ bicrystals, the J_c at 77 K varies from $\sim 1-5 \times 10^6$ A/cm^2 at 0° tilt to $\sim 1.2 \times 10^3$ A/cm^2 at 40° tilt. This study by Ivanov *et al.* is more closely related to this work both in the synthesis route and in the results obtained. The work reported by Garrison *et al.*[10] is the only prior study of study of J_c in a large number of YBCO films on YSZ with various amounts of texturing. Those results show definitively that in the films studied, texturing can lower J_c by almost four orders of magnitude. Although it may not be possible to infer the J_c of a film solely from its texturing, since other factors such as the oxygen content and intragranular defects also impact J_c, control of the texturing is a vital issue. Texturing is also likely to have an impact on the high frequency properties, electrical noise, and aging behavior of high-T_c films in addition to impacting J_c. Char *et al.*[2] and Laderman *et al.*[19] have related the density of high angle grain boundaries to microwave surface resistance losses in YBCO films on $SrTiO_3$ buffered sapphire and on MgO single crystals, respectively.

In *c*-axis oriented films on YSZ, epitaxy may occur with the YBCO *a*-axis parallel to the substrate ⟨100⟩ or ⟨110⟩ directions, causing 45° grain boundaries. In addition, YSZ frequently supports epitaxy with the YBCO *a*-axis making an angle of ~9° with the substrate ⟨100⟩. The YBCO unit cell is tetragonal during growth. The twinning which occurs as a result of the orthorhombic transformation during cooling introduces displacements and distortions which are small in comparison to the effective displacements of grain textures described above. Methods to identify the in-plane epitaxial orientations are well established.[5,7,9,10] Both x-ray diffraction phi scans (pole figures) and planar view transmission electron microscopy (TEM) are effective. Methods to characterize the effect of the texturing on the electrical properties are well established and several studies exist.[2,9–11,16–20] Finally, it is essential to understand how to control the texturing of YBCO on YSZ, MgO, and other substrates with poor lattice match or dissimilar crystal structure to YBCO. This paper is aimed at such an understanding. The ultimate applicability of the high temperature oxide superconductors rests heavily on our ability to grow materials in desired orientations. Among those working on these problems, the term "grain boundary engineering" is being used frequently to describe the ability to alter locally or globally the crystal orientation of epitaxial layers. Our investigation has concentrated on YSZ substrates where little work has been carried out previously, excluding artificially induced grain boundaries through the use of bicrystals.[18]

Although the details of the interface bonding between YBCO and YSZ are not understood, it is known that the relative amounts of the three identified *c*-axis configurations on YSZ (001) are easily perturbed by factors such as deposition temperature, pressure, stoichiometry, and the substrate surface preparation. Recently we reported that epitaxial YSZ grown on Si (001) by pulsed laser deposition supports epitaxy that is virtually free from 45° and low angle grain boundaries when the YBCO is grown in the same run as the YSZ.[11] Under those circumstances, the YBCO grows with the *a*-axis parallel to YSZ ⟨110⟩. Later, we reported that if the YSZ/Si films are removed and processed to make YSZ/Si mesa structures, the surface of the YSZ is altered in such a fashion that both 45° and 8–9° grain orientations result.[16] This problem was solved by growing a thin (~2 nm) layer of homoepitaxial YSZ on the processed YSZ surface prior to the YBCO film deposition. These results suggest (1) that the YSZ surface is easily altered, and (2) that only the *in situ* prepared YSZ surface has ideal properties for supporting epitaxy without texturing.

The nucleation of epitaxial grains in favor over nonepitaxial randomly oriented grains occurs in general due to the lower energy of the epitaxial configuration. In the case of YBCO on YSZ, the appearance of three, often coexisting, epitaxial configurations implies that the differences in total energy among these states are small and/or the kinetics are too limited to allow the configuration with the lowest total energy to grow exclusively, as would be the case in thermodynamic equilibrium. With energetic and/or kinetic limits on the growth, the order in which the overlayer constituents arrive on the substrate surface can become important in determining the epitaxial configuration, as we shall demonstrate below.

The observation of three principal textures in *c*-axis oriented YBCO films on YSZ substrates leads to the question of what processes govern their occurrence. The different in-plane orientations might be attributed to film growth originating with different cation layers of the YBCO unit cell. This is a testable conjecture. YBCO has four distinct cation layers normal to the *c*-axis, i.e., CuO_2 planes, CuO chains, BaO, and Y. These layers differ in their oxygen lattices, bond lengths, atomic sites, etc. (see Fig. 1). In most YBCO film deposition techniques, all of the constituents arrive simultaneously. The cation layer that resides at the substrate-film interface must separate from the other constituents. Streiffer *et al.*[21] have used image simulations of transmission electron micrographs of the YBCO/MgO interface to infer that Cu–O chains and BaO layers initiate the interface. Part of the present study is directed at understanding the effects of initiating the epitaxial growth with a flux composed of only one of the three different metal oxides on the YSZ surface.

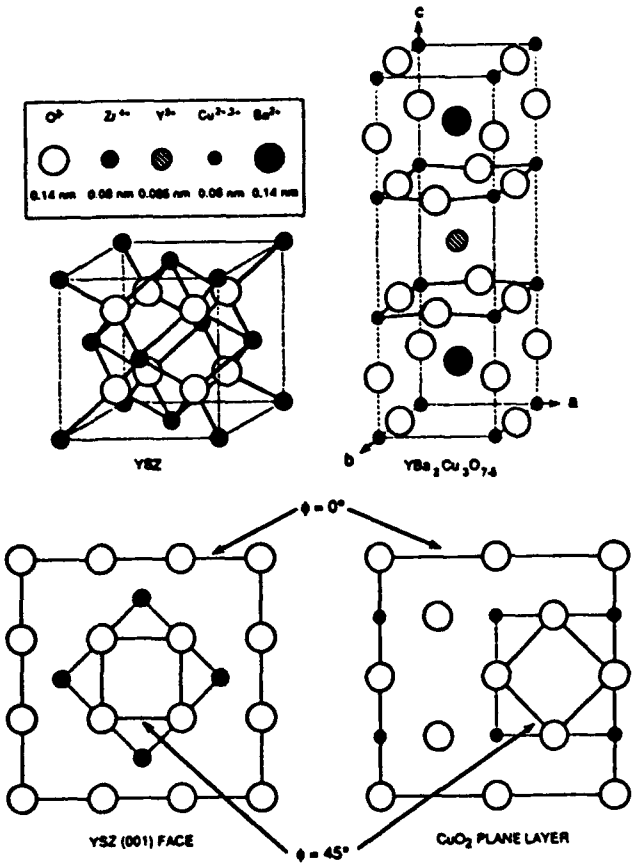

FIG. 1. The crystal structures of YSZ, YBCO, and {001} plan views of single layer slices of each structure. The YSZ unit cell is an idealized fluorite structure which does not illustrate the $Y^{3+}_{Zr^{4+}}$ substitutions or the $V_{O^{2-}}$ vacancies. In the case of YBCO, the CuO_2 plane layer is shown in plan view. For the $\phi = 0°$ orientation, 1.5 YSZ unit cells coincide with 2 YBCO unit cells. In the $\phi = 45°$ orientation, the oxygen sublattices are mismatched by about 6% when the [110] and [100] directions of the respective crystals are colinear.

This is done in an effort to eliminate as much as possible the role of diffusion in determining the cation layer at the substrate film interface.

Substrate film reactions, if sufficiently rapid, may also play a role in directing or disrupting heteroepitaxial alignments. Tietz *et al.*[7] have reported the occurrence of a reacted interfacial layer between YBCO and YSZ, and have provided evidence that the material is $BaZrO_3$. Cima *et al.*[22] have shown that $BaZrO_3$ is a stable end product of the reaction of YBCO with YSZ at 950 °C. To understand better how a $BaZrO_3$ interfacial layer can influence the orientation of YBCO on YSZ, we have grown layers of $BaZrO_3$ on YSZ prior to depositing YBCO. This experiment is important in trying to distinguish whether the Ba doped interface initiates YBCO growth with its Ba layer or whether it reacts to form other compounds. It should be noted that this experiment has as many variations as there are elements and compounds that can be deposited onto the YSZ surface prior to YBCO growth. We have explored several of the obvious choices. Similar variations are possible for many other film and substrate combinations.

Although studies of the control of YBCO texturing on YSZ substrates other than Refs. 14 and 16 have not been reported previously, some work on MgO substrates has appeared and will be mentioned here. Texturing of YBCO on MgO stems from the dissimilar crystal structures and lattice constants, and has been noted by numerous groups. Ravi *et al.*[23] have looked at the variety of grain orientations that appear and have shown that some of the orientations agree well with a near-coincident site lattice (NCSL) theory. The predominant orientation, however, is not explained by an NCSL theory. Eom[24] has observed that texturing of YBCO films on MgO substrates is possible by carefully selecting the deposition temperature. Moeckly *et al.*[20] report that high temperature treatment of the MgO substrate prior to YBCO growth improves the texturing.

In related work on other substrates, Inam *et al.*[25] have demonstrated orientational control via the selection of an appropriate buffer layer. They report that laser deposited $PrBa_2Cu_3O_{7-\delta}$ (PBCO) nucleates YBCO film growth with the *a*-axis normal to the substrate plane on (100) oriented $SrTiO_3$ and $LaAlO_3$ substrates at low temperature whereas YBCO alone does not nucleate homogeneous *a*-axis growth. The PBCO layer then acts as a template for the growth of *a*-axis PBCO or YBCO. Predictive understanding of these sorts of empirical observations is largely missing in the field of epitaxial oxide film growth and would be extremely useful. A final example of techniques developed to control the in-plane epitaxy of YBCO comes from the recent work on bi-epitaxial grain boundary junctions,[4,26,27] wherein 45° grain boundaries are produced along photolithographically defined lines by depositing seed and buffer layers. This work shows considerable promise for high-T_c integrated circuits.

II. EXPERIMENTAL PROCEDURES

YBCO films were deposited by pulsed laser deposition with a rotating polygon source (Kurt Lesker Co.) designed to accommodate up to ten different target materials during a single deposition run. This allowed us to modify the substrate surface with various materials prior to depositing YBCO. The polygon rotates at 5 to 10 Hz and is connected to a shaft encoder which allows precise triggering of our excimer laser to ablate from the appropriate target. The entire configuration is controlled by a microcomputer. Successive runs with different materials could be carried out systematically without alterations to the system aside from its software control. The deposition sources available on the polygon for these experiments included $(Y_2O_3)_x(ZrO_2)_{1-x}$ with $x = 0.05$, 0.09, and 0.30, CuO, Y_2O_3, Ba, $BaZrO_3$,

CeO_2, and a composite target of nominal composition $YBa_2Cu_3O_7$. The same YBCO target was used throughout this study. YBCO films were deposited on bare single crystal YSZ substrates, or on single crystal YSZ substrates whose surfaces had been modified with selected layers of the constituents listed above ranging in thickness from approximately 0.3 nm up to approximately 60 nm. The 0.3 nm layers were an attempt to introduce approximately one monolayer of material at the growth interface of YSZ and YBCO. No *in situ* characterization provided detailed information about the coverage of these layers or their thicknesses, which were inferred from depositions of thicker films.

A 308 nm XeCl excimer laser generated energy densities of 2.0 to 2.5 J/cm^2 on the targets with each 17 ns laser pulse. The homoepitaxial YSZ depositions were carried out in 0.4 mTorr background pressure of molecular oxygen, as described previously.[16] All other compounds, including YBCO, were deposited in 200 mTorr molecular oxygen with the exception of our study of the pressure effects on the YBCO epitaxy. All substrates used in this study were degreased in trichloroethane and followed by acetone, methanol, and isopropanol rinses prior to film deposition. The substrates were heated to 690–710 °C with a quartz lamp heater for all studies except for the effects of temperature. Studies of the effects of homoepitaxial YSZ, CuO, Y_2O_3, and BaO were carried out using substrates supplied from Ceres Corp. Studies of the effects of temperature, pressure, YSZ composition, CeO_2, and $BaZrO_3$ interfacial layers were carried out using substrates supplied from Commercial Crystal Labs. The nominal yttria content of all YSZ substrates was 9 mole %.

X-ray diffraction was carried out using a Siemens D5000 four-circle diffractometer with a Cu K_α source. The primary axes of the four-circle diffractometer are depicted in Fig. 2. In-plane texturing of the YBCO films was characterized by taking x-ray diffraction ϕ scans of the YBCO {103} reflections with the ϕ axis normal to the plane of the substrate. In this measurement, the instrument is sensitive to a fixed *d*-spacing which is nominally that of the YBCO {103} planes. Movement of the ϕ motor rotates *c*-axis aligned YBCO grains nominally about the [001] direction; their position in the plane is revealed by the value of ϕ for which they satisfy the Bragg condition. Phi scans of the YSZ {202} reflections were also taken to provide a crystallographic reference. Both the YBCO {103} and YSZ {202} reflections are gathered with an approximate χ angle of 45°. Reflections from the two materials are distinguished by their different 2θ angles. The relative orientational angles of film and substrate were measured directly from these ϕ scans.

Critical current densities were determined from the mutual inductance response, which was measured by placing the unpatterned films between drive and pickup coils in a fashion similar to Ref. 28. Resistivities and zero resistance transition temperatures were measured by the four-terminal resistance technique.

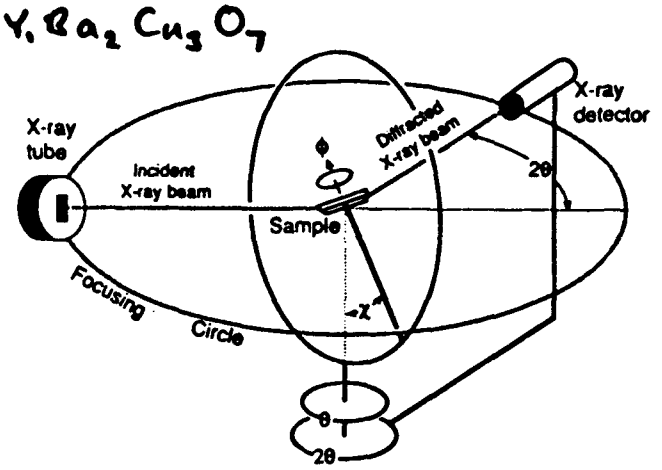

FIG. 2. Four-circle x-ray diffractometer geometry showing the principal axes and their configuration for ϕ scan measurements. In-plane texturing is determined by setting the 2θ angle to the appropriate angle for either the YBCO {103} reflections or for the YSZ {202} reflections, setting χ and θ to satisfy the Bragg condition ($\chi \approx 45°$ and $\theta \approx 2\theta/2$) and rotating the sample in ϕ by 180° or more.

III. RESULTS AND DISCUSSION

Figure 3 is a montage of x-ray diffraction ϕ scans of the YBCO {103} reflections from selected films grown in this experiment. This figure contains eight ϕ scans, seven of which (*a* through *f* and *h*) are from the specific layered structures indicated in the figure. The ϕ scans collected on the four structures indicated by the arrows converging on Fig. 3(g) were so nearly the same that the data were merged into a single representative ϕ scan. The transport properties and texturing data of some of the films grown in this study appear in Table I.

A. YBCO epitaxy on bare YSZ

Figure 3(a) is a typical x-ray diffraction ϕ scan of the YBCO {103} reflections for a film grown on a YSZ substrate supplied by Ceres Corp. without any processing of the surface other than the degreasing procedure used on all the substrates in this work. In this and all other ϕ scans, the zero of the ϕ angle is determined from the YSZ substrate. Three types of peaks in the spectrum are discernible. The peaks at $\phi = 0°$, 90°, etc. correspond to *c*-axis oriented YBCO grains with the *a*-axis parallel to YSZ ⟨100⟩, i.e., cube-on-cube epitaxy which will henceforth be referred to as ⟨100⟩ or $\phi = 0°$ material. Peaks at odd multiples of 45° manifest *c*-axis YBCO with the *a*-axis parallel to YSZ ⟨110⟩, henceforth referred to as ⟨110⟩ or $\phi = 45°$ material. The third class of material is manifested by the broad peaks forming satellites at an average of ±9° about the

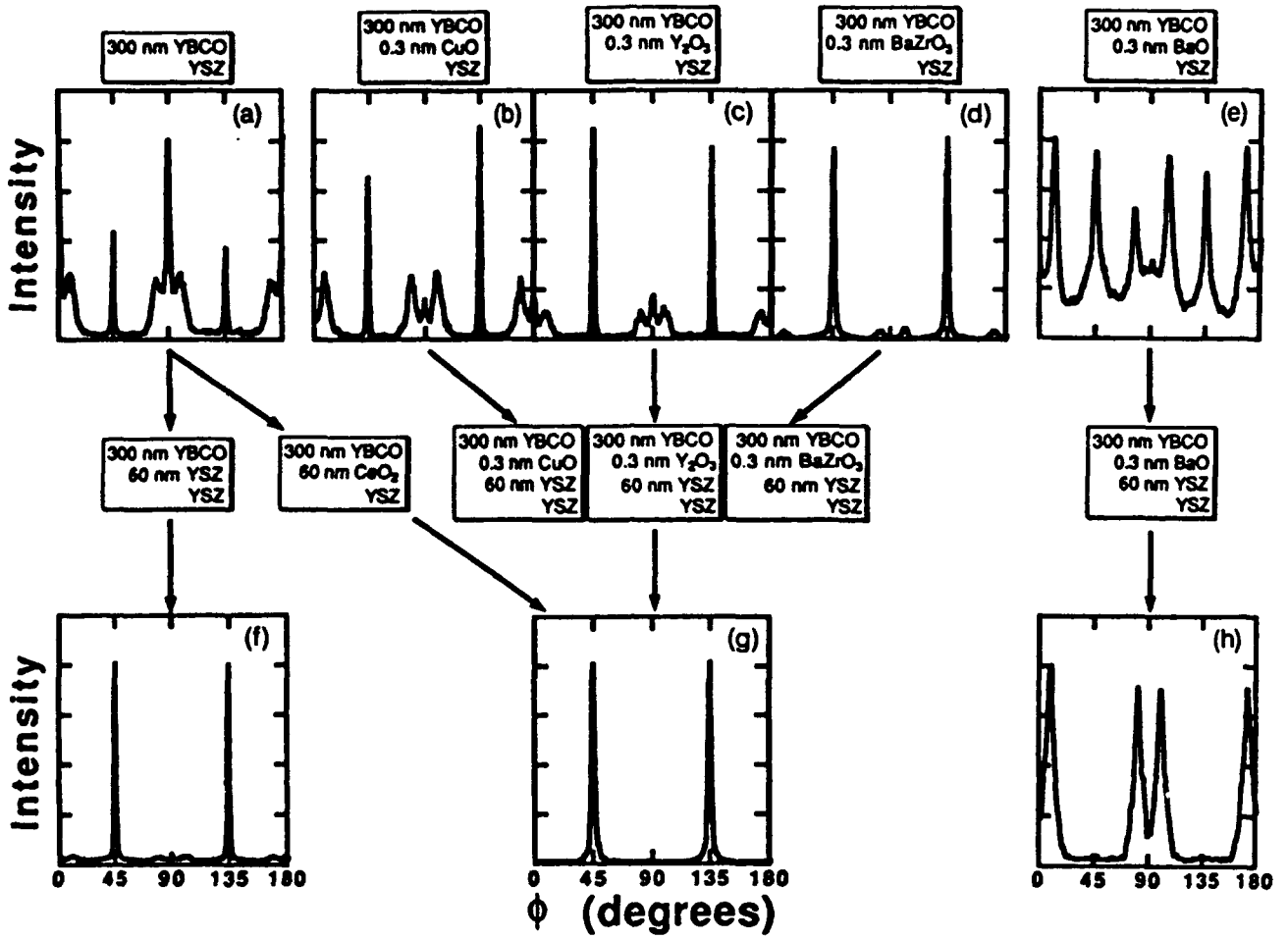

FIG. 3. Collection of x-ray diffraction ϕ scans of the YBCO {103} family of reflections for films grown on YSZ under the following conditions. $\phi = 0°$ was determined using the YSZ {202} reflection; hence the peak at $\phi = 0°$ manifests cube-on-cube oriented YBCO. (a) YBCO grown on single crystal 9 mole % YSZ with no *in situ* alterations to the surface. (b) YBCO grown on ~0.3 nm of CuO on single crystal 9 mole % YSZ. (c) YBCO grown on ~0.3 nm of Y_2O_3 on single crystal 9 mole % YSZ. (d) YBCO grown ~0.3 nm of $BaZrO_3$ on single crystal 9 mole % YSZ. (e) YBCO grown on ~0.3 nm of BaO on single crystal 9 mole % YSZ. (f) YBCO grown on 60 nm of 9 mole % YSZ grown on single crystal 9 mole % YSZ. (g) This figure represents data taken on YBCO grown on either of (1) 60 nm CeO_2, (2) ~0.3 nm of CuO on 60 nm 9 mole % YSZ, (3) ~0.3 nm of Y_2O_3 on 60 nm 9 mole % YSZ, (4) ~0.3 nm of $BaZrO_3$ on 60 nm 9 mole % YSZ, all on single crystal 9 mole % YSZ. (h) YBCO grown on ~0.3 nm of BaO on 60 nm 9 mole % YSZ on single crystal 9 mole % YSZ.

{100} peak. The grains corresponding to this material are not tightly locked into this orientation, but are instead responding to a "shallow potential." The fraction of the film composed of this third class of material varies greatly from almost none to nearly 100%, depending on the growth conditions. Keeping in mind that this material is broadly distributed, we will refer to it as $\phi \sim 9°$ material.

B. Homoepitaxial YSZ buffer layers

The first set of film depositions on modified surfaces revealed the effect of preparing the YSZ substrate surface with a homoepitaxial layer of YSZ prior to depositing YBCO. Briefly, the effect is to reduce the weak link behavior by greatly enhancing the amount of $\phi = 45°$ material (see Table I). Figure 3(f) is a YBCO {103} reflection ϕ scan of a film grown on a 60 nm layer of 9 mole % YSZ on a single crystal YSZ substrate supplied by Ceres Corp. Compared to Fig. 3(a), this scan shows a drastic reduction of the $\phi = 0°$ and $\phi \sim 9°$ components, which formed the dominant fraction of the YBCO film without the homoepitaxial layer. This result is in agreement with earlier results obtained on single crystal YSZ thin films on Si,[16] however, with the important difference that thicker layers of YSZ were required to produce films with mostly $\phi = 45°$ material. In Ref. 16, 2 nm of homoepitaxial YSZ on Si produced approximately the same effect as 60 nm on YSZ in this work. When we perform the same experiment on single crystals of YSZ with only 10 nm of YSZ film, mixed texturing still results, albeit with a larger $\phi = 45°$ component. This effect indicates that the features of the substrate which promote $\phi = 0°$

TABLE I. Layering, texturing, and transport properties of films generated in this work.

Sequence	ϕ scan	$\phi = 0°/\phi = 45°$	$\phi \sim 9°/\phi = 45°$	J_c (A/cm^2)	T_c (K)	ΔT_c (K)	ρ_{300}/ρ_{100}	ρ(100 K) ($\mu\Omega$-cm)
YBCO/YSZ	Fig. 3(a)	4.1	4.0	7.6×10^5	87.0	2.5	3.1	97
YBCO/10 nm YSZ/YSZ	...	0.28	0.51	4.8×10^5	88.0	1.5	2.9	107
YBCO/60 nm YSZ/YSZ	Fig. 3(f)	0.014	0.16	2.5×10^5	89.4	0.8	2.9	81
YBCO/0.3 nm CuO/YSZ	Fig. 3(b)	0.17	2.1	2.2×10^6	88.6	1.9	2.3	107
YBCO/0.3 nm Y_2O_3/YSZ	Fig. 3(c)	0.19	1.0	3.2×10^2	...	...	...	...
YBCO/0.3 nm $BaZrO_3$/YSZ	Fig. 3(d)	0.022	...	1.9×10^5	...	...	...	...
YBCO/0.3 nm BaO/YSZ	Fig. 3(e)	0.39	1.1	6.4×10^5	88.4	1.3	2.1	147
YBCO/0.3 nm CuO/60 nm YSZ/YSZ	Fig. 3(g)	0.017	< 0.007	2.3×10^6	88.8	0.7	3.3	76
YBCO/0.3 nm Y_2O_3/60 nm YSZ/YSZ	Fig. 3(g)	0.0015	0.008	9.6×10^5	88.8	1.1	3.6	66
YBCO/0.3 nm $BaZrO_3$/60 nm YSZ/YSZ	Fig. 3(g)	0.0029	...	1.9×10^6	...	...	...	...
YBCO/0.3 nm BaO/60 nm YSZ/YSZ	Fig. 3(h)	7.7	33.	9.6×10^5	...	...	...	...
YBCO/60 nm CeO_2/YSZ	Fig. 3(g)	0.0016	< 0.001	...	...	...	...	...

and $\phi \sim 9°$ orientations are not immediately buried but instead require some thickness to heal out. We have duplicated this result several times on substrates from Ceres Corp. and from Commercial Crystal Labs. The latter have a larger $\phi = 0°$ component at low coverages.

The nature of the interface modification resulting in the improved texturing remains unclear. The effect we observe with homoepitaxial YSZ has a variety of possible origins. Possible changes to the surface include morphological alterations such as better flatness, or the opposite, i.e., the generation of steps, screw dislocations, and other features. There are plenty of examples of how surface topology can influence epitaxy. The step morphology of silicon is critical to the epitaxy of GaAs on Si, for example. The surface terminating layer of YSZ (100) can contain either oxygen atoms or zirconia atoms. The surface dipole moment will depend on the surface termination. We do not currently know whether the homoepitaxial surfaces are terminated differently in comparison to polished single crystals. The Y dopants and oxygen vacancies are known to order in bulk YSZ,[29] and there is the possibility that such an ordering is playing a role in the subsequent YBCO epitaxy.

In the search for a cause of the effect described above, atomic force microscopy (AFM) provided a means to look for gross physical features that might be responsible. Our experiment consisted of taking AFM micrographs of polished YSZ substrates, YSZ substrates that were thermal cycled in the deposition environment to simulate the conditions prior to YBCO epitaxy, and YSZ substrates on which either 10 nm or 60 nm YSZ layers were grown. All four types of samples showed comparable morphology with a mean roughness of 0.2 nm. This result points the cause toward a local, possibly electronic effect, which is beyond the resolving power of AFM.

C. YSZ buffer layers of varied yttria content

We have sought to make a preliminary demonstration of the effects of the YSZ composition on the epitaxial behavior of YBCO on YSZ. The cubic $(Y_2O_3)_x(ZrO_2)_{1-x}$ solid solution extends over a broad range from approximately $x = 0.09$ to $x = 0.30$. Below approximately $x = 0.09$, tetragonal and monoclinic solid solutions start to appear.[30] The Y^{3+} ions situate substitutionally on the Zr^{4+} sites, and charge neutrality requires one oxygen anion vacancy for every two Y dopant atoms. The physical properties, i.e., ionic conductivity, plasticity, lattice constant, etc., are functions of the Y_2O_3 mole fraction; hence, an influence on the YBCO epitaxy is to be expected. As single crystals of various YSZ compositions were not available, we grew approximately 60 nm thin films of YSZ with the $x = 0.05$ and $x = 0.30$ compositions on single crystals with $x = 0.09$, and then deposited YBCO. The $x = 0.05$ sample had a 90% $\phi = 45°$ texture, with the remaining 10% divided between $\phi \sim 9°$ and $\phi = 0°$ components. The $x = 0.30$ sample had a greater than 99% $\phi = 45°$ texture, indicating clearly that the higher ~~doping~~ mole-fraction enhanced this orientation.

D. CeO_2 buffer layers

The above results show that homoepitaxial YSZ is effective for removing $\phi \neq 45°$ components of the *c*-axis YBCO epitaxy on YSZ; CeO_2 heteroepitaxial layers on YSZ also proved effective, and in addition have a closer lattice match to YBCO in the $\phi = 45°$ orientation. The mismatch of CeO_2 to YBCO at the growth temperature is about 1% for this orientation, whereas for YSZ it is about 5.6%. As represented by Fig. 3(g), deposition of a 60 nm layer of CeO_2 on bulk YSZ prior to YBCO deposition resulted in nearly 100% $\phi = 45°$ epitaxy. CeO_2 and

YSZ are both fluorite structure oxides; therefore it is not surprising that we observe that CeO_2 grows epitaxially on YSZ in a "cube-on-cube" fashion. Channeling on pulsed laser deposited CeO_2 on YSZ suggested earlier the likelihood of this epitaxial relationship,[31] as well as the chemical stability of the YBCO/CeO_2 interface.

E. Cu- and Y-oxide seed layers

The next set of surface modification experiments was aimed at determining the influence of initiating the growth with approximate monolayer coverages of CuO_x, Y_2O_3, and BaO. The effects may be summarized by saying that copper oxide and Y_2O_3 promote the growth of $\langle 110 \rangle$ $\phi = 45°$ material, and interfacial BaO promotes the formation of the $\phi \sim 9°$ distributed material. This series of experiments bears a relation to those of Kanai *et al.*,[32] who demonstrated the importance of the initiating layer in the epitaxy of Bi–Sr–Ca–Cu–O on $SrTiO_3$. While investigating laser molecular beam epitaxial growth of (Ca,Sr)CuO_2 layers on $SrTiO_3$, they observed that atomic layer growth was possible when the growth was initiated with SrO, whereas deposition of Cu as the initial material under oxidizing conditions resulted in three-dimensional growth.

Figure 3(b) shows a YBCO {103} reflection ϕ scan of a film prepared like that in Fig. 3(a) except for having 20 pulses (~0.3 nm) of copper oxide deposited on the substrate surface prior to YBCO growth. We observe more $\phi = 45°$ material than in Fig. 3(a), where the $\phi = 0°$ is the dominant orientation. A similar effect was observed in the case where 20 pulses of Y_2O_3 were deposited on the substrate surface prior to YBCO growth, as indicated in Fig. 3(c). Again, it is clearer that more $\phi = 45°$ material than in Fig. 3(a) was induced by the addition of Y_2O_3 to the interface.

Combination of this procedure with a YSZ homoepitaxial buffer layer consolidated the $\phi = 45°$ orientation almost completely. Figure 3(g) is representative of {103} ϕ scans taken on YBCO films grown following either 20 pulses of copper oxide on a 60 nm homoepitaxial YSZ layer or 20 pulses of Y_2O_3 on a 60 nm homoepitaxial YSZ layer. In both cases, about 1% of the scattering in the ϕ scans came from orientations not at $\phi = 45°$.

The x-ray results cannot reveal whether the initiating copper-oxide and yttrium-oxide layers, which are by intention the first arrivals at the YSZ surface, remain at the interface or are exchanged with other species. The results also cannot reveal the structure of the copper and yttrium oxides should they remain at the interface, i.e., whether they are incorporated into the YBCO structure or form a separate interface compound. Copper-oxide epitaxy on YSZ has not been reported; however, Y_2O_3 epitaxy on YSZ has been reported.[33] Y_2O_3 has the cubic bixbyite (Mn_2O_3) structure which contains cubic fluorite unit cells with vacant oxygen sites.[34] Thick (10 nm) Y_2O_3 layers were grown on YSZ on Si by Myoren *et al.*[12] to provide a suitable buffer layer structure for epitaxial YBCO. The crystallinity of their YBCO films without the Y_2O_3 layer was much poorer (Ba $\chi_{min} = 0.6$ instead of 0.06).

F. Ba-oxide seed layers

The results obtained by initiating YBCO growth with BaO differed from the related experiments with Y and Cu oxides. Figure 3(e) shows a YBCO {103} reflection ϕ scan of a film prepared like that in Fig. 3(a) except for having 20 pulses (~0.3 nm) of barium deposited in an oxidizing environment (200 mTorr O_2) on the substrate surface prior to YBCO growth. The $\phi = 0°$ grains which are dominant in Fig. 3(a) are almost absent in Fig. 3(e), and are replaced with $\phi = 45°$ and $\phi \sim 9°$ material. Figure 3(h) shows a film prepared with the same dose of barium oxide on a 60 nm homoepitaxial YSZ layer. The film is composed entirely of the broadly distributed $\phi \sim 9°$ material. This is to be contrasted with the $\phi = 45°$ epitaxy characteristic of the analogous experiments conducted with ytttrium and copper oxides. This experiment makes clear that interfacial Ba is involved in the nucleation of the $\phi \sim 9°$ material. This experiment also nicely demonstrates the sensitivity of the epitaxial texture to compositional fluctuations, with a rotation of the material by 36° being induced by approximately monolayer coverage of a species which is deposited in about 5 s.

G. $BaZrO_3$ seed layers

We have investigated $BaZrO_3$ interfacial layers in response to the observation that $BaZrO_3$ is a stable, interfacial end product of the reaction of YBCO with YSZ.[7] $BaZrO_3$ has the perovskite structure, and thus if grown as a thin layer, may support a chemically stable, homogeneous epitaxial transition from YSZ to YBCO. These experiments were carried out with substrates supplied by Commercial Crystal Labs. YBCO grown on these substrates without any treatment other than degreasing produced films with a dominant $\phi = 0°$ texture much like that indicated by Fig. 3(a). Addition of 20 pulses (~0.3 nm) of $BaZrO_3$ in an oxidizing environment resulted in transforming the texture to dominant $\phi = 45°$, as shown in Fig. 3(d). Inclusion of a 60 nm homoepitaxial YSZ layer produced the same results except for the removal of the $\phi \sim 9°$ grains, Fig. 3(g), and thicker $BaZrO_3$ produced the same $\phi = 45°$ texture with a broader ϕ width. These intentionally deposited $BaZrO_3$ layers have a significant effect on the YBCO in-plane texture, which is very different from the effect of the highly reactive BaO. When $BaZrO_3$ forms reactively

from with YBCO and YSZ, as has been observed by TEM, the influence on the in-plane epitaxy is difficult to ascertain. If the reacted layer forms immediately, there is the possibility that it reorients the YBCO. If the reacted layer forms only slowly, there may be little or no impact on the in-plane texture since these layers may form after several YBCO layers have grown, at which point the in-plane texture is essentially fixed.

H. Temperature effects on YBCO epitaxy

The next set of film depositions revealed the texturing trend as a function of temperature. YBCO films were grown on YSZ at approximate substrate temperatures of 740, 660, 630, and 600 °C and ϕ scans of the YBCO {103} reflections were taken as before. No treatment of the YSZ surface was performed prior to the YBCO deposition other than the degreasing procedure used for all the substrates in this work. The YSZ was supplied by Commercial Crystal Labs. Several epitaxial trends developed with temperature. There was a monotonic decrease in the fraction of $\phi = 0°$ oriented material as the substrate temperature was lowered. The ratio of the peak at $\phi = 0°$ to the peak at $\phi = 45°$ went from 1.9 at 740 °C down to 0.31 at 600 °C. In addition to becoming more dominant, the $\phi = 45°$ orientation developed a narrower rocking curve as the temperature was lowered. Finally, the amount of broadly distributed material about the $\phi = 0°$ orientation was almost negligible for the lowest three temperatures. Since the experiments with interfacial Ba reveal its role in generating low angle orientations, it is proposed that higher temperatures promote the separation of Ba to the interface during nucleation.

I. Pressure effects on YBCO epitaxy

A brief investigation into the effect of background pressure on the epitaxial texture of YBCO on YSZ was undertaken. YBCO thin films were grown directly on polished bulk YSZ substrates supplied by Commercial Crystal Labs at approximately 700 °C in 10 mTorr O_2 and 400 mTorr O_2. Three effects were observed. (1) The amount of $\phi = 0°$ material increased with the increase in pressure going from about 30% to about 70%. (2) There was no $\phi \sim 9°$ material formed in 10 mTorr whereas this accounted for about 15% of the film grown in 400 mTorr. (3) The ϕ width of the $\phi = 45°$ and $\phi = 0°$ components narrowed at the higher pressure. We note that even over a range covering 140 °C in substrate temperature and a factor of 40 in background pressure, the variation of these growth conditions was insufficient to produce 90% or larger dominance of a single orientation, unlike several of the surface modification procedures detailed above. This result has made us aware that seed layers deposited prior to YBCO are more effective for controlling the YBCO epitaxy than is temperature or pressure.

J. Cause of the three orientations

We will now discuss the origins of the principal textures observed in this experiment. There have been demonstrations of YBCO films on YSZ with either the $\phi = 0°$, $\phi \sim 9°$, or $\phi = 45°$ orientations dominating. Whereas this work has illustrated ways to isolate the $\phi \sim 9°$ and $\phi = 45°$ orientations, only the work of Garrison *et al.*[10] has reported films with near-complete $\phi = 0°$ orientation. Thus far, none of the procedures for altering the YSZ surface that we have tried enhances the $\phi = 0°$ orientation.

1. The $\phi = 0°$ orientation

The structures of YSZ and of YBCO appear in Fig. 1. YSZ has an oxygen deficient cubic fluorite structure; the anions form a simple cubic sublattice and the cation sublattice is face-centered cubic. At the growth temperature, the YSZ lattice constant is about 0.52 nm, and the YBCO lattice is tetragonal with an $a = 0.39$ nm.[35] For a $\phi = 0°$ orientation, i.e., with YBCO [100] or YBCO [010] parallel to YSZ [100], the lattices are almost exactly commensurate with a 4:3 ratio. The 2-dimensional repeat blocks for this commensuricity are diagrammed for YSZ (left) and YBCO (right) in the lower portion of Fig. 1. The oxygen sites at the corners of the repeat block are the coincident sites, which in the YSZ repeat block constitute one out of every nine oxygen sites. In the terminology of the coincident site lattice (CSL) theory,[36] this would therefore be classified as a $\Sigma \sim 9$ orientation. Note that the area of the CSL unit cell is nine times larger than the area of a unit cell of the YSZ oxygen sublattice. In the CSL theory, low values of Σ are correlated with low energy boundaries. This, we believe, explains why a fraction of the *c*-axis oriented grains on YSZ have this orientation.

2. The $\phi = 45°$ orientation

The simple cubic oxygen sublattice of YSZ has a spacing of 0.26 nm, whereas the nearest-neighbor oxygen-oxygen spacing in the square array of the CuO_2 planes in YBCO is 0.276 nm. Mating of the oxygen sublattices in this nearest-neighbor to nearest-neighbor fashion produces the $\phi = 45°$ orientation. This results in a 6% lattice mismatch with YBCO having the larger cell size. This is illustrated in the bottom of Fig. 1. The mating of sublattices is very local for this orientation, 0.26 nm between coincident sites compared with 0.78 nm for the $\phi = 0°$ orientation. Allowing a 6% compression of the CuO_2 plane layer, which may be

appropriate at very low coverage, the correspondence of anion sites with the YSZ lattice is unity, i.e., $\Sigma = 1$, whereas for the $\phi = 0°$ orientation the correspondence is one site in nine. It is generally assumed that a grain boundary may be of relatively low energy when the two adjoining crystal lattices have a relatively dense set of coincident lattice sites. This may explain the preponderance of the $\phi = 45°$ orientation under many of our experimental conditions. It may also explain the tendency of the $\phi = 45°$ orientation to have a narrower width in ϕ than the $\phi = 0°$ orientation.

Thus far, only the CuO_2 planes have been discussed in the context of coincident sites. Similar arguments apply to the chain layers. Both the Cu and the Y seed layers resulted in or enhanced the $\phi = 45°$ orientation. The Y plane has no oxygen, but is eightfold coordinated by the CuO_2 plane oxygens in YBCO as are (Zr, Y) nominally eightfold coordinated in YSZ. This implies that a direct transition from YSZ to YBCO initiated by the Y-layer should occur with Y going on the (Y, Zr) site. This causes the $\phi = 45°$ orientation and, as before, incurs a 6% lattice mismatch.

3. The $\phi \sim 9°$ orientation

Our results with barium at the interface show a dramatic redistribution of the epitaxial texture whose alignment, we believe, can also be explained in the context of a coincident site lattice model.[36] The coincident site lattice (CSL) is the lattice of points that overlap in two adjoining crystal lattices. In materials with the same lattice constant, the density of the CSL points is greatest without any relative rotation between grains (i.e., no boundary), and for cubic materials, the next most dense set of CSL points occurs with a relative rotation of 36.87°. This is referred to as a $\Sigma = 5$ boundary because the CSL unit cell volume is five times the area associated with each crystal lattice point. As mentioned above, it is assumed the low energy grain boundaries generally correspond to low values of Σ. The $\phi \sim 9°$ orientation, observed in particular in films grown with interfacial Ba, is very close to a $\Sigma = 5$ boundary originating from the $\phi = 45°$ orientation; an ideal $\Sigma = 5$ would result in $\phi = 45° - 36.87° = 8.13°$ and, as with the $\phi = 45°$ orientation, is mismatched by 6% at the growth temperature. Since the periodicity normal to the *c*-direction of all the YBCO layers is the same, the operation can be carried out similarly for all layers. The idealized $\Sigma = 5$ relationship is illustrated for the Ba–O plane in Fig. 4. Questions remain: for example, why we do not measure exactly $\phi = 8.13°$, and what particular role Ba is playing in causing the $\phi \sim 9°$ orientation? Without detailed simulations or surface structural measurements it is difficult to conclude very much more at this stage.

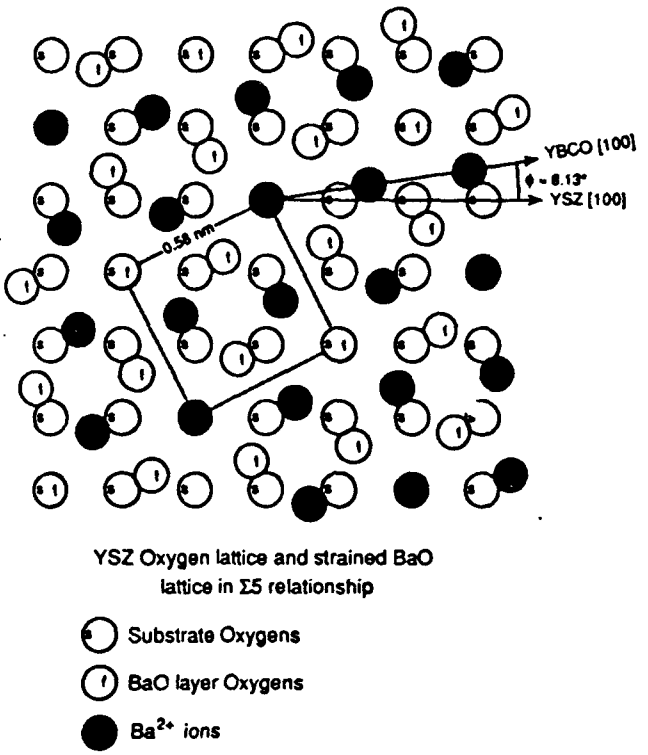

FIG. 4. Possible model for BaO layer overgrowth on YSZ. Overlay of the BaO and YSZ substrate layer lattices with a $\Sigma = 5$ relationship between the oxygen sublattices of the two compounds.

K. Transport correlations with epitaxial texture

The transport properties of some of the films grown in this study appear in Table I. To provide a semiquantitative measure of the epitaxial texture, the ratio of the peak areas of the $\phi = 0°$ and $\phi = 45°$ reflections was computed for each film. For all of the films the critical current density at 77 K was also measured. These two measurements appear in Table I, and appear graphically in Fig. 5. The correlation of J_c with the $\phi = 0°/\phi = 45°$ ratio is largely consistent with the results of Garrison *et al.*[10] (open circles in Fig. 5). The critical current density throughout the film is sensitive to the coupling between grains in the film. In films containing more than a few percent volume fraction of material making large angle grain boundaries with the dominant orientation, the J_c drops well below 10^6 A/cm^2 at 77 K. In films where the various methods described above resulted in a volume fraction of misaligned material on the order of 1% or less, the J_c lies near or above 10^6 A/cm^2 at 77 K.

Table I also contains the zero resistance transition temperature, transition width, resistance ratio ($\rho_{(300)}/\rho_{(100)}$), and the normal state resistivity at 100 K for some of the films listed. The T_c, transition width, resistivity, and the resistivity ratio are all dominated principally by intragranular properties; therefore, a strong dependence on texturing is not expected. For example, the J_c varied

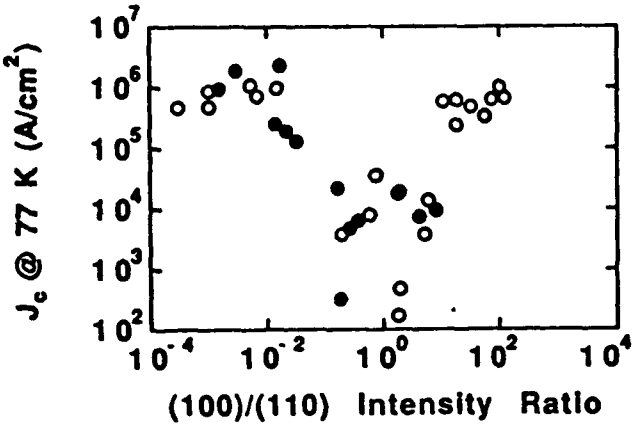

FIG. 5. Critical current density J_c measured at 77 K by the mutual inductance technique versus the intensity ratio of the YBCO (103) diffraction peaks representing the volume fraction of the film oriented with the $\phi = 0°$ and $\phi = 45°$ orientations. Solid circles refer to films from this work, and open circles are from Garrison *et al.*[10]

over about three orders of magnitude between films with heavily mixed and largely unmixed texture, whereas the normal state resistivity varied by about a factor of two.

IV. CONCLUSIONS

This work has been directed at controlling the epitaxial YBCO on YSZ system via straightforward *in situ* procedures. Variability in epitaxial quality is expected on the basis of variations in the surface quality, contamination, growth conditions, and substrate supplier. This work demonstrates that it is possible to make the film epitaxy insensitive to process variability such as modest fluctuations in temperature, stoichiometry, and substrate handling. Until recently, procedures for preparing substrates have focused on what goes on outside the growth chamber. This work suggests that most critical surface preparation procedures may be ones carried out *in situ*. This is frequently the case in semiconductor epitaxy and is an expected development in the refinement of YBCO film epitaxy. The surface of a polished YSZ single crystal supports *c*-axis epitaxy which is inherently tristable. The *in situ* prepared homoepitaxial YSZ surface enhances monostable *c*-axis epitaxy by favoring the $\phi = 45°$ orientation as do interfacial Y and Cu oxides. The effects of the YSZ homoepitaxial layer are enhanced as the mole fraction of the Y_2O_3 is increased. CeO_2 heteroepitaxial buffer layers were also proven to stabilize the $\phi = 45°$ orientation. This work has demonstrated that interfacial Ba is uniquely damaging among the YBCO cations, and has the effect of inducing a spread of low angle grain boundaries. Proximity to a low energy $\Sigma 5$ grain boundary may be the cause. The cause does not appear to be reactions that form barium zirconate. Degradation in film epitaxy at high temperatures and high pressures is manifested by low angle grain boundaries distributed about $\phi = 0°$. Finally, in spite of all our efforts, a procedure for isolating the $\phi = 0°$ epitaxial orientation remains elusive. The more long-range nature of the oxygen sublattice mating may be a factor.

ACKNOWLEDGMENTS

We gratefully acknowledge useful discussions with Stephen Streiffer of Stanford University, David Eaglesham of Bell Labs, and Jim Boyce and Neville Connell of Xerox PARC, and John M. Rowell and Nate Newman of Conductus, Inc. We thank Dick Johnson, Steve Ready, and Lars-Eric Swartz for their assistance developing our laser deposition system. Work at Xerox PARC was supported by the Air Force Office of Scientific Research (F49620-89-C-0017). DKF acknowledges an AT&T scholarship.

REFERENCES

1. A. B. Berezin, C. W. Yuan, and A. L. de Lozane, Appl. Phys. Lett. 57, 90 (1990).
2. K. Char, N. Newman, S. M. Garrison, R. W. Barton, R. C. Taber, S. S. Laderman, and R. D. Jacowitz, Appl. Phys. Lett. 57, 409 (1990).
3. X. D. Wu, R. E. Muenchausen, N. S. Nogar, A. Pique, R. Edwards, B. Wilkins, T. S. Ravi, D. M. Huang, and C. Y. Chen, Appl. Phys. Lett. 58, 304 (1991).
4. K. Char, M. S. Colclough, L. P. Lee, and G. Zaharchuk, Appl. Phys. Lett. 59, 2177 (1991).
5. D. K. Fork, K. Char, F. Bridges, S. Tahara, B. Lairson, J. B. Boyce, G. A. N. Connell, and T. H. Geballe, Physica C 162–164 121 (1989).
6. Q. Li, O. Meyer, X. X. Xi, J. Geerk, and G. Linker, Appl. Phys. Lett. 55, 1792 (1989).
7. L. A. Tietz, C. B. Carter, D. K. Lathrop, S. E. Russek, R. A. Buhrman, and J. R. Michael, J. Mater. Res. 4, 1072 (1989).
8. W. Shi, J. Shi, J. Sun, W. Yao, and Zh. Qi, Appl. Phys. Lett. 57, 822 (1990).
9. J. P. Zheng, S. Y. Dong, and H. S. Kwok, Appl. Phys. Lett. 58, 540 (1991).
10. S. M. Garrison, N. Newman, B. F. Cole, K. Char, and R. W. Barton, Appl. Phys. Lett. 58, 2168 (1991).
11. D. K. Fork, D. B. Fenner, R. W. Barton, Julia M. Phillips, G. A. N. Connell, J. B. Boyce, and T. H. Geballe, Appl. Phys. Lett. 57, 1161 (1990).
12. H. Myoren, Y. Nishiyama, N. Miyamoto, Y. Kai, T. Tamanaka, Y. Osaka, and F. Nishiyama, Jpn. J. Appl. Phys. 29, L955 (1990).
13. D. P. Norton, D. H. Lowndes, J. D. Budai, D. K. Christen, E. C. Jones, K. W. Lay, and J. E. Tkaczyk, Appl. Phys. Lett. 57, 1164 (1990); K. S. Harshavardhan, R. Ramesh, T. S. Ravi, S. Sampere, A. Inam, C. C. Chang, G. Hull, M. Rajeswari, T. Sands, T. Venkatesan, M. Reeves, J. E. Tkaczyk, and K. W. Lay, Appl. Phys. Lett. 59, 1638 (1991).
14. S. Witanachchi, S. Patel, Y. Z. Zhu, H. S. Kwok, and D. T. Shaw, J. Mater. Res. 5, 717 (1990); A. Kumar, L. Ganapathi, S. M. Kanetkar, and J. Narayan, Appl. Phys. Lett. 57, 2594 (1990); A. Kumar, L. Ganapathi, S. M. Kanetkar, and J. Narayan, J. Appl. Phys. 69, 2410 (1991); J. Saitoh, M. Fukutomi, K. Komori, Y. Tanaka, T. Asano, H. Maeda, and H. Takahara, Jpn. J. Appl. Phys. 30, L898 (1991); R. P. Reade, X. L. Mao, and R. E. Russo, Appl. Phys. Lett. 59, 739 (1991).

15. G.A. Samara, J. Appl. Phys. 68, 4214 (1990).
16. D.K. Fork, A. Barrera, T.A. Geballe, A.M. Viano, and D.B. Fenner, Appl. Phys. Lett. 57, 2504 (1990).
17. D. Dimos, P. Chaudhari, J. Mannhart, and F.K. LeGoues, Phys. Rev. Lett. 61, 219 (1988); D. Dimos, P. Chaudhari, and J. Mannhart, Phys. Rev. B 41, 4038 (1990).
18. Z.G. Ivanov, P.A. Nilsson, D. Winkler, G. Brorsson, T. Claeson, E.A. Stepantsov, and A. Ya. Tzalenchuk, presented at the International Conference on Superconducting and Quantum Effect Devices and their Applications, Berlin, Germany, June 18–21, 1991.
19. S.S. Laderman, R.C. Taber, R.D. Jacowitz, J.L. Moll, C.B. Eom, T.L. Hylton, A.F. Marshall, T.H. Geballe, and M.R. Beasley, PRB (accepted).
20. B.H. Moeckly, S.E. Russek, D.K. Lathrop, R.A. Buhrman, Jian Li, and J.W. Mayer, Appl. Phys. Lett. 57, 1687 (1990).
21. S.K. Streiffer, B.M. Lairson, C.B. Eom, A.F. Marshall, J.C. Bravman, and T.H. Geballe, in *High Resolution Electron Microscopy of Defects in Materials*, edited by R. Sinclair, D.J. Smith, and U. Dahmer (Mater. Res. Soc. Symp. Proc. 183, Pittsburgh, PA, 1990), p. 363.
22. M.J. Cima, J.S. Schneider, S.C. Peterson, and W. Coblenz, Appl. Phys. Lett. 53, 710 (1988).
23. T.S. Ravi, D.M. Huang, R. Ramesh, Siu Wai Chan, L. Nazar, C.Y. Chen, A. Inam, and T. Venkatesan, Phys. Rev. B 42, 10141 (1990).
24. C.B. Eom, private communication.
25. A. Inam, C.T. Rogers, R. Ramesh, K. Remschnig, L. Farrow, D. Hart, T. Venkatesan, and B. Wilkins, Appl. Phys. Lett. 57, 2484 (1990).
26. K. Char, M.S. Colclough, S.M. Garrison, N. Newman, and G. Zaharchuk, Appl. Phys. Lett. 59, 733 (1991).
27. L.P. Lee, K. Char, M.S. Colclough, and G. Zaharchuk, Appl. Phys. Lett. 00, 000 (1991).
28. A.T. Fiory, A.F. Hebard, P.M. Mankiewich, and R.E. Howard, Appl. Phys. Lett. 52, 2165 (1988).
29. D. Steele and B.E.F. Fender, J. Phys. C 7, 1 (1974).
30. V.S. Stubican, Adv. Ceram. 24, 71 (1988).
31. X.D. Wu, R.C. Dye, R.E. Muenchausen, S.R. Foltyn, M. Maley, A.D. Rollett, A.R. Garcia, and N.S. Nogar, Appl. Phys. Lett. 58, 2165 (1991).
32. Masaki Kanai, Tomoji Kawai, and Shichio Kawai, Appl. Phys. Lett. 58, 771 (1991).
33. H. Fukumoto, T. Imura, and Y. Osaka, Appl. Phys. Lett. 55, 360 (1989).
34. R.W.G. Wycoff, *Crystal Structures* (Interscience, New York, 1963), Vol. 2, p. 4.
35. J.D. Jorgensen, M.A. Beno, D.G. Hinks, L. Soderholm, K.J. Volin, R.L. Hitterman, J.D. Grace, Ivan K. Schuller, C.U. Segre, K. Zhang, and M.S. Kleefisch, Phys. Rev. B 36, 3608 (1987).
36. R.W. Balluffi, A. Brokman, and A.H. King, Acta Metall. 30, 1453 (1982).

EPITAXIAL GROWTH OF FERROELECTRIC THIN FILMS ON GaAs WITH MgO BUFFER LAYERS BY PULSED LASER DEPOSITION

K. Nashimoto[a)b)], D. K. Fork[a)c)], F. A. Ponce[a)], and T. H. Geballe[c)]

a) Xerox Palo Alto Research Center, Palo Alto, CA 94304.
b) Materials Research Laboratory, Fuji Xerox Co., Ltd., Kanagawa, Japan.
c) Department of Applied Physics, Stanford University, CA 94305.

ABSTRACT

Epitaxial growth of ferroelectric thin films on GaAs (100) by pulsed laser deposition was examined for integrated electro-optic device applications. To promote epitaxy of ferroelectrics and prevent interdiffusion, we have deposited several types of buffer layers. CeO_2 film reacted strongly with GaAs. Although Y_2O_3 9% stabilized-ZrO_2 films showed epitaxial growth, YSZ reacted with GaAs at 780°C. MgO grew epitaxially and was stable even at 780°C. HRTEM observation showed sharp interface between MgO and GaAs. $BaTiO_3$ and $SrTiO_3$ deposited on MgO/GaAs structures showed epitaxial growth. In-plain orientation was $BaTiO_3$ [100] // MgO [100] // GaAs [100]. Epitaxial $BaTiO_3$ films were c-axis oriented tetragonal phase and showed ferroelectric hysteresis.

INTRODUCTION

There have been growing efforts in preparing epitaxial ferroelectric films on oxide substrates such as PLZT on sapphire by rf-magnetron sputtering [1], $KNbO_3$ on MgO by ion beam sputtering [2], $Bi_4Ti_3O_{12}$ on $SrTiO_3$ by pulsed laser deposition [3], $PbTiO_3$ on $SrTiO_3$ by MOCVD [4], and $LiNbO_3$ on sapphire by sol-gel process [5]. Whereas, epitaxial growth of ferroelectric films on GaAs is very attractive to integrate semiconductor lasers and ferroelectric electro-optic devices on the same GaAs substrate. With this integration, monolithic electro-optic devices which emit visible laser light by second harmonic generation or scan the laser light by acousto-optic diffraction, for instance, will be fabricated. Furthermore, perovskite type ferroelectric materials are good host materials for epitaxial $YBa_2C_3O_{7-\delta}$ films. [6]

However, epitaxy of ferroelectric films on GaAs is not easy because of several factors such as the high growth temperature, interdiffusion, and the general lack of epitaxy to the zinc blend structure. GaAs begins to loose As over 400°C [7] without As_4 flux atmosphere which is incompatible with the growth technique of ferroelectric films. Pb diffusion from PLZT into the GaAs was detected [8]. Therefore, capping of GaAs with buffer layer which grows epitaxially at low temperature and works as a diffusion barrier is needed. Epitaxial oxide materials which have been grown on Si include $MgAl_2O_4$ [9], Y-stabilized ZrO_2 (YSZ) [10], CeO_2 [11], and MgO [12]. Such a buffer layer on GaAs has not been reported previously to our knowledge. While we have succeeded in growing epitaxial MgO on GaAs (100) and epitaxial $BaTiO_3$ thereon by pulsed laser deposition [13]. Pulsed laser deposition is a very useful technique because of its simplicity, high deposition rate and near stoichiometric deposition.

In this report, we will show growth of oxide materials such as CeO_2 (Fluorite, a=5.41134 Å), Y_2O_3 9% stabilized-ZrO_2 (YSZ) (Fluorite, a=5.139 Å), and MgO (NaCl, a=4.218 Å) on GaAs (Zinc blend, a=5.6534 Å). Then, we will present structures and properties of perovskite type thin films like $BaTiO_3$ (Perovskite, a=3.994 Å, c=4.038 Å) and $SrTiO_3$ (Perovskite, a=3.9051 Å) grown on buffer layers.

EXPERIMENTAL

The Pulsed laser deposition apparatus used was described previously [13]. Briefly, a XeCl excimer laser (308 nm) was used at a pulse rate of 4 Hz, a pulse length of 17 ns, and a laser energy of 130 mJ (an energy density of 1.3 J/cm^2 on targets.) The target-to-substrate distance was 50 mm and the base pressure was 3×10^{-7} Torr. We used stoichiometric CeO_2, YSZ, $BaTiO_3$, and $SrTiO_3$ targets, and Mg metal target. Mg is readily oxidized due to the molecule's high binding energy. The GaAs substrate was heated radiatively. Substrate temperature was measured by a thermocouple and by a pyrometer. The thermocouple overestimates the substrate temperature.

Si doped GaAs (001) off 0°±0.2° wafers, 6×6 mm square, were degreased, etched by H_2SO_4:H_2O_2:H_2O=10:1:1, then rinsed with deionized water, ethanol, and spin-dried with ethanol in flowing N_2. After these process, the substrate was immediately introduced into the deposition chamber. The substrate was heated at 680°C (600°C by pyrometer) for 2 min in the base pressure before deposition in order to sublimate surface oxides formed after etching.

RESULT AND DISCUSSION

We examined a few oxides as buffer layers. CeO_2 was deposited at 730°C in 1.2×10^{-3} Torr O_2. After deposition, surface of the substrate looked very rough to naked eyes meaning a strong reaction of CeO_2 with GaAs. YSZ films deposited between 630°C and 730°C in 0.5×10^{-3} Torr O_2 were epitaxial to GaAs with (200) orientation. Fig. 1 shows an X-ray θ-2θ diffraction pattern with Cu $K\alpha$ radiation from YSZ deposited at 680°C. However, YSZ deposited at 780°C was not epitaxial to GaAs. $BaTiO_3$ deposited on epitaxial YSZ prepared at 680°C showed unidentifiable peaks when $BaTiO_3$ was deposited at 780°C. Considering from these results YSZ looked reacted react with GaAs at 780°C.

MgO films were deposited between 250°C and 450°C. MgO films deposited in 5×10^{-6} Torr O_2 were all epitaxial in spite of low deposition temperatures a large lattice mismatch (25.5%) between MgO and GaAs. Fig. 2 is a typical X-ray diffraction pattern from MgO/GaAs structure showing reflections only from MgO (200) and GaAs (200). The rocking curve FWHM of MgO was 1.40° when MgO was deposited at 350°C in 5×10^{-6} Torr O_2.

$BaTiO_3$ films deposited in 1.2×10^{-3} Torr O_2 at 780°C on these epitaxial MgO were all epitaxial as shown in Fig. 3. According to the values of d spacing and the intensity ratio of (001) to (002) reflections, the films had tetragonal phase and c-axis orientation. The observation by scanning electron microscopy showed optically smooth surfaces of the films. The in-plane epitaxial relationship between $BaTiO_3$, MgO, and GaAs was verified as $BaTiO_3$ [100] // MgO [100] // GaAs [100] by X-ray

diffraction phi scan of the (202) reflections which are 45° off normal to the surface. $BaTiO_3$ films deposited on MgO films deposited below and over 5×10^{-6} Torr O_2 showed misoriented planes. The rocking curve FWHM of $BaTiO_3$ deposited on MgO which was deposited at 350°C in 5×10^{-6} Torr O_2 was 1.84°. Without MgO buffer layer, $BaTiO_3$ did not grow epitaxially although the lattice mismatch between $BaTiO_3$ and GaAs for [110] // [100] is 0.1%. While the lattice mismatch between $BaTiO_3$ and MgO for [100] // [100] is 5.2%. and

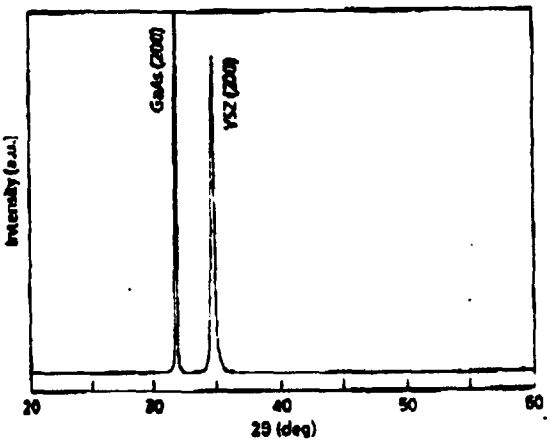

Fig. 1 X-ray diffraction pattern of YSZ on GaAs.

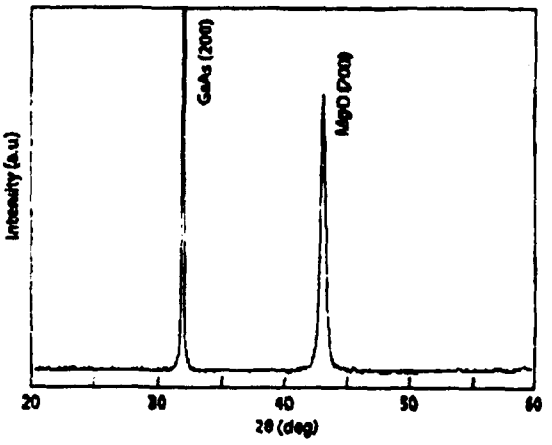

Fig. 2 X-ray diffraction pattern of MgO on GaAs.

The same deposition condition as $BaTiO_3$ was applicable for growing $SrTiO_3$ epitaxially on MgO/GaAs as shown in Fig. 4. Epitaxial $SrTiO_3$ was grown in 1.2×10^{-3} Torr O_2 at 780°C. The lattice mismatch between $SrTiO_3$ and MgO for [100] // [100] is 7.3% and larger than that between $BaTiO_3$ and MgO.

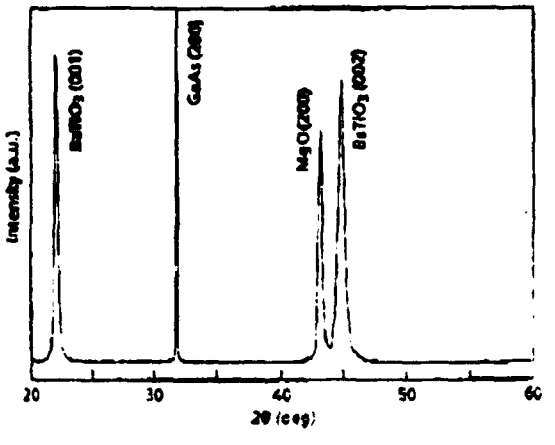

Fig. 3 X-ray diffraction pattern of $BaTiO_3$ on MgO/GaAs.

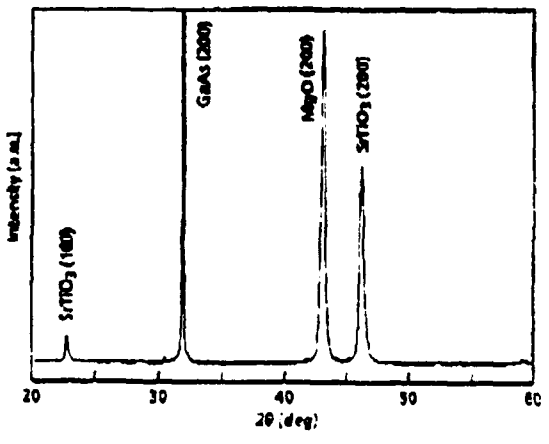

Fig. 4 X-ray diffraction pattern of $SrTiO_3$ on MgO/GaAs.

Misfit dislocations are observed at the interface at intervals of four atomic planes of MgO and 3 atomic planes of GaAs.

Lattice images of interfaces were observed in the [110] zone axis by high resolution transmission electron microscopy (HRTEM) for MgO grown at 350°C in 5×10^{-6} Torr O_2 and $BaTiO_3$ grown on the MgO at 780°C in 1.2×10^{-3} Torr O_2. The lattice images and electron diffraction patterns confirmed cube-on-cube crystallography. Fig. 5 is the MgO/GaAs interface. The interface is abrupt, and free ~~from formation~~ of secondary phases and oxides. ~~The detailed observation of the~~ image shows periodical ~~formation~~ of dots at ~~the~~ intervals of ~~four atoms for MgO~~ and ~~three atoms for GaAs.~~ These dots may be ~~caused by~~ the dislocation or ~~misfit~~. It is quite interesting that the mismatch between MgO and GaAs is 0.65% for a 4:3 lattice coincidence. Therefore, the epitaxial growth of MgO with a large lattice mismatch to GaAs may be promoted by relaxing its lattice constant to its bulk value through the formation of incommensurate interface as a 4:3 lattice coincidence. Fig. 6 is the $BaTiO_3$/MgO interface. $BaTiO_3$ was epitaxial on MgO as observed by X-ray diffractions. The interface is also sharp and free from formation of secondary phases. The formation of twin boundaries were visible in $BaTiO_3$ although no grain boundaries was observed.

Fig. 5 High resolution transmission electron micrograph of MgO/GaAs interface in [110] zone axis.

Rutherford Backscattering (RBS) spectra along random and the [001] directions for $BaTiO_3$ grown at 700°C in 1.2×10^{-3} Torr O_2 on MgO deposited at 350°C in 5×10^{-6} Torr O_2 showed a minimum yield of 55% at the surface. The defects observed by HRTEM may be a main reason for the relatively high RBS channeling yield.

CONCLUSIONS

Epitaxial YSZ and MgO were grown on GaAs (001) substrates as buffer layers by pulsed laser deposition. YSZ, however, reacted with GaAs at 780°C. Whereas, MgO grown between 250°C and 450°C was stable even at 780°C. The interface between MgO and GaAs was atomically sharp. $BaTiO_3$ and $SrTiO_3$ films deposited on MgO/GaAs showed epitaxial growth. Epitaxial relationship was $BaTiO_3$ [100] // MgO [100] // GaAs [100] in spite of a large lattice mismatch of 25.5% between MgO and GaAs. Grown $BaTiO_3$ showed ferroelectric hysteresis loops meaning formation of a tetragonal phase. Through this study, we demonstrated possibility of monolithic integration of semiconductor lasers and ferroelectric electro-optic devices on the same GaAs substrates.

ACKNOWLEDGMENT

The authors would like to thank J. M. Phillips of AT&T Bell Laboratories for RBS measurement, and J. C. Tramontana and R. Donaldson for technical assistance. We are also thankful to G. A. N. Connell and J. B. Boyce for their suggestions and encouragement during the course of the study. This work is supported in part by AFOSR (contract #F49620-89-C-0017). DKF was an AT&T scholar.

REFERENCES

1. H. Adachi, T. Kawaguchi, M. Kitabatake, and K. Wasa, Jpn. J. Appl. Phys. 22, suppl. 22-2, 11 (1983).
2. M. S. Ameen, T. M. Graettinger, S. H. Rou, H. N. Al-Shareef, K. D. Gifford, O. Auchiello, and A. I. Kingon, *Mat. Res. Soc. Symp. Proc.* 200 65 (1990).
3. R. Ramesh, K. Luther, B. Wilkens, D. L. Hart, E. Wang, and J. M. Tarascon, A. Inam, X. D. Wu, and T. Venkatesan, Appl. Phys. Lett. 57 1505 (1990).
4. M. de Keijser, G. J. Dormans, J. F. Cillessen, D. M. de Leeuw, and H. W. Zandbergen, Appl. Phys. Lett. 58 2636 (1991).
5. K. Nashimoto and M. J. Cima, Mater. Lett. 10 348 (1991).
6. D. K. Fork, K. Nashimoto, and T. H. Geballe, to be submitted. (unpublished)
7. J. Y. Tsao, T. M. Brennan, J. F. Klem, and B. E. Hammons, J. Vac. Sci. Technol. A7, 2138 (1989).
8. M. Ishida, S. Tsuji, K. Kimura, H. Matsunaga, and T. Tanaka, J. Cryst. Growth, 45 393 (1978).
9. M. Mikami, Y. Hokari, K. Egami, H. Tsuya, and M. Kanamori, Proceedings of 15th Conference on Solid State Devices and Materials, Tokyo, 31 (1983).
10. H. Fukumoto, T. Imura, and Y. Osaka, Jpn. J. Appl. Phys. 27, L1401 (1988).
11. T. Inoue, Y. Yamamoto, S. Koyama, S. Suzuki, and Y. Ueda, Appl. Phys. Let. 56, 1332 (1990).
12. D. K. Fork, F. A. Ponce, J. C. Tramontana, and T. H. Geballe, Appl. Phys. Lett. 58 2294 (1991).
13. K. Nashimoto, D. K. Fork, and T. H. Geballe, submitted to publish. (unpublished)

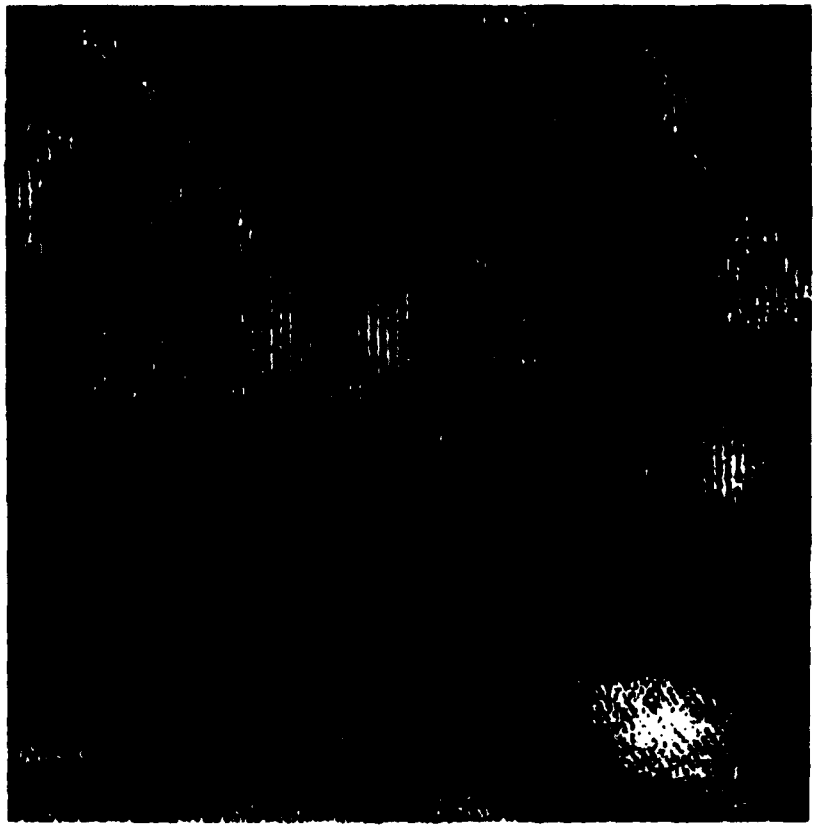

Fig. 6 High resolution transmission electron micrograph of $BaTiO_3$/MgO interface in [110] zone axis.

The ferroelectric hysteresis of the epitaxial films were measured with capacitor structure using Cr dots of 1 mm in diameter on the 1915Å $BaTiO_3$/ 343Å MgO/GaAs as shown in Fig. 7. The remanent polarization, the coercive field, and effective dielectric constant were about 0.6 $\mu C/cm^2$, 120 kV/cm, and 40 at applied voltage of 6V, respectively. Relatively large coercive field and small effective dielectric constant may result from existence of MgO buffer layer because of large voltage drop across MgO due to its high electric resistance and of small dielectric constant relative to $BaTiO_3$. Presentation of ferroelectric hysteresis means that the grown $BaTiO_3$ films are tetragonal phase as suggested from X-ray data.

The presence

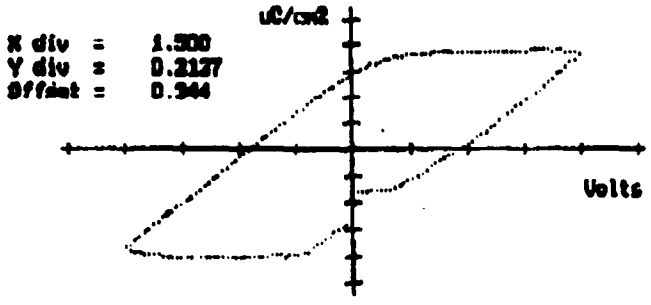

Fig. 7 Ferroelectric hysteresis loop of BaTiO3/MgO films on GaAs.

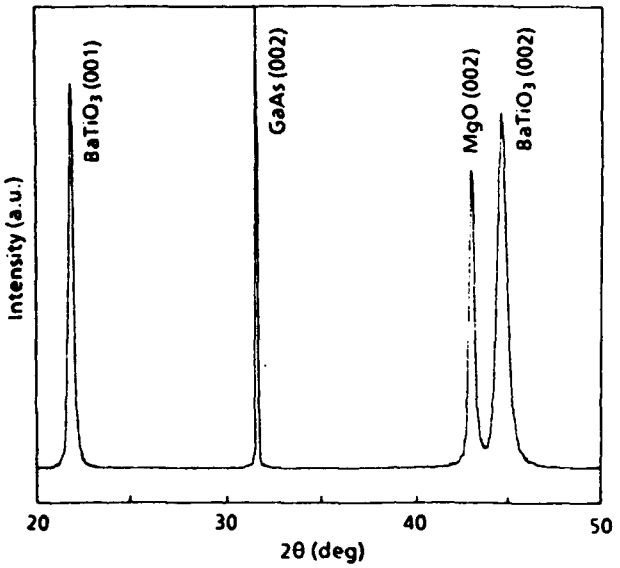

FIG. 1. X-ray diffraction pattern from $BaTiO_3$/MgO/GaAs structure.

However, $BaTiO_3$ films were polycrystalline with preferred (001) and (101) orientations. This result indicates that epitaxy of $BaTiO_3$ requires more than simple lattice matching (for [110]|| [100] the mismatch is 0.1%)

About 600-Å-thick $BaTiO_3$ films were deposited at 780 °C (700 °C by a pyrometer) in 1.2×10^{-3} Torr O_2 on MgO films deposited between 250 and 450 °C in the same run. MgO films deposited in 5×10^{-6} Torr O_2 and $BaTiO_3$ films deposited thereon were all epitaxial. The surface morphology of the films observed by scanning electron microscopy was quite smooth. Figure 1 is an x-ray θ-2θ diffraction pattern with Cu$K\alpha$ radiation from one of prepared $BaTiO_3$/MgO/GaAs structures showing reflections from $BaTiO_3$ (00*l*), MgO (002), and GaAs (002). No misoriented material was observed. The *d* spacing of deposited $BaTiO_3$ (002) was 2.02 Å, whereas the bulk values are 1.997 and 2.019 Å for (200) and (002) planes of the tetragonal phase and 2.016 Å for (200) of the cubic phase, respectively. While the intensity ratio of the deposited $BaTiO_3$ was 1.08 ± 0.08 ($n=8$) for (002) to (001), the bulk values of the tetragonal phase are 1.48 for (200) to (100) and 1.00 for (002) to (001), and the bulk value of cubic phase is 2.50 for (200) to (100). Therefore, the *c*-axis-oriented tetragonal phase seems to be formed although phase identification requires further analysis.

MgO layer thickness was measured by He-Ne laser ellipsometry. The deposition rate of MgO depended strongly on O_2 pressure and substrate temperature. Deposition rates were between 0.03 and 0.07 Å/pulse. According to Yadavalli *et al.*,[15] thermal desorption of Mg is inhibited by lower substrate temperature and Mg oxidation; both are consistent with Table I. The thickness of the MgO layer in Fig. 1 was about 440 Å. It was surprising, however, that only about a 40-Å-thick MgO layer worked well to give epitaxial $BaTiO_3$.

Misalignment of the crystal plane of the films parallel to the surface was evaluated by x-ray diffraction rocking curves as shown in Table II. The epitaxy of MgO was very

TABLE I. Ellipsometric data for MgO films on GaAs.

Heter. temp (°C)	O_2 pressure ($\times10^{-6}$ Torr)	Thickness (Å)	Refractive index
300	5	704 ± 21	1.706 ± 0.002
350	2	353 ± 6	1.687 ± 0.002
350	5	436 ± 4	1.719 ± 0.001
350	10	486 ± 7	1.725 ± 0.001
350	20	551 ± 8	1.717 ± 0.002
400	5	359 ± 5	1.717 ± 0.003
450	5	305 ± 18	1.676 ± 0.003

sensitive to O_2 pressure. Misoriented planes of $BaTiO_3$ were observed when the MgO films were deposited in O_2 pressure other than 5×10^{-6} Torr, although changes in the rocking curve FWHM (full width at half maximum) were relatively small over 5×10^{-6} Torr O_2. For both $BaTiO_3$ and MgO, the rocking curve FWHM of the films showed almost the smallest value at 350 °C. MgO deposited at 350 °C in 5×10^{-6} Torr O_2 had a rocking curve FWHM of 1.4°. This value is better than that for the epitaxial MgO on Si (2.5°),[14] although the lattice mismatch between MgO and GaAs (25.5%) is larger than that between MgO and Si (22.2%). It is interesting, however, that for a 4:3 lattice coincidence the mismatch between MgO and GaAs is 0.65% and that between MgO and Si is 3.43%. The relationship between FWHM of rocking curve for MgO (002) and $BaTiO_3$ (002) is proportional as shown in Fig. 2. This result indicates that crystallinity of $BaTiO_3$ films depends on the quality of underlying MgO films as in the case between films and substrates. The films deposited without the surface oxide sublimation step showed worse crystallographic quality as shown in Table II. The rocking curve resolution measured on GaAs (002) was 0.24°.

In-plane film texturing and twist misalignment was analyzed by the x-ray diffraction ϕ scan of the (202) reflections which are 45° off normal to the surface for cubic crystals as shown in Table II. The epitaxial relationship between $BaTiO_3$, MgO, and GaAs was verified as $BaTiO_3$ [100]|| MgO[100]|| GaAs[100] in spite of a large lattice mismatch between MgO and GaAs with this orientation. This result is identical to the growth of MgO on Si.[14] ϕ scan FWHMs were almost identical over 5×10^{-6} Torr.

TABLE II. X-ray diffraction data for $BaTiO_3$ and MgO on GaAs.

Heter. temp	O_2 for MgO	Rocking curve width for (002) (deg)		ϕ scan width for (202) (deg)	
(°C)	($\times10^{-6}$ Torr)	MgO	$BaTiO_3$	MgO	$BaTiO_3$
250	5	1.47	1.93	2.72	3.25
300	5	1.62	1.97	2.40	3.10
350[a]	2	2.85	...	...	...
350	5	1.40	1.84	2.21	2.74
350[a]	10	1.45	1.91	2.24	...
350[a]	20	1.29	1.53	1.95	2.54
400	5	1.89	2.37	2.50	3.16
450	5	2.11	2.37	2.63	3.36
350[a,b]	5	1.80	2.06	3.98	...

[a] $BaTiO_3$ contained misoriented planes.
[b] MgO was deposited without preheating at 680 °C.

Epitaxial growth of MgO on GaAs(001) for growing epitaxial $BaTiO_3$ thin films by pulsed laser deposition

Keiichi Nashimoto[a)] and David K. Fork
Xerox Palo Alto Research Center, Palo Alto, California 94304

Theodore H. Geballe
Department of Applied Physics, Stanford University, Stanford, California 94305

(Received 30 September 1991; accepted for publication 3 January 1992)

MgO buffer layers were deposited on GaAs by pulsed laser deposition for epitaxial growth of $BaTiO_3$. MgO was grown epitaxially on GaAs for the first time; the orientation is (001) on GaAs(001). The best crystallographic quality was obtained at 350 °C in 5×10^{-6} Torr O_2. $BaTiO_3$ films with (001) orientation grew epitaxially on MgO/GaAs. The in-plane epitaxial relationship was $BaTiO_3[100]\|$ MgO[100]$\|$ GaAs[100] in spite of a large lattice mismatch (25.5%) between MgO and GaAs.

Ferroelectric thin films have attracted attention for nonvolatile memories, electro-optic devices, and surface-acoustic-wave devices. For electro-optic applications using optical waveguides, in particular, epitaxial ferroelectric films are essential because of their low propagation loss. Extensive effort has produced epitaxial ferroelectric films mostly on oxide substrates by a variety of methods: $Pb_{1-x}La_x(Zr_{1-y}Ti_y)_{1-x/4}O_3$ (PLZT) on sapphire by rf-magnetron sputtering,[1] $NKbO_3$ on MgO by ion-beam sputtering,[2] $BaTiO_3$ on MgO (Ref. 3), and $Bi_4Ti_3O_{12}$ on $SrTiO_3$ (Ref. 4) by pulsed laser deposition, $PbTiO_3$ on $SrTiO_3$ by metalorganic chemical vapor deposition (MOCVD),[5] and $LiNbO_3$ on sapphire by the sol-gel process,[6] for instance.

Epitaxial growth of ferroelectric films on GaAs is desirable to integrate semiconductor lasers and ferroelectric electro-optic devices on the same GaAs substrate. Epitaxy of ferroelectric films directly on GaAs is rendered difficult by several factors, including the high growth temperature, interdiffusion, and the general lack of epitaxy to the zinc-blende structure. GaAs begins to lose As over 400 °C (Ref. 7) and layer-by-layer sublimation from GaAs was reported above 690 °C,[8] without As_4 flux atmosphere which is incompatible with ferroelectric film growth. Diffusion of Pb into the GaAs was detected, although epitaxial PLZT films with (110) orientation were prepared on GaAs(100) by rf diode sputtering.[9] Therefore, a capping buffer layer which grows epitaxially at low temperature and acts as a diffusion barrier is needed.

To our knowledge, such a buffer layer on GaAs has not been reported previously. Oxide materials which have been grown epitaxially on Si include $MgAl_2O_4$,[10] Y-stabilized ZrO_2 (YSZ),[11,12] CeO_2,[13] and MgO.[14] We selected a few oxides out of these materials as buffer layers since GaAs is also a tetrahedral semiconductor with a lattice parameter similar to Si. CeO_2 and YSZ were, however, reactive with GaAs according to our preliminary experiments, although YSZ grew epitaxially on GaAs with crystallography as observed in epitaxial YSZ on Si.[12]

Yadavalli *et al.* reported low-temperature homoepitaxial growth of MgO down to 140 K.[15] Low-temperature growth of MgO on Si was also observed by Fork *et al.*[14] MgO is an ionic solid with low-energy neutral (001) cleavage planes, and is known to grow with (001) orientation preferentially, regardless of substrate materials. MgO has been used as a substrate for deposition of ferroelectric and high-temperature superconductor films because of its refractory nature and of its crystal structure (NaCl, $a = 4.213$ Å) suitable for these depositions.

In this study, growth of $BaTiO_3$ thin films on GaAs was examined as a model perovskite ferroelectric material. Stoichiometry control and epitaxy on bulk MgO by pulsed laser deposition has been demonstrated.[3] $BaTiO_3$ is also a good host material for epitaxial $YBa_2C_3O_{7-\delta}$ films.[16]

Pulsed laser deposition is a powerful technique due to its simplicity, high deposition rate, and near-stoichiometric deposition. A 308-nm XeCl excimer laser (Lambda Physik EMG 103) was used at a pulse rate of 4 Hz, a pulse length of 17 ns, and a laser energy of 130 mJ which give an energy density of 1.3 J/cm^2 on targets. The target-to-substrate distance was 50 mm and the base pressure of 3×10^{-7} Torr. We used $BaTiO_3$ and Mg targets mounted on a Poly-Gun source (Kurt J. Lesker Co.) as in Ref. 14. Mg is readily oxidized due to the molecule's $\sim$10 eV binding energy. The GaAs substrate was heated radiatively. Temperature was measured by a thermocouple affixed to an inner wall of the box containing the lamp. The substrate and its holder form one wall of the box. The thermocouple overestimates the substrate temperature.

Si-doped GaAs(001) off $0°\pm0.2°$ wafers, 6×6 mm square, were degreased and immersed for 60 s in H_2SO_4:H_2O_2:H_2O = 10:1:1. The substrates were then rinsed with de-ionized water, ethanol, and spin dried with ethanol in flowing N_2, then immediately introduced into the deposition chamber. Reference 17 indicates that surface oxides desorb at 582 °C, hence the substrate was heated at 680 °C (600 °C by a pyrometer) for 2 min in the base pressure before deposition in order to sublimate surface oxides formed after etching.

$BaTiO_3$ films were deposited in condition ranging from 680 to 780 °C and from base pressure to 3×10^{-2} Torr O_2.

a)Currently at Materials Research Laboratory, Fuji Xerox Co., Ltd., Minamiashigara, Kanagawa 250-01, Japan.

 0003-6951/92/101199-03$03.00

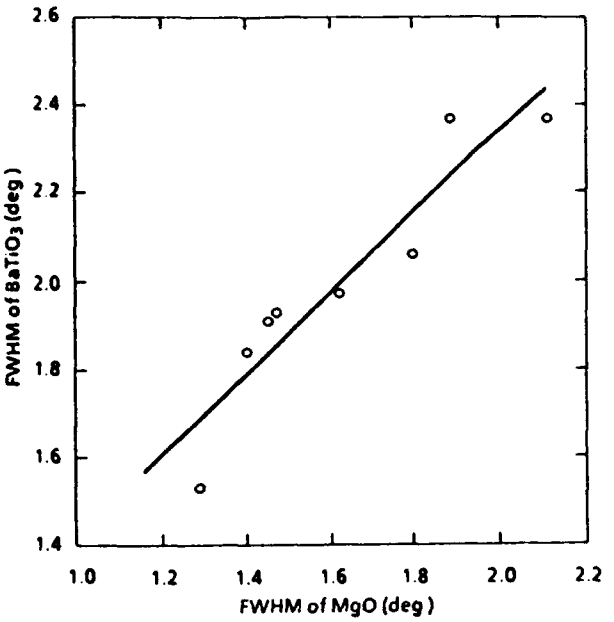

FIG. 2. Relationship between x-ray rocking curve FWHM for (002) reflections of $BaTiO_3$ films and for (002) reflections of underlying MgO films on GaAs.

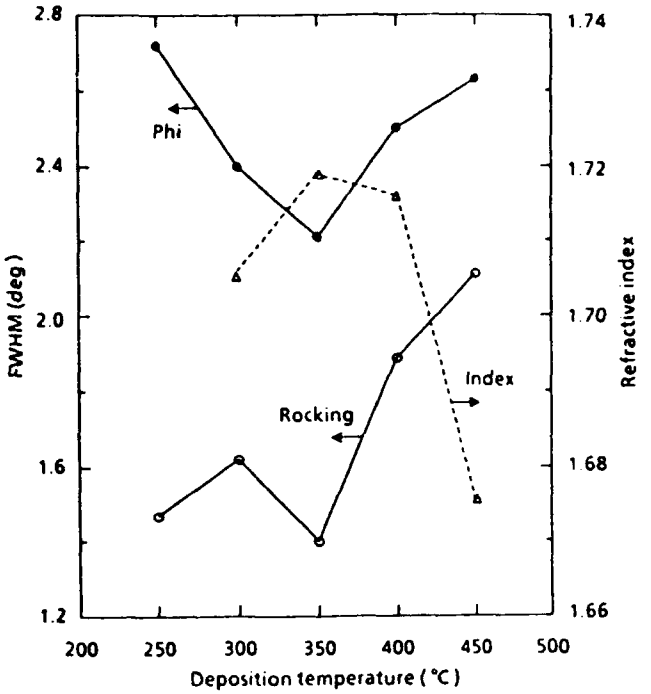

FIG. 3. X-ray diffraction data and refractive indices of MgO grown in 5×10^{-6} Torr O_2 as a function of deposition temperature.

The ϕ scan curve FWHMs for both $BaTiO_3$ and MgO were the smallest when the MgO film was grown at 350 °C. The ϕ resolution was 0.75° as measured on GaAs (202).

Refractive indices of MgO films measured by ellipsometry with a He-Ne laser also varied with O_2 pressure and substrate temperature like x-ray diffraction results as shown in Table I. Figure 3 shows x-ray diffraction data and refractive indices as a function of deposition temperature. The highest refractive index was 1.725 of the film deposited at 350 °C in 1×10^{-5} Torr O_2. This value is close to 1.735 of a single-crystal MgO,[18] indicating the MgO film is high density.

In conclusion, epitaxial growth of $BaTiO_3$ on GaAs by pulsed laser deposition was achieved by introducing epitaxial MgO buffer layers. MgO with the best crystallographic and optical quality was deposited around at 350 °C in 5×10^{-6} Torr O_2 using a Mg metal target. The epitaxial relationships are $BaTiO_3$ (001)|| MgO(001)|| GaAs(001) and $BaTiO_3$ [100]|| MgO[100]|| GaAs[100] in spite of a large lattice mismatch (25.5%) between MgO and GaAs. This is the first demonstration of a NaCl structure compound epitaxial to a zinc-blende structure material.

We thank Dr. G. A. N. Connell and Dr. J. B. Boyce for useful discussions and suggestions. M. Gidwani is acknowledged for technical assistant. This work is supported in part by AFOSR under Contract No. F49620-89-C-0017. D.K.F. is an AT&T scholar.

[1] H. Adachi, T. Kawaguchi, M. Kitabatake, and K. Wasa, Jpn. J. Appl. Phys. 22, Suppl. 22-2, 11 (1983).
[2] M. S. Ameen, T. M. Graettinger, S. H. Rou, H. N. Al-Shareef, K. D. Gifford, O. Auchiello, and A. I. Kingon, Mater. Res. Symp. Proc. 200, 65 (1990).
[3] M. G. Norton and C. B. Carter, J. Mater. Res. 5, 2762 (1990).
[4] R. Ramesh, K. Luther, B. Wikerns, D. L. Hart, E. Wang, and J. M. Tarascon, A. Inam, X. D. Wu, and T. Venkatesan, Appl. Phys. Lett. 57, 1505 (1990).
[5] M. de Keijser, G. J. Dormans, J. F. Cillessen, D. M. de Leeuw, and H. W. Zandbergen, Appl. Phys. Lett. 58, 2636 (1991).
[6] K. Nashimoto and M. J. Cima, Mater. Lett. 10, 348 (1991).
[7] J. Y. Tsao, T. M. Brennan, J. F. Klem, and B. E. Hammons, J. Vac. Sci. Technol. A 7, 2138 (1989).
[8] T. Kojima, N. J. Kawai, T. Nakagawa, and K. Ohta, Appl. Phys. Lett. 47, 286 (1985).
[9] M. Ishida, S. Tsuji, K. Kimura, H. Matsunaga, and T. Tanaka, J. Cryst. Growth 45, 393 (1978).
[10] M. Mikami, Y. Hokari, K. Egami, H. Tsuya, and M. Kanamori, *Extended Abstracts of the 15th Conference on Solid State Devices and Materials*, (Business Center for Academic Societies, Japan, Tokyo, 1983), p. 31.
[11] H. Fukumoto, T. Imura, and Y. Osaka, Jpn. J. Appl Phys 27, L1401 (1988).
[12] D. K. Fork, D. B. Fenner, G. A. N. Connell, J. M. Phillips, and T. H. Geballe, Appl. Phys. Lett. 57, 1137 (1990).
[13] T. Inoue, Y. Yamamoto, S. Koyama, S. Suzuki, and Y. Ueda, Appl. Phys. Lett. 56, 1332 (1990).
[14] D. K. Fork, F. A. Ponce, J. C. Tramontana, and T. H. Geballe, Appl. Phys. Lett. 58, 2294 (1991).
[15] S. Yadavalli, M. H. Yang, and C. P. Flynn, Phys. Rev. B 41, 7961 (1990).
[16] D. K. Fork, K. Nashimoto, and T. H. Geballe (unpublished).
[17] A. J. SpringThorpe and P. Mandeville, J. Vac. Sci. Technol. B 6, 754 (1988).
[18] K. Nunomura, A. Ishitani, T. Matsubara, and I. Hayashi, J. Cryst. Growth 45, 355 (1978).

Published without author corrections

G. W. Bailey, Editor, Proceedings of the 49th Annual Meeting of the Electron Microscopy Society of America
 Published by San Francisco Press, Inc., Box 6800, San Francisco, CA 94101-6800, USA

SEGREGATION IN Fe-SUBSTITUTED $YBa_2Cu_3O_7$ FILMS

F. A. Ponce, J. B. Boyce, F. Bridges and J. C. Tramontana

Xerox Palo Alto Research Center, Palo Alto, CA 94304

Understanding of the role played by the Cu(2)-O and the Cu(1)-O chains is crucial in the high T_c material $YBa_2Cu_3O_7$ (YBCO). One approach has been to substitute[1,2] other atoms such as Co, Fe, Ni and Zn for some of the Cu. A linear decrease in the T_c has been observed for several dopants, in particular for Fe substituted bulk samples[1], $T_c \rightarrow 0$ at 14-15%. Bulk sample studies show some variation in the amount of T_c suppression with concentration, possibly related to the method of materials preparation. The materials discussed here were prepared using the laser ablation technique[3,4]. Successive ablations from a series of targets was used in order to achieve in principle a mixing on an atomic scale as the components are deposited about an atomic layer at a time. An XeCl laser deposition system was used, equiped with a computer controlled rotating target holder enclosed in a water-cooled shroud. The holder, containing 10 targets, rotates at speeds up to 10 hz and the laser is fired each time a desired target is correctly oriented. Details on the deposition conditions are contained in reference 2. The targets were made of pressed fine powders of Cu-deficient YBCO, CuO and two mixtures of CuO and FeO-$(CuO)_{1-x}(FeO)_x$, with $x = 0.33$ and 0.67. The substrates were $LaAlO_3$ crystals, in the <100> orientation. Figure 1 shows the resitivity for several YBCO films substituted with various concentrations of Fe. Figure 2 shows the transition temperature Tc as a function of Fe concentration, and the results are compared between our thin films and results obtained elsewhere on bulk samples.

In order to understand the apparent discrepancy between the thin film and bulk materials shown in figure 2, we have studied the structure of the films with TEM. We report here on the structure of YBCO films with 17% concentration Fe. Figure 3 is a bright-field plane-view image of the film and some of the substrate. The image is characterized by (a) moire patterns, (b) circular precipitates, and (c) platelets along directions mutually perpendicular. The moire patterns are due to the interference of 200 reflections of film with substrate. The moire patterns occur with periods of 25nm, and using the lattice parameter of $LaAlO_3$ of 3.792Å, gives a lattice parameter for YBCO of 3.85Å which is consistent with those measured by x-ray diffraction and compares well with that of tetragonal YBCO (3.82,3.88,11.67). The circular precipitates produce moires which are consistent with cubic Y_2O_3, and are attributed to a Ba-defficient target. The platelet density increases with Fe concentration in the samples that we have studied. The platelets are oriented parallel to {100} YBCO planes, and produce streaks in the diffraction pattern as shown in figure 4. Lattice images, such as the one in figure 5, show that the platelets are coherent precipitates with good match in the direction parallel to the platelet, and a hexagonal-like structure in the normal direction. X-ray energy dispersive analysis of the platelets show a dramatically high density of Fe, an order of magnitude larger that the Fe in the YBCO matrix.

The results presented here show that Fe substituted for Cu in YBCO has a tendency to segregate with the production of Fe-rich precipitates. The apparent discrepancy between thin film and bulk data can therefore be explained in terms of effective solubilities of Fe for different materials preparation techniques.

References

1. J. M. Tarascon et al., Phys. Rev. 37, 7458 (1988).
2. F. Bridges et al., Mat. Res. Soc. Proc. 191, 159 (1990).
3. T. Venkatesan et al., Appl. Phys. Lett. 53, 243 (1988).
4. J. B. Boyce et al., SPIE 1187, 136 (1989).

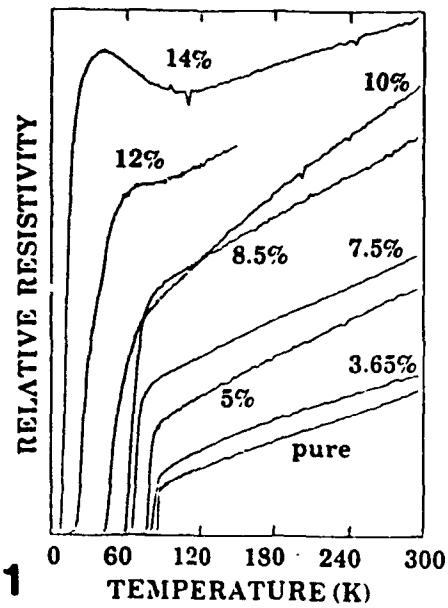

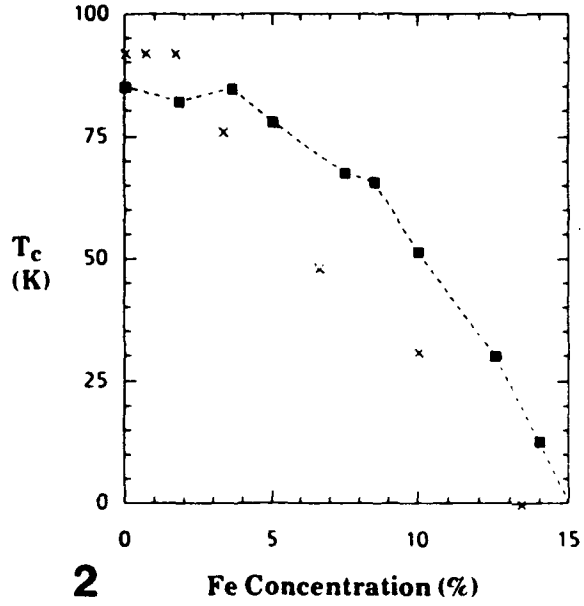

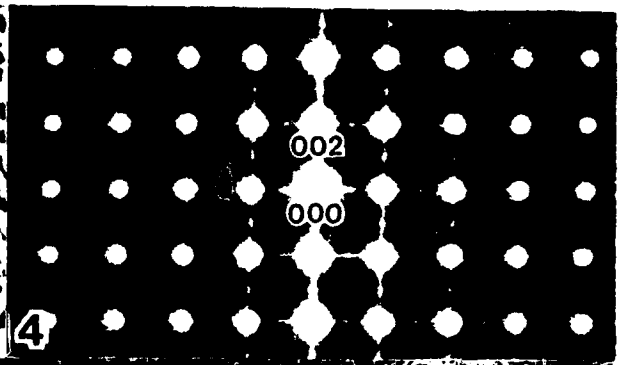

FIG. 1.--Relative resistivity vs. temperature for the Fe-substituted YBCO thin films grown on $LaAlO_3$ substrates[2] (The Fe concentration is with respect to Cu).
FIG. 2.--Midpoint transition temperature Tc as a function of the Fe concentration[2] (The crosses are the data on bulk samples from Tarascon, et al.[1]).
FIG. 3.--Bright-field micrograph of 17% Fe substituted film.
FIG. 4.--Selected area diffraction pattern of area shown in figure 2.
FIG. 5.--HRTEM of Fe-rich precipitate in YBCO film.

Ferroelectric bismuth titanate/superconductor (Y-Ba-Cu-O) thin-film heterostructures on silicon

R. Ramesh, A. Inam, B. Wilkens, W. K. Chan, T. Sands, and J. M. Tarascon
Bellcore, Red Bank, New Jersey 07701

D. K. Fork and T. H. Geballe
Stanford University, Stanford, California 94305

J. Evans and J. Bullington
Radiant Technologies, Albuquerque, New Mexico 87106

(Received 27 March 1991; accepted for publication 29 July 1991)

The growth by pulsed-laser deposition of *c*-axis-oriented bismuth titanate (BTO)/$YBa_2Cu_3O_7$(YBCO) superconductor heterostructures on [001]-oriented Si with epitaxial yttria-stabilized ZrO_2 as a buffer layer is reported. X-ray-diffraction studies of the heterostructures show that all the layers grow in the *c*-axis orientation, with a rocking angle of 1.0°–1.2° for the bismuth titanate layer and 0.6°–0.8° for the YBCO layer. Rutherford backscattering ion channeling yields of 28% at the surface have been obtained. Transmission electron microscopy of cross-sectioned samples reveal that the BTO layer has a significant density of translational boundaries that propagate at 45° to the film surface. The BTO film exhibits ferroelectric hysteresis and a dielectric constant in the range of 180–200.

There is presently a considerable amount of research being focused on the growth and device fabrication aspects of thin-film ferroelectrics for a variety of applications including nonvolatile memories, electro-optic switches, and detectors.[1–4] Earlier research in this area had been influenced by three problems. (i) Devices were fabricated from thick films and hence required very high switching voltages, thus making them incompatible with semiconductor device technology; (ii) the films are polycrystalline when grown on silicon with Pt or Al as the bottom electrode (these films may be susceptible to problems related to the granularity, i.e., chemical and charge segregation leading to aging, fatigue, time-dependent breakdown, etc.); (iii) maintaining proper stiochiometry in the ferroelectric film and congruence between the target and film composition. Sputtered lead zirconate titanate films (PZT), for example, are grown from targets enriched in Pb to compensate for Pb loss.

In a recent paper,[5] we reported preliminary results on the growth of epitaxial bismuth titanate (BTO/$Bi_2Sr_2CuO_{6+x}$ (2201) heterostructures on single-crystal [001]-oriented $SrTiO_3$, $LaAlO_3$, and yttria-stabilized ZrO_2 (YSZ) substrates. These *c*-axis-oriented films exhibit better crystalline quality compared to polycrystalline films. The 2201 layer is metallic at room temperature and is used as the bottom electrode. The BTO/2201 heterostructure is closely lattice matched (2201: $a = 5.4$ Å, $b = 5.41$ Å, $c = 24.6$ Å, and BTO: $a = 5.41$ Å, $b = 5.45$ Å, $c = 32.815$ Å) and the two layers have similar crystal chemistry, thus yielding a BTO film of good crystalline quality. These films exhibit ferroelectric hysteresis and a dielectric loss tangent of less than or equal to 0.02.

In general, growth of oxides such as $YBa_2Cu_3O_7$ directly on Si has proven to be difficult due to interfacial reaction at the growth temperature. This is further complicated by the large difference in thermal-expansion coefficients between YBCO and Si, leading to cracking upon cooling. Consequently, there has been a continuous search for suitable buffer layers that will provide both the chemical barrier and reduce the effect of thermal-expansion mismatch. $MgAl_2O_4$ and YSZ have both been shown to possess such properties. Growth of high-quality epitaxial Y-Ba-Cu-O (YBCO) films on YSZ/Si (Ref. 6) and $MgAl_2O_4/BaTiO_3$/Si (Ref. 7) has been demonstrated. In our research we are using YSZ/Si as the substrate to grow BTO/YBCO heterostructures.

Details of deposition of YSZ on Si are reported elsewhere.[6] The BTO/YBCO heterostructure is grown *in situ* using a 248-nm pulsed excimer laser which is directed at a rotating, sintered polycrystalline target of the required material and the resulting plume is caught on a heated substrate. The targets are mounted onto a four-target rotating carousel, thus enabling *in situ* deposition of the multilayered structure. The substrate heater is maintained at a temperature in the range of 650–820 °C. The substrate surface temperature is, in general, about 50 °C lower than the substrate heater temperature. The deposition is carried out in an oxygen pressure of 50–200 mTorr and the films are grown at the rate of 0.5–1.0 Å/s. After both the layers are deposited, the heterostructure is cooled in 200–600 Torr oxygen. The YBCO layer thickness is typically in the range of 1000–2000 Å while the BTO layer is generally 2000–10 000 Å thick.

Specifically, we present here results for a heterostructure in which the YBCO layer is ~2000 Å thick and the BTO layer is ~6000 Å thick. X-ray-diffraction studies show that only the *c*-axis orientation of both YBCO and BTO, in addition to the $(002)_{YSZ}$ and $(004)_{Si}$ peaks, are present as illustrated in Fig. 1. The ω rocking curve full width at half-maximum (FWHM) for the $(005)_{YBCO}$ peak

 0003-6951/91/391782-03$02.00

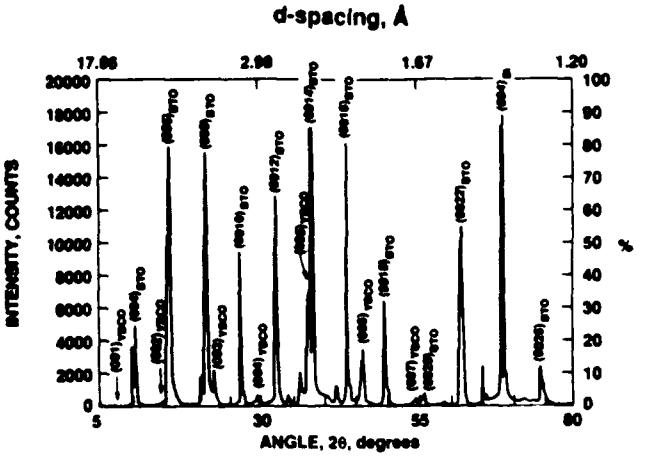

FIG. 1. X-ray-diffraction pattern from the BTO/YBCO heterostructure, grown on [001] Si with [001] YSZ as the buffer layer, showing the presence of only the 00*l* lines for BTO and YBCO along with those of YSZ and Si.

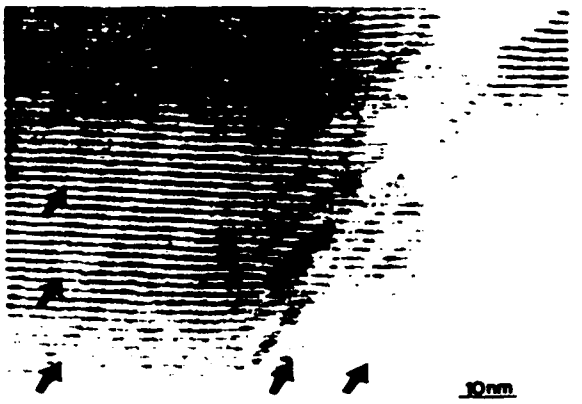

FIG. 3. High resolution electron microscope (HREM) image of the BTO film showing the presence of a large density of "translational boundaries." These boundaries are likely to be the cause for the progressive ion dechanneling in the film.

is in the range of 0.6°–1.0°. The corresponding value for the BTO layer is in the range of 0.8°–1.0°. These values for BTO compare quite favorably with the 0.7°–0.8° obtained for similar heterostructures grown on [001] $SrTiO_3$. As a comparison, bismuth titanate films grown under identical conditions, on Si with Pt as the bottom electrode, yield a rocking curve FWHM of 10°–12°, although they show some preferential alignment of the *c* axis.

Rutherford backscattering (RBS) spectra along the [001] and along random directions were obtained using 2.8-MeV He ions to characterize the crystalline quality along the [001] direction and the composition of the different layers. In Fig. 2 is shown the RBS spectrum, the corresponding best-fit simulation, and the ion channeling spectrum for the heterostructure described in the inset. Due to the large number of chemical species and the consequent overlapping peaks, compositional information is approximate and was independently confirmed by scanning electron microscopy x-ray microanalysis. The ion chaneling spectrum shows a minimum yield of 28% at the surface with evidence for dechanneling as the ions travel through the bismuth titanate film. Some possible reasons for this are found by examination of cross sections of the film by transmission electron microscopy (TEM).

Typically, TEM of the bismuth titanate films shows a large density of "translational boundaries" that propagate at 45° to the film surface, illustrated in Fig. 3. In contrast to the cuprate superconductors,[8] no polytypoidic stacking defects are observed. The large density of these boundaries coupled with their orientation in the film is likely to be the main reason for the progressive ion dechanneling into the film. We are at present carrying out a comprehensive study of the interface and defect structure in these heterostructures that will be reported in the future.

The ferroelectric properties of the films were probed using a pulsed measurement technique. An array of 200-μm^2 gold pads was evaporated onto the surface of the film using a TEM grid shadow mask. The films were probed as shown in the inset to Fig. 4. The pulsed-polarization test applies a series of five 2-ms triangular pulses to

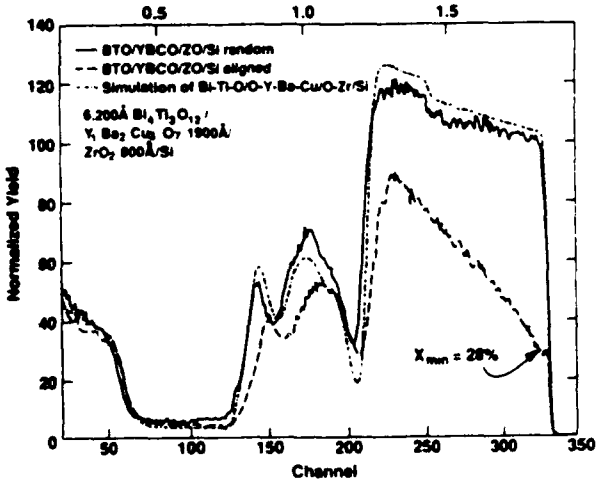

FIG. 2. RBS spectrum from the heterostructure showing ion channeling *minimum* yield of 28% at the surface, with progressive dechanneling into the film. The simulation shows reasonable fit with the nominal composition of the different layers which was independently confirmed by SEM x-ray microanalysis.

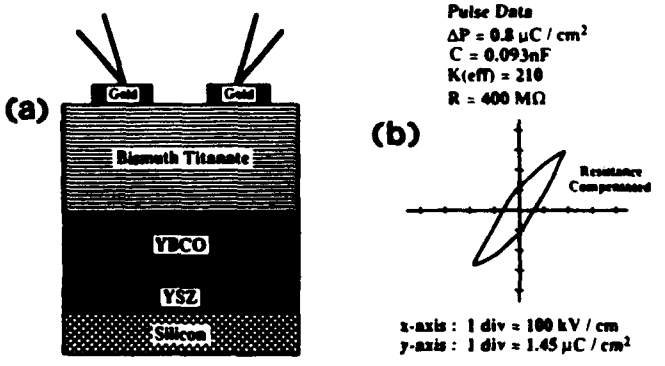

FIG. 4.(a) Schematic diagram of the electrical measurement procedure; (b) hysteresis loop along with pulsed measurement data for a 0.8-μm-thick film.

the sample with 100 ms delay between each pulse. The films exhibit a dielectric constant in the range of 180–200, which is commensurate with the *c*-axis value of 220. Figure 4 shows a hysteresis loop obtained at a maximum applied voltage of 9.5 V. The hysteretic remanence is in the range of 0.7–1.2 $\mu C/cm^2$ with a coercive field in the range of 50–60 kV/cm. As shown in the data in Fig. 4(b), the remanence ΔP in the pulsed measurement is 0.8 $\mu C/cm^2$. The difference in remanence between the hysteresis and the pulse measurement indicates some leakage. The resistivity of the films is in the range of 10^8–10^{10} Ω cm (depending on the voltage). For comparison, bismuth titanate films grown on Si (with a Pt bottom electrode), show a resistivity in the range of 10^{11}–10^{12} Ω cm. The exact reasons for the lower values in these heterostructures is not clear at the moment. We speculate that this may be related to the structural and chemical nature of the electrode/film interfaces. This is currently under investigation.

In summary, we have demonstrated the growth of YBCO/bismuth titanate heterostructures on Si using a YSZ-grown buffer layer. All the oxide layers can potentially be grown *in situ* without breaking the vacuum. These heterostructures are structurally preferable to those grown on Si(Pt). It is also demonstrated that the cuprate superconductors can be used as metallic bottom electrodes. However, considerable further work needs to be done to improve the ferroelectric performance and to understand the role of the defect microstructure, structural interfaces, and processing conditions on the ferroelectric properties.

We wish to acknowledge the support and encouragement of V. G. Keramidas and P. L. Key. The support of Professor G. Thomas and the staff of the National Center for Electron Microscopy, Lawrence Berkeley Laboratory, is greatly appreciated.

[1] J. F. Scott and C. A. Paz de Araujo, Science, 246, 1400 (1989); M. Sayer and K. Sreenivas, Science, 247, 1056 (1990).
[2] A. F. Tasch, Jr., and L. H. Parker, Proc. IEEE 77, 374 (1989); L. H. Parker and A. F. Tasch, Jr., IEEE Circuits and Devices CD-6, 17 (1990).
[3] G. H. Haertling and C. E. Land, J. Ceram. Soc. 54, 1 (1971).
[4] S. Y. Wu, W. J. Takei, and M. H. Francombe, Ferroelectrics 10, 209 (1976).
[5] R. Ramesh, A. Inam, W. K. Chan, B. Bilkens, K. Myers, K. Remschnig, D. L. Hart, and J. M. Tarascon, Science 252, 944 (1991).
[6] D. K. Fork, D. B. Fenner, R. W. Barton, J. M. Phillips, G. A. N. Connell, J. B. Boyce, and T. H. Geballe, Appl. Phys. Lett. 57, 1161 (1990).
[7] X. D. Wu, A. Inam, M. S. Hedge, B. Wilkens, C. C. Chang, D. M. Hwang, L. Nazar, T. Venkatesan, S. Miura, S. Matsubara, Y. Miyasaka, and N. Shohata, Appl. Phys. Lett. 54, 754 (1989).
[8] R. Ramesh, D. M. Hwang, T. Venkatesan, T. S. Ravi, L. Nazar, A. Inam, X. D. Wu, B. Dutta, G. Thomas, A. F. Marshall, and T. H. Geballe, Science 247, 57 (1990).

Fatigue and Aging of Ferroelectric YBCO/PZT/YBCO Heterostructures

R.Ramesh, W.K.Chan, B.Wilkens, T.Sands J.M.Tarascon and V.G.Keramidas
Bellcore, Red Bank, NJ 07701.
D.K.Fork
Xerox Palo Alto Research Center ← cap
Palo Alto, CA 94305.
J.J.Lee and A.Safari
Rutgers University
Piscataway, NJ 08754.

spell out acronym

We report results of fatigue and aging studies on PZT thin films grown with Y-Ba-Cu-O(YBCO) thin film top and bottom electrodes. Such heterostructures have been grown in-situ on yttria-stabilized ZrO_2 buffered [100] Si as well as on [001] $LaAlO_3$ by pulsed laser deposition. Both the a-axis and c-axis orientations of the YBCO lattice have been grown using suitable changes in growth conditions. These symmetrical capacitor structures show very good fatigue and aging characteristics, which are much superior to those with Pt top electrodes.

Nice paper Ramesh. Aside from some structural changes and the need for references the paper should go out soon. The cause for the effect is damned elusive. Depletion layers, Schottky barriers, interdiffusion, ... could be playing a role. It will be interesting to learn what the SIMS tells us.

- Dave

In the past few years there has been a strong resurgence of research and development in the area of ferroelectric materials. Specifically, sub-micron thick films are being grown by a variety of techniques for potential use as non-volatile, random access memories integrated with existing CMOS transistor circuitry. Conventionally the ferroelectric thin films, such as lead zirconate titanate (PZT), are deposited onto Pt coated Si wafers with Pt metal being the top contact electrode to form the capacitor structure. A variety of techniques including sol-gel spin-on, sputtering, chemical vapor deposition, and pulsed laser deposition are being used to deposit the thin films.

In an earlier paper, we reported the growth of Y-Ba-Cu-O(YBCO) / Pb-Zr-Ti-O(PZT) heterostructures on single crystalline $LaAlO_3$ substrates. These heterostructures showed ferroelectric and dielectric properties that were very desirable for non-volatile memory applications. In such structures, the metallic properties of the YBCO bottom layer at room temperatures was used in conjunction with Pt/Au top electrodes to form the test capacitors for ferroelectric measurements. Subsequent studies of the fatigue and aging characteristics showed that the remnant polarization, ΔP (ΔP = switched polarization - non-switched polarization, both measured at the bottom of the applied pulse) dropped to 50% of the initial value after about 10^8-10^9 bipolar cycles, which is insufficient for the types of applications envisioned. Although the exact reasons for this drop is still unclear, it appears to be related to an internal field, which is generated due to differences between the two electrodes and the ferroelectric. In order to be useable as memories, these capacitors have to be integrated with appropriate CMOS drive circuitry. In this letter, we report results of the first stage of this process in which we have grown such heterostructures on yttria-stabilized ZrO2 buffered [100] Si. The use of a YBCO top electrode has dramatically improved the fatigue and aging characteristics of the PZT layer.

The YBCO/PZT/YBCO heterostructures are grown in-situ pulsed laser deposition onto YSZ-buffered Si and [100] $LaAlO_3$. The details of the deposition conditions for the YSZ buffer layer on Si and subsequent growth of the YBCO/PZT heterostructures are described in earlier papers. We have grown both c-axis and a-axis oriented YBCO top and bottom electrodes through appropriate changes in the substrate temperature. For example, we describe here results from heterostructures in which both the top and bottom YBCO layers were a-axis oriented and grown on buffered Si. The heterostructures were characterized structurally and chemically using x-ray diffraction and Rutherford Backscattering(RBS) analyses. RBS studies were used to ensure that the three layers were of the required composition. 100μm diameter capacitors were defined by photolithography and finally Ag/Au contacts were

YBCO/PZT/YBCO/YSZ/Si(100)

---

footnote is best of (...)? Also, use consistant symbols, ie ΔP or ∂P but not both.

give citations.

your designation for thin film layers seems to flip forwards and backwards. Compare in fig. 3 - "Pt/PZT/YBCO" and throughout paper. Try to adopt a consistent formulation like

evaporated on top; the test structure is schematically illustrated in Fig.1(a). The bottom electrode is contacted through capacitive coupling using an electrode pad that is much larger (>100 times) than the test capacitor. The ferroelectric properties were evaluated using a pulsed testing system (Radiant Technologies, RT66A) in conjunction with an external pulse generator. The pulse trains used to measure the polarization and fatigue characteristics are shown in the insets to Figs.1(b)&2. In the fatigue experiments, frequencies up to 40kHz, 8.6μsec wide pulses were generated using the RT66A hardware, which is illustrated in the inset to Fig.2(a). For high frequency testing, an external pulse generator was used in conjunction with the RT66A system. The capacitors were fatigued for a specific number of cycles, after which they were automatically tested for the switched and non-switched polarization values using the same pulse train shown in Fig.1(b).

X-ray diffraction scans showed that the YBCO layers were essentially a-axis oriented while the PZT layer was c-axis oriented. Fig.1(b) shows a pulsed hysteresis loop from one test capacitor. The inset to this figure also shows the pulse train that is used to measure the pulsed polarization values. The film resistivities are typically in the range of $5x10^8$ - $5x10^9$ Ω.cm. There are two important differences between the capacitors with YBCO top electrode and Pt top electrode. Firstly, the switched polarization in this case is much smaller than when the top electrode is Pt. Secondly, the coercive voltage is also much smaller (1-1.5V) than with the Pt top electrode(2.2-2.7V). We speculate that the reduction in switched polarization is due to the clamping effect of the top electrode as the ferroelectric film is cooled down through the phase transition, while the lower coercive voltage is primarily due to the type of contact at the interface. The exact reasons are still unclear, but this may be due to the difference in work functions between PZT and the electrodes leading to differences in contact behaviour (i.e., Pt electrode forms a Schottky barrier while the YBCO electrode forms an ohmic contact).

The capacitors were then fatigued with square, bipolar pulses at various frequencies to study their fatigue characteristics. Fig.2 shows normalized remnant polarization, ∂P (∂P= switched polarization - nonswitched polarization) for the two cases, viz., YBCO and Pt top electrodes. In the case of the Pt top electrode, the remnant polarization is relatively unchanged up to about 10^7 cycles, after which there is a sharp drop to 50% of the initial polarization in 10^8-10^9 cycles. In the case of the YBCO electrode, the remnant polarization does not change significantly. Similar experiments were carried out at a cycling frequency of 1MHz up to 10^{12} cycles, the results of which are shown in Fig.3. The capacitor with YBCO top electrode shows a 8-10% decay of remnant polarization after 10^{12} cycles, while the capacitor

with Pt electrodes shows about 90% decay after the same number of cycles. We have also found that the loss of switched remnant polarization due to fatigue can be "rejuvenated" by pulse poling, the details of which are presented in a separate paper. Similar improvements in fatigue behaviour have been observed by several groups using other metallic oxides such as RuO2 and La.5Sr.5CoO3, thus pointing to a common cause, i.e., the electronic properties of the electrode-ferroelectric interface.

Give citations. ↳

In order to confirm that the capacitors can still retain a logic state (either "1" or "0") after cycling, we have also carried out retention experiments on capacitors in the same array after fatiguing to 10^{12} cycles at 6V. The retention test was carried out by using a -6V write voltage (pulse width of 8.6μsec) and reading with either 5V(for the logic state "1") and -5V(for the logic state "0"). In both cases, the read voltage pulse width was 2msec. The pulse polarization was measured both at the top of the pulse (saturation value) as well as at the bottom of the pulse (remnant). The results are shown in Fig.4. Clearly, the difference between the two logic states (corresponding to P^* and $P^\wedge$) is sufficiently large (~5μC/cm^2) even after cycling to 10^{12} cycles. More importantly, this difference does not decrease after 10^5 seconds of retention. We are presently continuing this experiment to longer times as well as at higher temperatures, the results of which will be reported in subsequent publications.

In conclusion, it has been demonstrated that the use of symmetric conducting oxide electrode such as the cuprate superconductors can dramatically alleviate the problem of fatigue in ferroelectric capacitors. These preliminary results look promising for further studies and subsequent integration into non-volatile memory structures. The exact roles of crystalline quality and epitaxy on the ferroelectric properties are still unresolved questions. The results so far indicate that as far as fatigue is concerned, the primary issue is the nature of the electrode-film interface. We wish to acknowledge many stimulating discussions with J.T.Evans(Radiant Technologies).

plural →

You might be able to slip this in by the time the paper is ready or accepted.

FIGURE CAP... ...S

Figure 1: (a) A schematic illustration of the capacitor test structure used to evaluate the ferroelectric properties, in which the bottom electrode is capacitively coupled using a very large top electrode; (b) a typical pulsed hysteresis loop obtained from the YBCO/PZT/YBCO heterostructure. The inset to this image shows the pulse train used to measure the pulsed polarization values.

Figure 2: A plot of remnant polarization ∂P(∂P=switched remnant polarization - nonswitched remnant polarization) versus fatigue ccycles at 5V and 40kHz for the YBCO/PZT/YBCO capacitor, compared with a Pt/PZT/YBCO capacitor. The inset shows the pulse train used for this test.

Figure 3: ∂P versus fatigue cycles at 1MHz and 5V showing that the YBCO/PZT/YBCO capacitor structure shows very little fatigue upto 10^{12} cycles.

Figure 4: A plot of remnant polarization, both at the top and at the bottom of the read pulse for the two logic states after fatiguing for 10^{12} cycles at 5V. The write voltage is -5V and the read voltage is either -4V (for logic state "0") and 4V(for logic state "1"). The capacitor shows sufficient distinction (~5μC/cm2) between these two states.

In Fig. 4, I think you need to make it a little more clear which data is saturation and which is remanant. It is obvious once you think about it though. The r subscript is not actually delineated anywhere in the paper.

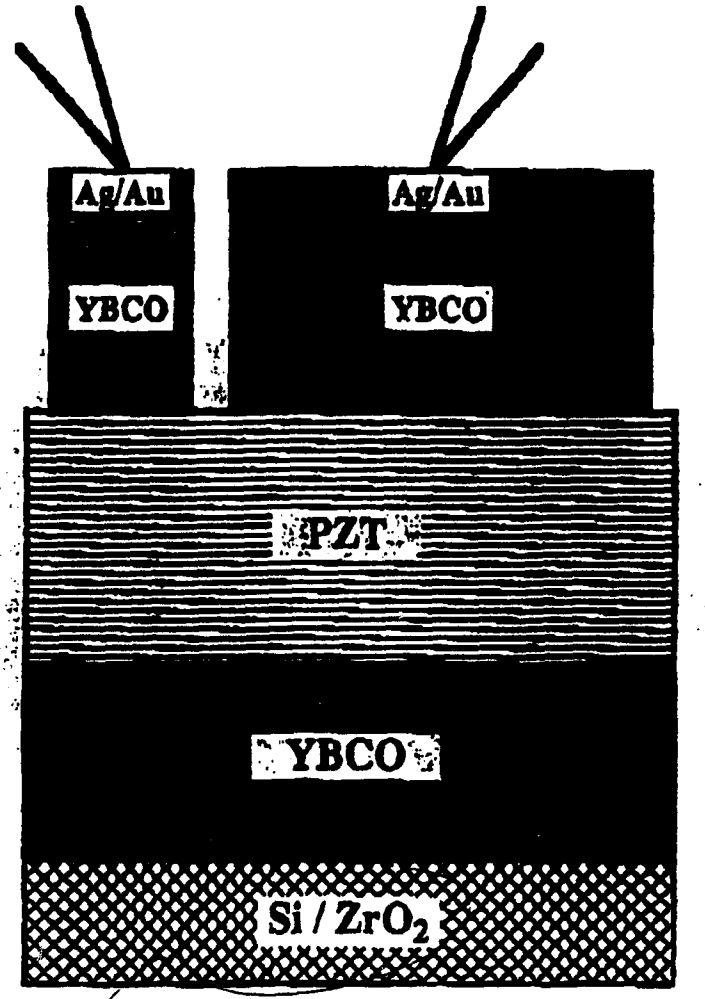

Virtual Ground Mode
or Sawyer-Tower Mode

This convention could signify "silicon grown on YSZ substrate" instead of YSZ grown on Silicon

Fig. 1(a)

Effect of top electrode on Fatigue performance
5V ; 40kHz

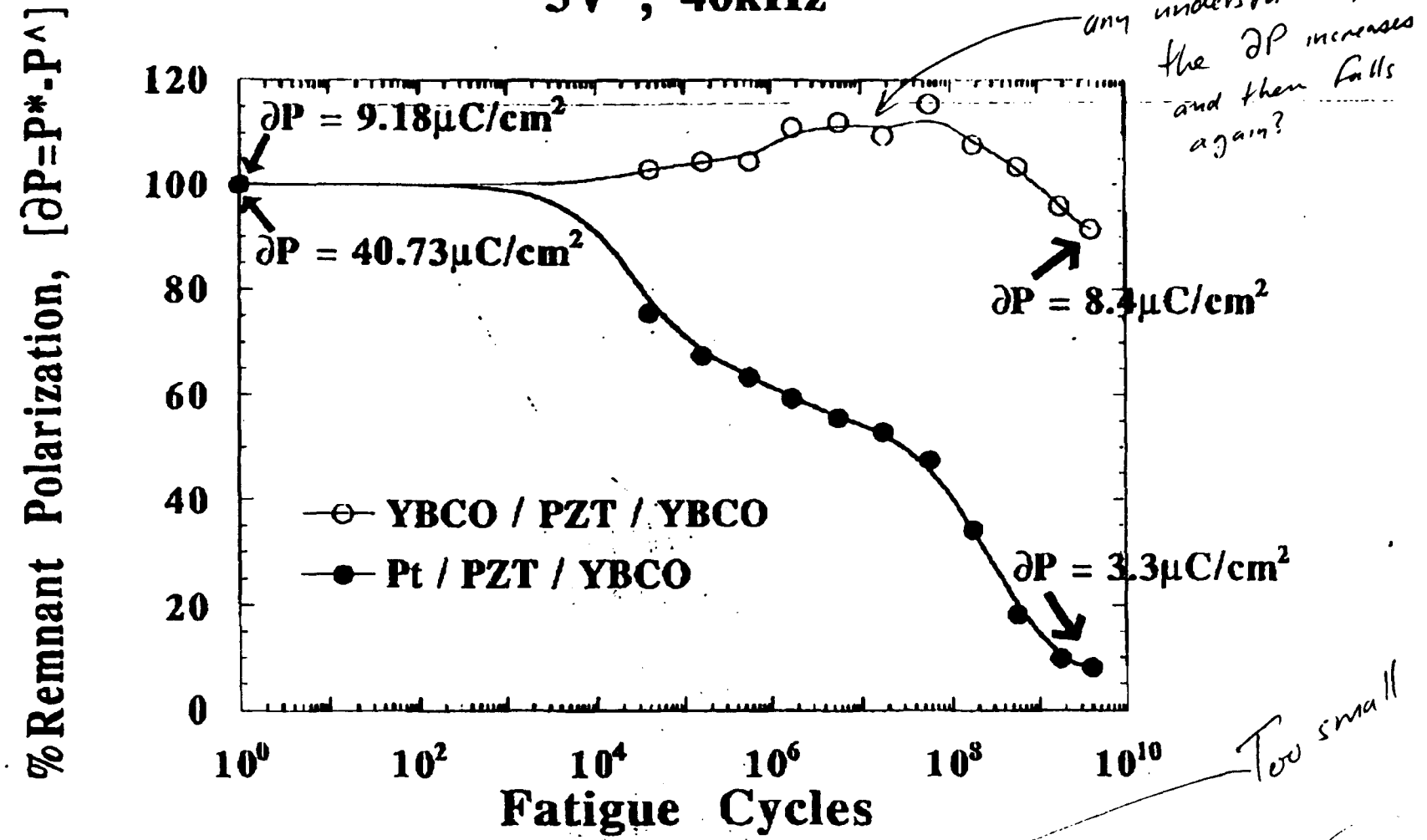

Too small

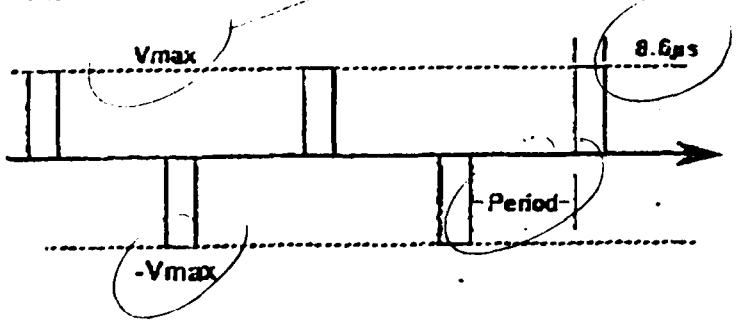

Fig. 2

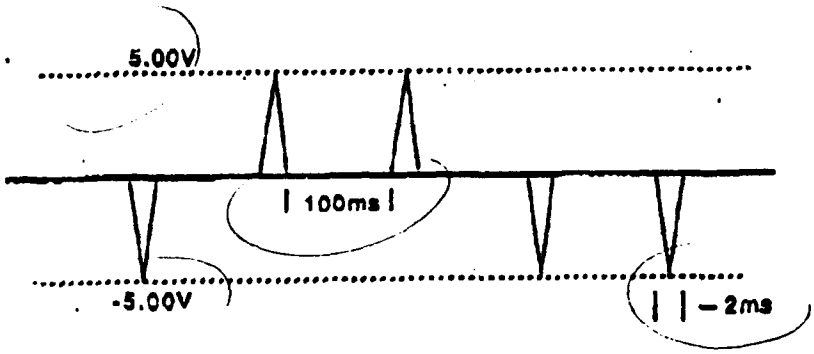

These character are too small to survive the reduction in the final figure. See the APS style manual.

Pulsed Hysteresis

PZT
Resistance
Compensated

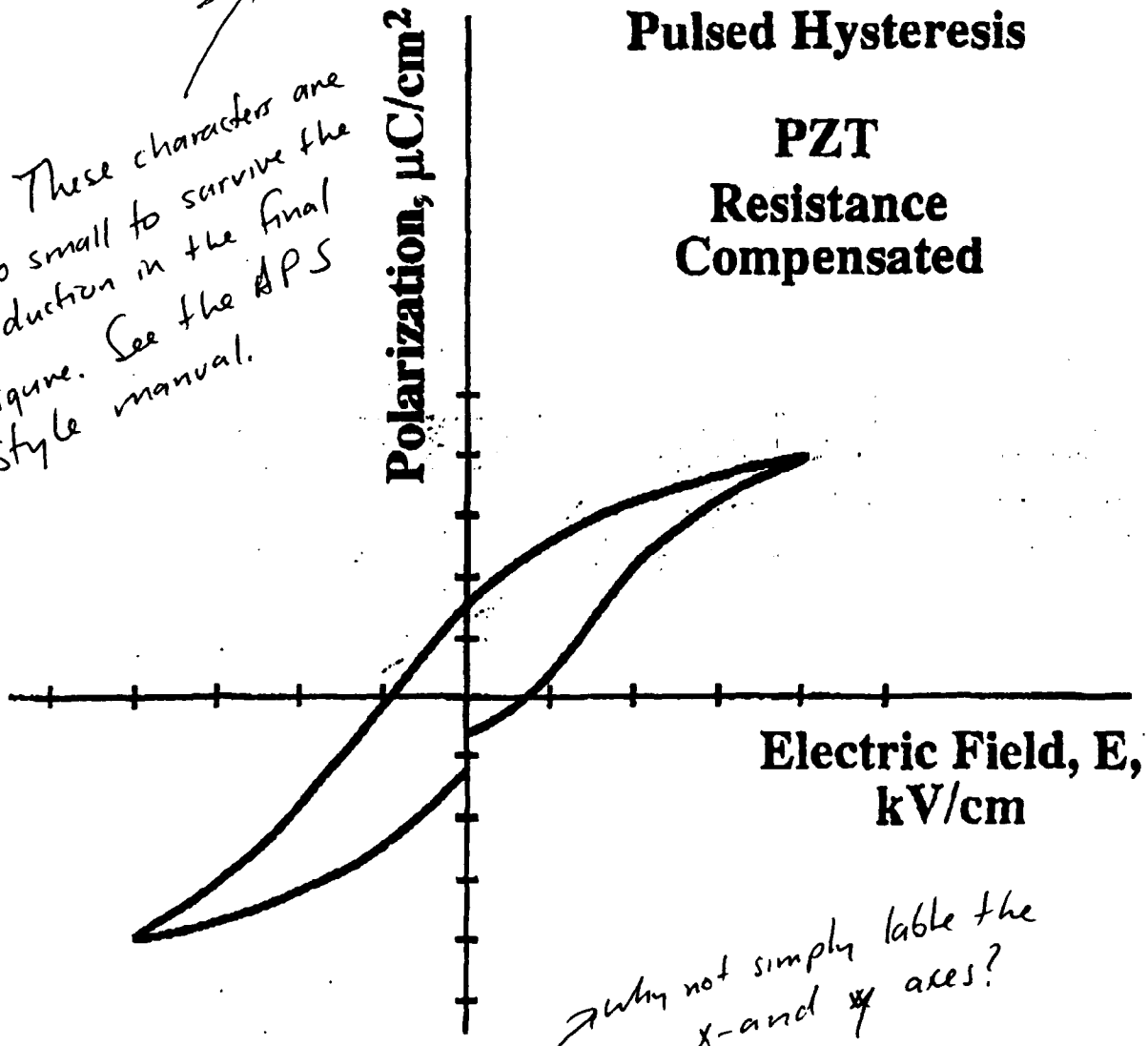

why not simply lable the x- and y- axes?

x-axis : Electric Field : 1 div = 50 kV / cm
y-axis : Polarization : 1 div = 6.8 μC / cm²

Fig. 1(b)

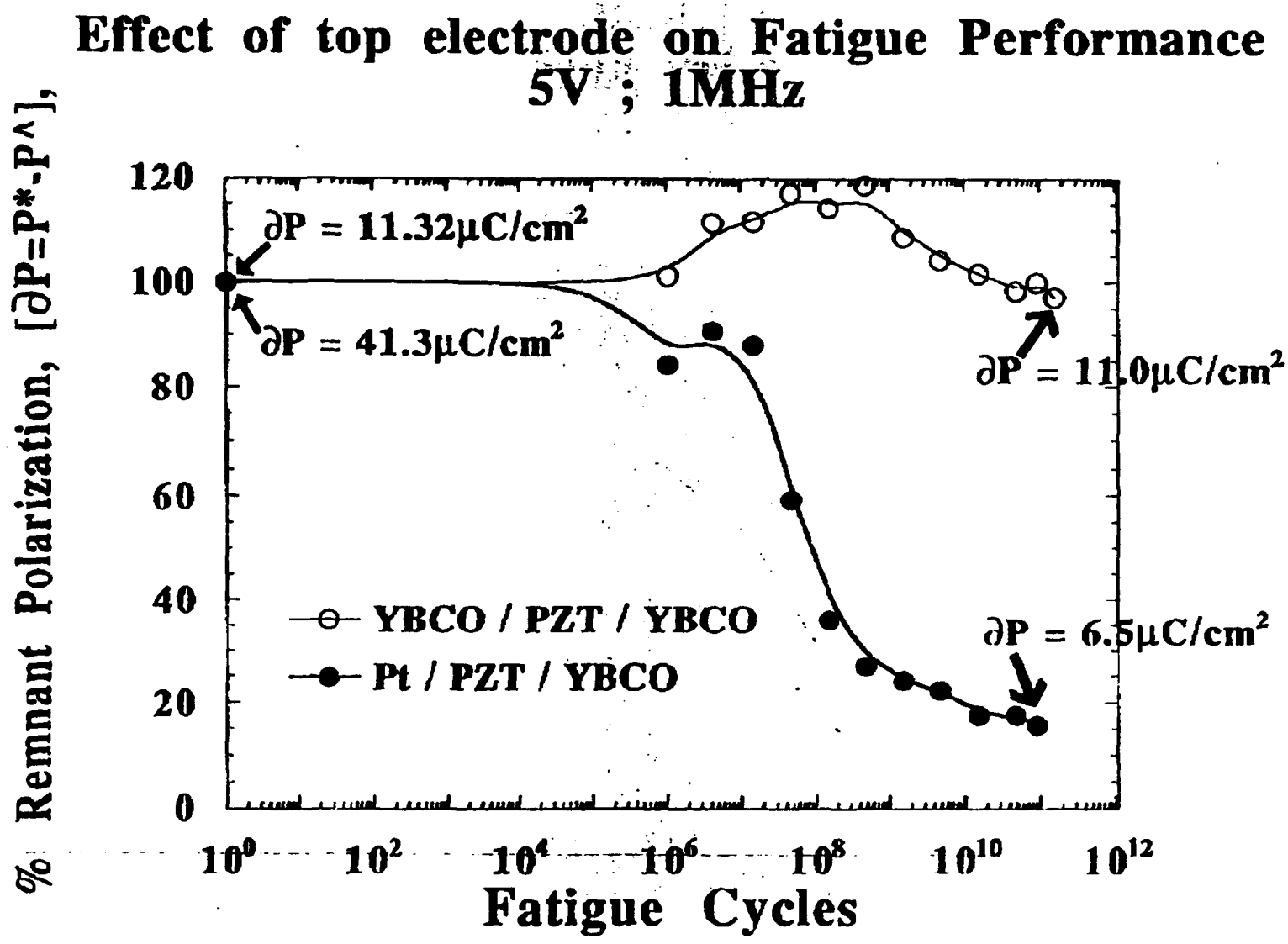
Effect of top electrode on Fatigue Performance
5V ; 1MHz
% Remnant Polarization, [∂P=P*-P^],
120
100
80
60
40
20
0
∂P = 11.32μC/cm²
∂P = 41.3μC/cm²
∂P = 11.0μC/cm²
∂P = 6.5μC/cm²
YBCO / PZT / YBCO
Pt / PZT / YBCO
10⁰
10²
10⁴
10⁶
10⁸
10¹⁰
10¹²
Fatigue Cycles

Fig 3

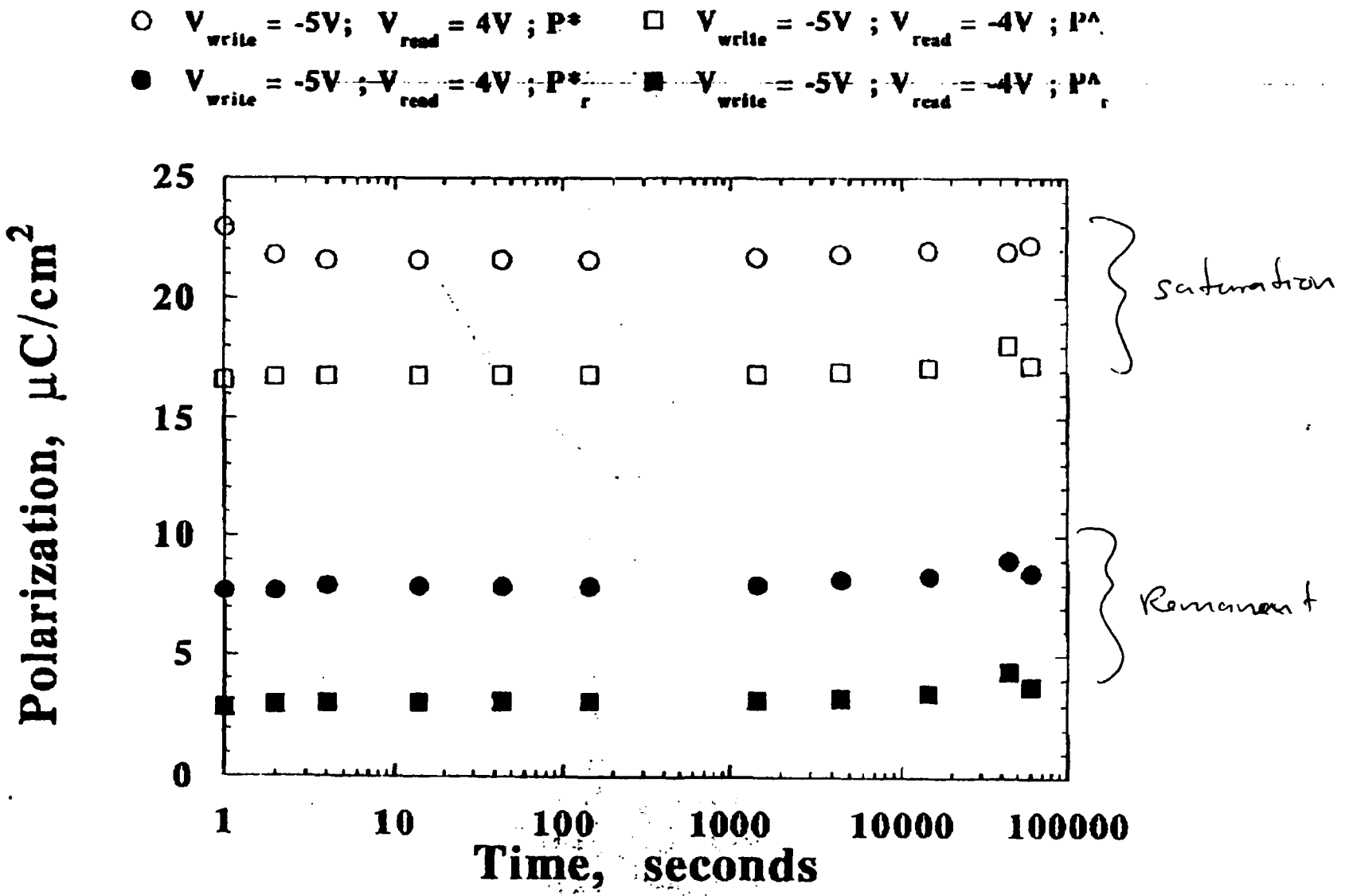
○ V_{write} = -5V; V_{read} = 4V ; P*
□ V_{write} = -5V ; V_{read} = -4V ; P^
● V_{write} = -5V ; V_{read} = 4V ; P^*_r
■ V_{write} = -5V ; V_{read} = -4V ; $P^_r$
Polarization, μC/cm²
25
20
15
10
5
0
1
10
100
1000
10000
100000
Time, seconds
saturation
Remanent

Fig. 4

Feasibility of infrared imaging arrays using high-T_c superconducting bolometers

S. Verghese and P. L. Richards
Department of Physics, University of California and Materials Sciences Division, Lawrence Berkeley Laboratory, Berkeley, California 94720

K. Char
Conductus Inc., Sunnyvale, California 94086

D. K. Fork
Xerox Palo Alto Research Center, Palo Alto, California 94304, and Department of Applied Physics, Stanford University, Stanford, California 94305

T. H. Geballe
Department of Applied Physics, Stanford University, Stanford, California 94305

(Received 21 October 1991; accepted for publication 27 November 1991)

The design of high-T_c superconducting bolometers for applications such as infrared imaging arrays is discussed. The dependence of bolometer sensitivity on excess voltage noise in the thermometer is a function of the detector area and thus of the wavelength to be detected. Measurements of the voltage noise in thin films of $YBa_2Cu_3O_{7-\delta}$ on Si, Si_3N_4, and sapphire substrates are used to predict the performance of different bolometer architectures. Useful opportunities exist for bolometers made on both Si and Si_3N_4 membranes. A readout scheme for two-dimensional arrays of bolometers is also described in which real-time signal integration is performed on the chip.

I. INTRODUCTION

Much recent work has focused on the high-T_c superconducting bolometer as an infrared detector.[1-9] Such bolometers consist of an infrared radiation absorber thermally coupled to a high-T_c superconducting thermometer operated at its resistive transition, both weakly coupled to a liquid-nitrogen-cooled heat sink at 77 K. For the purposes of this paper we consider only relatively sensitive slow composite bolometers that absorb radiation directly and are constructed on thin substrates that are thermally isolated from the heat sink. We will not consider the fast bolometers obtained when a high-T_c film is deposited directly on a bulk substrate[10-13] or the antenna-coupled microbolometer.[14,15]

For wavelengths $\lambda < 20\ \mu$m, photovoltaic infrared detectors such as HgCdTe give excellent performance at 77 K. For wavelengths $\lambda > 20\ \mu$m, the sensitivity of semiconducting detectors at or above 77 K is poor and room-temperature thermal detectors such as the pyroelectric detector, the thermopile, or the Golay cell are used in applications where a liquid-nitrogen-cooled high-T_c bolometer could be conveniently used. The high-T_c bolometer offers higher sensitivity under these conditions, primarily because of the sensitivity with which small changes in the temperature of the bolometer can be detected. Applications for composite high-T_c bolometers exist in far-infrared laboratory spectroscopy[9] and space observations of bright sources such as planets[5,6] using radiatively cooled systems. Applications as large format infrared imagers may also exist.

Some of us have recently built composite high-T_c bolometers cooled by liquid nitrogen with $D^* > 4\times10^9$ cm $Hz^{1/2}$ W^{-1}.[8,9] The areas of these bolometers were chosen from 1 to 10 mm^2 to match the throughput of laboratory Fourier transform spectrometers. For such large areas, there are stringent requirements on thermometer sensitivity which require the use of high-quality epitaxial c-axis $YBa_2Cu_3O_{7-\delta}$ (YBCO) films on favorable substrates with sharp resistive transitions and low voltage noise under current bias. Arrays of much smaller bolometers are potentially useful for thermal imaging. The absorbing area A can be as small as the diffraction limit $A = \lambda^2/\Omega$, where Ω is the solid angle of the pixel's field of view. The lower heat capacity of such small bolometers relaxes the requirement on thermometer sensitivity. The possibility then exists that YBCO on amorphous substrates like silicon nitride (Si_3N_4) could be used. Researchers at Honeywell are working on linear arrays of micromachined bolometers on substrates of Si_3N_4 membranes for thermal imaging at 10 μm.[16]

This paper describes the dependence of bolometer design on area. The discussion is directly relevant to the design of imaging arrays of high-T_c bolometers for wavelengths from 10 to 1000 μm. The required thermometer sensitivity for various areas will be compared with the voltage noise V_N measured for current-biased YBCO films on various substrates. We will also discuss a scheme for reading out two-dimensional bolometer arrays that performs real-time signal integration on the chip.

II. THEORY

The voltage responsivity for a signal modulated at angular frequency ω can be written as

$$S(\omega) = \frac{IR}{G\Delta T(1+\omega^2\tau^2)^{1/2}}, \tag{1}$$

 0021-8979/92/062491-08$04.00

where I is the bias current, G is the thermal conductance to the heat sink, and τ is the thermal time constant. The temperature coefficient of resistance $dR(T)/dT = R/\Delta T$ has been written in terms of half the width ΔT of the superconducting transition, and the resistance R at the operating point near the midpoint of the transition.[1] We neglect the effects of the positive thermal feedback from the bias current I which reduces the thermal conductance to an effective value $G - I^2R/\Delta T$. To maintain thermal stability we constrain the current by the condition

$$I^2R < 0.3G\Delta T. \tag{2}$$

The noise equivalent power (NEP) is calculated by summing the important sources of statistically uncorrelated noise in quadrature,

$$\mathrm{NEP} = \left(4kT_c^2G + \frac{4kT_cR}{|S|^2} + \frac{V_N^2}{|S|^2} + \frac{e_n^2 + (i_nR)^2}{|S|^2}\right)^{1/2}. \tag{3}$$

The first term, phonon noise, in Eq. (3) is an important limit on the sensitivity of the bolometer. The last three terms, Johnson noise, excess film noise, and amplifier noise, respectively, are voltage noise contributions to the NEP from the temperature read-out. In the ideal case, the responsivity S is large enough to make these terms less than or equal to the phonon noise. If these terms can be made very much less than the phonon noise for $\omega\tau \simeq 1$, then the NEP can be further reduced by operating the bolometer with reduced G and $\omega\tau > 1$. The minimum heat capacity C of a practical bolometer with a given area is limited by materials and fabrication considerations. The thermal conductance G to the heat sink can be limited by the permissible temperature rise under the background power loading P, or by the required response time $\tau = C/G$, or by materials or fabrication considerations.

Our own measurements on YBCO films and those of others[17,18] indicate that the excess voltage noise in current-biased films depends sensitively on film quality. It can be modeled as resistance fluctuations, $V_N^2 = (I\delta R)^2$, where $[\delta(\ln R)]^2$ usually has a frequency dependence between ω^{-1} and ω^{-2}, and scales roughly as the reciprocal of the film volume.[19] A resistance fluctuation δR can be written as a temperature fluctuation by using the slope of the resistive transition $\delta T = \delta(\ln R)\Delta T$. The noise equivalent temperature, $\mathrm{NET} = \delta(\ln R)\Delta T$, is introduced as a convenient figure of merit for YBCO transition-edge thermometers. The NET is the minimum temperature difference that can be measured in approximately 1 s of integration time. The thermometer contribution to the NEP can then be written as

$$\begin{aligned}\mathrm{NEP}_T &= \delta(\ln R)\Delta T G(1 + \omega^2\tau^2)^{1/2} \\ &= \mathrm{NET}\, G(1 + \omega^2\tau^2)^{1/2}.\end{aligned} \tag{4}$$

The film noise will dominate other contributions to the readout noise if the bias current is large enough that

$$I\delta R > [4kT_cR + e_n^2 + (i_nR)^2]^{1/2}. \tag{5}$$

As will be discussed below, this condition can be met for all of the YBCO films we have measured to date without exceeding the constraint (2) set by bias heating.

Phenomena such as thermopower, Bi film resistance, gas expansion, and dielectric constant changes have been used as thermometers for thermal far-infrared detectors operating above 77 K.[20–25] For applications with frequencies less than 100 Hz, the best NET of these technologies is in the range of 10^{-6} K/Hz$^{1/2}$. If these thermometer technologies are restricted to thin films useful for large micromachined arrays,[22–26] such as bismuch films, the NET is $> 10^{-5}$ K/Hz$^{1/2}$. High-T_c thin-film thermometers promise values of NET $< 10^{-8}$ K/Hz$^{1/2}$, and hence orders of magnitude increase in detector sensitivity.

For a given optical system, the area of a pixel which couples optically to n spatial modes is proportional to the wavelength squared $A = \lambda^2 n/\Omega$. Many considerations enter the choice of the constant of proportionality n/Ω. The optical filling factor is the ratio of the area of the infrared absorber to the area of the unit cell for a single pixel (which may include other components such as charge-storage capacitors or readout circuitry). For $\lambda = 10$ μm, an acceptable filling factor of (50%–60%) can be achieved[26] with $A/\lambda^2 \simeq 50$. Diffraction-limited pixels ($n = 1$) with $f/6$ optics ($\Omega = 0.02$ sr) and $A = 5 \times 10^{-5}$ cm^2 are useful at 10 μm for applications requiring high spatial resolution. Multimode pixels ($n = 10$) with $f/2$ optics ($\Omega = 0.2$ sr) are useful at 10 μm for applications requiring high sensitivity when detector noise limited. The specific detectivity $D^* = A^{1/2}/\mathrm{NEP}$ is convenient for comparing detectors with different areas. We will use these concepts to discuss the sensitivity of imaging arrays of high-T_c bolometers as a function of thermometer NET, bolometer area, and wavelength.

III. FILM PROPERTIES

Fabrication of useful high-T_c composite bolometers requires films on very thin substrates to minimize heat capacity. We have chosen to study films on sapphire, silicon, and silicon nitride substrates which are strong enough to be made thin. Table I summarizes the properties of four YBCO films that were deposited by laser ablation at Conductus and Xerox. These are representative of the best performance that has been obtained to date. Samples A and B were epitaxial c-axis films deposited on crystalline substrates with buffer layers. Sample A was made *in situ* by depositing a 20-nm-thick buffer layer of $SrTiO_3$ on $\{1\bar{1}02\}$ sapphire followed by 300 nm of epitaxial c-axis YBCO.[27] After breaking vacuum, silver contact pads were sputter deposited through a shadow mask and annealed in oxygen at 500 °C for 60 min. Sample B was made using a silicon substrate. A process was specifically developed to provide a pristine Si surface for epitaxial growth.[28,29] First, a weak HF and ethanol solution was used to strip the native SiO_2 layer and to terminate the exposed silicon bonds with hydrogen. Then the Si substrate was transferred to the deposition system via a nitrogen gas-purged glove box and load lock. The substrate was heated in vacuum to drive off the hydrogen and 40 nm of YBCO was deposited *in situ* on

TABLE I. Characteristics of YBCO films measured for use as thermometers on high-T_c bolometers.

Sample	Source	Geometry	$\left(\frac{1}{R}\frac{dR}{dT}\right)^{-1}$ (K)	δ (ln R) (Hz$^{-1/2}$)	NET (K Hz$^{-1/2}$)	ρ_{dc} ($\mu\Omega$ cm) at midpoint
A	Conductus	1×1 mm^2 300 nm YBCO/20 nm $SrTiO_3/Al_2O_3$	1	3×10^{-8}	3×10^{-8}	37
B	Xerox	1×3 mm^2 40 nm YBCO/50 nm YSZ/Si	2.6	3×10^{-8}	8×10^{-8}	55
C	Conductus	3×3 mm^2 300 nm YBCO/20 nm YSZ/Si_3N_4	6	4×10^{-7}	2.4×10^{-6}	270
D	Xerox	1×3 mm^2 40 nm YBCO/50 nm YSZ/Si_3N_4	5	10^{-6}	5×10^{-6}	190

a 50-nm-thick yttria-stabilized zirconia (YSZ) buffer layer. Because of the difference in the thermal expansion between silicon and YBCO, the YBCO films are under tensile stress and must be grown thinner than ~50 nm to avoid cracking. Silver contacts were again sputter deposited but were not annealed to avoid driving surface contaminants into the thin YBCO film. Samples C and D were mostly c-axis YBCO deposited on amorphous Si_3N_4 films with YSZ buffer layers. The Si_3N_4 films were deposited on Si at 850 °C by low-pressure chemical-vapor deposition (LPCVD) at 350 mTorr using SiH_2Cl_2 and NH_3. The YBCO films were deposited by a laser ablation process similar to that used for sample A.

We measured the voltage noise with an ac-coupled, room-temperature transformer and a field-effect transistor (FET) amplifier. The samples were mounted on a temperature-controlled stage in a cryostat and current biased at values typical for bolometer operation. Figure 1 shows the voltage noise for epitaxial samples A and B. The experiment was done by integrating the noise in a 2 Hz bandwidth for 15 min at each temperature point. The noise at the steepest part of the resistive transition for sample A (YBCO/$SrTiO_3/Al_2O_3$) gives NET = 3×10^{-8} K/Hz$^{1/2}$. This sample was as quiet as the best YBCO films that we have measured to date on any substrate. In general, films that satisfy other standard requirements for quality (e.g., large J_c small ΔT) consistently show low noise before processing. Samples A and B had high critical current ($J_c > 10^6$ A/cm^2, $T = 77$ K) and, as shown in Table I, narrow resistive transitions, and low resistance fluctuation noise. Processing, especially in the form of narrow, patterned lines, has been observed to increase noise. Therefore, we have avoided extensive processing of the films after deposition by using large area YBCO thermometers with the minimum resistance necessary to satisfy Eq. (5). Poor quality films tend to degrade more rapidly with processing than high-quality films. At present, our yield for samples of YBCO/$SrTiO_3/Al_2O_3$ with NET < 6×10^{-8} K/Hz$^{1/2}$ after processing is higher than 50%. After the substrate thickness of sample A was reduced by grinding to 25 μm, it was used in a composite bolometer with a sapphire substrate.[8,9] The best NET yet obtained for YBCO on a silicon substrate is NET = 7×10^{-8} K/Hz$^{1/2}$.

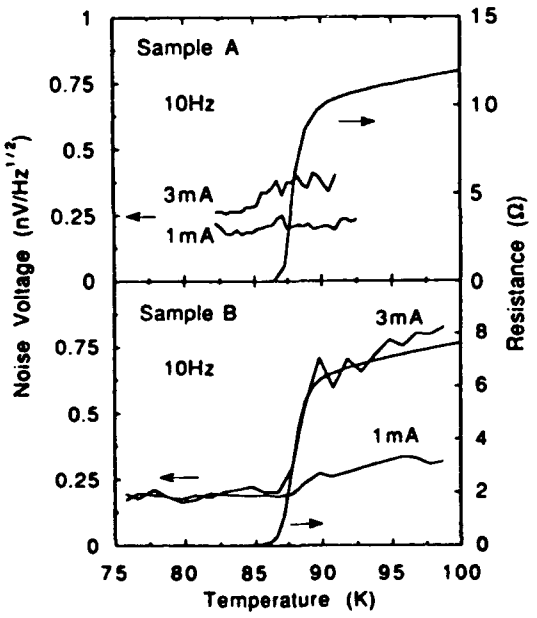

FIG. 1. Resistance and voltage noise at 10 Hz in current-biased YBCO films measured as a function of temperature. The noise in the measurement system is 0.15 nV/Hz$^{1/2}$. Sample A is 300 nm of epitaxial YBCO on a 20 nm buffer layer of $SrTiO_3$ on sapphire. Sample B is 40 nm of epitaxial YBCO on a 50 nm buffer layer of yttria-stabilized zirconia on silicon.

The resistive transitions for samples C and D of YBCO/YSZ/Si_3N_4 shown in Fig. 2 are significantly broader than for samples A and B and the voltage noise is higher. Consequently, the values of NET are about 100 times poorer. In general, we expect that YBCO samples with poor epitaxy make noisier thermometers. One contribution is switching noise from thermally activated flux motion. Flux can move more easily along regions of reduced energy-gap parameter such as grain boundaries.[30] The frequency dependence of δ(ln R) is determined by the distribution of activation energies for the switching processes[31] and the amplitude of δ(ln R) depends on the number of such processes. We have strong evidence for such processes from noise measurements in an external magnetic field of both YBCO/MgO samples and YBCO/Al_2O_3 samples.[32] The YBCO/Al_2O_3 film had poorer in-plane epitaxy, as determined by x-ray analysis,[33] and higher noise, which increased with applied magnetic field. Based on experience with other substrates, we expect that the NETs for YBCO films on Si_3N_4 will improve as that technology matures.

For practical reasons, bolometers for use in large for-

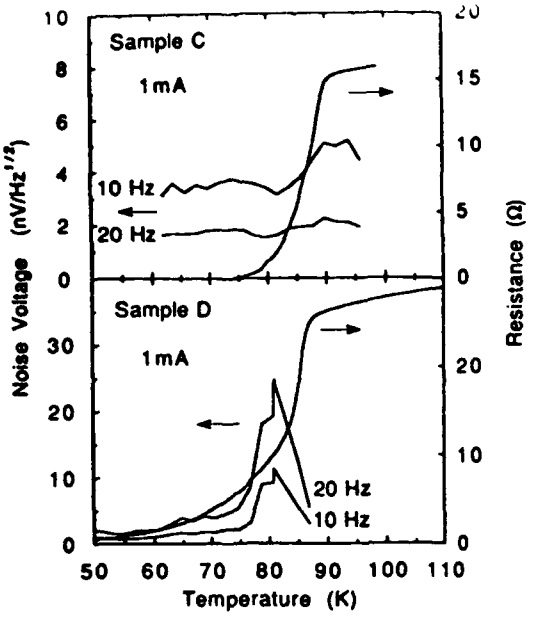

FIG. 2. Resistance and voltage noise at 10 Hz in current-biased YBCO films measured as a function of temperature. The noise in the measurement system is 0.15 $nV/Hz^{1/2}$. Sample C is 300 nm YBCO on a 20 nm buffer layer of yttria-stabilized zirconia on Si_3N_4. Sample D is 40 nm YBCO on a 50 nm buffer layer of yttria-stabilized zirconia on Si_3N_4.

mat imaging arrays must be produced by optical lithography and micromachining. Such techniques are desirable even for single bolometer elements. Our interest has focused on bolometers that consist of a high-T_c thermometer and a radiation absorber such as gold black[34,35] or a Bi film[36] deposited on a thin membrane that is isolated from the heat sink by two thin legs of the same membrane material (Fig. 3). Bolometers made on thin Si_3N_4 membranes can have very low heat capacity per unit area C_A and can be made with very low G because of the mechanical strength and the low bulk thermal conductivity of Si_3N_4. The relatively high NET of our present thermometers on Si_3N_4, however, limits the use of this substrate to relatively small bolometers with high responsivity to minimize the contribution of film noise in Eq. (4). Such bolometers are well suited, for example, to imaging arrays for $\lambda \sim 10$ μm. Bolometers made on Si membranes have smaller values of

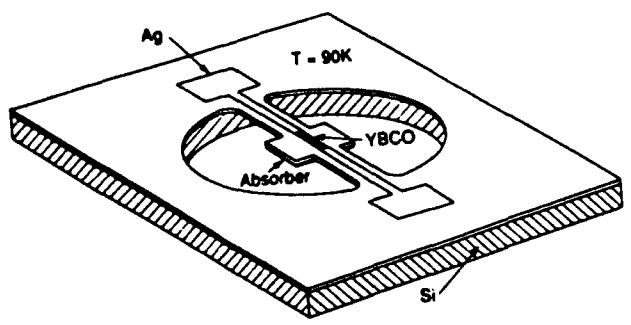

FIG. 3. Diagram of a membrane bolometer. The bolometer consists of a radiation absorber and a YBCO thermometer deposited on a membrane of Si or Si_3N_4 which is isolated from the heat sink by two thin legs.

NET, but will probably be limited to larger values of C_A and G. They are therefore appropriate for higher throughput applications at longer wavelengths. The very low values of NET obtained on thinned sapphire substrates make this technology appropriate for very large bolometers. We will quantify this argument by calculating the dependence of the detectivity D^* on area and thus on λ for each of the above technologies using the values of NET from Table I.

The bolometer substrate technology chosen sets material limits to the heat capacity per unit area C_A that can be achieved. In addition, for the membrane technologies, there is a minimum practical value for the thermal conductance G_{min} set by the strength of the legs. If we assume that the required response time τ and the factor $A/\lambda^2 = n/\Omega$ are set by the application, then the required $G = C_A A/\tau$ will be equal to G_{min} at a specific wavelength λ_0 given by

$$\lambda_0 = \left(\frac{G_{min}\tau}{C_A}\frac{\Omega}{n}\right)^{1/2}. \tag{6}$$

For $\lambda < \lambda_0$ the bolometer will be faster than is required and therefore less sensitive than optimum. For $\lambda > \lambda_0$, the available range of G includes the optimum value.

We estimate C_A and G_{min} for a Si_3N_4 bolometer based on a 0.75-μm-thick Si_3N_4 membrane which was built at Berkeley by other workers.[37] This membrane was supported by two Si_3N_4 legs with dimensions $0.75\times0.75\times20$ μm.[3] For a bolometer with two such legs, we calculate $G_{min} \approx 0.3$ μW/K by using a handbook value for the thermal conductivity of bulk Si_3N_4 at 90 K. For a Si membrane bolometer with two undoped Si legs of the same dimensions, $G_{min} \approx 30$ μW/K. From handbook data,[38] we estimate that G_{min} of doped Si legs might be roughly $0.5G_{min}$ of undoped Si legs at 90 K. We expect the heat capacity of the YBCO thermometer and silver electrical contacts to dominate the substrate heat capacity, so we choose $C_A = 2.7\times10^{-5}$ J K^{-1} cm^{-2} for both Si and Si_3N_4 membrane bolometers.

Figure 4 shows the prediction for D^* as a function of the normalized wavelength λ/λ_0 for a fixed value of A/λ^2 and $\tau = 10$ ms. The solid line shows the upper limit on D^* imposed by phonon noise,

$$D^* = (A/4kT_c^2G)^{1/2}. \tag{7}$$

For $\lambda > \lambda_0$, $G \propto A$, so $D^*(\lambda)$ is constant. For $\lambda < \lambda_0$, $G = G_{min}$, so $D^*(\lambda) \propto \lambda$.

The performance of the bolometer is limited by thermometer noise if NET $> 10^{-8}$ $K/Hz^{1/2}$. The dashed lines show the limits on D^* from thermometer noise for various values of NET calculated from

$$D^* = \left(\frac{A}{G^2(\mathrm{NET})^2(1+\omega^2\tau^2)}\right)^{1/2}. \tag{8}$$

For $\lambda > \lambda_0$, $D^*(\lambda) \propto 1/\lambda$. For $\lambda < \lambda_0$, G is held constant at G_{min} and $D^*(\lambda) \propto \lambda$. Hence D^* peaks at $\lambda = \lambda_0$ for a pixel limited by thermometer noise. The wavelength λ_0 for Si_3N_4 is 0.1 of the value of λ_0 for Si since the thermal conductivity of Si_3N_4 is $\sim 1/100$ that of Si at 90 K.

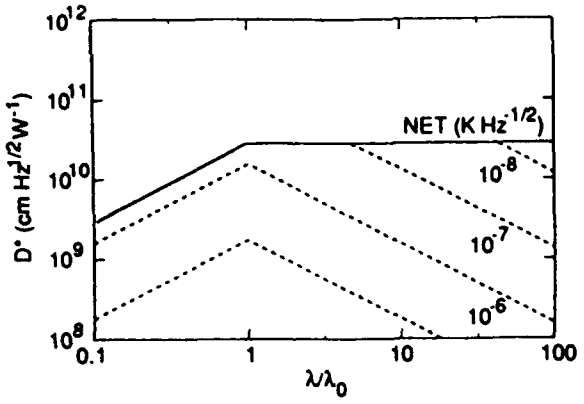

FIG. 4. Specific detectivity D^* as a function of reduced wavelength λ/λ_0 where λ_0 depends on the minimum achievable values of the heat capacity per unit area C_A and thermal conductance G_{min} as well as the response time τ, the number n of electromagnetic modes that couple, and the solid angle Ω of the pixel's field of view. The solid line shows the predicted phonon noise limit for a bolometer on a thin membrane. The dashed lines show upper limits on D^* for thermometers with various values of NET.

For a given value of A/λ^2, response time τ, and combination of YBCO thermometer and substrate, we can compute λ_0 and plot the curve from Fig. 4 as D^* vs λ. Figure 5 shows this plot for $A/\lambda^2 = 50$ and $\tau = 10$ ms for our best YBCO thermometers on both Si_3N_4 and Si membranes. For comparison, Fig. 5 also shows the performance of typical pixels in several different large format arrays operated at 77 K along with the photon noise limits for photovoltaic and photoconductive detectors that view 300 K radiation in a 0.02 sr field of view. The predicted performance for YBCO/YSZ/Si_3N_4, shown in Fig. 5, could be competitive with HgCdTe at $\lambda = 10$ μm and one order of magnitude more sensitive than HgCdTe at $\lambda = 20$ μm.[39] The performance of this array at longer wavelengths is

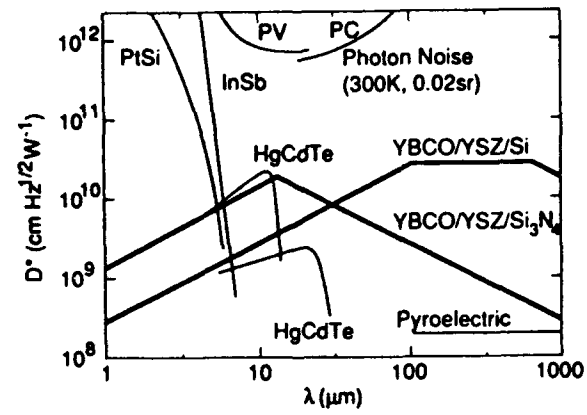

FIG. 5. Specific detectivity D^* as a function of wavelength for diffraction-limited pixels with $\Omega = 0.02$ sr ($f/6$ optics) and $\tau = 10$ ms. The thick lines show the predicted D^* for high-T_c bolometers on silicon and Si_3N_4 membranes using YBCO thermometers. These lines were calculated using estimates for the minimum achievable heat capacity and thermal conductance and using measurements of voltage noise in high-T_c thermometers. Typical values of D^* for InSb, PtSi, and HgCdTe detectors in two-dimensional staring arrays operated at 77 K are shown for comparison. Also shown are the photon noise limits for photovoltaic and photoconductive detectors which view 300 K radiation in a 0.02 sr field of view.

better than room-temperature detectors, but is rapidly degraded by thermometer noise. An array optimized for longer wavelengths can have a better peak value of D^*. Choosing $A/\lambda^2 = 5$ and $\tau = 10$ ms, the peak in D^* is three times higher and occurs at $\lambda = 45$ μm for the same thermometer NET.

The predicted performance for a YBCO/YSZ/Si bolometer with the same assumed geometry as for Si_3N_4 is also shown in Fig. 5. The region of phonon-noise-limited D^* appears at longer wavelengths than for Si_3N_4 because of the higher bulk thermal conductivity of silicon. The limit to D^* from thermometer noise is higher than that of bolometers on Si_3N_4 because of the lower NET of YBCO on silicon. Arrays of high-T_c bolometers on Si membranes may be useful for imaging applications for $\lambda > 20$ μm. One example is long-wavelength atmospheric imaging from NASA planetary probes such as Cassini.[5,6]

The most important potential impact of the high-T_c bolometer is in a liquid-nitrogen (LN)-cooled large format imaging array for 8–14 μm. This possibility depends both on the performance of the bolometer arrays as discussed above and also on the performance available from the competing HgCdTe technology. Although accurate predictions are not possible, this important question deserves further discussion. Two-dimensional (2D) staring arrays for 300 K thermal imaging in the atmospheric window from 8 to 14 μm require high D^* per pixel, good uniformity, and low-noise readout electronics. The predicted D^* of a high-T_c bolometer used from 8 to 14 μm is worse than the D^* of a HgCdTe photovoltaic detector in a single pixel or linear array format. However, it is difficult to make 2D arrays of HgCdTe photovoltaic detectors that are larger than 128×128 pixels.[16] Even these arrays suffer from low yields and high costs. The performance of arrays of HgCdTe detectors which operate from 8 to 14 μm also suffers from high backgrounds and high leakage currents. These currents rapidly saturate the charge-storage capacity of a CCD readout and can restrict the integration time of the signal.[16,40] Many thermal imaging systems that require high spatial resolution across the field of view operate at shorter wavelengths so as to use more mature technologies[41] with larger numbers of pixels such as PtSi (Ref. 42) or InSb. Although the yield and uniformity of such arrays are excellent, the atmosphere is more opaque at these wavelengths. Also, radiation from a 300 K blackbody is weaker at 4 μm than at 10 μm but stray light from visible sources such as the sun is stronger at 4 μm than at 10 μm. We believe large 2D arrays of high-T_c bolometers on Si_3N_4 membranes will have useful sensitivity from 8 to 14 μm and could have advantages in yield and cost over large 2D arrays of HgCdTe. Without building such an array, we cannot quantitatively predict the uniformity of the responsivities of pixels across the array. Equation (1) shows the uniformity in S depends only on variations in I, G, and $dR(T)/dT$. Temperature gradients across the array could produce variations in $dR(T)/dT$ from pixel to pixel. But, temperature gradients that are smaller than $\sim 0.1\Delta T$ should not seriously degrade uniformity since $R(T)$ is mostly linear on this temperature scale.

IV. ARRAY DESIGN AND READOUT

We have predicted useful sensitivity for a single pixel high-T_c bolometer with a dedicated low-frequency amplifier. Many imaging applications require large arrays of bolometers where constraints on power dissipation and filling factor only allow for a small number of amplifier channels. In simple circuits, the electrical signal from a pixel is only integrated for a tiny fraction of the observation time. The electrical noise from a pixel in an array can therefore be much greater than the noise from a single pixel with a dedicated amplifier. We now discuss a scheme that provides signal integration over the full observation time, but does not require one amplifier per pixel.

The NEP of a bolometer pixel has contributions from thermal fluctuations, including infrared source fluctuations, as well as the phonon noise, represented by the first term in Eq. (3). It also has contributions from voltage fluctuations in the thermometer, represented by the second and third terms in Eq. (3). Thermal fluctuations occurring for $\omega_{fluct}\tau \gg 1$ are integrated by the thermal response time of the bolometer. Therefore, a bolometer that operates in the source noise or phonon noise limit with τ equal to the frame time does not require additional electrical integration. In principle, however, a bolometer optimized for sensitivity has equal contributions to the NEP from both thermal fluctuations and voltage fluctuations. In practice, the bolometer designs that we have described above are sometimes limited by voltage noise fluctuations. Therefore, integration of the electrical signal is desirable.

Photovoltaic detectors in a CCD array integrate the photocurrent with a charge storage well next to each detector. Ideally, the storage capacity of the well is larger than the product of the photocurrent and the time interval between samplings by the readout amplifier. Consequently, charge fluctuations that occur faster than the sampling rate are averaged. A bolometric detector outputs a voltage equal to the product of the absorbed infrared power and the responsivity (1). An RC filter could be implemented next to the bolometer which integrates voltage fluctuations occurring on time scales shorter than RC. The RC time should approximately equal the frame time.

As a specific example, we consider a 64×64 imaging array of high-T_c bolometers similar to existing arrays of bismuth bolometers built at Honeywell.[26] Since both the readout amplifiers and the bolometers have $1/f$ noise, we assume the incident radiation is chopped at 60 Hz. This leads to a frame rate of 30 Hz and a thermal time constant $\tau = 3$ ms for each bolometer pixel. The pixels are continuously biased and dissipate less than 5 μW each. The whole array is read out once while observing the target, and again while observing the chopper blade. The two frames are then digitally subtracted. Assuming four readout amplifiers, each pixel is sampled for a maximum time $\tau_{sample} = 3$ μs. Electrical noise in the thermometer occurring at higher frequencies than 60 Hz is then aliased across the bandwidth of the readout amplifier. An RC filter next to each pixel would roll off this high-frequency noise before it is aliased.

Figure 6 shows a schematic implementation of the

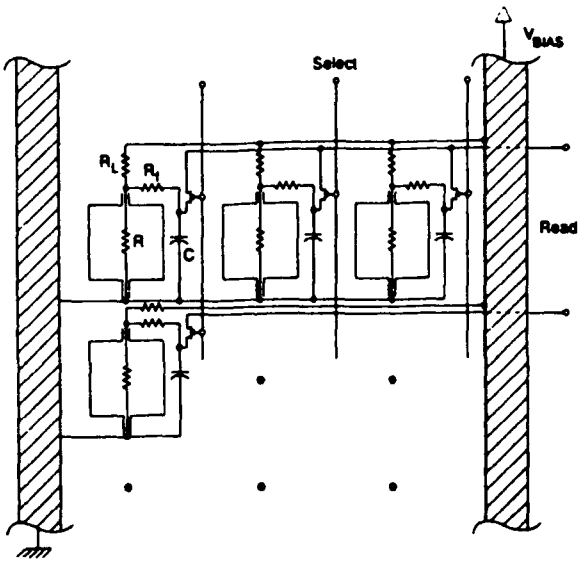

FIG. 6. Schematic layout of a possible implementation of a high-T_c bolometer array with a novel readout scheme in which above-band electrical noise from each pixel is integrated by an R_fC filter. In this scheme, a multiplexed readout amplifier that undersamples a given pixel does not alias above-band noise into the signal channel. The unit cell consists of an YBCO thermometer R, an R_fC filter, an access transistor, a load resistor R_L, and bias lines. The voltage across R appears on the appropriate "READ" line when the "SELECT" voltage is high. All pixels are constantly under bias. The readout circuit elements would be implemented on a separate Si wafer which could be indium bump bonded to the bolometer pixels. The optical fill factor will probably be limited by geometrical constraints on the bolometer imposed by requirements for thermal isolation.

readout circuit for a two-dimensional bolometer array. The readout circuit elements could be fabricated on a separate silicon wafer which is bonded to the bolometer array with indium bumps. The R_fC filter appears in parallel with the high-T_c thermometer. For conceptual simplicity, we will first consider passive circuit components. In practice, circuits with active components may consume less power and surface area. Active components are frequently used in CCD arrays.[43,44] A polysilicon resistor with $R_f = 10$ MΩ and a trench capacitor with $C = 300$ pF would give a time constant $R_fC = 3$ ms. Typically, $R_f \gg R$ so the contribution to the NEP from Johnson noise is mostly from R_f. This contribution will be negligible if the constraint (5) is modified to

$$I\delta R > \left(4kT_cR_f + \frac{e_n^2 + (i_nR_f)^2}{f_{chop}\tau_{sample}}\right)^{1/2}. \quad (9)$$

The divisor $f_{chop}\tau_{sample}$ accounts for the reduced integration time of noise from the readout amplifier. The resulting amplifier noise contribution to the NEP is negligible for available amplifiers.[45] For example, a bolometer on a Si_3N_4 membrane using sample C could satisfy conditions (9) and (2) for $R_f = 10$ MΩ and the array parameters described above if the YBCO is patterned into a meander line with $R = 50$ kΩ at T_c.

It may be difficult to satisfy conditions (9) and (2) using only passive components because of size constraints

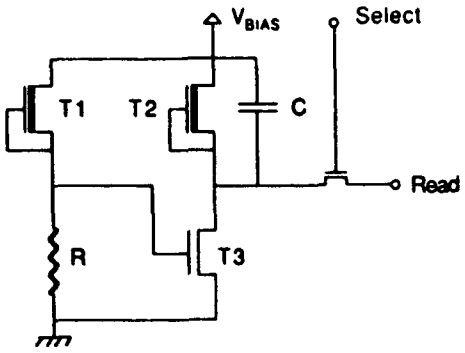

FIG. 7. Schematic layout of a readout for a single pixel which is functionally similar to a single cell in Fig. 6 but uses active devices. This circuit has both an anti-aliasing filter and voltage gain to buffer the signal from noise in the "select" transistor. The power consumption and size of this circuit can be much smaller than the circuit shown in Fig. 6.

on the capacitors or difficulty in making high-resistance meander strips of YBCO. Although exact requirements on the anti-aliasing filter are specific to the system, we will mention two approaches for meeting the above conditions. First, the R_fC time constant could be reduced by reading out the array more frequently. For example, most of the signal integration could be performed by a bank of larger capacitors, called a frame averager, which is located outside the focal plane. In this scheme, multiplexers transfer charge from a small capacitor next to a pixel to a much larger capacitor out of the focal plane at a faster rate than the chopping frequency. Then the readout amplifier samples the capacitors in the frame averager at the chopping frequency. Second, two-transistor amplifiers with anti-aliasing filters could be fabricated in silicon for each pixel. Figure 7 shows a schematic diagram of a circuit that is functionally similar to Fig. 6 but which uses active components. The depletion-mode transistor T1 presents a current bias to the bolometer without dissipating much power. The depletion-mode transistor T2 functions both as R_f for the anti-aliasing filter and as a load resistance for the common source buffer stage made from T3. This circuit has both an anti-aliasing filter and voltage gain to buffer the signal from noise in the "select" transistor. If a specific application requires a higher resistance from the active load, a current mirror could be used in place of the depletion-mode transistor.[46] The transistors can be metal-oxide-semiconductor FETs in most applications. Some applications may benefit from the lower $1/f$ noise of junction field effect transistors (JFET).

V. SUMMARY

We have discussed the optimization of high-T_c bolometers for imaging arrays for wavelengths longer than 10 μm. An analysis of the thermometer sensitivity required for different pixel sizes indicates that there are useful applications for small Si_3N_4 membrane bolometers at $\lambda \sim 10$ μm and larger Si membrane bolometers at longer wavelengths. A readout scheme for an array of bolometers that provides real-time signal integration on chip has also been described.

ACKNOWLEDGMENTS

The authors gratefully acknowledge useful discussions with Paul Kruse and Matts Gustaffson. This work was supported in part by the Director, Office of Energy Research, Office of Basic Energy Sciences, Materials Sciences Division of the U.S. Department of Energy under Contract No. DE-AC03-76SF00098 (for S.V. and P.L.R.), by Conductus Inc. (for K.C.), by the Air Force Office of Scientific Research (AFOSR) under Contract No. F49620-89-C-0017 (for D.K.F. and T.H.G.), and by Xerox Palo Alto Research Center (for D.K.F.). S.V. acknowledges a Department of Education predoctoral fellowship, and D.K.F. acknowledges an ATT predoctoral fellowship.

[1] P. L. Richards, J. Clarke, R. Leoni, P. H. Lerch, S. Verghese, M. R. Beasley, T. H. Geballe, R. H. Hammond, P. Rosenthal, and S. R. Spielman, Appl. Phys. Lett. 54, 283 (1989).
[2] P. L. Richards, S. Verghese, T. H. Geballe, and S. R. Spielman, IEEE Trans. Magn. MAG-25, 1335 (1989).
[3] L. Xizhi, Y. Caibing, C. Xiaoneng, F. Xizeng, S. Xiangqing, L. Shuqin, X. Yizhi, Z. Bairu, Y. Caiwen, Z. Yinzi, Z. Yuying, L. Yong, W. Huisheg, S. Yinhuan, G. Ju, and L. Lin, Int. J. Infrared Millimeter Waves 10, 445 (1989).
[4] J. C. Brasunas, S. H. Moseley, B. Lakew, R. H. Ono, D. G. McDonald, J. A. Beall, and J. E. Sauvageau, J. Appl. Phys. 66, 4551 (1989).
[5] J. C. Brasunas, S. H. Moseley, B. Lakew, R. H. Ono, D. G. McDonald, J. A. Beall, and J. E. Sauvageau, SPIE Proc. 1292, 155 (1990).
[6] J. C. Brasunas, S. H. Moseley, B. Lakew, R. H. Ono, D. G. McDonald, J. A. Beall, and J. E. Sauvageau, SPIE Proc. 1477, 166 (1991).
[7] B. Dwir, L. Pavesi, J. H. James, B. Kellett, D. Pavuna, and F. K. Reinhart, Supercond. Sci. Technol. 2, 314 (1989).
[8] S. Verghese, P. L. Richards, K. Char, and S. A. Sachtjen, SPIE Proc. 1292, 137 (1990).
[9] S. Verghese, P. L. Richards, K. Char, and S. A. Sachtjen, IEEE Trans. Magn. MAG-27, 3077 (1991).
[10] G. L. Carr, M. Quijada, D. B. Tanner, C. J. Hirschmugl, G. P. Williams, S. Etemad, B. Dutta, F. DeRosa, A. Inam, T. Venkatesan, and X. Xi, Appl. Phys. Lett. 57, 2725 (1990).
[11] W. S. Brocklesby, D. Monroe, A. F. J. Levi, M. Hong, S. H. Liou, J. Kwo, C. E. Rice, P. M. Mankiewich, and R. E. Howard, Appl. Phys. Lett. 54, 1175 (1989).
[12] J. G. Forrester, M. Gottleib, J. R. Gavaler, A. I. Braginski, Appl. Phys. Lett. 53, 1332 (1988).
[13] H. S. Kwok, J. P. Zheng, and Q. Y. Ying, Appl. Phys. Lett. 54, 2473 (1989).
[14] Qing Hu and P. L. Richards, Appl. Phys. Lett. 55, 2444 (1989).
[15] M. Nahum, Qing Hu, and P. L. Richards, IEEE Trans. Magn. MAG-27, 3081 (1991).
[16] T. G. Stratton, B. E. Cole, P. W. Kruse, and R. A. Wood, in SC Global 90 International Superconductor Applications Convention Proceedings, CA, January, 1990; also T. G. Stratton, B. E. Cole, P W. Kruse, R. A. Wood, K. Beauchamp, T. F. Wang, B. Johnson, and A. M. Goldman, Appl. Phys. Lett. 57, 99 (1990).
[17] P. Rosenthal, R. H. Hammond, M. R. Beasley, R. Leoni, P. Lerch, and J. Clarke, IEEE Trans. Magn. MAG-25, 973 (1989).
[18] R. C. Lacoe, J. P. Hurrell, K. Springer, I. D. Raistrick, R. Hu, J. F. Burch, and R. S. Simon, IEEE Trans. Magn. MAG-27, 2832 (1991).
[19] F. N. Hooge and A. M. H. Hoppenbrouwers, Physica 45, 386 (1969).
[20] See, for example, the Barnes thermopile detector, EDO Corp., Shelton, CT.
[21] T. L. Hwang, S. E. Schwarz, and D. B. Rutledge, Appl. Phys. Lett. 34, 773 (1978).
[22] D. P. Neikirk, W. W. Lam, and D. B. Rutledge, Int. J. Infrared Millimeter Waves 5, 245 (1984).
[23] T. W. Kenny, W. J. Kaiser, S. B. Waltman, and J. K. Reynolds, Appl.

Phys. Lett. 59, 1820 (1991).
[24] M. J. E. Golay, Rev. Sci. Instrum. 20, 816 (1949).
[25] See, for example, the P-41 detector, Molectron Corp., Sunnyvale, CA.
[26] P. W. Kruse (private communication).
[27] K. Char, N. Newman, S. M. Garrison, R. W. Barton, R. C. Taber, S. S. Laderman, and R. D. Jacowitz, Appl. Phys. Lett. 57, 409 (1990).
[28] D. K. Fork, D. B. Fenner, R. W. Barton, J. M. Phillips, G. A. N. Connell, J. B. Boyce, and T. H. Geballe, Appl. Phys. Lett. 57, 1161 (1990).
[29] D. K. Fork, A. Barrera, T. H. Geballe, A. M. Viano, and D. B. Fenner, Appl. Phys. Lett. 57, 2504 (1990).
[30] M. J. Ferrari, M. Johnson, F. C. Wellstood, J. Clarke, D. Mitzi, P. A. Rosenthal, C. B. Eom, T. H. Geballe, A. Kapitulnik, and M. R. Beasley, Phys. Rev. Lett. 64, 72 (1990).
[31] P. Dutta and P. M. Horn, Rev. Mod. Phys. 53, 497 (1981).
[32] S. Verghese, P. L. Richards, K. Char, S. M. Garrison, and R. W. Barton (unpublished).
[33] K. Char, D. K. Fork, T. H. Geballe, S. S. Laderman, R. C. Taber, R. D. Jacowitz, F. Bridges, G. A. N. Connell, and J. B. Boyce, Appl. Phys. Lett. 56, 785 (1990).
[34] L. Harris and J. K. Beasley, J. Opt. Soc. 42, 134 (1952).
[35] L. Harris, J. Opt. Soc. 51, 80 (1960).
[36] J. Clarke, G. I. Hoffer, P. L. Richards, and N.-H. Yeh, J. Appl. Phys. 48, 4865 (1977).
[37] Matts Gustaffson (private communication).
[38] Y. S. Touloukian, *Thermophysical Properties of Matter: Thermal Conductivity of Metallic Elements and Alloys* (IFI/Plenum, New York, 1970), p. 326.
[39] E. R. Fossum, Innovative Long Wavelength Infrared Detector Workshop Proceedings, JPL Publication 90-22, p. 117, July 1990.
[40] A. Rogalski and J. Piotrowski, Prog. Quantum Electron. 12, 87 (1988).
[41] P. R. Norton (unpublished).
[42] J. Mooney (private communication).
[43] M. B. Reine, Innovative Long Wavelength Infrared Detector Workshop Proceedings, JPL Publication 90-22, p. 61, July 1990.
[44] N. Bluzer and A. S. Jensen, Opt. Eng. 26, 241 (1987).
[45] An amplifier built with a Toshiba 2SK137 JFET input stage can have a noise temperature of 100 mK at frequencies lower than 100 Hz with $\sim$ 10 MΩ noise resistance.
[46] P. R. Gray and R. G. Meyer, *Analysis and Design of Analog Integrated Circuits* (Wiley, New York, 1984), p. 710.